MESENCHYMAL STROMAL CELL THERAPY FOR LIVER FIBROSIS

by

Debashis Haldar

A thesis submitted to the University of Birmingham for the degree of

DOCTOR OF PHILOSOPHY

Centre for Liver Research
Institute of Immunology and Immunotherapy
College of Medical and Dental Sciences
University of Birmingham
June 2019

Mesenchymal stromal cell therapy for liver fibrosis

Substantial uncertainty exists from pre-clinical liver fibrosis models as to whether mesenchymal stromal cells (MSCs) are anti-fibrotic, and yet clinically they have been proposed as a putative anti-fibrotic therapy for patients. This research was set out to examine whether MSC therapy can reduce liver fibrosis.

An assessment of the depth and persistence of fibrosis in two murine liver fibrosis models (12 doses of intraperitoneal carbon tetrachloride, or 16 weeks of oral thioacetamide) allowed a statistically powered analysis of MSC intervention. Human umbilical cord MSCs were peripherally injected after liver fibrosis was established, or during fibrogenesis. Finally, the effect of MSC conditioned medium on the biology of human stellate-cell line, LX2 cells, was examined.

MSC administration neither resolved established fibrosis, nor abrogated fibrogenesis in either model. Peripherally injected MSCs were sequestered in the lungs. However, MSC conditioned medium attenuated the expression of collagen type-1 mRNA and promoted apoptosis in LX2 cells. The discordance between the *in vivo* and *in vitro* findings requires further exploration. Nevertheless, this statistically powered robust examination of human umbilical cord MSCs suggests no discernible anti-fibrotic influence *in vivo*, and future testing would require a significant deviation in protocol to overcome a documented barrier from this research.

Acknowledgments

ওঁ মা সরস্বতী

This work was a product of the help and support I received throughout my research.

Gideon saw potential when I did not. Phil opened doors I did not know existed. Neil showed me the forest through the trees.

The Wellcome Trust believed in my vision, and the Tavernors were incredibly generous in funding my development. Steve Elliman and the rest of Orbsen trusted me with their magic cells, and BioInVision helped me see them.

My brother blazed a trail for me to follow; my parents armed me with resilience – I needed it.

James and Geoff offered friendship when I did not expect it. Maggie, Emma, Mirka, Ashnila, Dan, Gwil, Sarah, Abhi, Tickle, tall Richard, short Richard and Killer Chung made work fun. Mohammed, Ditte, Annika, Thin and Vas were generous with their patience and time in teaching me "to lab". Yuri reminded me that one could always work harder. Janine, Subin and Gary enabled me to do just that. Suggestions, help and carbohydrate sustenance were never difficult to find in the Liver Labs, and I thank each and every one of my colleagues who made my life better.

Then there was Monica, for when my resilience was not enough…

Dissemination and publications

Directly related to data presented in thesis

Haldar D, Wilkin R, Hedegaard D, Alfaifi M, Vigneswara V, Luu N, et al. Study of anti-fibrotic activity of human umbilical-cord tissue-derived mesenchymal stromal cells during fibrogenesis or resolution in murine models of liver fibrosis. J Hepatol 2019;70:e194.

Ciccocioppo R, Dos Santos CC, Baumgart DC, Cangemi GC, Cardinale V, Ciacci C, Haldar D, et al. Proceedings of the signature series event of the international society for cellular therapy: "Advancements in cellular therapies and regenerative medicine in digestive diseases" London, United Kingdom, May 3, 2017. Cytotherapy 2018.

Haldar D, Henderson NC, Hirschfield G, Newsome PN. Mesenchymal stromal cells and liver fibrosis: a complicated relationship. FASEB J 2016;30:3905–28.

Parallel to data presented in thesis

King A, Houlihan DD, Kavanagh D, Haldar D, Luu N, Owen A, et al. Sphingosine-1-Phosphate Prevents Egress of Hematopoietic Stem Cells From Liver to Reduce Fibrosis. Gastroenterology 2017.

Wilhelm A, Aldridge V, Haldar D, Naylor AJ, Weston CJ, Hedegaard D, et al. CD248/endosialin critically regulates hepatic stellate cell proliferation during chronic liver injury via a PDGF-regulated mechanism. Gut 2016;65:1175–85

Than NN, Tomlinson CL, Haldar D, King AL, Moore D, Newsome PN. Clinical effectiveness of cell therapies in patients with chronic liver disease and acute-on-chronic liver failure: a systematic review protocol. Syst Rev 2016;5:100.

Other first-author publications during research

Haldar D, Kern B, Hodson J, Armstrong MJ, Adam R, Berlakovich G, et al. Outcomes of liver transplantation for non-alcoholic steatohepatitis: A European Liver Transplant Registry study. J Hepatol 2019.

Haldar D, Cockwell P, Richter AG, Roberts KJ, Hirschfield GM. An overview of the diagnosis and management of immunoglobulin G4-related disease. CMAJ 2016

Haldar D, Hirschfield GM. Deciphering the biology of IgG4-related disease: Specific antigens and disease? Gut 2018;67.

*__Bold__ denotes first author.

Contents

Chapter 1 Introduction 1

1.1. The clinical imperative for an anti-fibrotic agent 2

1.2. Mechanisms of fibrogenesis and resolution in liver disease 7

1.3. Potential targets for therapy in fibrosis pathways 12

1.4. Mesenchymal stromal cells – a therapeutic option? 13

1.5. Do mesenchymal stromal cells prevent fibrosis, rather than promote its resolution? 17

1.6. Can mesenchymal stromal cells have a direct anti-fibrotic effect? 25

1.6.1. Tipping the balance of TIMPs and MMPs 25

1.6.2. Secreted anti-fibrotic agents and the effects on the fate of myofibroblasts 28

1.7. Do BM-MSC contribute to fibrosis? 33

1.8. Do liver resident MSCs contribute to fibrosis? 40

1.9. Aims of the research 41

Chapter 2 Materials and Methods 42

2.1. Isolation of mesenchymal stromal cells from human umbilical cord tissue 43

2.2. Storage, culture, subculture and use of human MSC 44

2.2.1. Preparation and storage of MSC conditioned medium 47

2.3. Characterisation of MSC 48

2.3.1. Characterisation of MSCs by flow cytometry 48
2.3.2. Characterisation of MSC by adipogenic differentiation 50
2.3.3. Characterisation of MSC by chondrogenic differentiation 51
2.3.4. Characterisation of MSC by osteogenic differentiation 53
2.4. Animal Husbandry 55
2.5. Inducing toxin-mediated hepatic injury and fibrosis 56
2.5.1. Carbon tetrachloride 56
2.5.2. Thioacetamide 56
2.6. Investigating the therapeutic effect of MSCs *in vivo* 58
2.7. Mouse euthanasia; tissue and blood collection for analysis 59
2.8. Flow cytometry analysis for myeloid cells 61
2.8.1. Isolation of immune cells from mouse liver 61
2.8.2. Isolation of immune cells from mouse blood 62
2.8.3. Antibody staining 62
2.8.4. Gating strategies for myeloid cells 64
2.9. Liver biochemical tests 65
2.10. Hepatic hydroxyproline assay 66
2.10.1. Preparation of Chloramine-T solution 66
2.10.2. Preparation of Ehrlich's solution 66

2.10.3. Preparation of hydroxyproline standards 67

2.10.4. The hydroxyproline assay 67

2.11. Preparing slides from formalin-fixed paraffin embedded tissue for staining 69

2.11.1. Haematoxylin and eosin staining 69

2.11.2. Immunohistochemistry (IHC) 70

2.11.3. Picrosirius red staining 71

2.11.4. Digitising slide images for analysis 72

2.11.5. Morphometric analysis of PSR and IHC stained liver tissue sections 73

2.12. *In vivo* localisation of MSC after IV injection 74

2.12.1. Flow cytometric analysis of QuantumDot® labelled cells 75

2.13. *In vitro* methodology 76

2.13.1. Storage, culture and subculture of LX2 cells 76

2.13.2. Immunocytochemistry 78

2.13.3. Senescence associated β-galactosidase assay 81

2.13.4. Cell proliferation assay 81

2.13.5. Cell apoptosis assay 83

2.14. Quantitative PCR 85

2.14.1. RNA extraction from mouse liver tissue 85

2.14.2. RNA extraction from LX2 cells 86

2.14.3. cDNA synthesis 86

2.14.4. Real time quantitative polymerase chain reaction (qPCR) 87

2.15. Statistics 90

Chapter 3 Models of liver fibrosis and resolution 91

3.1. Background and context 92

3.1.1. An ideal model to test the effect of a therapeutic agent on established liver fibrosis. 92

3.1.2. CCl_4-induced hepatotoxicity 94

3.1.3. TAA-induced hepatotoxicity 95

3.1.4. Choice of genetic background 96

3.2. Aims of the chapter 97

3.3. Establishing models of liver fibrosis and resolution: CCl_4 98

3.3.1. Fibrosis and resolution model: Low dose CCl_4 98

3.3.2. Fibrosis and resolution model: High dose CCl_4 102

3.3.3. Determining period of continued inflammation and hepatocyte injury after toxin-cessation: High dose CCl_4 model 110

3.4. Establishing models of liver fibrosis and resolution: TAA 113

3.4.1. Feasibility and safety of IP TAA protocol 113

3.4.3. Feasibility and safety of oral TAA protocol 115

3.4.4. Fibrosis and resolution model: oral TAA 123

3.4.5. Determining the profile of inflammation and hepatocyte injury after toxin-cessation: oral TAA model 129

3.5. Discussion 131

3.5.1. Feasibility and safety 131

3.5.2. Peak fibrosis and resolution 131

3.5.3. Defining a time frame for intervention 134

3.5.4. Variation in fibrosis despite identical injury 134

3.5.5. Summary 137

Chapter 4 Characterising MSCs 138

4.1. Background and context 139

4.1.1. Mesenchymal stromal cell selection by prospective enrichment 140

4.1.2. Umbilical-cord tissue derived mesenchymal stromal cells 142

4.1.3. Syndecan-2 143

4.2. Aims of the chapter 144

4.3. Morphology and plastic adherence of MSCs 145

4.4. The mesogenic process – mesodermal differentiation of MSCs 147

4.5. Cell-surface marker analysis 149

4.6. Discussion 152

4.6.1. The characterisation of MSCs 152

4.6.2. Moving goal posts – finessing the characterisation of MSCs 152

4.6.3. The effect of *in vitro* confluence on MSC biology 153

4.6.4. Summary 154

Chapter 5 The therapeutic effect of systemic human UCT-MSC therapy on liver fibrosis in murine models 155

5.1. Background and context 156

5.2. Aims of the chapter 158

5.3. Intervention to enhance fibrosis resolution in the absence of ongoing hepatocyte injury or inflammation 159

5.3.1. The effect of human UCT-MSCs on established CCl_4-induced liver fibrosis 159

5.3.2. The effect of human UCT-MSCs on established TAA-induced liver fibrosis 167

5.4. Intervention to enhance fibrosis resolution in the presence of ongoing hepatocyte injury or inflammation 172

5.5. Intervention to reduce fibrogenesis during ongoing hepatic injury 179

5.5.1. The effect of human UCT-MSCs during CCl_4-induced liver fibrosis 180

5.5.3. The effect of human UCT-MSCs during TAA-induced liver fibrosis 187

5.6. Discussion 192

5.6.1. Summary 197

Chapter 6 Bio-distribution and persistence of human MSCs injected by tail-vein in mice with established liver fibrosis 199

6.1. Background and context 200
6.1.1. Cryoviz™ imaging of nanocrystal labelled MSCs 200
6.2. Aims of the chapter 202
6.3. Qdot® nanocrystal labelling of human UC MSCs 204
6.3.1. Labelling uptake efficacy 204
6.3.2. The effect of label uptake on cellular viability 205
6.4. Bio-distribution and persistence of Qdot® labelled UC MSCs 206
6.5. Discussion 212
6.5.1. MSC labelling efficiency is consistent 212
6.5.2. The pulmonary "first-pass" effect – Big round pegs don't fit through small square holes 213
6.5.3. Changing the bio-distribution of systemically injected MSCs 213
6.5.4. MSC homing to areas of injury 215
6.5.5. The fate of MSCs after systemic injection 216
6.5.6. Summary 217
Chapter 7 The effect of MSC conditioned media on LX2 cell biology 218
7.1. Background and context 219
7.2. Aims of the chapter 220
7.3. Characterising LX2 cells 221

7.4. The effect of MSC conditioned media on LX2 cell activation....230

7.5. The effect of MSC conditioned media on LX2 senescence, proliferation and viability....232

7.6. Discussion....235

7.6.1. Aligning the findings to the existing literature....235

7.6.2. *In vitro* models need to improve....239

7.6.3. Summary....242

Chapter 8 Conclusions and Discussion....243

8.1. Summary of findings....244

8.2. Strengths and limitations....245

8.3. Further experiments....248

8.4. Commentary on broader aspects of MSC research....249

8.5. Commentary on broader aspects of pre-clinical fibrosis research....251

Chapter 9 References....255

Table of Figures

Figure 1-1 A summary of major mechanisms and pathways that regulate liver fibrosis[45] 11

Figure 1-2 Mechanisms by which MSCs may reduce fibrosis[45] 31

Figure 2-1: Flow cytometry gating strategy for myeloid cell populations 64

Figure 3-1 Schematic of ideal fibrosis model for planned anti-fibrotic intervention 93

Figure 3-2: Schematic of IP CCl_4 chronic hepatic injury (low dose) and resolution 98

Figure 3-3: Mouse weight changes; IP CCl_4 chronic hepatic injury (low dose) 99

Figure 3-4: Staining of collagen deposition by PSR; IP CCl_4 chronic hepatic injury (low dose) and resolution 100

Figure 3-5: Quantitative analysis of collagen deposition; IP CCl4 chronic hepatic injury (low dose), and resolution 101

Figure 3-6: Schematic of IP CCl_4 chronic hepatic injury (high dose) and resolution 102

Figure 3-7: Mouse weight changes; IP CCl_4 chronic hepatic injury (high dose) 103

Figure 3-8: Staining of collagen deposition by PSR; IP CCl_4 chronic hepatic injury (high dose), and resolution 104

Figure 3-9: Quantitative analysis of collagen deposition; IP CCl_4 chronic hepatic injury (high dose), and resolution 105

Figure 3-10: Gross histopathological assessment of hepatic tissue by H&E staining; IP CCl_4 chronic hepatic injury (high dose), and resolution 106

Figure 3-11: Staining for activated myofibroblasts by αSMA; IP CCl_4 chronic hepatic injury (high dose), and resolution 107

Figure 3-12: Quantitative analysis of myofibroblast activation; IP CCl_4 chronic hepatic injury (high dose), and resolution 108
Figure 3-13: Gene expression analysis by qPCR of fibrosis-associated genes; IP CCl_4 chronic hepatic injury (high dose), and resolution 109
Figure 3-14: Assessment of inflammatory infiltrate by CD45 staining; IP CCl_4 chronic hepatic injury (high dose), and resolution 110
Figure 3-15: Quantitative analysis of inflammatory infiltrate by CD45 staining; IP CCl_4 chronic hepatic injury (high dose), and resolution 112
Figure 3-16: Serum ALT as a marker of hepatocyte injury; IP CCl_4 chronic hepatic injury (high dose), and resolution 112
Figure 3-17: IP TAA chronic hepatic injury feasibility experiment 113
Figure 3-18: Schematic of oral TAA chronic hepatic injury - feasibility experiment 115
Figure 3-19: Mouse weight changes; oral TAA chronic hepatic injury model – feasibility experiment 115
Figure 3-20: Gross histopathological assessment of hepatic tissue by H&E staining; oral TAA chronic hepatic injury - feasibility experiment 117
Figure 3-21: Assessment of inflammatory infiltrate by CD45 staining; oral TAA chronic hepatic injury - feasibility experiment 118
Figure 3-22: Quantitative analysis of inflammatory infiltrate by CD45 staining and hepatocyte injury by serum ALT measurements; oral TAA - feasibility experiment 119
Figure 3-23: Staining of collagen deposition by PSR; oral TAA chronic hepatic injury - feasibility experiment 119

Figure 3-24: Quantitative analysis of collagen deposition; oral TAA chronic hepatic injury - feasibility experiment 120
Figure 3-25: Staining for activated myofibroblasts by αSMA; oral TAA chronic hepatic injury - feasibility experiment 121
Figure 3-26: Gene expression analysis by qPCR of fibrosis-associated genes; oral TAA chronic hepatic injury - feasibility experiment 122
Figure 3-27: Schematic of oral TAA chronic hepatic injury model and resolution 123
Figure 3-28: Mouse weight changes; oral TAA chronic hepatic injury model and resolution 123
Figure 3-29: Staining of collagen deposition by PSR; oral TAA chronic hepatic injury model and resolution 124
Figure 3-30: Quantitative analysis of collagen deposition; oral TAA chronic hepatic injury model and resolution 125
Figure 3-31: Staining for activated myofibroblasts by αSMA; oral TAA chronic hepatic injury model and resolution 126
Figure 3-32: Quantitative analysis of myofibroblast activation; oral TAA chronic hepatic injury model and resolution 127
Figure 3-33: Gene expression analysis by qPCR of fibrosis-associated genes; oral TAA chronic hepatic injury model and resolution 128
Figure 3-34: Assessment of inflammatory infiltrate by CD45 staining; oral TAA chronic hepatic injury model and resolution 129
Figure 3-35: Quantitative analysis of inflammatory infiltrate by CD45 staining and hepatocyte injury by serum ALT measurements; oral TAA chronic hepatic injury model and resolution 130

Figure 4-1: Bright field image of human UCT-derived MSCs 145
Figure 4-2: Bright field images of human UCT-derived MSCs at different confluences 146
Figure 4-3: Tri-lineage differentiation of human UCT-derived MSCs 147
Figure 4-4: Flow-cytometric analysis of human UCT-derived MSCs by the expression of MSC-defining markers 149
Figure 4-5: Flow-cytometric analysis of syndecan-2 expression in human UCT-derived MSCs by their mode of selection and cellular confluence *in-vitro* 150
Figure 5-1: Schematic of experiment to explore the effect of MSC therapy on the resolution of established liver fibrosis using the IP CCl_4 chronic hepatic injury model: Experiment 1 159
Figure 5-2: Analysis of collagen deposition in Experiment 1 161
Figure 5-3: Analysis of myofibroblast activation in Experiment 1 162
Figure 5-4: Gene expression analysis by qPCR of fibrosis-associated genes in Experiment 1 163
Figure 5-5: Analysis of inflammatory infiltrate by CD45 staining and hepatocyte injury by serum ALT measurements and in Experiment 1 164
Figure 5-6: Flow cytometric analysis of myeloid cells from hepatic tissue and sera in Experiment 1 165
Figure 5-7: Schematic of experiment to explore the effect of MSC therapy on the resolution of established liver fibrosis using the oral TAA chronic hepatic injury model: Experiment 2 167
Figure 5-8: Analysis of collagen deposition in Experiment 2 168
Figure 5-9: Analysis of myofibroblast activation in Experiment 2 169
Figure 5-10: Gene expression analysis by qPCR of fibrosis-associated genes in Experiment 2 170

Figure 5-11: Analysis of inflammatory infiltrate by CD45 staining and hepatocyte injury by serum ALT measurements and in Experiment 2 171
Figure 5-12: Schematic of experiment to explore the effect of MSC therapy on the resolution of established liver fibrosis in the presence of on-going inflammation using the IP CCl_4 chronic hepatic injury model: Experiment 3 172
Figure 5-13: Analysis of collagen deposition in Experiment 3 173
Figure 5-14: Analysis of myofibroblast activation in Experiment 3 174
Figure 5-15: Gene expression analysis by qPCR of fibrosis-associated genes in Experiment 3 175
Figure 5-16: Analysis of inflammatory infiltrate by CD45 staining and hepatocyte injury by serum ALT measurements and in Experiment 3 176
Figure 5-17: Flow cytometric analysis of myeloid cells from hepatic tissue and sera in Experiment 3 177
Figure 5-18: Schematic of experiment to explore the effect of MSC therapy on fibrogenesis using the IP CCl_4 chronic hepatic injury model: Experiment 4 180
Figure 5-19: Analysis of collagen deposition in Experiment 4 181
Figure 5-20: Analysis of myofibroblast activation in Experiment 4 182
Figure 5-21: Gene expression analysis by qPCR of fibrosis-associated genes in Experiment 4 183
Figure 5-22: Analysis of inflammatory infiltrate by CD45 staining and hepatocyte injury by serum ALT measurements and in Experiment 4 184
Figure 5-23: Flow cytometric analysis of myeloid cells from hepatic tissue and sera in Experiment 4 185

Figure 5-24: Schematic of experiment to explore the effect of MSC therapy on fibrogenesis using the oral TAA chronic hepatic injury model: Experiment 5 187

Figure 5-25: Analysis of collagen deposition in Experiment 5 188

Figure 5-26: Analysis of myofibroblast activation in Experiment 5 189

Figure 5-27: Gene expression analysis by qPCR of fibrosis-associated genes in Experiment 5 ... 190

Figure 5-28: Analysis of inflammatory infiltrate by CD45 staining and hepatocyte injury by serum ALT measurements and in Experiment 5 191

Figure 6-1: Image acquisition using Cryoviz™ technology: localising MSCs 203

Figure 6-2: Flow cytometric analysis of Qdot® uptake by MSCs in culture 204

Figure 6-3: Cell viability of Q-dot®-labelled and unlabelled MSCs 205

Figure 6-4: Schematic of experiment to explore the bio-distribution tail-vein-injected MSCs in a model of liver fibrosis 206

Figure 6-5: 3-dimensional rendering of Cryoviz™ images to illustrate the distribution of MSCs in the injected CCl_4-injected mice at advancing time points after tail-vein injection 207

Figure 6-6: 3-dimensional rendering of Cryoviz™ images to illustrate the distribution of MSCs in the lungs, liver and spleen at advancing time points after tail-vein injection 208

Figure 6-7: Analysis of MSC numbers in the lungs, liver and spleen at advancing time points after tail-vein injection 210

Figure 6-8: Changes in relative proportions of detectable cells in the liver in lung with advancing time 211

Figure 7-1: Expression of intermediate filaments by LX2 cells in different culture media 222

Figure 7-2: mRNA expression of genes related to stellate cell activation in different culture media 224

Figure 7-3: Response of LX2 cells to PDGF-BB 225

Figure 7-4: Proliferation and senescence of LX2 cells in different culture media 226

Figure 7-5: Apoptosis of LX2 cells in different culture media 228

Figure 7-6: mRNA expression of genes related to stellate cell activation in MSC conditioned media 230

Figure 7-7: Expression of αSMA in LX2 cells in MSC conditioned media 231

Figure 7-8: LX2 cell senescence in MSC conditioned media 233

Figure 7-9: LX2 cell proliferation and viability in MSC conditioned media 234

Table of Tables

Table 1-1: Clinical studies investigating the effect of MSC therapy in chronic liver disease[45] 14

Table 1-2: Effect of adoptively transferred MSCs in animal models[45] 19

Table 1-3: Animal model studies investigating the role of BM-derived cells in fibrogenesis[45] 37

Table 2-1: Antibody set up for MSC characterisation flow cytometry 49

Table 2-2: Primary antibody mixture for myeloid panel 63

Table 2-3: Antibodies for immunohistochemistry 71

Table 2-4: Antibodies for immunocytochemistry 80

Table 2-5: Probes for qPCR 89

Table 3-1: Summary comparison of fibrosis at peak and after recovery in the IP CCl_4 and oral TAA model 133

Table 3-2: Sample size calculations for intervention experiment based on time course experiments in both models 136

Table 5-1: Application of standardised guidelines to improve reliability of outputs from animal experimentation to explore liver fibrosis 192

Abbreviations

ACLF	acute-on-chronic liver failure
AIH	autoimmune hepatitis
APC	allophycocyanin
ARLD	alcohol-related liver disease
ALT	alanine transaminase
AST	aspartate aminotransferase
AT	adipose tissue
Ath-HFD	atherogenic high-fat diet
BDL	bile duct ligation
BLD	bi-lineage differentiation
BM	bone marrow
BMSU	Biomedical Services Unit
BMT	bone marrow transplant
BSA	bovine serum albumin
CCl4	carbon tetrachloride
CI	confidence interval
CM	conditioned medium
CPA	collagen proportionate area
Ct	cycling threshold
Dlk	delta-like
DMN	dimethylnitrosamine

DBA	dilute brown non-agouti
DDC	3,5-diethoxycarbonyl-1,4-dihydrocollidine
DMEM	Dulbecco's Minimum Essential Media
DMSO	dimethylsulfoxide
ECM	extracellular matrix
EDTA	ethylenediaminetetraacetic acid
EGFP	enhanced green fluorescent protein
FACS	fluorescence-activated cell sorting / flow cytometry
FBS	foetal bovine serum
FCS	foetal calf serum
18F-FDG	18F-fluorodeoxyglucose
FGF	fibroblast growth factor
(F)ISH	fluorescent in situ hybridisation
FFPE	formalin-fixed paraffin embedded
FGF	fibroblast growth factor
GFP	green fluorescent protein
GFAP	glial fibrillary acidic protein
GvHD	graft versus host disease
HBV	hepatitis-B virus
HCV	hepatitis-C virus
HFD	high fat diet
HGF	hepatocyte growth factor

HSC	hepatic stellate cells
ICC	immunocytochemistry
ICR	Institute for Cancer Research
IGF	insulin-like growth factor
IGFBP	insulin-like growth factor binding protein
IHC	immunohistochemistry
IFN	interferon
IL	interleukin
IP	intra-peritoneal
ISCT	International Society of Cellular Therapy
LUC	luciferase
MACS	magnetic-activated cellular sorting
MCP	monocyte chemotactic protein
MF	myofibroblast
MHC	major histocompatibility complex
MLD	multi-lineage differentiation
MMP	matrix metalloproteinases
MSC	mesenchymal stromal cell
NACWO	named animal care and welfare officer
NASH	non-alcoholic steatohepatitis
NK	natural killer
NOD	non-obese diabetic

NSG	NOD/SCID/IL-2R γ -null
OTL	Orbsen Therapeutics Limited
OD	once a day
OG	oral gavage
PA	plastic adherent
PBC	primary biliary cholangitis
PBS(-T)	phosphate buffered saline (with tween)
PDGF	platelet-derived growth factor
PET	positron emission tomography
PPAR	peroxisome proliferator activated receptor
PSR	picrosirius red
(rt-)PCR	real time polymerase chain reaction
SA- β -gal	senescence-associated expression of β -galactosidase
S1P	sphingosine-1-phosphate
S2	syndecan 2 (CD362)
SC	subcutaneous
SCID	severe combined immunodeficiency
siRNA	small interfering ribonucleic acid
SMc	Schistosoma Mansoni cercaria
TAA	thioacetamide
TBS(-T)	tris-buffered saline (with tween)
TGF β	transforming growth factor beta

TIMP	tissue inhibitor of metalloproteinases
TLD	tri-lineage differentiation
TRAIL	tumour necrosis factor-related apoptosis-inducing ligand
TNF	tumour necrosis factor
UCT	umbilical cord tissue
UDCA	ursodeoxycholic acid
UK	United Kingdom
USA	United States of America
WB	whole body
WT	wild type
α MEM	Minimal Essential Media- alpha
α SMA	alpha smooth muscle actin

Chapter 1

Introduction

1.1. The clinical imperative for an anti-fibrotic agent

Liver disease is the third commonest cause of premature death in the United Kingdom (UK), with 62,000 years of potential working life lost every year[1]. The HEPAHEALTH project – established to describe the epidemiology of liver disease and their risk factors in European countries - estimates the prevalence of cirrhosis (advanced liver scarring) to be approximately 600 per 100,000 population in the UK – equating to approximately 0.6% of the population[2]. Of those with cirrhosis, approximately 1 in 10 will get hepatocellular carcinoma. Alcohol and obesity are the two primary causes of liver disease, and the combined costs of these two entirely preventable drivers of disease to the UK National Health Service is almost £10 billion per year[1].

These numbers only give a snapshot of the current state of affairs. Of greater concern are the adverse trends. There has been a fivefold increase of cirrhosis in people between the ages of 35 and 55 over the past 10 years[3]. Mortality from liver disease has increased fourfold since 1970, and fivefold in those of working-age[4]. Rates of premature deaths continue to increase, with those living in the most deprived areas being considerably more vulnerable and being twice as more likely to die prematurely from liver disease[5].

The systematic under-prioritisation of liver disease in health policies was epitomized by the absence of a National Liver Strategy and emphasized in a striking summary statement in the 2012 Chief Medical Officer's Annual Report whereby liver disease was recognised as "the only major cause of mortality and morbidity which is on the increase in England"[6]. It was highlighted as one of the three key issues for population health, and reassuringly, since this report, there has been a

greater impetus to tackle "tomorrow's catastrophe"[7]. The 2014 All-Party Parliamentary Hepatology Group Inquiry into Improving Outcomes in Liver Disease made 20 key recommendations centering on themes of early recognition and prevention. *The Lancet* commissioned a blueprint to address liver disease in the UK, which it described as "the glaring exception to the vast improvements made during the past 30 years in health and life expectancy for chronic disorders".[1] Four Lancet Commission reports have now been published, which not only outline the evidence base for action, but set out priorities[1,3,8,9]. Moreover, the National Institute for Health and Clinical Excellence, the British Association for the Study of the Liver, the British Society of Gastroenterology and the Royal Colleges of Physicians and General Practitioners have published several clinical practice guidelines for afflictions of the liver.

90% of liver disease is preventable[10]. Thus, it is entirely appropriate that the focus of the multi-faceted efforts have been on public health measures and strategies directed at early detection and prevention[3]. These measures will undoubtedly dampen the risk and scale of "tomorrow's catastrophe", but we still face the legacy of "today's complacency"[7]. This is not just the case in the UK where 600,000 people have some sort of liver disease, accounting for over 60,000 hospital admissions and 11,000 deaths per year. The estimated 5-10% of the world population with established chronic liver disease are at risk of cancer, morbidity and premature death[11]. Global burden of disease estimates suggest that 3.5% of all deaths worldwide are attributable to cirrhosis or liver cancer – an increase of 0.5% since 2000[12]. Effective measures to address viral hepatitis have unmasked the burdens of alcohol-related liver disease (ARLD)[13] and non-alcoholic steatohepatitis (NASH)[14] - lifestyle diseases in areas of the world where the infrastructure to deliver widespread

screening and behavioural change may be considerably limited. Thus, today's successes in health policies should not seed complacency in the fight to tackle an evolving problem.

Nobel laureates Burnet and Medawar's work on immune tolerance paved the way for organ transplantation in the 1960s[15,16]. Tom Starzl, Roy Calne and colleagues took brave, innovative and field-changing steps to introduce and subsequently refine procedures in liver transplantation[17,18]. 50 years later, it remains the mainstay of treatment for those with end-stage liver disease, with most recipients living for over 10 years after a transplant.

The successes of public health and preventative measures and improvements in transplantation techniques, technologies and peri-operative care have been the highlights of the past 50 years of endeavour. The relative scarcity of donor organs and limitations of transplantation service infrastructure remain steep barriers to a wider availability of transplantation to all in need and has resulted in an increase of liver transplant waiting list mortality in North America and Europe to almost 20%[19]. Moreover, over 30 years of research have heralded a greater understanding of the pathways of fibrosis, cirrhosis and resolution without yielding a clinically available anti-fibrotic agent that can resolve established fibrosis to augment the natural capacity of the liver to regenerate[20]. This is not an isolated failing of those investigating liver disease. Common and unique mechanisms are known to regulate fibrosis in various chronic fibroproliferative disease that are thought to account for nearly 45% of all deaths in the developed world; yet, despite this enormous impact, there are currently no approved treatments that directly target mechanisms of

fibrosis in any disease setting[21]. A safe and effective therapy to tackle dysfunctional fibrosis and cirrhosis remains the holy grail of Hepatology.

Liver fibrosis is a dynamic, bi-directional process. The progression of fibrosis can be halted and advanced fibrosis and cirrhosis can be reversed in both animal models and in real-world clinical practice if the primary disease aetiology can be eliminated or suppressed. Historically this has been most evident as a consequence of effective antiviral therapy against hepatitis B[22–24] and C[25], iron depletion in patients with haemochromatosis[26], and immunosuppression in those with autoimmune hepatitis[27,28]. Lifestyle interventions can interrupt disease progression and promote fibrosis resolution in NASH[29] and ARLD[30]. However, certain phenotypes of cirrhosis, or advanced fibrosis may not regress spontaneously[31–33]. Patients are consequently subject to the risk of liver failure, hepatocellular carcinoma and death – it is for these patients that an anti-fibrotic agent may be most impactful.

Autologous cell therapies have been explored in the treatment of liver fibrosis, with haematopoietic stem cells and macrophages showing potential promise[34,35]. Modest evidence of efficacy alongside practical and cost constraints with autologous cells have resulted in the consideration of allogeneic approaches, in particular mesenchymal stromal cells (MSCs). They have been demonstrated to home to areas of inflammation[36–38], reduce inflammatory damage[39] and oxidative stress[40,41], and even contribute to differentiated epithelium[42]. These findings have led to many clinical trials using MSCs to modulate the body's response to injury in different organs including the liver[43]. Alongside the anti-inflammatory action of MSCs, there are suggestions they

may be able to exert direct anti-fibrotic effects, although enthusiasm for their use in patients with liver fibrosis has been tempered by concerns about a possible pro-fibrotic role of endogenous MSCs in response to injury.

The overarching aim of my PhD was to investigate the therapeutic potential of MSCs to treat liver fibrosis. This introductory section will summarise the current evidence base and highlight the remaining controversies and unanswered questions in the field, and thereby provide context for the body of work that follows.

1.2. Mechanisms of fibrogenesis and resolution in liver disease

Fibrosis is a wound healing response to chronic injury characterised by the accumulation of extracellular matrix (ECM) or "scar" tissue[44]. The primary mediators of fibrogenesis and the composition of scar are generally conserved across different types of injury. ECM replaces damaged regions of tissue; a process that ultimately leads to cirrhosis whereby normal hepatic architecture is replaced by a nodular structure of functional regenerative hepatocytes encapsulated by fibrous septa[45]. An associated increase in vascular tone, maladaptive micro- and macro-circulatory changes and hepatocellular dysfunction results in the clinical sequelae of portal hypertension, liver failure and increased risk of hepatocellular carcinoma. A simplified depiction of the complex interplay of fibrogenic and resolution pathways is shown in figure 1.1.

The liver's response to tissue injury is multifaceted, and the component parts, which mediate both fibrosis and its resolution, are interlinked in an exquisitely complex way. The initial consequence of injury is almost invariably hepatocyte death or activation, which drives inflammatory and fibrogenic pathways in infiltrating and non-parenchymal cells[46]. This includes activating hepatic stellate cells (HSCs) - the principal precursor population for myofibroblasts.

Myofibroblasts are the primary effector cells and the major source of ECM (including fibril-forming collagens (I, III, V), glycoproteins (e.g. laminin, fibronectin)) during liver fibrogenesis. Following liver injury HSCs undergo trans-differentiation to become matrix-secreting myofibroblasts[45,47,48]. They shed their vitamin A stores, up-regulate expression of markers such as myosin and alpha-smooth muscle actin (αSMA), transdifferentiate and proliferate in response to locally increased

cytokines such as platelet-derived growth factor (PDGF) and transforming growth factor-beta (TGF β 1)[49]. Myofibroblasts also secrete tissue inhibitors of metalloproteinases (TIMP), which act to block ECM degradation by matrix metalloproteinases (MMP), thus supporting ECM persistence. With time and fibrotic density, myofibroblasts gain a progressive resistance to death or inactivation which is thought to contribute to resistance to regression[50]. Further to their scar-production and maintenance, the pro-fibrotic myofibroblast acquires proliferative, migratory, immunomodulatory, phagocytic and contractile properties, that directly contribute to sinusoidal tone and portal hypertension. In resolution, myofibroblasts either die by apoptosis, or undergo a change to a non-fibrogenic phenotype – inactivation or senescence, whereby they do not secrete ECM or TIMP[45,48]. Fate-tracing experiments using Cre-loxP-based labelling to mark the fate of collagen type-I expressing myofibroblasts in a murine model of hepatic injury (carbon tetrachloride (CCl_4)) demonstrated that the majority of the remaining HSCs in resolution (1 month after injury) were inactivated myofibroblasts[51].

Macrophages derived from circulating monocytes are equally critical to the biology of tissue injury, with different subpopulations playing functionally distinct roles[45]. However, the traditional classification based upon their mode of activation (M1 and M2 macrophages), does not fully reflect the range of distinct sub-populations involved in fibrogenesis and resolution[52,53]. Though less well characterised in humans, rodent studies have shown that the expression of Ly-6C and Gr1 on macrophages better describes their role in fibrosis[45]. Macrophages with a high expression of Ly-6C or Gr1 are pro-fibrogenic[54,55] and are the dominant source of TGF β, PDGF and insulin-like growth factor-1 (IGF1), which serves to activate HSCs, as well as providing an NF-κB-

mediated survival signal to myofibroblasts[56]. They also recruit other circulating inflammatory cells by their secretion of chemokines, cytokines and growth factors[57]. Conversely, macrophages with low expression of Ly-6C[55,58,59] describe a terminally differentiated, collagenase-secreting, phagocytic "restorative" macrophage responsible for the resolution of fibrosis[35]. They produce MMPs which directly break down ECM[31,60], and promote HSC apoptosis via caspase-9 and a tumour necrosis factor-related apoptosis-inducing ligand (TRAIL) dependent mechanism. Their effects are augmented by the recruitment of phagocytic neutrophils[35] and natural killer (NK) cells[61]. This duality of macrophage function has been demonstrated in a range of murine models of fibrosis including CCl_4, dimethylnitrosamine (DMN), and thioacetamide (TAA))[52,62,63], whereby macrophage depletion during chronic injury abrogates fibrogenesis, and macrophage depletion post-cessation of chronic injury abolishes the resolution of fibrosis[52].

Matrix is continually turned over during the liver's response to injury, and there is an increased expression of MMPs and collagenases even in the fibrotic liver[45,64]. However, ECM accumulates in fibrogenesis owing to the activity of high levels of TIMP (especially myofibroblast-derived TIMP-1), which inhibits the activity of MMPs[45]. TIMPs also provide an autocrine anti-apoptotic stimulus for myofibroblasts[33]. A reduction in functional TIMP in resolution allows the unopposed action of MMPs to degrade scar tissue[65], and promote myofibroblast apoptosis[66]. The most potent collagenase is MMP-1 in humans and Mmp-13 in rodents, both of which are predominantly secreted by macrophages[45].

The reversibility of fibrosis remains a matter of debate, and the concept and its definition is likely to change with advancing knowledge and understanding. Dense and longstanding fibrosis or cirrhosis is marked by thick bands of ECM with extensive cross-linking[67,68] and elastin[60] on a pauci-cellular scaffold[33] with decreased MMP activity. Myofibroblasts adopt a resistance to apoptosis with scar maturation[50].

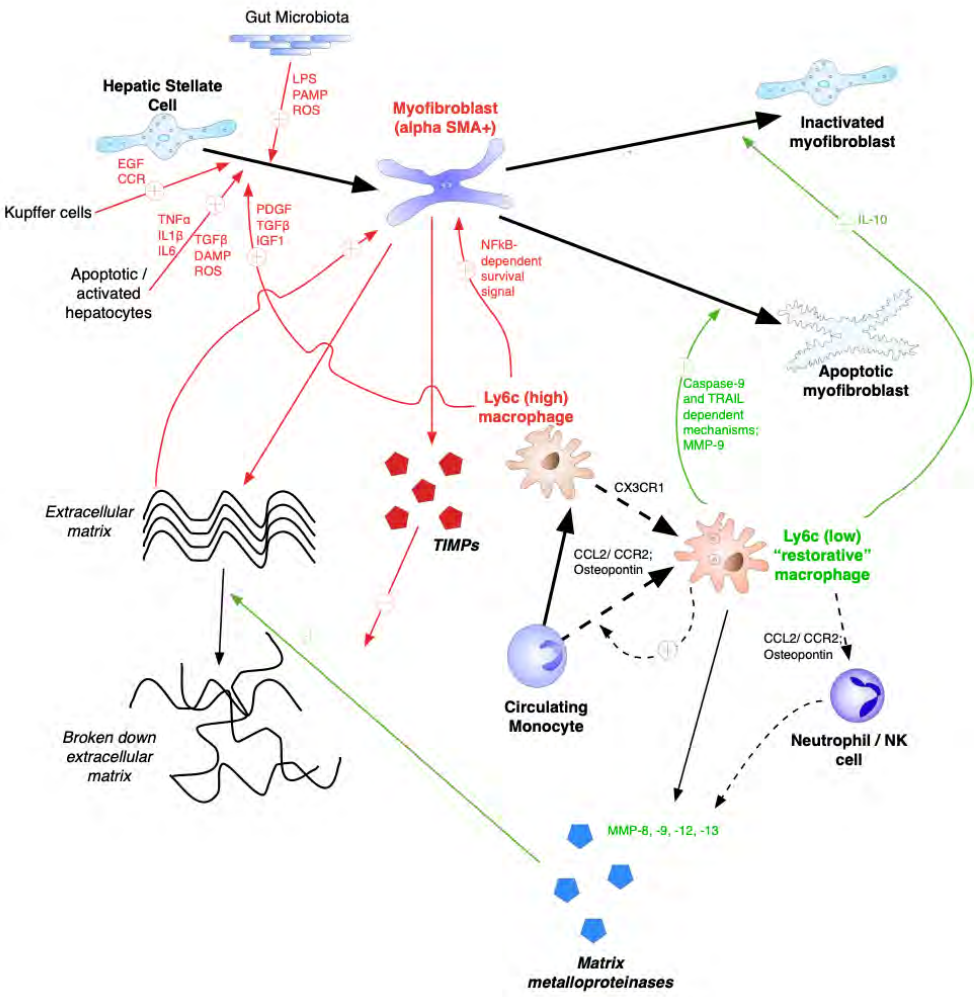

Figure 1-1 A summary of major mechanisms and pathways that regulate liver fibrosis[45]

Adapted from Haldar *et al.*[45]

Fibrosis pathways are in red, and resolution pathways are in green. Fibrogenesis: myofibroblasts are activated and stimulated by a number of different stimuli. They produce ECM and TIMPs, which inhibit MMPs. Ly6c^{hi} macrophages are recruited and secrete pro-fibrotic cytokines, in turn recruiting other inflammatory cells, and augmenting myofibroblast survival. Resolution: myofibroblasts undergo inactivation, senescence or apoptosis. Ly6c^{lo} restorative macrophages stimulate apoptosis and inactivation of myofibroblasts, secrete MMPs and recruit other mediators of resolution including neutrophils and NK cells. TIMP levels decline, which allows unopposed ECM degradation by MMPs. DAMP, damage associated molecular patterns; EGF, epidermal growth factor; IL, interleukin; PAMP, pathogen associated molecular patterns; PDGF, platelet-derived growth factor; ROS, reactive oxygen species; TGF, transforming growth factor; TNF, tumour necrosis factor; TRAIL, TNF-related apoptosis-inducing ligand.

1.3. Potential targets for therapy in fibrosis pathways

Myofibroblasts and ECM are the primary targets of any putative anti-fibrotic therapeutic agents. However, the complex interplay with other cells in the microenvironment governs fibrogenic activation or regression. Our current understanding is distilled to the existence of two multicellular functional units – one centred around perisinusoidal pericytes (HSCs) that is likely to be dominant and the other around portal myofibroblasts[69,70], though some investigators have also described intermediary myofibroblasts with distinct morphology and functional microenvironment[71]. There are nuanced differences in the nature of myofibroblast precursors from different sites[72], though in advanced fibrotic disease the boundaries between the functional units overlap as dense septa form cirrhotic nodules.

Fibrogenic and resolution pathways are complex. A putative anti-fibrotic agent could interfere at a crucial bottleneck of the fibrogenic pathway, simultaneously interfere with discrete pathways or enhance the resolution phase[45]. Moreover, any anti-fibrotic effect must be appropriate to requirements and reset homeostasis to a non-injured, non-fibrotic set point.

Therapies that target myofibroblasts or ECM are labelled direct anti-fibrotic agents, whereas those that target other aspects of the fibrosis or resolution pathways are indirect agents[73]. A vast catalogue of agents have been trialled pre-clinically, but only a few have made it to phase 2 clinical trials or beyond and are the subject of an excellent recent review[74] – yet as stated, none have come into clinical use.

1.4. Mesenchymal stromal cells – a therapeutic option?

MSC are stromal cell progenitors with the ability to differentiate down mesodermal cell lineages[66], and have wide-ranging immuno-modulatory properties[45]. The current concept of MSCs can be traced to classical experiments by Friedenstein and colleagues in the 1960s and 1970s who demonstrated the osteogenic potential of a subset of bone marrow (BM) derived cells by heterotopic transplantation[75]. They are now thought to reside in perivascular niches/matrices within tissue[76], and can be isolated for use from almost every postnatal connective tissue including adipose tissue (AT)[77], umbilical cord (UCT)[78], dental pulp[79], synovium[80] and many others. Their three defining properties, as decreed by the International Society of Cellular Therapy (ISCT)[81,82], are: (i) the ability to adhere to plastic, (ii) a characteristic immunophenotype with expression of CD73, CD 90 and CD105, and lack of expression of class-II major histocompatibility complex (MHC) and CD14, CD34 and CD45, (iii) and ability to readily differentiate to form multiple skeletal tissues (bone, cartilage, adipose tissue).

Early therapeutic interest in MSC revolved around their capacity for multi-lineage differentiation including reported epithelial and endodermal differentiation[83], although the current focus relates to their immunomodulatory effects[45]. MSC have been found to modify the activity of both the innate[84] and adaptive immune system[85–87], and can also exert other cytoprotective[40], pro-angiogenic[88] and anti-fibrotic[89] effects.

Table 1-1: Clinical studies investigating the effect of MSC therapy in chronic liver disease[45]

Primary author; year	Type of Study	Cell Therapy	Dose/Route	Disease aetiology	Number of patients	Follow up	Main Results
Mohamadnejad[90]; 2007	Uncontrolled trial	Autologous BM-MSC; 10 - 60x10^6	Single dose / peripheral vein	Cryptogenic; AIH	4	12 months	↓ MELD* in 50% of patients; ↑ QoL
Kharaziha[91]; 2009	Uncontrolled trial	Autologous BM-MSC; 3-5x10^7	Single dose / portal vein	HBV; HCV; ARLD; Cryptogenic	8	24 weeks	↓ MELD
Amer[92]; 2011	Controlled trial	Autologous BM-MSC; 2x10^7 – 2x10^8	Single Dose / intrahepatic, intrasplenic	HCV	10 intrahepatic; 10 splenic; 20 controls	6 months	↓MELD; ↓ oedema
Peng[93]; 2011	Controlled trial	Autologous BM-MSC; 3.4x10^8	Single dose / hepatic artery	HBV	53 treatment 105 controls	192 weeks	↓ MELD
Shi[94]; 2012	Controlled trial	Allogeneic UCT-MSC; 0.5x10^6/kg bw	Multiple doses / peripheral vein	ACLF (HBV background)	43 treatment 24 controls	72 weeks	↓ MELD; Improved PT, bilirubin, albumin
El-Ansary[95]; 2012	Controlled trial	Autologous BM-MSC; 1x10^6/kg bw	Single dose / peripheral vein	HCV	15 treatment 10 controls	6 months	↓ MELD
Zhang[96]; 2012	Randomised controlled trial	Allogeneic UCT-MSC; 0.5x10^6/kg bw	Multiple doses / peripheral vein	HBV	30 treatment 15 controls	48 weeks	↓ MELD-Na
Mohamadnejad[97]; 2013	Randomised controlled trial	Autologous BM-MSC; 1.2 – 2.9x10^8	Single dose / peripheral vein	CC; PBC; HBV; HCV; AIH	14 treatment 11 controls	12 months	No difference between groups
Salama[98]; 2014	Controlled trial	Autologous BM-MSC; 0.5x10^8	Single dose / peripheral vein	HCV	20	6 months	↓ MELD; Improved PT, bilirubin, albumin
Wang[99]; 2014	Uncontrolled trial	Allogeneic UC-MSC; 0.5x10^6/kg bw	Multiple doses / peripheral vein	UDCA-refractory PBC	7	12 months	↓ ALP, ↑ QoL; No change in MELD
Suk[100]; 2016	Randomised controlled trial	Autologous BM-MSC; 5x10^7	One or two doses / hepatic artery	Abstinent (6 months) ARLD	19 (2 doses) & 18 (1 dose) treatment; 18 control	12 months	↓ fibrosis; ↓ CPS
Lin[101]; 2017	Randomised controlled trial	Allogeneic BM-MSC; 1-10x10^5	Multiple (4) doses / peripheral vein	ACLF (HBV background)	56 treatment; 54 controls	24 weeks	↑ survival, ↓infection; ↓MELD
Liang[102]; 2017	Uncontrolled trial	Allogeneic; UCT- or cord blood or BM; 1x10^6	Single dose / peripheral vein	PBC, systemic autoimmune dis.	23 UCT-MSC, 2 cord blood-MSC, 1 BM-MSC	2 years	↑ albumin; no change in MELD

Adapted from Haldar *et al.*[45]

*Model for end-stage liver disease (MELD) is a composite measure for the extent of liver disease. MELD-Na is a variant thereof. Higher scores equate to more advanced disease. ACLF, acute-on-chronic liver failure; AIH, autoimmune hepatitis; ARLD, alcohol-related liver disease; ALP, alkaline phosphatase; BM, bone marrow; bw, body weight; CC, cryptogenic; CPS, Child-Pugh score; HBV, hepatitis B virus; HCV, hepatitis C virus; MSC, mesenchymal stromal cells; PBC, primary biliary cholangitis; QoL, quality of life; UCT, umbilical cord tissue; UDCA, ursodeoxycholic acid.

The highlight of translational MSC-therapy research has been the successful application to treat patients with steroid-refractory severe graft-versus-heart-disease (GvHD). In May 2012, the United States of America (USA)-based biotech Osiris received market approval in Canada and New Zealand for their proprietary plastic adherent (PA)-MSC formulation (*Prochymal™*) to treat specific cases of GvHD – representing the world's first market approved allogeneic ("off-the-shelf") stem cell medicine. Furthermore, MSC therapy has been shown to be safe and effective in the treatment of patients with systemic lupus erythematosus and fistulising bowel disease (Crohn's disease)[103]. This work has culminated in TiGenix™ (Euronex Brussels) acquiring Food and Drug Association approval in the USA through Special Protocol Assessment for use of their proprietary platform of allogeneic AT-MSC (Cx601) in a phase III randomised, double blinded, parallel group, placebo-controlled multicentre study to treat complex perianal fistulas in Crohn's disease patients[104]. Other phase I and II trials are underway in different disease settings.

There have been a number of published MSC trials investigating the therapeutic effect of plastic-adherent MSC in patients with liver cirrhosis (Table 1.1), with many more on going[45]. The majority of these studies recruited patients with advanced cirrhotic disease, in whom MSC therapy was deemed safe. Though the majority of these studies suggested a clinical benefit too, only four randomised controlled trials have been reported to date, with three demonstrating a favourable clinical effect. Despite these findings, the scientific community still has significant concerns about the efficacy and safety of their use in patients with liver fibrosis. One major cause for apprehension is borne out of pre-clinical studies reporting MSC may be inherently fibrogenic, making their use to treat fibrosis seemingly illogical[45].

In the following sections, the pre-clinical evidence supporting MSC therapy for liver fibrosis will be critically appraised to provide a balanced exploration of the evidence surrounding their role in liver fibrosis.

1.5. Do mesenchymal stromal cells prevent fibrosis, rather than promote its resolution?

There is an increasing body of work supporting the anti-fibrotic effects of adoptively transferred MSC in rodent models of liver fibrosis (Table 1.2), however, the timing of therapy may be a critical consideration as the effect on fibrosis may be mediated through a reduction in inflammation rather than promoting its degradation directly[45].

Notably, the majority of rodent studies have infused MSC during on-going injury and provided evidence to suggest that MSC reduce inflammation and subsequently fibrosis. Tsai *et al* injected $5x10^5$ human UCT-MSC into the sub-hepatic capsule of CCl_4-injured rats[78] four weeks after the onset of injury (twice per week CCl_4 by oral gavage), with the injury continuing for a further 4 weeks until the rats were sacrificed. MSC reduced metabolic activity in the injured liver to pre-injury levels, as detected by MicroPET (positron emission tomography) after ^{18}F-FDG injection; this was crudely used as a surrogate for inflammation – an assumption that has its limitations[105]. The presumed reduction in inflammation translated to a dramatic reduction in fibrosis compared to those injured for 8 weeks without MSC treatment. Morphometric analysis of collagen-proportionate area (CPA) (picrosirius red (PSR) staining: 0.07 ± 0.02% vs. 9.56 ± 2.03%; $p<0.05$) suggested fibrosis was reduced to uninjured levels, and this was supported by a 66% relative reduction of TGFβ protein expression in the MSC treated group. Similarly, Seki *et al* established that injection of MSC whilst injury is on-going can affect both inflammation and fibrosis[77]. They injected $1x10^5$ green-fluorescent protein (GFP)-labelled murine AT derived stromal cells every two

weeks in a NASH model of fibrosis (34 weeks of atherogenic high-fat diet) and demonstrated a 50% reduction in fibrosis by morphometric analysis ($p<0.05$), allied with fewer detectable αSMA+ myofibroblasts ($p<0.001$). They interrogated the hepatic inflammatory infiltrate by immunohistochemistry (IHC) and flow cytometry to show that MSC led to a significant decrease in the number of cells of myeloid (CD11b+) origin and granulocyte/antigen presenting cells (Gr1+) in the liver, whilst increasing CD4+ T-cell numbers. Ezquer *et al* also observed injection of syngeneic BM-MSC into mice 33 weeks into 50 weeks of high-fat diet (HFD) prevented development of fibrosis[106]. MSC-treated mice did not develop fibrosis, whereas the untreated mice did, although both groups of mice did developed obesity, insulin resistance and hepatic steatosis. Gene expression for both *Col-1* and *Tgf-β1* were significantly reduced with treatment ($p<0.01$), though there was no significant change in the hepatic expression of *αSMA*. The decreased fibrosis was allied to attenuated levels of inflammatory cytokines (*IL-1ß*, *IFN-γ*, and *TNF-α*), though only the expression of *TNF-α* was significantly reduced ($p<0.05$)

Table 1-2: Effect of adoptively transferred MSCs in animal models[45]

Primary Author; Year	MSC treatment			Injury model	Output: Significant effects on fibrosis
	Source of MSC; ***Route of delivery***	**Dose (cells)**	**Timing of treatment**		
Oyagi 2006	Rat; BM; HGF-primed *Tail vein*	$3x10^6$	At onset of injury	Fisher 344 rats; chronic IP CCl_4	• HGF-primed MSC led to ↓ in fibrosis; un-primed MSC did not
Fang 2004	Mouse; BM *Tail Vein*	$1x10^6$	At onset of injury, or 1 wk after injury start	Mice; chronic OG CCl_4	• MSC delivered at onset of injury led to a ↓ in fibrosis; later delivery did not.
Seki 2013	Mouse ; AT *Splenic capsule / portal vein*	**Split** $1x10^5$ 17 doses	Twice every 2wks	C57Bl/6 mice; chronic Ath + HFD	• MSC treatment led to ↓ in fibrosis and changes in profile of hepatic inflammatory cell infiltrate.
Hong 2014	Human; UCT *Tail vein*	**Varied** $1x10^6$; $3x10^6$; $6x10^6$	During injury	Sprague Dawley rats; chronic DEN in water	• Comparison of effects of MSC therapy at varied doses given during injury: ↑ doses led to greater ↓ in fibrosis. • Splitting the dose trended to deliver a greater ↓ in fibrosis against the single equivalent dose.
		Split $1x10^6$; 3 doses or $1x10^6$; 6 doses	Split doses were given every 3 days		
Tsai 2009	Human; UCT *Sub-hepatic*	$5x10^5$	4wks after onset of injury	Sprague Dawley rats; chronic OG CCl_4	• MSC led to ↓ in fibrosis, and a ↓ in metabolic activity.
Rabani 2010	Mouse; BM *Tail vein*	$1x10^6$	4wks after onset of injury	NMRI mice; chronic IP CCl_4	• MSC led to ↓ in fibrosis.
Kamada 2009	Mouse; AT FGF-primed *Intra-splenic*	$1x10^5$	4wks after onset of injury	C57Bl/6 mice; chronic IP CCl_4	• FGF-unprimed MSC led to ↑ fibrosis; FGF-primed MSC led to a ↓in fibrosis.
M'ounesi 2013	Human; BM *Tail vein*	$3x10^6$	4wks after onset of injury	NMRI mice; chronic IP CCl_4	• Comparison of effects of MSC therapy delivered as single dose, or split dose: single dose did not ↓ fibrosis; split dosing did.
		Split $1x10^6$; 3 doses	At weeks 4,5,6 of injury		
Li 2013	Human; UCT *Intrahepatic*	Exosomes	6wks after onset of injury	Kunmingbai mice; chronic IP CCl_4	• MSC exosome used as therapy: led to a ↓ in fibrosis.
Meier 2015	Human; UCT *IP*	$1.5x10^6$	During (unclear exactly when)	DBA-1 mice; BDL or chronic SC CCl_4	• MSC ↓ fibrosis in both the BDL and CCl_4 models.
Jang 2014	Human; UCT *Intrahepatic*	**Split** $2x10^6$; 2 doses	At wk 6 and 8 of injury	Sprague Dawley rats; chronic IP TAA	• MSC led to ↓ in fibrosis.
Baligar 2016	Mouse; AT *Intra-splenic*	$0.25x10^6$	8wks after onset of injury	C57Bl/6 mice; chronic IP CCl_4	• MSC led to ↓ in fibrosis.
Abdel-Aziz 2012	Mouse; BM *Tail vein*	No information available	8wks after Schistosoma injection	Balb/C mice; single SMc injection	• MSC led to ↓ in fibrosis.

Ezquer 2011	Mouse; BM *Tail vein*	**Split** $0.5x10^6$; 2 doses	At 33 and 37wks of HF diet	C57Bl/6 mice; chronic HFD	• MSC treatment prevented the establishment of fibrosis, no effect on obesity, insulin resistance or hepatic steatosis.
Chen 2014	Mouse BM *Tail vein*	**Split** $0.5x10^6$; 2 doses	Day 60 and 61 of injury	C57Bl/6 mice; chronic IP CCl_4	• MSC led to ↓ in fibrosis. ; associated with changes of hepatic cytokine and inflammatory cell infiltrate profiles. • All MSC-related effects negated if mice were pre-treated with dexamethasone prior to MSC delivery.
Q'tanilha 2014	Canine BM *Tail vein*	**Split** $2x10^6$; 4 doses	At wk10, 11, 12, 13 of injury	NOD/ SCID mice; chronic IP TAA	• MSC led to r↓ in fibrosis with better redox homeostasis.
Raafat 2015	Rat BM Tail vein	$3x10^6$	At cessation of injury	Albino rats; chronic SC CCl_4	• MSC led to ↓ in fibrosis.
Zhao 2005	Rat; BM *Tail vein*	$3x10^6$	At cessation of injury	Wistar rats; chronic IP CCl_4	• ↓ in fibrosis when MSC given at cessation of CCl_4 injury.
			Day 10, or day 20 of injury	chronic IP DMN	• ↓ in fibrosis was more marked when MSC were delivered early during injury compared to later.
Jung 2009	Human; UCT *Tail vein*	$1x10^6$	At cessation of injury (details unclear	Sprague Dawley rats; chronic IP CCl_4	• MSC led to ↓ in fibrosis.
Carvalho 2008	Rats BM *Portal vein*	$1x10^7$	At cessation of injury (details unclear)	Wistar rats; chronic IP CCl_4 & simultaneous alcohol liquid diet	• MSC <u>did not</u> ↓ fibrosis.
M'heimer 2011	Rats; BM (cirrhotic) *Portal vein*	$1.6x10^7$			• MSC did not affect injury-related changes in portal vein diameter.
Motawi 2014	Rat; BM *Tail vein*	$3x10^6$	1 day after final injury	Wistar rats; chronic IP CCl_4	• MSC led to ↓ in fibrosis.
Briquet 2014	Human; BM, UCT, Liver *Tail vein*	$0.5x10^6$	2 days after final injury	NSG mice; chronic IP CCl_4	• MSC <u>did not</u> ↓ fibrosis.
Chang 2009	Human; BM *Portal vein*	$1x10^6$	3.5 days after final injury	Wistar rats; chronic SC CCl_4	• MSC led to ↓ in fibrosis.

Adapted from Haldar *et al.*[45]

Ath+HFD, atherogenic + high fat diet; AT, adipose tissue; BDL, bile duct ligation; BM, bone marrow; CCl_4, carbon tetrachloride; DBA, dilute brown nonagouti; DMN, dimethylnitrosamine; FGF, fibroblast growth factor; HGF, hepatocyte growth factor; IP, intraperitoneal; MSC, mesenchymal stromal cell; NMRI, Naval Medical Research Institute; NOD-SCID, non-obese diabetic-severe combined immunodeficiency; NSG, NOD-SCID-gamma; OG, oral gavage; SC, subcutaneous; SMc, Schistosoma Mansoni cercaria. ; TAA, thioacetamide; UCT, umbilical cord tissue; wk, week.

Fang *et al* compared the therapeutic effects of MSC given at the onset of injury to that given during injury, and demonstrated that syngeneic BM-MSC infusion ($1x10^6$ cells via tail vein) administered at the onset of injury (5 weeks of CCl_4 by oral gavage twice per week) significantly reduced surrogate markers of fibrosis (hepatic hydroxyproline, serum hyaluronic acid and pro-collagen III-N-peptide) and inflammation compared to no treatment (all $p<0.01$). However, the anti-fibrotic and anti-inflammatory effects were not seen if the MSC therapy was given 1 week after the onset of injury, which is an unexpected finding in light of other studies showing an anti-fibrotic effect when MSC are given during injury. This may reflect the use of Balb/C mice in this study, which are prone to a more profound fibrotic response[107], and thus conceivably more resistant to resolution once fibrosis starts to form.

A number of studies have shown that MSC injected at or near to the end of injury also lead to a reduction in fibrosis. Chen *et al* injected $0.5x10^6$ syngeneic BM-MSC on the last 2 days of a 61-day hepatic injury (twice per week CCl_4 by oral gavage)[108] and then analysed the effects 3 and 6 days later. Morphometric analysis of CPA showed the MSC treated group had a significant reduction in fibrosis compared to the untreated group (4% vs. 7%; $p<0.001$), with a significant reduction in αSMA+ cell staining by IHC (4% vs. 12%; $p<0.001$). MSC led to a statistically significant reduction in serum inflammatory markers IFNγ, TNFα, IL-1β (all $p<0.001$) and IL-17A ($p<0.01$), and an increase in IL-10 ($p<0.01$). Overall leucocyte infiltration into the liver was abrogated by MSC infusion; CD4+/IFNγ+ and CD4+/IL-17+ T-cells were significantly decreased ($p<0.001$), whereas regulatory T-cells (CD4+/CD25+/Foxp3+) were increased ($p<0.01$). These results differ from those of Ezquer *et al* who demonstrated that CD4+ cells increased after MSC infusion (with no effect of

CD8 cell infiltration). However, they did not sub-stratify the CD4+ population, and the experiment used a different, NASH, model of injury[106]. Quintanilha *et al* also showed the anti-fibrotic effects of MSC administered near the end of injury. They administered $2x10^6$ canine BM-MSC into mice subjected to hepatic injury by twice-a-week intra-peritoneal (IP) injection of TAA for 13 weeks. MSC were given by tail-vein injection at weeks 10, 11, 12 and 13, and the mice analysed 3 days after the last injection. MSC significantly reduced fibrosis in comparison to untreated mice, when analysed by CPA (5.1±2.9% vs. 8.3±1.7%), serum hyaluronic acid or procollagen N-terminal peptide expression (all $p<0.05$). Moreover, the authors demonstrated that MSC treatment was associated with better redox homeostasis with higher total antioxidant levels ($p<0.001$) and lower lipid peroxidation ($p<0.05$) establishing a possible cytoprotective effect on hepatocytes (which was subsequently demonstrated in *vitro*).

Jung *et al* demonstrated that MSC continue to have an anti-fibrotic effect even when administered in the absence of on-going injury[109]. They administered $1x10^6$ hUCT-MSC via tail vein to rats at the end of eight weeks of CCl_4 injury (IP, 3/week). There was a significant reduction in fibrosis compared to untreated control, as measured by histological staging and serum hyaluronic acid and laminin ($p<0.05$). Furthermore, the authors determined an 80% relative reduction in the gene expression of hepatic *Col-I*, *αSMA*, and *Tgfβ*, four weeks after MSC therapy ($p<0.05$). This was allied to a significant reduction in serum AST and ALT in the treatment arm ($p<0.05$), but the inflammatory signature and mechanisms of therapeutic effect were not explored further. Similarly, Chang *et al* showed a reduction in fibrosis from MSC treatment 3.5 days after cessation of injury[110]. They injected GFP-transfected human BM-MSC into the portal vein of rats that had been injured

by subcutaneous (SC) CCl_4 injections twice a week for 4 weeks, and analysed the effects 4 weeks later. Masson's trichrome staining demonstrated large bands of collagen in the untreated cohort, whereas collagen accumulation was not seen in the MSC-treated cohort. The authors suggested that the MSC might have directly contributed to the degradation of fibrosis by expressing MMPs; they showed that human-specific MMP co-localised with MSC in treated livers. Motawi *et al* also established that MSC given at the cessation of injury can lead to a reduction in fibrosis, and allied this to a significant increase in MMP-1 ($p<0.01$), and decrease in TIMP-1 ($p<0.001$). They administered syngeneic BM-MSC via the tail-vein of CCl_4-injured rats (IP twice a week for 6 weeks), 1 day after the cessation of injury, and analysed the effects 8 days later. Zhao *et al* demonstrated the anti-fibrotic effect of rat BM-MSC, in two different chronic models of rat liver fibrosis, and compared the administration of MSC at different points during, and at the end of injury[111]. They injected $3x10^6$ MSC via tail vein at the end of CCl_4 injury (2x per week SC injections for 6 weeks), and sacrificed the mice 28 days later. MSC led to a significant reduction in fibrosis and myofibroblast numbers compared to sham treatment as measured by CPA (40% reduction; $p<0.05$), hepatic hydroxyproline, serum laminin and hyaluronic acid ($p<0.01$), and staining for αSMA+ cells ($p<0.05$). They then showed very similar results in a DMN-induced liver injury (3 consecutive days every week for 6 weeks), in which they infused MSC at day 10 of injury, or at day 20 of injury, before sacrificing the mice 7 days after the end on injury. This demonstrated that the anti-fibrotic effect was apparent in both treatment arms, but more pronounced in the earlier treatment arm. The authors did not explore this further, though it is clear that MSC had an anti-fibrotic effect in both models of injury, and at all three time points. Collectively these studies

suggest multiple mechanisms by which MSC may attenuate fibrogenesis or degrade established fibrosis, which may in turn be governed by the timing of therapy in relation to on-going injury.

However, at least three studies have demonstrated that MSC given at, or after the cessation of injury may not deliver an effect on fibrosis. Carvalho *et al*[112] administered $1x10^7$ syngeneic BM-MSC via the portal vein of rats at the end of injury (alcohol-infused diet and IP CCl_4) and demonstrated no improvement in serum biochemical markers of liver disease, nor in morphometric analysis for CPA 2 months later (4.8±0.6% in MSC-treated group vs. 5.4±1.1% in sham-treated group; p=0.6). The MSC were both radiolabelled and labelled with Hoechst 3342, and were seen to be viable and concentrated in the liver 6 hours after injection, but were not detected after 4 or 8 weeks. Mannheimer *et al* undertook a similar experiment using MSC isolated from the bone marrow of cirrhotic rats and found no difference in fibrosis nor portal-vein diameter in the MSC treatment arm compared to the control[113]. The authors did deliver a bi-modal hepatic injury (alcohol-infused diet and IP CCl_4) and did so over a much longer time than other experiments (14 weeks vs. 4-8 weeks in other papers), which may deposit a more resistant scar. Furthermore, Mannheimer used BM-MSC from cirrhotic rats, which may affect the functionality of MSC. Briquet *et al* injected human BM-MSC, UCT-MSC and liver MSC, into NOD/SCID/IL-2Rγ-null (NSG) mice subjected to 4 weeks of IP CCl_4-induced liver fibrosis, 2 days after the cessation of injury. They demonstrated no therapeutic effect of MSC therapy on relative fibrosis area, plasma albumin, ALT and AST after injection, despite evidence of homing and persistence in liver[114]. The NSG mice develop only very mild peak fibrosis (0.7% CPA by morphometric analysis), which makes it difficult to observe differences in response to therapy.

1.6. Can mesenchymal stromal cells have a direct anti-fibrotic effect?

The mechanisms by which MSC reduce hepatic fibrosis are not well developed, though clues exist from existing data (Figure 1.2). In the setting of on-going inflammation, MSC may influence the pro-fibrotic stimuli by immuno-modulation, or act to protect parenchymal cells from oxidative stress. MSC may also influence the degradation of ECM, either directly by secreting locally acting MMPs, or indirectly by stimulating the influx of restorative macrophages or dendritic cells to up-regulate MMPs. Furthermore, they may effect myofibroblast inactivation or death, which is the main determinant of fibrogenesis/fibrinolysis. Myofibroblasts not only secrete the majority of ECM, but are also the main source of TIMP-1, which acts to stem the collagenase activity of MMPs. MMP concentrations are increased in both fibrosis and resolution, although different MMPs may dominate in injury and resolution, and the TIMP:MMP balance favours the latter in resolution. In the following sections, we will discuss the purported direct ant fibrotic effects of MSC.

1.6.1. Tipping the balance of TIMPs and MMPs

A number of studies that have demonstrated the anti-fibrotic potential of murine MSC after syngeneic treatment in models of chronic hepatic injury have also investigated the effects on MMPs and TIMPs. It is not possible to extract a consistent profile of effects on MMPs, due to inconsistencies in what has been tested. Nevertheless, syngeneic rodent MSC treatment in models of CCl_4-induced liver injury leads to increased expression of MMP-1/13[115–117] and MMP-12[118], a reduction in the expression of MMP-2[108,119], and no or limited effect on MMP-9[108,115,118] in the setting of resolving fibrosis. What remains unclear is whether these fluxes in MMPs reflect

maturation/changes in the inflammatory infiltrate[77,120] – including HSCs, neutrophils, macrophages and dendritic cells (driven by MSC), or whether MSC actually secrete MMPs themselves.

MMP-12 is an elastase (metalloelastase) and is critical to the resolution of advanced scars in which elastin is a prominent feature. They are secreted by hepatic restorative macrophages[60], and it is likely that the changes seen with MSC therapy reflect the maturation of macrophages to a restorative phenotype. Rodent MMP-13 is an interstitial collagenase (human MMP-1) that is also expressed by mature macrophages[31], and which is also expressed transiently by maturing HSC early in their activation[121], but is subsequently down-regulated when HSC reach a fully fibrogenic phenotype[122].

MMP-2 (Gelatinase-A) is secreted by myofibroblasts and has been functionally linked with the naïve/proliferative phenotype[123]. Thus, it follows that the MSC-induced resolution leads to a reduction in MMP-2.

Seki *et al* reported a decrease in both MMP-8 and -9 following syngeneic AT-MSC injection in a NASH model of murine liver injury[77]. They also described a significant decrease in the number of cells of myeloid lineage (CD11b+), and granulocytes/antigen presenting cells (Gr1+), which may account for the flux of MMPs. This was not investigated further, but it is known that neutrophil collagenase (MMP-8) is expressed by both neutrophils and macrophages[124], and that Gelatinase-B (MMP-9) is expressed by inflammatory macrophages, dendritic cells[125] and Kupffer cells[126].

Therefore, it is likely that the changes in the inflammatory profile described by Seki *et al* explain the reported changes in MMPs.

Of note, none of the cited studies designated MMP secretion directly to MSC. Chang *et al* administered human BM-MSC to rats via the portal vein 3.5 days after cessation of chronic CCl_4 injury and demonstrated an improvement in biochemical markers of liver injury and function (albumin, ammonia, fibrinogen)[110]. They reported that engrafted human GFP-transfected BM-MSC co-localised with human-specific MMP expression in the injured liver, and had no fibrosis 4 weeks after therapy. However, the effect of sparsely engrafted MSC secreting MMPs is unlikely to be functionally significant by itself.

TIMP molecules inhibit the extracellular function of MMPs by stabilising the pro-enzyme, and inhibiting the active moiety[127]. Both TIMP-1 and -2 are expressed by myofibroblasts; TIMP-1 expression mirrors that of other markers of HSC activation (such as αSMA, and collagen-1), to the extent that TIMP-1 correlates with numbers of activated HSC. TIMP-2 is also expressed by both active and quiescent phenotypes of HSC, and during resolution myofibroblasts undergo apoptosis or revert to a quiescent state. As such, the expression of TIMP-1 falls[128–130]. Despite, no major fluxes in MMP expression, they are liberated to remodel fibrotic matrix. Thus, the downregulation of TIMP is critical to allow the degradation of scar tissue.

MSC therapy leads to a decrease in the expression of TIMP-1 in the setting of resolving liver fibrosis[115–117,119], which was invariably allied with either a decrease in αSMA+ staining, collagen-1

or TGFβ expression. It is likely to be a consequence of HSC inactivation or apoptosis, though the exact mechanisms by which MSC enact this have not been well developed in these studies.

1.6.2. Secreted anti-fibrotic agents and the effects on the fate of myofibroblasts

The switch from fibrogenesis to resolution in the body's response to injury requires control of the injury and the inactivation of myofibroblasts (by reversion to a quiescent state or apoptosis). Investigators have tried to determine methods by which MSC may influence myofibroblast fate. Purported hypotheses include a direct effect by cell-cell contact, a direct effect by MSC-secreted cytokines / growth factors, or an indirect effect by cellular mediators such as macrophages or even hepatocytes.

In vitro experiments have demonstrated that MSC can suppress HSC activation and proliferation by direct cellular contact. Chen *et al* established that HSC undergo proliferative arrest on direct cell-cell contact with BM-MSC[131]. MSC induce HSC cell arrest of in G_0 through a Notch-dependent pathway – blockade of Notch signalling pathway with Notch1 siRNA increased expression of phospho-Akt and increased the proliferation of co-cultured HSC. Whilst adoptively transferred MSC preferentially home to areas of injury, they never do at levels to make sufficient direct cell-cell interactions for this to be a plausible mechanism of their effect [39].

Evidence suggests that secreted factors are critical to the therapeutic MSC armamentarium. Meier *et al* elegantly demonstrated that MSC mediate an anti-fibrotic effect by releasing soluble molecules *in vitro* and *in vivo*[132]. The authors encapsulated human BM-MSC in an alginate-

polyethylene glycol hybrid hydrogel, which is permissive to soluble factors (oxygen, glucose cytokines), but not to antibodies or direct cellular interaction. The authors observed that IP injected micro-encapsulated MSC decrease inflammation and liver fibrosis in murine models of chronic liver injury – CCl_4 and BDL – suggesting the effects can be solely attributed to factors secreted by MSC; in particular they were shown to secrete IL-1Ra, increase endogenous serum IL-10 levels and hepatic MMP-9 expression. *In vitro* experiments subsequently suggested a direct anti-fibrotic effect of MSC conditioned medium (CM) on TGFβ-stimulated LX-2 and primary HSC, implicating a possible role for insulin-like growth factor binding protein-2 (IGFBP-2), IL-6, IL-1Ra, and monocyte chemotactic protein-1 (MCP-1) without wholly interrogating the mechanism.

Similarly, Li *et al* determined the anti-fibrotic effects of microvesicles (or exosomes) from hUCT-MSC in a CCl_4-induced model of chronic hepatic injury in rats[133]. Microvesicles are cell-derived vesicles that act as functional parcels containing proteins and nucleic acid variants that are characteristic of the parent cell[134]. Li *et al* directly transplanted microvesicles into injured livers whereby they significantly attenuated the fibrotic response. Allied *in vitro* experiments demonstrated MSC microvesicles induced a reversal of TGFβ-induced activation of HSC, as in Meier *et al*; however, the contents of the microvesicles were not interrogated further.

Tsai *et al* demonstrated a concomitant rise in hepatocyte growth factor (HGF) and Met-P expression after MSC treatment[78], which they hypothesised may modulate either MSC action or homing to areas of injury. In fact the HGF/c-Met signalling pathway has been shown to be critical to MSC homing to the liver in an acute ischaemic liver injury model in rats, as subsequently

confirmed by Transwell *in vitro* studies[135]. Furthermore, Ishikawa *et al* demonstrated the critical role of the HGF/c-Met pathway in the resolution of 3,5-diethoxycarbonyl-1,4-dihydrocollidine (DDC)-induced hepatic fibrosis. It was found to be critical to mobilising and differentiating the native hepatic stem cell niche (oval cells), and for the recruitment of MMP-9-expressing mature macrophages[136]. Studies have also established that HGF promotes MMP expression *in vivo*, and also causes HSC apoptosis *in vitro*[137].

Parekkadan *et al* showed that human BM-MSC induced replicative arrest and apoptosis of activated HSC in an indirect co-culture experiment, and HGF was deemed to be the major pro-apoptotic agent, as its neutralisation attenuated HSC apoptosis[137]. MSC-derived IL-10 and TNF-α inhibited HSC proliferation and collagen synthesis, whilst their blockage allowed HSC proliferation despite the presence of MSC. Of interest, HSC-derived IL-6 stimulated IL-10 secretion by MSC. *In vivo* verification would allow for a robust evaluation of these pathways.

Pan *et al* injected $1x10^6$ murine BM-MSC via tail vein after mice had been subject to 4 weeks of IP CCl_4-induced liver injury[138]. They demonstrated a significant decrease in fibrosis as measured by morphometric analysis (60% reduction of fibrosis area; $p<0.05$), and both collagen and αSMA expression (approximately 80% relative reduction in expression of both; $p<0.05$).

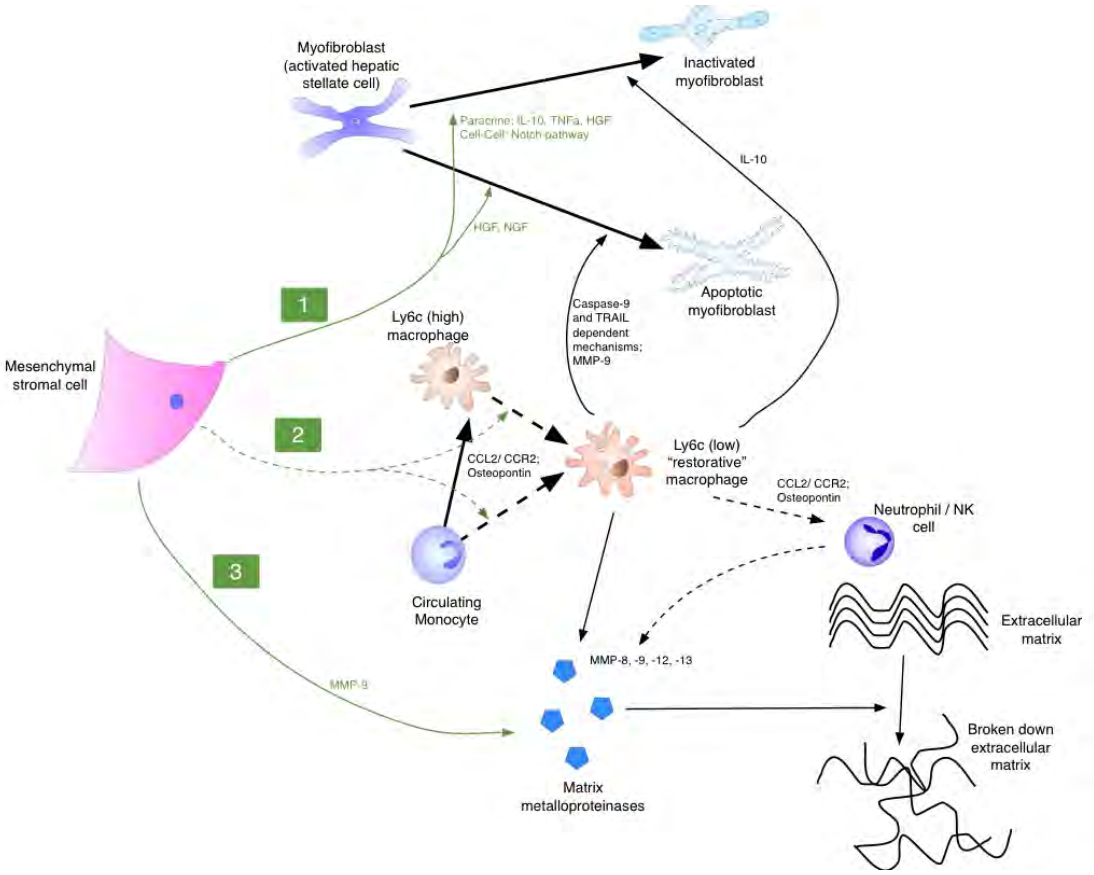

Figure 1-2 Mechanisms by which MSCs may reduce fibrosis[45]

Adapted from Haldar *et al.*[45]

1) Alter the fate of hepatic myofibroblasts to a non-fibrogenic inactive phenotype, or by promoting their apoptosis. 2) Alter the macrophage phenotype to promote resolution. The ability of MSCs to alter macrophage fate has been documented outside the liver and needs to be explored in the setting of liver disease. 3) MSCs may themselves secrete MMP and contribute to the breakdown of ECM. HGF, hepatocyte graft factor; IL, interleukin; MMP, matrix metalloproteinase; NGF, nerve growth factor; TNF, tumour necrosis factor; TRAIL, TNF-related apoptosis-inducing ligand.

They then went on to establish the critical role of hepatocyte-derived cytokine, delta-like 1 (Dlk1), in HSC activation and showed both *in vivo* and subsequently *in vitro* that MSC-derived fibroblast growth factor (FGF) 2 is critical in the down-regulation of hepatocyte Dlk1 expression, and subsequent HSC activation. This provides an insight on the indirect and amplifying paracrine

mechanisms by which MSC may deliver an anti-fibrotic effect. However, not all studies have shown MSC to have the desired inhibitory effect on HSCs. Baligar *et al* cultured primary HSC with conditioned medium from adipose tissue derived MSC, and showed both increased activation (expression of αSMA and collagen-1) and proliferation (Ki-67) of HSC in this environment. A significant increase ($p<0.05$) in MSC-derived TGF-β was noted in the conditioned media compared to the control media. An inhibitor to TGF-β receptor kinase significantly barred the MSC-CM induced activation of HSC, proving MSC derived TGF-β contributes to HSC activation *in vitro*. TGF-β is a well-described agent of MSC-mediated immuno-regulation in settings of acute inflammation[139,140], though its application in models of chronic liver injury is doubtful as most studies describe a decrease in TGF-β with MSC therapy. They injected $0.5x10^6$ human AD-MSC in to the spleens of mice subjected to 8 weeks of IP CCl_4-induced liver injury at week 4 of injury. The MSC-treated group had a significant reduction in fibrosis by CPA (5% vs. 6%; $p<0.05$), however there was no reduction (or increase) in αSMA+ staining. The authors did not investigate TGF-β or TIMP levels, but did report a three-fold increase in MMP-12 expression ($p<0.05$). As previously discussed, MMP-12 is expressed by restorative macrophages, so it possible that MSC exert their anti-fibrotic effect in this experiment by influencing macrophage polarity, though the authors did not investigate this further.

1.7. Do BM-MSC contribute to fibrosis?

The contribution of BM-derived cells to fibrogenesis has been a contentious issue, and significant studies are summarised in table 1.3. In an early study, Baba *et al* suggested BM-derived HSC might co-localise with scar tissue after CCl_4 injury. They transplanted $1x10^5$ unsorted whole bone marrow cells from GFP transgenic mice (GFP-tg) into irradiated WT mice. Recipient mice were sacrificed after 8 weeks of CCl_4 injury. 31.7% of isolated GFAP+ and desmin+ HSC from uninjured livers expressed GFP. In injured liver, αSMA-expressing cells co-localised with GFP near areas of scar, but this was not quantified, and a functional contribution to fibrosis was not described[141].

In an elegant series of gender mismatched BM reconstitution studies Russo *et al* showed that BM cells contribute to HSC, hepatic myofibroblasts, and to collagen expression using 2 models of murine hepatic injury (CCl_4 and TAA)[142]. The group demonstrated BM reconstitution after they injected $1x10^6$ un-sorted BM cells from male donors into age-matched female recipients. They used fluorescent *in situ* hybridisation (FISH) to reveal that 14% of HSC were of BM (male) origin in the absence of injury, which increased to 70% after 12 weeks of CCl_4 injury. Myofibroblast numbers (defined by the expression of αSMA – activated HSC) increased with duration of injury to approximately 400 cells per unit area (10 high power fields), but the proportion of BM-derived myofibroblasts remained constant at around 70%, suggesting an axis of renewal from the BM. Using BM cells with a β-gal reporter under the control of a α2(I)collagen enhancer they demonstrated the presence of β-gal expressing cells around areas of scarring in the liver after 12 weeks of CCl_4 injury. *In situ* hybridisation for mRNA for pro(α1)I collagen and Y chromosome along with IHC for αSMA, confirmed collagen expression in BM-derived cells. The authors went on to

establish whether the BM cells functionally contributed to the fibrotic phenotype in liver injury; irradiated mice received BM transplants from Col-1a1rr mice, which have a mutated collagenase-resistant collagen, and on injury wild-type mice developed extensive peri-cellular fibrosis similar to that seen in the Col-1a1rr mice. The phenotype of fibrosis, as measured by histopathological assessment and hydroxyproline assay, was markedly greater than that seen in mice receiving wild type (WT) BM. Notably, the proportion of myofibroblasts of BM origin from Col-1a1rr mice was 63% compared to 49% in mice receiving BM from WT mice, suggesting that the genotype of the BM-derived myofibroblasts could influence their homing/engraftment to the liver as well as the injured organ's fibrotic response. To determine which cells within the BM were responsible the authors performed a series of gender mismatched reconstitution studies demonstrating that marrow stromal and not haematopoietic stem cells were responsible for BM-derived myofibroblasts in the liver. It is not clear how similar the marrow stromal cells used in this study were to MSC, as data were not provided on cell surface marker expression or tri-lineage differentiation.

The same group also published a case series of male patients who had received liver transplants from female donors, who had then gone on to require another transplant for cirrhosis[143]. Explanted liver tissue was analysed for Y chromosome by in-situ hybridisation together with IHC for HSC and myofibroblast and identified that 14-45% of myofibroblast were deemed to be of recipient origin. Similarly, they showed 25% of hepatic myofibroblasts found in the explant of a female cirrhotic patient who had previously received an HLA-matched BMT from a male donor for β-thalassemia, were of BM origin.

More recently, Li *et al* reconstituted the BM of irradiated WT mice with enhanced GFP (EGFP) transgenic whole BM. They defined BM-derived myofibroblasts as αSMA^+ cells that also expressed EGFP and showed that the proportion of BM-derived myofibroblasts increased with duration of injury up to 80% after 6 weeks of twice-weekly IP CCl_4 in C57Bl/6 mice. They then used $1.2x10^6$ MSC (plastic-adherent; $CD90^+$, $CD105^+$, $CD166^+$, $CD34^-$, $CD45^-$, $CD14^-$) from EGFP transgenic mice to reconstitute the BM of irradiated WT mice (with $1.08x10^7$ whole BM from a WT donor) and demonstrated that after two weeks of CCl_4 injury 70% of myofibroblasts were of BM-MSC origin. Furthermore, they showed that BM cell homing to the injured liver was sphingosine-1-phosphate (S1P) dependent such that blockade of the S1P receptor 3 with suramin reduced BM cell homing by 80%[144]. Notably, the effect of this blockade on fibrosis was not reported, and no direct contribution to fibrosis was reported in this study. Nevertheless, Kong *et al* repeated Li's experiment using $EGFP^+$ MSC reconstitution of irradiated BM in WT mice, and blocked the S1P dependent pathway with the partial S1P agonist FTY720[145]. In the setting of CCl_4 injury, they demonstrated a relative reduction in the mRNA expression of αSMA (88% reduction), *Col*α*1(I)* (75%), *Col*α*1(III)* (60%), *Tgf-*β*1* (60%), compared to mice untreated with FTY720. They repeated the experiment using SCID-beige mice (an immunodeficient mouse affecting T-, B- and NK-cell populations) to eliminate any signal from FTY720 action on effector leucocytes and found very similar results suggesting that BM-derived stromal cells contribute to liver fibrosis.

Di Bonzo *et al* irradiated NOD/SCID mice prior to tail vein infusion with human MSC to attain BM reconstitution, although this was not confirmed. MSC were plastic-adherent and had a

characteristic CD antigen signature (CD45, CD14 (low); CD106, CD16 (med); CD29, CD90, CD44, CD105 (high)) with tri-lineage differentiation properties. After chronic injury with 6 weeks of CCl_4 they demonstrated 7% of liver cells were positive for human HLA-I antigens[146], of which half exhibited a myofibroblast morphology and were either αSMA or GFAP positive[146]. It was unclear what proportion of the total HSC and myofibroblast populations were BM-derived although the contribution was considerably less than had been described in other papers which may reflect the xenogeneic nature of the study.

In contrast to Russo *et al* who reported that it was BM stromal cells and not haematopoietic stem cells that contributed to liver fibrosis, Miyata *et al* reported a dominant role for haematopoietic stem cells[147]. They transplanted haematopoietic stem cells from transgenic EGFP mice into irradiated mice, and demonstrated that after 12 weeks of injury with CCl_4, up to 60% of the GFP-positive cells in the liver were myofibroblasts. Data on the percentage of HSC and myofibroblasts that were derived from the haematopoietic lineage was not provided.

Table 1-3: Animal model studies investigating the role of BM-derived cells in fibrogenesis[45]

Primary Author; year	Type & Source of BM	Dose of transplanted cells*	Recipient character -istics	Mode of liver injury; duration of injury	Time for BMT to liver injury	Timing of analysis	BM contribution to HSC / MF Functional contribution to fibrosis; Key conclusions
Baba[141]; 2004	Unsorted whole BM cells; transgenic GFP mice	$1x10^5$	Mice; c57Bl/6	SC CCl_4 every 3 days 1.5 wks (5 doses)	8 weeks after BMT	96 hours after injury cessation	• 31.7% of isolated HSC expressed GFP in uninjured liver • IHC of uninjured liver showed GFP cells expressing GFAP and desmin (not αSMA) • GFP-cells co-localised with αSMA in injury. • No functional contribution to fibrosis demonstrated
Russo[142]; 2006	Unsorted whole BM cells; Male mice;	$1x10^6$	Mice (female); Balb/c	IP CCl_4 every 5 days varying duration	4 weeks after BMT	72 hours after cessation of injury	• BM-derived HSCs defined as Y-chromosome positive and $GFAP^+$ • 14% of HSCs were BM-derived in uninjured liver • Proportion of BM-derived HSC increased with duration of injury (70% at 12 weeks), yet total numbers of GFAP+ cells remained constant with increasing duration of injury (around 380 cells/ unit high power field area). • 69% of MFs (αSMA) in injury were of BM origin – this remained constant with longer injury, even though total MF numbers increased.
				IP TAA 3x/wk 4 weeks			
				IP CCl_4 Every 5 days 8 weeks		8 weeks after cessation of injury	• No αSMA^+ cells in recovery; the proportion of $GFAP^+$ cells was as it was before injury, with 16% being of BM origin; a $desmin^+$ cell group congregated around residual scarring - 42% of which were of BM origin - indicating the heterogeneity of expression, and how this may be source-dependent
	Unsorted Whole BM cells; Male; col1a2 mice - express β-gal (reporter), under control of alpha2(I) collagen enhancer	$1x10^6$	Mice (female); c57Bl/6	IP CCl_4 Every 5 days 12 weeks		72 hours after injury cessation	• Cells expressing β-gal confirmed to be of BM origin (Y-chromosome co-localisation); more BM derived αSMA cells (226 cells / unit area) than BM-derived β-gal cells (161 cells / unit area) – suggesting not all αSMA cells express collagen. • Other: ISH for pro(α1)I together with FISH for Y-chromosome used to demonstrate collagen transcription in BM derived cells. • Both these results suggest a BM-cell derived collagen expression
	Unsorted Whole BM cells; Male; $Col1\alpha1^{rr}$ mice - mutated, collagenase resistant collagen expression	$1x10^6$		IP CCl_4 Every 5 days 8 weeks		1 week after injury cessation	• Test mice had a more profound and characteristic peri-cellular fibrosis compared to mice with WT BM: Hyp - 2.5mM/mg vs. 2.0mM/mg. • 63% of MF were of BM origin compared to 49% in mice receiving BM from WT mice. This suggested that the genotype of the BM-derived MF could influence the injured organ's fibrotic response.
	MSC (female mice) + haematopoietic stem cells (male mice)	$1.2x10^6$ MSC; $2.3x10^5$ haematopoietic stem cells. MSC were PA; no further characterisation	Mice (female); Balb/c	IP CCl_4 Every 5 days 6 weeks		72 hours after injury cessation	• 53% of MF were of BMMSC origin
	MSC (male mice) + haematopoietic stem cells (female mice)						• 8% of MF were of BM haematopoietic stellate cell origin
Di Bonzo[146]; 2008	Human BM-MSC; HLA expressing; some pre-labelled with fluorescent tag	$1x10^6$ cells. MSC characterised by PA, cell surface markers and tri-lineage differentiation.	Mice; NOD/SCID	IP CCl_4 every 5 days 4-6 weeks	4 weeks after BMT	72 hours after injury cessation	• 7% of cells in liver were HLA^+, after 6 weeks of injury. • Approximately half (3.33% of total) of HLA^+ cells had MF morphology and were either $GFAP^+$, or αSMA^+. • No functional contribution to fibrosis demonstrated. • Unclear what proportion of total MF or HSC were of BM origin.

Li[144]; 2009	Unsorted whole BM cells; transgenic EGFP mice	1.5x10^7 cells	Mice; ICR	IP CCl_4 2x/wk varying duration	4 weeks after BMT	24 hours after injury cessation	• $EGFP^+/\alpha SMA^+$ co-expressing cells defined BM derived MF • Proportion of MF of BM origin increased with duration of injury - 80% with 6 weeks of CCl_4 injury
	BM-MSC ($EGFP^+$ mice) + Whole BM (EGFP- mice)	1.2x10^6 BMMSC; 1.08x10^7 whole BM cells.		IP CCl_4 2x/wk 2 weeks			• 70% of the MFs were BM-derived, suggesting a predominant contribution from BMMSC • Mice were injured in the presence or absence of suramin (S1P receptor 3 blocker). Suramin led to decreased $EGFP^+$ cells in liver (80% relative reduction), though no data on how this affected liver fibrosis was offered
	MSC were PA. Immunophenotyping: **pos –** CD44, CD105, CD166; **neg –** CD34, CD45, CD14						
Kong[145]; 2014	BM-MSC (EGFP+ mice) + Whole BM (EGFP- mice)	1.2x10^6 BM-MSC; 1.08x10^7 whole BM cells;	Mice; ICR + SCID-beige	IP CCl_4 2x/ week 4 weeks	4 weeks after BMT	24 hours after injury cessation	• Mice were injured in the presence or absence of FTY720 (blocking partial S1P agonist). FTY720 led to relative reduction in the mRNA expression of *αSMA* (88% reduction), *Colα 1(I)* (75%), *Colα 1(III)* (60%), *TGF-β 1* (60%). • Similar results in ICR, and SCID-beige mice
	MSC were PA. Immunophenotyping: **pos –** CD44, CD105, CD166; **neg –** CD34, CD45, CD14						
Hi'yama[148]; 2009	Unsorted whole BM cells; transgenic mice harbouring tissue-specific enhancer/ promoter sequences of α2(I) collagen gene linked to EGFP or LUC	5x10^6 cells	Mice; C57Bl/6	IP CCl_4 every 3 days 13 weeks (30 doses)	8 weeks after BMT	48 hours after cessation of injury	• Activation of the Col1α2 promoter was assessed by confocal microscopic examination detecting EGFP signals and LUC activity by assays of liver homogenates. • After CCl_4 injury or BDL only negligible contributions of the BM to collagen production demonstrated. • BM cells did localise to areas of scarring, but they did not produce collagen, and did not stain for macrophage or Kupffer cell markers
				BDL 14 days			
Med'cke[47]; 2013	Unsorted whole BM cells; transgenic LratCre mGFP, mTom. LratCre faithfully expressed in HSC; Liposome clodronate for macrophage depletion	1x10^7 cells	Mice; C57Bl/6	IP CCl_4 20 doses	Not stated	5-6 months after BMT	• Authors did not detect LratCre-labelled HSCs in normal liver or fibrotic livers after BDL or chronic CCL4. • HSC isolated from these mice did not express mGFP, whereas controls did show abundant mGFP expression. • These data strongly suggest the HSC population is from liver resident cells. • These data were in the context of other data to confirm HSC as the predominant source of MFs in liver injury of different aetiologies.
				BDL 3 weeks			

Adapted from Haldar *et al.*[45]

All studies involved BM irradiation and reconstitution with donor cells. All cell transplantation was done by tail vein injection. αSMA, alpha smooth muscle actin; BDL, bile duct ligation; BM, bone marrow; BMT, BM transplant; CCl_4, carbon tetrachloride; FACS, fluorescence-activated cell sorting; (F)ISH, fluorescence *in situ* hybridisation; GFAP, glial fibrillary acidic protein; GFP, green fluorescent protein; HLA, human leukocyte antigen; HSC, hepatic stellate cell; ICR, Institute of Cancer Research; IP, intraperitoneal; LUC, luciferase; MF, myofibroblast; PA, plastic adherent; S1P, sphingosine-1-phosphate; SCID, severe combined immunodeficiency; TGFβ, tissue growth factor beta; wk, week; WT, wild-type.

In contrast to the aforementioned studies, Higashiyama *et al*[148] reported no role for BM-derived cells in the generation of liver fibrosis. In their studies BM of wild-type mice was replaced by cells obtained from transgenic animals harbouring tissue-specific enhancer/promoter sequences of α_2(I) collagen gene (Colα1-2) linked to EGFP or firefly luciferase (LUC) gene. Expression of collagen by such cells as would occur after adoption of a myofibroblast phenotype would result in EGFP fluorescence or luciferase expression. After CCl_4 or BDL injury, only negligible contributions of the bone marrow to collagen production were demonstrated in either model. BM cells did localise to areas of scarring, but they were not collagen producing, and did not stain for macrophage or Kupffer cell markers. A further novel fate-tracing study by Mederacke (using BM reconstitution of irradiated mice with whole BM from mTom/LratCre transgenic mice; LratCre faithfully reports HSCs) demonstrated that resident hepatic stellate cells were not of bone marrow origin in either CCl_4 or BDL injury[47]. As with Higashiyama, BM cells ($mTom^+$) were seen to populate scarred areas but the identity of these cells was not further characterised, although they did not report LratCre.

Reconciling the disparate findings between these studies is challenging and possibly reflects differences in BM reconstitution, models of liver injury and methods used to confirm cellular identities. *In situ* hybridisation and IHC co-staining can lack sensitivity and specificity although confocal imaging as used by Russo *et al* provides greater confidence. Additionally, studies relying on αSMA production as a surrogate for collagen-producing cells may over-estimate the functional contribution of such cells to liver fibrosis as not all αSMA positive cells produce collagen[149]. Furthermore, not all collagen-producing cells are positive for αSMA[150].

1.8. Do liver resident MSCs contribute to fibrosis?

A very recent study by Kramann *et al* identified a subpopulation of PDGFβ receptor (PDGFβR)-positive pericytes that express Gli1, and that can be found in all solid organs[151]. $Gli1^+$ $PDGFβR^+$ cells demonstrate classical hallmarks of being MSC; they had the potential for tri-lineage mesenchymal differentiation regardless of their origin, and expressed CD29, Sca1, Cd44, Cd105, but not CD31, CD45 and CD34. The authors established that resident perivascular Gli1+ cells underwent proliferative expansion after injury and differentiated into myofibroblasts *in vivo*, the extent of which varied across organs. In a model of renal fibrosis (unilateral ureteric obstruction), 45% of myofibroblasts were of Gli1 origin, whereas only 39% of $αSMA^+$ cells were of Gli1 origin after a CCl_4-induced hepatic fibrosis. Nevertheless, they demonstrated that a Gli1 knockout led to a 50% amelioration of renal fibrosis in the UUO model, although the equivalent experiment in liver fibrosis was not reported. Though the idea of perivascular cells contributing to fibrosis in different organ systems is not novel[152], this was the first genetic fate-tracing experiment to conclusively demonstrate that a resident population of MSC can react in this way. Kramann *et al* also demonstrate that neither circulating nor BM-derived Gli^+ cells contributed to the myofibroblast pool in kidney fibrosis by the use of both a BM transplant and a parabiosis model.

1.9. Aims of the research

The contribution of endogenous MSC to hepatic fibrogenesis remains contentious due to conflicting reports. In contrast, there are no convincing reports of exogenous MSC contributing to liver fibrosis; rather, their anti-fibrotic potential makes them an attractive agent, apparently exploiting mechanisms that modulate inflammation, induce the degradation of ECM, and switch off the drivers of fibrosis (Figure 1.2). The therapeutic potential of MSCs in the regression of fibrosis after the cessation of injury has not yet been comprehensively investigated and is clinically relevant in an era of better cure rates of hepatitis C, and for cirrhotic patients with alcoholic liver disease who have maintained abstinence.

The primary aim of this body of work is to determine the therapeutic effect of MSC therapy on established liver fibrosis. In order to do this, I will:

- Delineate the time-course and ascertain the reproducibility of fibrosis regression using two toxin-mediated models of murine liver fibrosis
- Characterise human UCT-MSCs provided by industry collaborators
- Determine the effect of MSC therapy on the resolution of established liver fibrosis and on fibrogenesis
- Detail the bio-distribution and persistence of peripherally intravenously injected MSCs in mice subject to chronic hepatic fibrosis using CryoViz^{TM} imaging technology.
- Ascertain any effect of MSCs on LX2 (human stellate cell line) biology *in vitro* in an effort to determine any potential direct anti-fibrotic action.

Chapter 2

Materials and Methods

2.1. Isolation of mesenchymal stromal cells from human umbilical cord tissue

Orbsen Therapeutics Limited (OTL) (Galway, Ireland) provided human UCT-derived syndecan 2-positive (S2)-cells for use. They isolated, enriched and cultured the cells for use by previously described methods.[153] Briefly, human UCT was collected from Caesarean deliveries by Tissue Solutions Ltd. (Glasgow, UK) in accordance with local legal and ethical requirements. Tissue was transported to OTL and processed for cell isolation within 48 hours of delivery. Whole tissue was manually dissociated, and enzymatically digested by collagenase 1, hyaluronidase 1 and DNase for 2 hours at 37°C. The resulting single cell suspension was stained with CD362-APC (allophycocyanin) (clone 305515, 1:50 dilution; R&D systems, UK). After 30 minutes at 4°C, the cells were washed and suspended in magnetic-activated cell sorting (MACS) buffer (80µL/10^7 cells). MACS buffer is phosphate buffered saline (PBS) with 2% heat-inactivated FCS, and 1mM of ethylenediaminetetraacetic acid (EDTA). Anti-APC beads (20µL/10^7 cells) were added to the cells for 15 minutes at 4°C. The stained cells were then isolated using MS columns (Miltenyi Biotec; UK). Each cell fraction was counted, seeded for expansion (as described in section 2.2) and cryopreserved at passage 2 for shipment to the University of Birmingham.

2.2. Storage, culture, subculture and use of human MSC

Cells were packaged and received on dry ice in 1mL cryovials containing $1x10^6$ cells in 1mL of serum with 10% dimethyl sulfoxide (DMSO), and promptly stored in liquid nitrogen until needed. For use, cells were thawed in a 37°C water bath, and contents transferred to a 15mL conical-bottom polypropylene tube containing 12mL of pre-warmed complete MSC culture medium at 37°C. Complete MSC culture medium was prepared in a biological safety cabinet and consisted of Minimum Essential Media – alpha with GlutaMAX™ supplement (32561029; Gibco, UK) (αMEM), with 10% heat-inactivated FCS (F9665; Sigma-Aldrich, UK), 1% penicillin/streptomycin (10,000U/mL; 15140122; Gibco, UK) and 1ng/mL of recombinant human FGF (100-18B; Peprotech, UK) and stored at 4°C.

The suspension was then centrifuged for 5 minutes at a relative centrifugal force of 400g at 20±5°C. The supernatant was subsequently discarded, and the pellet gently re-suspended in 5mL of complete MSC culture medium by flicking the bottom of the tube and using a Pasteur pipette. The cell suspension was then transferred to a T-175cm^2 cell culture flask with a vented cap containing 25mL of pre-warmed complete MSC culture medium (total volume = 30mL). Cells were then incubated at 37°C in a hypercapnic (5% CO_2) atmosphere. The flasks were inspected for cellular confluence and contamination daily, and the spent medium changed every 2-3 days or earlier if a significant pH change was indicated by the phenol red (i.e. if it turned yellow). 70-80% confluence could be expected at day 4 or 5, at which point the cells could be sub-cultured for expansion if required, or prepared for infusion. Passage 4 cells were used for all experiments. For either, the medium was removed, and the cells washed with 10mL of sterile PBS, twice. The cells

were then bathed in 10mL of pre-warmed (to 37°C) 1X TrypLE™ Express Enzyme (12605010; Gibco, UK), and incubated for 5 minutes in a 37°C incubator. The contents of the flask were then examined using an inverted light microscope to ensure the cells had dislodged from the surface of the flask. If not, the flask contents were incubated for a further 2 minutes, and then re-examined. The trypsin was neutralised by adding 20mL of complete MSC culture medium to the flask, and the cell suspension then aspirated and transferred to a 50mL conical-bottom polypropylene tube. They were centrifuged for 5 minutes at a relative centrifugal force of 400g at 20±5°C. The supernatant was discarded, and the pellet re-suspended in 5mL of complete MSC culture medium. After ensuring adequate re-suspension of the cells, 20µL were mixed with an equal volume of 0.4% trypan blue solution (15250061; Gibco, UK). 10µL of the cell suspension with trypan blue mixture was applied to the haemocytometer affixed with a moistened glass coverslip. Under an inverted light microscope using 10X objective, the live cells (unstained cells) were counted in each of the 4 corner sets of 16 squares using a hand tally counter:

The number of viable cells was then calculated:

The sum of viable cells in the 4 corner sets of 16 squares divided by 4 = X.

X multiplied by 10^4 to give the number of cells per mL = y

y multiplied by dilution factor with trypan blue (=2), which is then multiplied by volume of original cell suspension in mL (5), to give total volume of cells in suspension.

The remaining suspension was then spun in a centrifuge for 5 minutes at a relative centrifugal force of 400g at 20±5°C. The supernatant was discarded and cell pellet re-suspended fit for purpose.

- For sub-culturing cells the pellet was re-suspended in complete MSC culture medium; $1x10^6$ cells in suspension were then be transferred to a T-175cm^2 cell culture flask containing pre-warmed complete medium as previously described.
- For long-term storage of cells, they were suspended in Cryostor® cell cryopreservation medium CS5 (CS299; Sigma Aldrich, UK) at a density of $1x10^6$ cells/mL, and 1mL transferred to 1.5mL cryovials. The cryovials were frozen at -80°C in a Mr. Frosty™ Freezing Container (51000001; Thermo Scientific, UK) to ensure a cooling rate of -1°C/minute, before they were transferred to liquid nitrogen storage.
- For preparation of cells for injection into mice, the pellet was re-suspended in an appropriate volume of sterile 0.9% saline to give a final concentration of 5c/mL, where c = number of cells being infused per mouse. 300µL of cell suspension in saline was transferred to a 1.5mL Eppendorf tube, and transferred on ice to the Biomedical Services Unit (BMSU) (where the mice were housed). The cells were re-suspended by gentle flicking of the Eppendorf tube, followed by gentle mixing by the use of a 1mL pipette. 200µL (containing number of cells = c) of the cell suspension was then injected via lateral tail vein in a pre-warmed mouse (37°C), using an appropriate micro-injector syringe (500µL syringe) with a 28-gauge needle. The mice were observed for acute deterioration for 15 minutes before being housed for standard observations and follow up. The duration from bench (when

cells suspended in saline in biological safety cabinet) to mouse (when tail vein injection performed) was kept to less than 45 minutes.

2.2.1. Preparation and storage of MSC conditioned medium

Syndecan-2 selected MSCs at passage 4 were seeded in 6-well plates at a density of $5x10^4$ cells per well and incubated as previously described in 2mL of MSC complete culture medium without FGF supplementation. The media were changed every 48 hours, or earlier in the event of a media colour change. Cells were grown to a confluence of 60-80%, which typically required 2-4 days before the spent media was exchanged for fresh Dulbecco's Minimum Essential Media with GlutaMAX™ supplement (11584456; Gibco, UK) (DMEM) with 10% FCS. After 24 hours, the media were collected via aspiration, transferred to a 50mL conical-bottom polypropylene tube and centrifuged for 5 minutes at a relative centrifugal force of 400g at 20±5°C. The supernatant was then carefully aspirated, and diluted in fresh MSC culture medium (without FGF) as required, and stored as 1mL aliquots in 1.5mL Eppendorf tubes at -80°C for later use. On the day of use, the conditioned media were thawed at 37°C, and used. Unused conditioned media were discarded and not refrozen.

2.3. Characterisation of MSC

2.3.1. Characterisation of MSCs by flow cytometry

MSCs were cultured to passage 3 in complete medium as described, dislodged with trypsin, and suspended to a concentration of $1x10^7$ cells/ mL of flow cytometry (FACS) buffer (same as MACS buffer). The BD Stemflow™ Human MSC Analysis Kit (562245; BD biosciences, UK) was set up as per manufacturer's instructions. $1x10^6$ cells in 100µL of FACS buffer were added to FACS tubes, and antibodies were added as described in Table 2.1. The cells were incubated for 30 minutes at 4°C, shielded from light

On completion, the samples were washed twice in 2mL of ice-cold FACS buffer and centrifuged for 5 minutes at a relative centrifugal force of 400g at 4°C. The resulting pellets were stained with a live-dead marker (conjugated with APC Cy7; 1µL in 1000µL PBS): incubating in 100µL for 30 minutes at 4°C shielded from light. The samples were then washed twice as already described, and resuspended in 500µL of FACS buffer, passed through a 50µm filter before analysing on a Cyan ADP flow cytometer (Beckman Coulter, UK).

Table 2-1: Antibody set up for MSC characterisation flow cytometry

Assignment	Antibody	Fluorescence tag	Antibody volume	
Single colour compensation	CD90	FITC	5µL	
Single colour compensation	CD44	PE	5µL	
Single colour compensation	CD105	PerCP-Cy 5.5	5µL	
Single colour compensation	CD73	APC	5µL	
Live-dead single colour compensation	Live-dead	APC Cy7	1µL	
Unstained control	Unstained	-	-	Each of these tubes repeated for every MSC batch used
Positive and negative isotype control cocktails, (and live-dead marker)	mIgG1, κ	FITC	20µL	
	mIgG2b, κ	PE		
	mIgG1, κ	PerCP-Cy 5.5		
	mIgG1, κ	APC		
	mIgG1, κ	PE	20µL	
	mIgG2a, κ	PE		
	(Live dead)			
Positive and negative cocktails, (and live-dead marker)	CD90	FITC	20µL	
	CD44	PE		
	CD105	PerCP-Cy 5.5		
	CD73	APC		
	CD34	PE	20µL	
	CD11b	PE		
	CD19	PE		
	CD45	PE		
	HLA-DR	PE		
	(Live dead)			

As per BD Stemflow™ Human MSC Analysis Kit manufacturer's instructions. Volumes of antibodies were added to 1x106 cells in 100µL of FACS buffer.

MSCs from OTL were also examined for their expression of S2/CD362. MSC from each batch received were cultured to passage 3, washed and suspended to a density of $1x10^5$ cells/ 100µL of FACS buffer. $1x10^5$ cells were loaded per well of a 96-well plate. 2µL of the human CD362 APC-conjugated antibody (FAB2965A; R&D systems, UK) were added to each of the test wells. An unstained control and an appropriate isotype control were used – 1µl of APC-conjugated monoclonal rat IgG2b (IC013A; R&D systems, UK). The cells were left to incubate for 30 minutes

at 4°C shielded from light, then washed twice in FACS buffer, and finally suspended in 500µL of FACS buffer before analysing.

2.3.2. Characterisation of MSC by adipogenic differentiation

2.3.2.1. Preparing adipogenic differentiation medium

Complete adipogenic medium was a product of the StemPro® Adipocyte Differentiation Kit (A1007001; Gibco, UK), whereby 90mL of StemPro® Adipocyte Differentiation Basal Medium was added to 10mL of StemPro® Adipocyte Supplement and gentamycin (15750060; Gibco, UK) at a concentration of 5µg/mL.

2.3.2.2. Stimulating adipogenic differentiation

MSC were seeded at passage 3 in a 12-well tissue culture plate at a density of $5x10^4$ cells/well, in complete MSC culture medium (2mL/well) and cultured as described in section 2.2. At 70-80% confluence, the spent media were removed, and the cells washed in a working volume of sterile PBS, before replacing with pre-warmed complete adipogenesis differentiation medium. The cells were checked daily for differentiation, and evidence of fat vacuoles. The spent media were aspirated and discarded every 3 days, and replaced with complete adipogenesis differentiation medium. The culture continued for 14 days before the cells were washed twice in sterile PBS and fixed in 2mL of 10% neutral-buffered formalin. Following 30 minutes of incubation at room temperature, the cells were washed twice in sterile PBS, and stored at 4°C bathed in PBS until such time as to perform Oil Red O staining.

2.3.2.3. Oil Red O staining

Oil Red O (00625; Sigma Aldrich, UK) was dissolved in 99% isopropanol at a concentration of 3g/L to make a stock solution. A working solution was made on the day of staining by diluting the stock solution in distilled water (1.5:1) and filtering through Whatman paper (WHA10010155, Aldrich, UK). Fixed cells were washed in PBS. 2mL of 60% isopropanol was added to each well. After 5 minutes, the isopropanol was aspirated and discarded, and 2mL of the freshly-prepared oil red O working solution was added to each well. After 15 minutes, the working solution was discarded, and the cells were washed twice in distilled water to ensure the water runs clear. 2mL of filtered 25% Mayer's haematoxylin (008011; ThermoFisher Scientific, UK) was added as a nuclear counterstain to the wells. After 5 minutes, the counterstain was aspirated and discarded. The cells were washed with warm tap water, and the plate/wells kept wet to ensure the integrity of the lipid vacuoles. The cells were then visualised using a phase contrast inverted light microscope at 10X and 20X magnification.

2.3.3. Characterisation of MSC by chondrogenic differentiation

2.3.3.1. Preparing chondrogenic differentiation medium

An "incomplete" and "complete" chondrogenic media were prepared from the Human Mesenchymal Stromal Cell differentiation BulletKit™ – chondrogenic (PT-3003; Lonza, USA). An incomplete chondrogenic medium was prepared by adding SingleQuots™ of dexamethasone, ascorbate, insulin-transferrin-selenium supplement, gentamycin, amphotericin-B, sodium pyruvate, proline and L-glutamine to 185mL of chondrogenic differentiation basal medium.

Complete chondrogenic medium was made on the day of intended use by adding recombinant human TGFβ3 (100-36E, Peprotech, USA) to incomplete medium at a concentration of 10ng/mL.

2.3.3.2. Stimulating chondrogenic differentiation

At passage 4, $2.5x10^5$ MSC in complete MSC culture medium were transferred to a 15mL conical-bottom polypropylene tube and washed in sterile PBS, by gentle resuspension and centrifuging at a relative centrifugal force of 150g at 20±5°C for 5 minutes. The cells were then washed in incomplete chondrogenic medium, and the supernatant discarded from the resultant pellet. The cells were resuspended in 500µL of freshly-made complete chondrogenic medium, and left to incubate at 37°C in a hypercapnic (5% CO_2) atmosphere. The lids of the tubes were not fully tightened to allow gas exchange. A pellet was allowed to form, and the cells were left undisturbed for 48 hours. The spent medium was aspirated and discarded every 3 days, and replaced with freshly made complete chondrogenic medium; the bottom of the tube was gently agitated / flicked every 2-3 days to ensure the pellet remained free-floating. After 28 days of culture, the spent medium was fully aspirated, and the pellet embedded in PolyFreeze Tissue Freezing Medium (SHH0026; Sigma, UK), and snap-frozen in liquid nitrogen. The pellet was stored in a -80°C freezer, until cryo-sectioning to a thickness of 4µm.

2.3.3.3. Toluidine Blue staining

0.1% toluidine blue solution was prepared in acetic acid–sodium acetate buffer solution (pH 4.0). The buffer solution was prepared and pH balanced by adding 8.47mL of glacial acetic acid

(10060000; Fisher Scientific, UK) to 1.53mL of sodium acetate (S2889; Sigma-Aldrich, UK) solution (from anhydrous). Frozen sections were cut to 4µm thickness and fixed onto X-tra® glass microscope slides (3800050; Leica, UK). The slides were defrosted for 30 minutes. A wax boundary was drawn around the tissue on the slide. 200µL of 0.1% toluidine blue solution was applied to the sample. After 2 minutes, the slides were rinsed in tap water until it was running clear. The slides were serially dehydrated in 99% ethanol thrice, followed by clearing in xylene thrice. Each rinse was undertaken for 3 minutes. The slides were mounted with coverslips using non-aqueous DPX mounting medium (1005790500, EMD Millipore, UK).

2.3.4. Characterisation of MSC by osteogenic differentiation

2.3.4.1. Preparing osteogenic differentiation medium

Complete osteogenic medium was a product of the StemPro® Osteogenesis Differentiation Kit (A1007201; Gibco, UK), whereby 90mL of StemPro® Osteocyte Differentiation Basal Medium was added to 10mL of StemPro® Osteocyte Supplement and gentamycin (15750060; Gibco, UK) at a concentration of 5µg/mL.

2.3.4.2. Stimulating osteogenic differentiation

MSC were seeded at passage 3 in a 12-well tissue culture plate at a density of $1x10^4$ cells/well, in complete MSC culture medium (2mL/well) and cultured as described in section 2.2. At 60-70% confluence, the spent media were removed, and the cells washed in a working volume of sterile PBS, before replacing with pre-warmed complete osteogenesis differentiation medium. The cells

were checked daily for differentiation, and contamination. The spent media were aspirated and discarded every 3 days, and replaced with fresh complete osteogenesis differentiation medium. The culture continued for 14 days before the cells were washed twice in sterile PBS and fixed in 2mL of 10% neutral-buffered formalin. Following 30 minutes of incubation at room temperature, the cells were washed twice in water.

2.3.4.3. Alizarin Red-S staining

1% Alizarin Red S solution was prepared by diluting 1g of Alizarin Red S powder (A5533; Sigma-Aldrich, UK) in 100mL of distilled water, and pH adjusted to 4.1-4.3 using sodium hydroxide solution. The solution was filtered as previously described prior to use. Formalin-fixed cells in a 12-well plate as detailed in section 2.3.4.2 were washed in water. 0.5mL of the 1% Alizarin Red S solution was added to each well, and the plate left to agitate on a gently shaking platform for 30 minutes. The staining solution was then removed, and the wells washed in water and left to air dry, before being examined under an inverted light microscope.

2.4. Animal Husbandry

Male C57Bl/6 mice were purchased from Charles River UK Ltd. (Margate, UK) and acquired at an age of 7-9 weeks. They were housed and cared for at the University of Birmingham Biomedical Services Unit (Birmingham, UK) by standard care protocols. All procedures on the animals were carried out in accordance with the Animals (Scientific Procedures) Act 1986, UK, under project licence 70/7707 (care of Professor Philip Newsome) and underwent ethical review prior to approval and enactment. Male C57Bl/6 mice, aged between 8-10 weeks were used for the experiments. Mice were clinically assessed and weighed at least weekly throughout experiments. A 10% decrease in weight was deemed significant and warranted the mouse to be excluded from further injury and thus the experiment. Other signs of clinical distress were assessed during the standard observation period. If mice were found to be suffering and the situation deemed unsalvageable, the mice were euthanised. Otherwise, mice would be euthanised per protocol as scheduled by the experimental design (see relevant results sections)

2.5. Inducing toxin-mediated hepatic injury and fibrosis

2.5.1. Carbon tetrachloride

Protocols of chronic hepatic injury by CCl_4 have been conducted at the University of Birmingham BMSU previously[154]; a feasibility experiment was therefore not required.

CCl_4 (289116; Sigma-Aldrich, UK) was diluted 1:3 with mineral oil (M8410; Sigma, UK) in sterile conditions (biological safety cabinet), and transported to the BMSU in an autoclaved glass container. The mice were subject to twice-a-week IP injections of this solution at a dose of either 1 or 2µL/g body weight (b/w) for 6 weeks (12 doses in total), by the use of an appropriate syringe and a 28-30-gauge single-use needle. The mice were clinically assessed and weighed prior to every injection to instruct correct dosing. They were closely observed for any signs of acute clinical deterioration for 15 minutes after injection, before being housed for standard observations and follow up.

2.5.2. Thioacetamide

Protocols of chronic hepatic injury by TAA have not been conducted at the University of Birmingham BMSU previously. As such, small-scale feasibility studies were conducted to determine the safety of the proposed protocols. TAA (163678; Sigma-Aldrich, UK) was diluted in sterile UV treated water to a final concentration of 20mg/mL in a biological safety cabinet (stock solution) and passed through a sterile 0.22µm filter prior to use.

2.5.2.1. Intraperitoneal thioacetamide

The stock solution was transported to the BMSU in an autoclaved glass container. Mice were subject to IP injection of TAA (150mg/kg bodyweight) by the use of an appropriate syringe and a 28-30-gauge single-use needle[155–157]. Following 15 minutes of close observation, the mice were housed for standard observations and follow up.

2.5.2.2. Oral thioacetamide

The mice were housed and provided chow as per usual BMSU protocols, but their drinking water was substituted for TAA solution. Mice were given TAA in 1:5 diluted fruit squash (Robinson's orange and pineapple, single strength, no added sugar) at a dose of 100mg/L for 3 days, and then 300mg/L for 3 days, followed by 600mg/L for the rest of the duration (up to 16 weeks) (diluted from stock of 20mg/mL). Mice were weighed and clinically assessed for signs of distress daily (see Section 2.4 for exclusion criteria). The drinking bottles were weighed daily to determine adequate oral liquid intake.

2.6. Investigating the therapeutic effect of MSCs *in vivo*

The therapeutic effects of MSCs on the resolution of established fibrosis, or fibrogenesis were examined by injecting MSCs at different time points. These details are described in the experimental design sections of the results chapters. MSCs or a matched volume of their carrier (sterile 0.9% saline) were injected into the tail veins of experimental mice as described in section 2.2, and the mice euthanised per protocol as scheduled by the experimental design.

2.7. Mouse euthanasia; tissue and blood collection for analysis

Upon completion of an experiment, blood and tissue were collected from mice by the following methods:

- **Blood and serum**: Cardiac puncture under terminal anaesthesia by isoflurane. Up to 1000µL of blood was aspirated through a 25-gauge needle with an appropriate syringe and collected in a 1.5mL Eppendorf tube. The mice were immediately euthanised by cervical dislocation, and death confirmed. The clotted blood was centrifuged at 10,000 rpm for 10 minutes. The serum supernatant was aspirated and re-centrifuged under the same settings to clarify the supernatant from any cell debris. The serum was then collected and stored at -80°C.
- **Liver:** Abdominal contents were exposed by sleeve laparotomy and reflection. For cases intended for flow-cytometric (and not hydroxyproline) analysis the inferior vena cava was cannulated with a 26-gauge needle to flush the liver with 10mL of PBS. Swelling and pallor of the liver would confirm adequate flushing. The portal vein was cut to allow the flushed contents to escape the circulation. The liver was subsequently surgically dissected from the abdomen, and the gallbladder rejected.
    - The left lobe of the liver was placed in 10% neutral buffered formalin – for formalin-fixed paraffin embedding OR placed in RPMI 1640 Medium, GlutaMAX™ Supplement, HEPES (RPMI) with 2% FCS (7240021; Gibco, UK) for flow cytometry.

The other lobes were snap-frozen on liquid nitrogen:

- The median lobe was used for preparing acetone fixed frozen sections on glass slides

- The right lobe was used for hepatic hydroxyproline assay
- The caudate and quadrate lobes were used for molecular biology including RNA isolation

2.8. Flow cytometry analysis for myeloid cells

2.8.1. Isolation of immune cells from mouse liver

The left lobe of experimental mouse livers was collected in RPMI with 2% FCS as described in section 2.7 from the BMSU on ice. Upon return to the laboratory, all processing was undertaken in a biological safety cabinet. The liver tissue was manually homogenised using a sterile plunger in an appropriately sized vessel (6-well plate). The homogenised tissue was then passed through a 70µm cell strainer with RPMI/2%FCS in to a 15mL conical-bottom polypropylene tube, which was topped up with RPMI/2%FCS and centrifuged at 2000 RPM at 4°C for 5 minutes. The supernatant was discarded, and the pellet was resuspended in 5mL of RPMI/2%FCS. The cell suspension was then gently layered upon 7mL of cold (4°C) Optiprep solution in a 15mL conical-bottom polypropylene tube and centrifuged at a relative centrifugal force of 1000g at 20°C for 25 minutes, with the brakes off. Optiprep solution was made by diluting 1 unit of OptiPrep™ Density Gradient Medium (D1556; Sigma, UK) in 2.75 units of PBS. The resulting band of cells at the interface between the RPMI and the Optiprep solution was aspirated using a sterile Pasteur pipette and transferred to a 15mL conical-bottom polypropylene tube, and washed in RPMI/2%FCS by centrifugation at 2000 RPM at 4°C for 5 minutes. The supernatant was then discarded, and the pellet resuspended and washed in FACS buffer. The resulting pellet was then re-suspended in 300µL of FACS buffer.

2.8.2. Isolation of immune cells from mouse blood

Upon terminal anaesthesia, blood was collected from experimental mice by cardiac puncture as described in section 2.7. 200µL of blood was collected in EDTA collection tubes (459036; Grenier Bio-One Ltd, UK). The blood was incubated at room temperature in an equal volume of 1X RBC lysis buffer (00-4333-57; eBioscience, Invitrogen, UK) for 5 minutes. The reaction was stopped by adding 20mL of PBS and centrifuged at 2000 RPM for 5 minutes. The pellet was then twice washed in FACS buffer by centrifugation, before re-suspending in 300µL of FACS buffer.

2.8.3. Antibody staining

200µL of the each cell suspension samples were loaded to a well of a 96-well plate. The plate was centrifuged at a relative centrifugal force of 1700g with brakes attenuated to a setting of 3 on a Harrier benchtop 15/80 centrifuge. The supernatant from each well was discarded. The cells were incubated with 100µL of APC CY7-conjugated live/dead stain (1:1000 concentration) for 30 minutes at 4°C, protected from light. The cells were then twice washed with FACS buffer, before adding 60µL of the myeloid primary antibody mixture to each test well, mixed, and left to incubate at 4°C, protected from light for 30 minutes. The cells were then twice washed in FACS buffer and fixed for 20 minutes in 200µL of 3% formalin (37% formaldehyde (F1635, Sigma, UK)) at room temperature. Cells were then twice washed and subsequently re-suspended in 200µL of FACS buffer before analysing on a Cyan ADP flow cytometer (Beckman Coulter, UK).

Alongside the test-samples, unstained cells, single colour samples and IMCs were used as controls.

The primary myeloid antibody mixture was prepared as described in Table 2.2. The dilution factors had been pre-optimised by others in the Newsome laboratory.

Table 2-2: Primary antibody mixture for myeloid panel

Antibody	Cat#, supplier	*Isotype (IMC Source)*	Fluorescence tag	Dilution factor	Antibody volume
CD11b	53-0122-80, eBioscience	*Rat IgG2b (400633, BioLegend)*	FITC	100	0.6µL
Ly6c	128031, BioLegend	*Rat IgG2c (400725, BioLegend)*	BV 421	20	3µL
CD45	45-0451-82, eBioscience	*Rat IgG2b (400631, BioLegend)*	PerCP-Cy 5.5	200	0.3µL
Gr1	108411, BioLegend	*Rat IgG2b (400611, BioLegend)*	APC	100	0.6µL
CD11c	117318, BioLegend	*Armenian hamster IgG (400921, BioLegend)*	PE-Cy7	100	0.6µL
CD3	100233, BioLegend	*Rat IgG2b (400547, BioLegend)*	BV 510	20	3µL
F4/80	123109, BioLegend	*Rat IgG2a (400507, BioLegend)*	PE	20	3µL
PBS / well					48.9µL
Total vol / well					60µL

Antibodies to isolate and analyse myeloid cells from mouse liver and serum cells. 60µL of cell suspension were incubated in a primary antibody panel as described in this table for 30 minutes at 4°C, protected from light. Single colour staining of cells and IMC staining of cells were done using the same dilution factors as described in the table.

FlowJo 8.7 for Mac (Ashland, Oregon, USA) was used to analyse the data. The software's in-built compensation matrix (Compensation Wizard) was used to compensate for the different fluorochromes. Data was analysed and represented as cells/mg of liver tissue or per 100µL of blood.

2.8.4. Gating strategies for myeloid cells

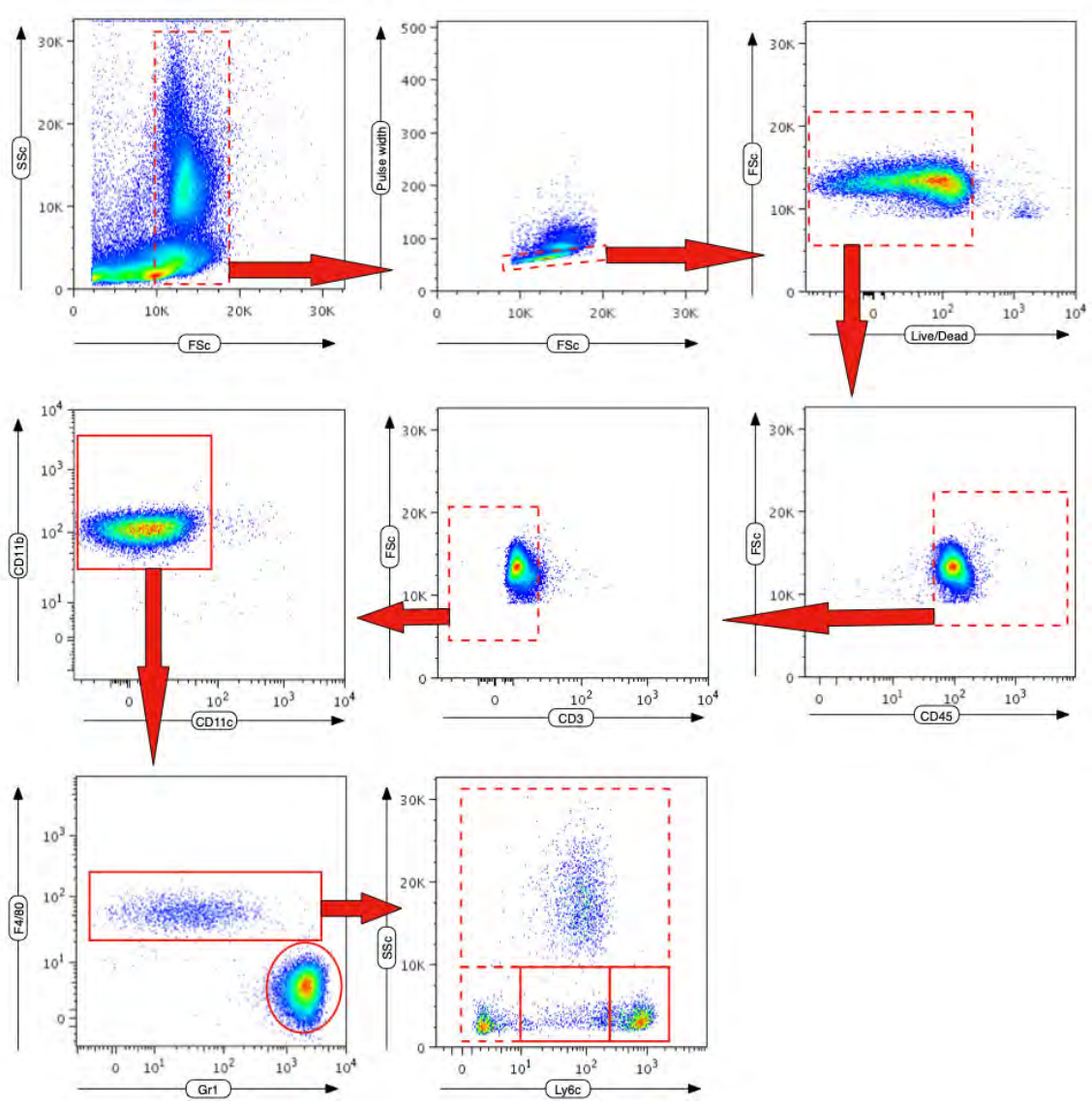

Figure 2-1: Flow cytometry gating strategy for myeloid cell populations

Cells of myeloid origin were isolated from mouse liver and blood and analysed by flow cytometry. A generous gate was selected by forward scatter (FSc) and side scatter (SSc). Singlets were selected by gating FSc by pulse width. Live cells (not taking up the live-dead marker) were selected, and cells were subsequently gated as CD45+ (leucocytes), CD3- (non-lymphoid). CD11b+/CD11c- cells select out myeloid non-DC cells. F4/80+ cells select out the macrophages (and eosinophils), and the Gr1+/F4/80- population select out neutrophils. The F4/80 cells with high side scatter likely represent eosinophils, whereas the low side scatter cells are macrophages that can be subdivided by their Ly6c expression. $Ly6c^{hi}$ cells represent pro-fibrogenic inflammatory macrophages, and the $Ly6c^{lo}$ macrophages represent mature restorative macrophages.

2.9. Liver biochemical tests

100µL of serum (from each mouse) was analysed for alanine aminotransferase (ALT), measured by an Olympus AU400 analyser (OLY-AU400; Beckman Coulter, USA) at the clinical biochemistry laboratory of the Birmingham Women's Hospital (Birmingham, UK) as a surrogate for on-going hepatocellular damage or membrane dysfunction.

2.10. Hepatic hydroxyproline assay

The hydroxyproline assay is a biochemical surrogate measure of collagen content of a tissue, which assumes that collagen is nearly unique as a protein that contains the amino acid hydroxyproline.

2.10.1. Preparation of Chloramine-T solution

A buffer was prepared by mixing 25g citric acid monohydrate (C1909; Sigma-Aldrich, UK), 6mL of glacial acetic acid (10060000; Fisher Scientific, UK), 60g of sodium acetate trihydrate (236500; Sigma-Aldrich, UK), 17g of sodium chloride (S9888-M; EMD Millipore, UK), and dissolving in water to a total volume of 500mL. The buffer was corrected to pH 4 and stored at 4°C until required. Chloramine-T solution was prepared by dissolving 1.75g of sodium N-chloro-p-toluenesulfonamide (402869; Sigma Aldrich, UK) in 10mL of distilled water, 10mL of 2-propanol (I9516; Sigma, UK), 80mL of buffer and 500mL of distilled water. The solution was adjusted to pH 6.

2.10.2. Preparation of Ehrlich's solution

Ehrlich's solution was prepared by dissolving 7.5g of p-dimethylaminobenzaldehyde (S156477; Sigma Aldrich, UK) in 30mL of 2-propanol (I9516; Sigma, UK) and 13mL of 60% perchloric acid (1.00518; EMD Millipore, UK). This was made freshly on the day of use.

2.10.3. Preparation of hydroxyproline standards

The hydroxyproline standards deliver a "standard curve" of absorbance values against which to determine the hydroxyproline content of the test samples. 25mg of trans-4-hydroxy-L-proline (H54409; Aldrich, UK) was dissolved in 250mL of 0.001N hydrochloric acid (13-1683; SAJ, UK) to make stock solution of 100µg/mL. To make standards, we diluted stock solution to 4, 2, 1, 0.5, 0.25, and 0µg in 50µL of distilled water.

2.10.4. The hydroxyproline assay

50-100mg of the right lobe of the liver was used for this assessment. The wet weight of each sample was noted, before it was transferred to a 1.5mL Eppendorf tube containing 0.5mL of ice-cold double distilled water. The tissue was then manually homogenised using a hand-held pellet pestle (Z359971; Sigma, UK), before a further 0.5mL of ice-cold distilled water was added to the sample. 125µL of 3.05N trichloroacetic acid solution (T0699; Sigma, UK) was added to the sample before being left to incubate on ice at 4°C for 30 minutes. The sample was centrifuged at 15,000 rpm for 5 minutes at 20±5°C. The supernatant was discarded from each sample, and the resultant pellet extracted with a fresh non-plugged glass Pasteur pipette (612-1701; VWR, UK) and transferred to a 12x75mm borosilicate Schott® culture tube (Z620246-50EA; Aldrich, UK). 500µL of 6N hydrochloric acid (13-1683; SAJ, UK) was then added to each tube, and a screw lock lid with rubber insert was applied tightly. Each tube and lid were checked for defects prior to use to ensure there was no escape of hydrochloric acid gas from the subsequent step. The samples were left at 120°C for 16 hours to allow hydrolysis, before the lids were removed, and the samples were left for a further 48 hours at 80°C for complete desiccation. The samples were then removed from the

oven and left to cool to room temperature. The desiccated precipitate was suspended in 500µL of distilled water with the aid of a long glass Pasteur pipette (612-1701; VWR, UK), and mixed using a laboratory bench-top vortex mixer. The mixture was then added to the top chamber of a sterile 1.5mL Costar® Spin-X® polypropylene centrifuge tube with a 0.45µm nylon filter membrane (CLS8163; Corning, UK). The tubes were centrifuged at 15,000 rpm for 5 minutes. 50µL of the filtered solution was then transferred to a clean 2mL clear borosilicate tube with solid top rubber lined cap (224721; DWK, UK). The hydroxyproline standards were prepared as described in section 2.10.3 to run alongside the test samples. 950µL of double-distilled water was added to each sample in the tubes. 500µL of chloramine-T solution (section 2.10.1) was added to each sample, lids applied, and mixed by use of a laboratory bench-top vortex mixer. After 20 minutes at room temperature, 500µL of Ehrlich's solution (section 2.10.2) was added to each sample, mixed by vortex, and left at 65°C for 15 minutes in a pre-warmed oven. Samples were then passively cooled to room temperature. 200µL of each sample were loaded to a clear, flat-bottom 96-well plate in triplicates. A plate reader (micro-well plate colorimeter) was then used to measure light absorbance at 561nm. The test readings were normalised by weight of liver tissue used for each sample.

2.11. Preparing slides from formalin-fixed paraffin embedded tissue for staining

Formalin-fixed tissue (left lobe of liver) was prepared in tissue cassettes and embedded in paraffin wax to form tissue blocks that were stored at room temperature. The formalin-fixed paraffin embedded (FFPE) tissue blocks were cut at a thickness of 3µm onto X-tra® glass microscope slides (3800050; Leica, UK) using a heated water bath and stored at room temperature until subsequently required. The slides were de-waxed by serial rinsing in xylene thrice, followed by 99% ethanol thrice, and rehydrated in water twice. Each rinse/wash was undertaken for 3 minutes.

2.11.1. Haematoxylin and eosin staining

Following dewaxing, dehydrating and washing, slides were placed in Harris haematoxylin stain (PRC/R/51; PFM Medical, UK) for 4 minutes, then in water for 2 minutes, and differentiated in 1% acid alcohol for 30 seconds. They were then washed in water for 2 minutes, then Scott's Tap Water (PRC/R/76; PFM Medical, UK) for 30 seconds and then in water again for a further 2 minutes before being stained in 1% aqueous eosin (PRC/11/1; PFM Medical, UK) for 1 minute. The slides were then washed in water for 4 minutes before being serially dehydrated in 99% ethanol for 3 minutes thrice, followed by clearing in xylene for 3 minutes thrice. The slides were mounted with coverslips using non-aqueous DPX mounting medium (1005790500, EMD Millipore, UK).

2.11.2. Immunohistochemistry (IHC)

Paraffin embedded sections on glass slides were prepared, cleared, dehydrated and washed as described in section 2.11. A wax pen was used to draw a boundary around the sections on each slide, and the slides placed in a rocking humidified chamber for all subsequent steps. Endogenous peroxidase activity was blocked by treating sections with 150µL of Dako REAL peroxidase blocking solution (S202386-2; Agilent, UK) for 20 minutes. Slides were then serially washed for 5 minutes at a time with 0.1% Tween-20 (P2287; Sigma, UK) in BioUltra tris-buffered saline, pH 7.6 (94158; Sigma, UK) (TBS-T), twice. Antigen retrieval was performed by immersing the slides in the pre-warmed solution of pH-adjusted buffer and heating at high power in a microwave oven for 15 minutes. The slides were retrieved after 20 minutes of passive cooling to room temperature, and washed in TBS-T, twice. Non-specific antibody binding was blocked by applying 150µL of 2X casein buffer solution (10X casein buffer (SP-5020; Vector laboratories, UK) diluted in TBS) to the sections for 20 minutes. This was replaced with 200µL of primary antibody, diluted to the required concentration as described in Table 2.3. After an hour, the sections were washed in TBS-T, twice, before adding the appropriate ImmPRESS™ horseradish peroxidase conjugated secondary antibody (Vector laboratories, UK). After 30 minutes, the slides were twice washed with TBS-T. 200µL of ImmPACT DAB peroxidase™ substrate (SK-4105; Vector laboratories, UK) was added to the sections for up to 90 seconds, or until a colour change was noted in the positive control, before washing rapidly in water. For sections that were counterstained, 200µL of filtered 1:4 diluted Mayer's haematoxylin (008011; Thermo Fisher, UK) was used for 15 seconds before serial washing in a warm, and then cold water bath for 2 minutes with agitation. The slides were dehydrated, cleared, washed and mounted with a coverslip as described in section 2.11.1. The

IHC experiments were performed with isotype controls, no primary antibody controls and negative tissue controls for each antibody.

Table 2-3: Antibodies for immunohistochemistry

Antibody	Supplier; cat #	Antigen retrieval	Conc.	Clonality	Host; isotype	Target	Diluent; dilution	Secondary; cat #
CD45	Invitrogen, UK; 14-0451-81	pH 8	0.5mg/mL	mono	Rat; IgG2b, κ	mouse	TBS; 1/200	Anti-rat, from goat; MP-7404
Isotype control	*Invitrogen, UK; 14-4031-81*	*pH 8*	*0.5mg/mL*	*mono*	*Rat; IgG2b*	*-*	*TBS; 1/200*	*Anti-rat, from goat; MP-7404*
αSMA	Abcam, UK; ab5694	pH 8	0.2mg/mL	poly	Rabbit; IgG	mouse	TBS; 1/200	Anti-rabbit from horse; MP-7401
Isotype control	*Abcam, UK; ab37415*	*pH 8*	*5mg/mL*	*poly*	*Rabbit; IgG*	*-*	*TBS; 1/5000*	*Anti-rabbit from horse; MP-7401*

2.11.3. Picrosirius red staining

Formalin-fixed paraffin embedded sections cut to 8µm onto glass slides were used. The slides were prepared, cleared, dehydrated and washed as described in section 2.11. A wax pen was used to draw a boundary around the sections on each slide, and the slides placed in a humidified chamber. Sections were moistened with distilled water prior to applying 200µL of 0.5% polymolybdic acid (HT153; Sigma, UK), for 5 minutes. The slides were transferred to a metal slide rack and bathed in PSR solution at room temperature on a rocking plate for 90 minutes. The PSR solution was made by dissolving 100mg of Direct Red 80 (365548; Sigma Aldrich, UK) in 100mL of saturated picric acid (P6744; Sigma, UK). The slide rack was then removed from the PSR solution,

and serially rinsed with agitation in 2 baths of acidified water (0.5% glacial acetic acid (10060000; Fisher Scientific, UK)) for 30 seconds, a bath of 0.1% (w/v in acidified water) fast green FCF (F7252; Sigma, UK) for 1 minute, 2 further baths of acidified water for 30 seconds, 3 baths of fresh 99% ethanol for 30 seconds, before finally being transferred to xylene. After 5 minutes, the slides were mounted with coverslips using non-aqueous DPX mounting medium (1005790500, EMD Millipore, UK).

2.11.4. Digitising slide images for analysis

Physical slides were converted to virtual slides by the use of an automated slide scanner (Axio Scan.Z1; Zeiss, Germany). A fixed acquisition protocol was designed and used on designated imaging and analysis software (Zen slidescan 2012 SP1, blue edition; Zeiss, Germany):

Camera	Hitachi HV F202
Objective	20x
Pixel resolution	0.22µm/pixel
Contrasting technique	Transmitted light brightfield
Z stack	Yes
Compression	Lossless
Stitching	Online
File format	.czi

The .czi files containing the whole section were opened in the aforementioned Zen image processing software, and images magnified to ensure adequate detail was obvious, and colour contrast adjusted uniformly amongst a batch of slides. The visible image on the screen was

captured and saved in a .png format; further images from the same slide were acquired to ensure at least 80% of each entire slide / section was captured.

2.11.5. Morphometric analysis of PSR and IHC stained liver tissue sections

The .png file was opened in Image J (NIH/LOCI, University of Wisconsin, USA) software, and converted to an RGB stack image. The image was then set to the green channel for PSR stained slides, and the blue channel for DAB, and AEC stained slides. An automatic threshold was utilised and adjusted to ensure no aberrant positive areas were demarcated. Areas of the slide that were dead space (e.g. biliary trunk) were removed from analysis using the lasso tool. The positive area was then calculated by the software as a % area of the working field. An arithmetic mean of the values from images of the same slide estimated the overall positively stained % area.

2.12. *In vivo* localisation of MSC after IV injection

At passage 4, the required number of MSCs were collected (10^6 MSC / mouse + $2x10^6$ for flow cytometry) in complete MSC culture medium at a suspension concentration of $1x10^7$ cells/mL to undertake the experiment as designed (detailed in Chapter 6). The Qtracker® 605nm cell labeling kit (Q25001MP; Life technologies, Invitrogen, UK) was used to label the MSCs in culture with fluorescent nanocrystals. 1µL of Component A and Component B of the kit were mixed in a 1.5mL Eppendorf tube and incubated for 5 minutes at 20±5°C. 200µL of complete MSC culture medium was added to the labelling solution and mixed by vortex for 30 seconds. 100µL of the cell suspension (containing $1x10^6$ cells) was added to the labelling solution and incubated at 37°C in a hypercapnic environment for 1 hour. The cells were then washed in sterile saline twice. $1x10^6$ cells were tested for nanocrystal uptake and fluorescence on a Cyan ADP flow cytometer (Beckman Coulter, UK), against unstained cells. Labelled cells were otherwise prepared for injection into mice as described in section 2.2, injected into mice as described in section 2.6, and the mice euthanised by CO_2 inhalation. The carcasses were submerged and embedded in PolyFreeze Tissue Freezing Medium (SHH0026; Sigma, UK), and rapidly frozen on a bed of dry ice. They were then stored at -80°C until shipment to BioInVision Inc. in Cleveland, USA. BioInVision Inc. use CryoViz™ cryo-imaging technology to detect, spatially map and quantify fluorescent units (in this case, QuantumDot® labelled MSCs) at a microscopic resolution within a macroscopic (whole mouse) field of view. The technology and software rendered three-dimensional maps of the fluorescent cells in the mice, quantified the number of cells in whole organs, and two-dimensional virtual sections for analysis.

2.12.1. Flow cytometric analysis of QuantumDot® labelled cells

To determine the fidelity of uptake of the fluorescent nanocrystals, labelled cells were washed and suspended in FACS buffer before analysing on a Cyan ADP flow cytometer (Beckman Coulter, UK).

2.13. *In vitro* methodology

2.13.1. Storage, culture and subculture of LX2 cells

The immortalised human hepatic stellate cell line, LX2, was obtained from Dr Scott Friedman (Mount Sinai School of Medicine, New York, USA) and stored by Dr Emma Shepherd (Centre for Liver and Gastrointestinal Research, University of Birmingham, Birmingham, UK), in our laboratories. Cells were stored in liquid nitrogen at a concentration of $1x10^6$ in 1mL of serum with 10% DMSO.

Low-serum LX2 medium was used for cell culturing. It was prepared in a biological safety cabinet and consisted of DMEM with GlutaMAX™ supplement (11584456; Gibco, UK) with 2% heat-inactivated FCS (F9665; Sigma-Aldrich, UK), 1% penicillin/streptomycin (10,000U/mL; 15140122; Gibco, UK) and stored at 4°C.

For use, cells were transported from liquid nitrogen to the working laboratory on dry ice. The cells were then rapidly thawed in a 37°C water bath, and contents transferred to a 15mL conical-bottom polypropylene tube containing 12mL of pre-warmed complete low-serum LX2 culture medium at 37°C. The suspension was then centrifuged for 5 minutes at a relative centrifugal force of 400g at 20±5°C. The supernatant was subsequently discarded, and the pellet gently re-suspended in 8mL of complete low-serum LX2 culture medium by flicking the bottom of the tube and using a Pasteur pipette. The cell suspension was then transferred to 4 T-75cm^2 cell culture flasks ($2.5x10^5$ cells / flask) with a vented cap containing 15mL of pre-warmed complete low-serum LX2 culture medium

(total volume = 20mL / flask). Cells were incubated at 37°C in a hypercapnic (5% CO_2) atmosphere. They were inspected for confluence and contamination daily, and the medium changed every 2 days or earlier if a significant pH change was indicated by the phenol red (i.e. if it turned yellow). 70%-80% confluence could be expected at day 3, at which point the cells could be sub-cultured for expansion if required or prepared for seeding into multi-well plates for further analysis. For either, the medium was removed, and the cells washed with 10mL of sterile PBS, twice. The cells were then bathed in 7mL of pre-warmed (to 37°C) 1X TrypLE™ Express Enzyme (12605010; Gibco, UK), and incubated for 5 minutes in a 37°C incubator. The contents of the flask were then examined using an inverted light microscope to ensure the cells had dislodged from the surface of the flask. If not, the flask was kept on incubation for a further 2 minutes. The trypsin was neutralised by adding 15mL of complete medium (containing serum) to the flask, and the cell suspension then aspirated and transferred to a 50mL conical-bottom polypropylene tube. They were spun for 5 minutes at a relative centrifugal force of 400g at 20±5°C. The supernatant was subsequently discarded, and the pellet re-suspended in 5mL of complete medium. After ensuring adequate re-suspension, live cell numbers were calculated using a haemocytometer as described in section 2.2.

The remaining suspension was then spun for 5 minutes at a relative centrifugal force of 400g at 20±5°C. The supernatant was subsequently discarded and the cell pellet re-suspended fit for purpose.

- For sub-culturing cells the pellet was re-suspended in complete low-serum LX2 culture medium; $2.5x10^5$ cells in suspension were transferred to T-75cm^2 cell culture flasks as previously described.
- For long-term storage of cells, they were suspended in Cryostor® cell cryopreservation medium CS5 (CS299; Sigma Aldrich, UK) at a density of $1x10^6$ cells/mL, and 1mL transferred to 1.5mL cryovials. The cryovials were frozen at -80°C in a Mr. Frosty™ Freezing Container (51000001; Thermo Scientific, UK) to ensure a cooling rate of -1°C/minute, before they were transferred to liquid nitrogen storage.

2.13.2. Immunocytochemistry

LX2 cells were cultured as already described and seeded to 24-well plates with cover glass inserts at a density of $3x10^4$ cells per well.

LX2 cells were seeded in complete low-serum culture medium for 8 hours, and serum starved (supplemented with 0.1% bovine serum albumin (15260037, Gibco, UK) (BSA)) for 24 hours before exchanging the media for the test- or control-media. After 48 hours, the cells were washed in PBS twice before fixing in 10% neutral buffered formalin for 10 minutes. The cells were washed in ice-cold PBS and the plate stored at 4°C with 2mL of PBS in each well until such time that the cells were stained.

For staining, the PBS was removed, and the cells gently washed in PBS for 5 minutes. Cells were permeabilised in 0.1% Triton-X 100 (X100; Sigma-Aldrich, UK) in PBS for 10 minutes, before

washing twice for 5 minutes at a time with 0.1% Tween-20 (P2287; Sigma, UK) in PBS (PBS-T). Non-specific antibody binding was blocked by incubating the cells in 200µL of 2X casein buffer solution (10X casein buffer (SP-5020; Vector laboratories, UK) diluted in TBS) for 20 minutes. 200µL of primary antibody diluted in PBS to the required concentration as described in Table 2.4, was then added to the cells for 1 hour at room temperature. After washing twice in PBS-T, the appropriate ImmPRESS^{TM} horse radish peroxidase conjugated secondary antibody (Vector laboratories, UK) was added to the cells. After 30 minutes, the slides were washed twice with PBS-T. 200µL of AEC horseradish peroxidase substrate (SK-4200; Vector laboratories, UK) was added to the sections for up to 25 minutes, or until a colour change was noted in the positive control, before washing in water. The cells were then counterstained in 200µL of filtered 1:4 diluted Mayer's haematoxylin (008011; Thermo Fisher, UK) for 15 seconds before serial washing in a warm, and then cold-water bath for 2 minutes, until the water was running clear. The cover glass inserts were carefully removed, and mounted to microscope slides (3800050; Leica, UK) by using VectaMount AQ aqueous mounting medium (H-5501; Vector laboratories, UK). The immunocytochemistry (ICC) experiments were performed with isotype controls.

Table 2-4: Antibodies for immunocytochemistry

Antibody	Supplier; cat #	Conc.	Clonality	Host; isotype	Target	Diluent; dilution	Secondary; cat #
Vimentin (EPR3776)	abcam, UK; ab92547	0.5mg/mL	mono	Rabbit; IgG	human	PBS; 1/500	Anti-rabbit from horse; MP-7401
Isotype control (EPR25A)	*abcam, UK; ab172730*	*1.5mg/mL*	*mono*	*Rabbit IgG*	-	*PBS; 1/1500*	*Anti-rabbit from horse; MP-7401*
αSMA	abcam, UK; ab5694	0.2mg/mL	poly	Rabbit; IgG	human	PBS; 1/200	Anti-rabbit from horse; MP-7401
Isotype control	*abcam, UK; ab37415*	*5mg/mL*	*poly*	*Rabbit IgG*	-	*PBS; 1/5000*	*Anti-rabbit from horse; MP-7401*
Ki-67 (MIB-1)	Agilent, Dako, UK; M7240	0.2mg/mL	mono	Mouse; IgG1, κ	human	PBS; 1/200	Anti-mouse from horse; MP-7402
P21 (WAF1/Cip1)	Agilent, Dako, UK; M7202	0.2mg/mL	mono	Mouse; IgG1, κ	human	PBS; 1/200	Anti-mouse from horse; MP-7402
Isotype control	*Invitrogen, UK; 14-4714-81*	*0.5mg/mL*	*mono*	*Mouse; IgG1, κ*	-	*PBS; 1/100*	*Anti-mouse from horse; MP-7402*

2.13.2.1. Quantifying positively stained cells

Physical slides were converted to virtual slides by the use of an automated slide scanner and processed for analysis as described earlier. The .png file was then be opened in Image J software. All available cells (up to a maximum of 500) (nuclei stained by Mayer's haematoxylin) in serial high power fields were counted, and all positively stained cells were separately recorded. The % of positively stained cells was used to estimate the total positive staining on the whole slide.

2.13.3. Senescence associated β-galactosidase assay

Senescent cells display increased senescence-associated expression of β-galactosidase (SA-β-gal) activity. A senescence detection kit (ab65351; abcam, UK) was used to detect senescence in LX2 cells in 12-well plates.

$5x10^4$ LX2 cells were seeded per well in complete low-serum culture medium for 8 hours. After confirmation of adherence to the bottom of the wells by microscopy, the cells were serum starved and supplemented with 0.1% BSA for 24 hours. They were then gently washed twice with sterile PBS, before adding 3mL of either control or test media.

After 36-48 hours (at 70-80% confluence), the spent media were removed from the wells, and the cells washed with PBS. The cells were fixed with 0.5mL (470µL staining solution + 5µl staining supplement + 25µl of X-gal solution (20mg/mL) in DMSO) of supplied fixative solution for 15 minutes at room temperature, and then washed twice in PBS. 0.5mL of the supplied staining solution mixture was added to each well and incubated at 37°C (normal CO_2 atmosphere), shielded from light for 12 hours. The cells were then observed under a light microscope to determine blue (positive) colour development and photographed using a digital camera. The images (saved as .jpeg files) were used for qualitative analysis.

2.13.4. Cell proliferation assay

The CyQUANT® Cell Proliferation Assay Kit (C7026; Thermo Scientific, UK) was used to determine the density of cells in culture, and thus used as a proliferation assay.

It utilises a fluorescent green dye that exhibits enhancement when bound to cellular nucleic acids. Frozen cells are thawed and lysed in the presence of a solution containing the green dye, and the fluorescence is measured using a microplate reader.

$5x10^3$ LX2 cells were seeded into wells of 5 identically designed flat-bottomed clear 96-well plate, and incubated in complete low-serum LX2 culture medium for 8 hours. The cells were serum starved and supplemented with 0.1% BSA. The medium was exchanged for test or control medium after 24 hours (time zero), and plates were serially frozen at 0, 24, 36, 48 and 72 hours.

The reagent (herein described as Cy-solution) was prepared as per manufacturer's recommendation but modified to detect up to $1x10^5$ cells in a 200µL volume. Subsequently, the plates were thawed at room temperature, and 200µL of the Cy-solution was added to each well, alongside standard curve samples. After 5 minutes of incubation, shielded from the light, the sample reading of fluorescence were measured using a fluorescence microplate reader with filters appropriate for 480nm excitation and 520nm emission maxima.

2.13.4.1. CyQUANT® standard curve

A reference standard curve was created to convert sample fluorescence values in to absolute LX2 cell numbers. LX2 cells were cultured in complete culture media, detached, and collected as a pellet as previously described. Cells were washed in sterile PBS twice, and suspended to a density of 10^6 cells / mL of PBS. The cell suspension was then divided in to aliquots of 1mL in 1.5mL

Eppendorf tubes, and centrifuged at 1,500 rpm for 5 minutes. The supernatant was discarded, and the pellet was frozen at -80°C.

At the time of analysis, the pellet was thawed at room temperature, and re-suspended in 1mL of the Cy-solution by vortexing. A dilution series was generated in a 96-well plate (flat-bottom, clear) using the Cy-solution as the diluent to make dilutions corresponding to cell numbers of $5x10^3$ to $1x10^5$, ensuring to include a sample with no cells as a negative control. As with the test samples, the standard curve samples were analysed in technical triplicates. After 5 minutes of incubation, shielded from light, the fluorescence was measured on a microplate reader as described.

2.13.5. Cell apoptosis assay

The induction of apoptosis in LX2 cells was assessed in different culture conditions by the use of an Annexin-V apoptosis detection kit (ab14085; abcam, UK). $3x10^5$ cells were seeded in to wells of a 6-well plate in complete low-serum LX2 culture medium. After 8 hours, the cells were serum starved and supplemented with 0.1% BSA for 24 hours. The media were then exchanged for test and control media (5mL per well) as required for 48 hours. A positive control was designed, whereby cells were cultured in compete medium for 44 hours, and then gliotoxin (G9893; Sigma, Aldrich, UK) was added at a concentration of 6nM for the final 4 hours. Upon completion of 24 hours, the media were collected from each well in 15mL conical-bottom polypropylene tubes, and the remaining adherent cells were detached with trypsin as previously described. Enzymatic activity was neutralised with one volume of serum-containing medium, and the cells transferred to the same corresponding polypropylene tubes. The cells were collected by centrifugation (400g

for 5 minutes), the supernatant discarded, and the cells suspended in warm PBS, counted, pelleted, and re-suspended to a density of 1-5x10^5 cells in 500µL of 1X binding buffer supplied in the kit in a 1.5mL Eppendorf tube. 5µL each of Annexin V-FITC and propidium iodide were added to each cell suspension and incubated at room temperature for 5 minutes shielded from light, before analysing on a Cyan ADP flow cytometer (Beckman Coulter, UK).

2.14. Quantitative PCR

2.14.1. RNA extraction from mouse liver tissue

The RNeasy Mini Kit (74104; Qiagen, UK) was used to extract RNA from murine hepatic tissue. All instruments and general consumables were pre-treated in an ultraviolet light box for 20 minutes prior to use. 20-30mg of the caudate or quadrate lobe of the sample mouse liver was homogenised in a sterile GentleMACS M tube (130-093-236; Miltenyi Biotec, UK) containing 600µL of RLT buffer supplemented with 10µL/mL of 2-β-mercaptoethanol (M6250; Aldrich, UK). Samples were then mechanically homogenised and disrupted in a GentleMACS Dissociator (130-093-235; Miltenyi Biotec, UK) using program RNA.01_01. Following centrifugation for 1 minute at 2,000 rpm, the homogenate was transferred to a 1.5mL Eppendorf tube, and centrifuged for 3 minutes at 13,000 rpm. The supernatant was aspirated (the debris discarded) and mixed with one volume (600µL) of 70% ethanol. The sample was then transferred to the upper chamber of a RNeasy Spin Column and centrifuged at 13,000 rpm for 20 seconds. The flow-through was discarded from the lower collection tube. 350µL of RW1 buffer was added to the upper chamber of the spin column and centrifuged at 13,000 rpm for 20 seconds. The flow-through was discarded. 80µL of RNase-free DNase solution (79254; Qiagen, UK) was carefully added to the silica membrane of the spin column. After 15 minutes, 350µL of RW1 buffer was added to the upper chamber of the spin column and centrifuged at 13,000 rpm for 20 seconds. The flow-through was discarded. 500µL of RPE buffer was then added to the upper chamber of the spin column and centrifuged at 13,000 rpm for 20 seconds. This was then repeated, with the flow through being discarded on each occasion. The spin column was then transferred to a new collection tube and centrifuged for 2

minutes at 13,000 rpm. Upon completion, the spin column was transferred to a nuclease-free 1.5mL Eppendorf tube, and 50µL of sterile pre-warmed nuclease-free water (12994; Qiagen, UK) was added to the spin column membrane and centrifuged at 13,000 rpm for 1 minute. The eluate was then replaced on to the spin column membrane and re-centrifuged at 13,000 rpm. The spin column was then discarded, leaving the eluate (RNA) for analysis and use. The concentration of the RNA was determined by measuring the absorbance at 260nm in a spectrophotometer. The purity was estimated by measuring the ratio of readings at 260nm and 280nm (target value 1.9±0.1), and at 260nm and 230nm (target value 2.1±0.1). In the event that the RNA was not an adequate purity, it was discarded, and the extraction process was repeated.

2.14.2. RNA extraction from LX2 cells

A washed pellet of 1-5x10^6 cells was disrupted in 600µL RLT buffer and homogenised by passing the disrupted lysate through a blunted 21-gauge needle attached to a sterile plastic syringe 10 times. Otherwise the protocol was as described in the section above.

2.14.3. cDNA synthesis

All instruments and general consumables were pre-treated in an ultraviolet light box for 20 minutes prior to use. 2µg of RNA from each sample was made up to a total volume 10.5µL with sterile nuclease-free water in a 0.2mL DNase- and RNase-free PCR microtube (Z374873; Sigma, UK). 0.5µL of random primers (C1181; Promega, UK) and 1µL of 10mM-each dNTP mix (R0192Thermo Scientific, UK) were then added to each sample, and the sample tubes transferred

to a pre-heated thermo-cycler plate and incubated for 5 minutes at 65°C. The sample tubes were quickly chilled on ice, and the contents of the tubes collected to the bottom by brief centrifugation. 4µL of 5x First Strand Buffer (18064; Invitrogen, UK), 2µL of 0.1M dithiothreitol (18064; Invitrogen, UK) and 1µl of nuclease free water was added and mixed to each sample. The samples were left to incubate for 2 minutes at 25°C. Finally, 1µL of SuperScript™ II reverse transcriptase (18064; Invitrogen, UK) was added to each sample, and mixed gently. Samples were incubated at 42°C for 50 minutes, and then the reaction was inactivated by heating at 70°C for 15 minutes. The samples were then stored at -20°C until ready for use.

2.14.4. Real time quantitative polymerase chain reaction (qPCR)

All instruments and general consumables were pre-treated in an ultraviolet light box for 20 minutes prior to use. LightCycler® 384 multi-well plates (04729749001; Roche, UK) were used, and samples were prepared on ice. Samples were made up in a final volume of 10µL containing 5µL of TaqMan® minor groove binder gene probe (Table 2.5) with a 5' FAM reporter dye (4331182, 4351372; Thermo Fisher, UK), 0.3µL of 2X reaction TaqMan® Universal PCR Master Mix II (4304437; Applied Biosystems, UK), 4.2µL of nuclease free water and 0.5µL of cDNA. Each sample and gene were tested in technical triplicate. No-RNA, and no-cDNA samples were used as negative controls. Samples were collected to the bottom of the wells by centrifugation at 1,500 rpm for 1 minute and sealed using the supplied sealing foil (04729757001; Roche, UK). The samples were processed using a LightCycler® 480 Instrument II (05015243001; Roche, UK). The PCR acquisition programme consisted of polymerase activation (95°C for 10 minutes), then denaturing and annealing over 40

cycles (95°C for 15 seconds, 60°C for 1 minute), with the fluorescence being recorded at the end of each cycle.

The amplification curves for each reaction were analysed against their technical replicates; sample results with obvious errors (high background noise, or no discernible curve) were discarded. A threshold to analyse cycling threshold (Ct) was manually set in the bottom third of the log-linear exponential phase, above any background noise, and kept constant per plate. Relative differences between samples were determined using the ΔΔCt method / $2^{-\Delta\Delta Ct}$ [158], whereby:

- ΔCt (sample) = Ct (target gene) – Ct (housekeeping gene)
- ΔΔCt = ΔCt (test sample) – ΔCt (control)

The ratio of the target gene in sample of interest against a control sample was calculated by $2^{-\Delta\Delta Ct}$.

Table 2-5: Probes for qPCR

Mouse gene probes	TaqMan® ID	Species	Assignment
Tgfb1; transforming growth factor, beta 1	Mm01178820_m1	Human	target
Col1a1; collagen, type I, alpha 1	Mm00801666_g1	Human	target
Col3a1; collagen, type III, alpha 1	Mm00802331_m1	Human	target
Acta2; Actin, alpha 2 smooth muscle	Mm00725412_s1	Human	target
Mmp2; Matrix metallopeptidase 2	Mm00439498_m1	Human	target
Mmp9; Matrix metallopeptidase 9	Mm00442991_m1	Human	target
Timp1; Tissue inhibitor of metalloproteinase 1	Mm00441818_m1	Human	target
Actb; Actin, beta	Mm02619580_g1	Human	reference
Human gene probes	TaqMan® ID	Species	Assignment
COL1A1; collagen type I, alpha 1	Hs00164004_m1	Human	target
ACTA2; actin, alpha 2 smooth muscle	Hs00426835_g1	Human	target
PPARG; peroxisome proliferator activated receptor gamma	Hs01115513_m1	Human	target
PDGFRB; platelet derived growth factor receptor beta	Hs01019589_m1	Human	target
SRSF4; serine and arginine rich splicing factor 4	Hs00900675_m1	Human	reference

2.15. Statistics

Data were analysed using GraphPad Prism version 8.1.0 for Windows (San Diego, California, USA). Data sets were tested for normality by the Shapiro-Wilk test. Non-parametric data were summarised using median and 95% confidence interval (CI) and compared using the Mann-Whitney test. Parametric data were summarised using the mean and standard deviation and compared using the unpaired Student's-t test. Power calculations were conducted to determine the necessary sample size for the intervention experiments to achieve a change of 25% of PCR CPA to a statistical power of 90% with a specific α error of 0.05. The data was presumed to be parametrically distributed for the purposes of the calculation and a two-tailed test was performed.

Chapter 3

Models of liver fibrosis and resolution

3.1. Background and context

The over-arching aim of this body of work is to examine the therapeutic effect of a putative anti-fibrotic agent – namely mesenchymal stromal cells – in the setting of established liver fibrosis. Animal models remain the gold standard of pre-clinical fibrosis research owing to their reported discrimination to the complex interplay between the multiple cell types and pathways that govern fibrosis *in vivo*.

3.1.1. An ideal model to test the effect of a therapeutic agent on established liver fibrosis

A model, by definition will differ from the original against which it is compared. An ideal model should have fidelity, by which the overall proportionate difference is minimal, and discrimination, by which the extent the model reproduces a particular property of the original is conserved[159]. Such models may not be readily accessible. Therefore, a pragmatic approach is to accept low fidelity, under the assumption of high discrimination – in this case, for fibrosis. Though the field accepts that the fibrogenic pathways for many of the available rodent models do not have human counterparts, the final scar is comparable, and results from experiments that examine effects on the scar may be translatable to human disease[160]. Rodent models are practical due to their fast reproductive cycle, ease of manipulation and ease of pathway targeting owing to an in-depth understanding of their biology, and a perceived reproducibility of injury using standard protocols. Moreover, they are "tried and tested", and the wealth of published available data provides comparability and context[73,74].

The intended beneficiaries of this project are those with persistent fibrosis or cirrhosis after the cessation of injury (i.e. patients with treated viral hepatitis, abstinent patients with ARLD, etc.). Therefore, I chose models in which the injury could be easily stopped once fibrosis was established, with a view to treating a persistent residual scar in the absence of on-going injury: chemically induced fibrosis models, CCl_4 and TAA. For the purposes of my intervention experiments, it was critical to describe the depth of fibrosis at peak injury, the resolution of fibrosis after cessation of injury, and the reproducibility / variability of both.

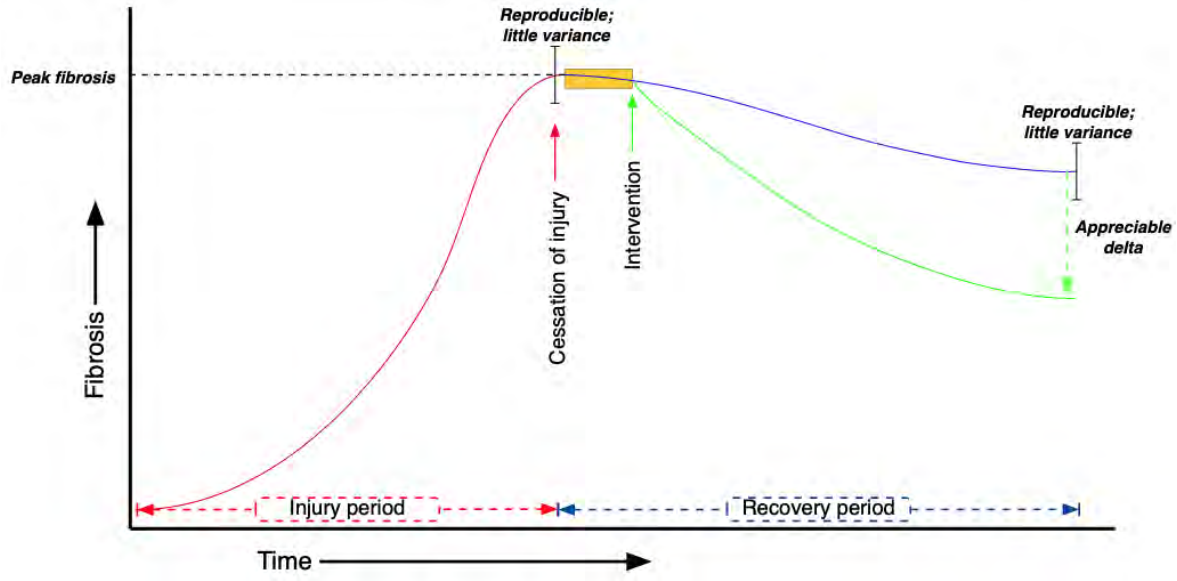

Figure 3-1 Schematic of ideal fibrosis model for planned anti-fibrotic intervention

Chemical-induced fibrosis models should deliver a peak fibrosis that is easily measurable by standard fibrosis readouts. The scar should persist after the cessation of injury, and only resolve slowly (blue recovery period, yellow box depicts the limits of any ongoing inflammation or hepatocyte damage after injury cessation). Under identical injury and maintenance environments, the injury and recovery should be reproducible, with little variance. These conditions would allow intervention (green arrow) to be instigated in the absence of ongoing injury and liver damage; any anti-fibrotic effect should be easily appreciated.

3.1.2. CCl_4-induced hepatotoxicity

CCl_4 hepatotoxicity is the best-characterised murine fibrosis model[161], with significant fibrosis, or even cirrhosis with 6-8 weeks on injury (dependent on genetic strain and dosing regimen)[162].

None of the reported effects by which CCl_4 is thought to be hepatotoxic are likely to act in isolation[163]. CCl_4 requires metabolic activation in the liver by cytochrome P450; the toxicity of the resulting trichloromethyl radical, CCl_3*, results from both primary interaction with critical target molecules (e.g. nucleic acids, proteins, lipids), and secondary interactions via a prior alteration process such as lipid peroxidation or ROS formation.

- CCl_4-mediated hypomethylation of RNA can impede protein synthesis, and hypomethylation of phospholipids can impede lipoprotein secretion – both processes affect cellular integrity and function.
- CCl_3* reacts with oxygen to form the highly reactive trichloromethylperoxy radical CCl_3OO*. This drives lipid peroxidation, which in turn destroys phospholipid-associated polyunsaturated fatty acids. The permeability of cellular and intracellular organelle membranes is compromised, with loss of calcium sequestration and cellular homeostasis[164].
- CCl_3*-mediated fatty acid breakdown also releases reactive aldehydes, which can inhibit protein (enzyme) function.

These processes contribute to cellular damage via either apoptosis or necrosis predominantly in zone 3. Moreover, at the molecular level, CCl_4 activates cytokines that drive apoptosis (TNFα) and fibrosis (TGFβ).

The culmination of these multiple injury modes is a four-phase progressive fibrotic injury: 1) acute injury, 2) initiation of fibrosis, 3) advanced fibrosis, 4) resolution after injury is ceased. The first phase is characterised by hepatocyte damage and Kupffer cell activation, both of which recruit inflammatory mediators of the tissue-injury response including macrophages, NK cells, neutrophils and lymphocytes and activate myofibroblasts. Within 2-3 weeks of iterative injury, fibrosis ensues, which progresses to bridge (central-central, followed by central-portal) after 6-8 weeks[162]. A number of investigators have shown the natural regression of fibrosis after cessation of injury, but the time course of this seems to vary, and is less-well characterised[161,162,165].

3.1.3. TAA-induced hepatotoxicity

Like the CCl_4 model, TAA-induced fibrosis follows a multiphasic fibrogenic pathway which is propagated by inflammation, and resolves when the hepatotoxic insult is removed. It is frequently applied to verify findings obtained in other models (like the CCl_4 model).

However, unlike the CCl_4 model, the mechanisms by which TAA induces hepatotoxicity and fibrosis are less-well characterised. TAA is first oxidised to TAA-S,S-oxide by the cytochrome P450 pathway or by FAD-containing monooxygenases. This in turn leads to oxidative stress, lipid peroxidation and glutathione depletion. The result of these include centrilobular cellular injury and the fibrosis

progression[166]. Moreover, TAA-S,S-oxide, covalently binds to cellular proteins and lipids, which has a multitude of cytopathic downstream effects including enzyme inhibition, dysfunctional protein folding, and aberrant mitochondrial chaperone function[167].

The resulting fibrosis is often more pronounced than seen in CCl_4, and microscopy reveals hepatocyte vacuolization, a mixed inflammatory infiltrate involving portal tracts, with ductal proliferation and portal-portal and portal-central bridging. Other differences with CCl_4 model include a prolonged latency period between drug exposure and the development of fibrosis. However, published data suggests that the fibrosis does not resolve quite as readily as with the CCl_4 model, thus providing a more stable substrate on which to test an anti-fibrotic agent[167].

3.1.4. Choice of genetic background

Both CCl_4 and TAA-induced hepatotoxicity is strain dependent. Though BALB/c mice are more sensitive to fibrosis, I chose to experiment with C57Bl/6 mice as they afforded greater scope for genetic modification if required, without overly compromising the potential for fibrosis deposition[168].

3.2. Aims of the chapter

The aims of the work in this chapter were to:

- establish two models of chemical-induced liver fibrosis
- determine the safety of the models
- establish the reproducibility and variance of peak fibrosis
- determine the time course and variance of fibrosis resolution of both models
- examine the duration of continued inflammation and hepatocyte damage after final injury in both models

3.3. Establishing models of liver fibrosis and resolution: CCl_4

3.3.1. Fibrosis and resolution model: Low dose CCl_4

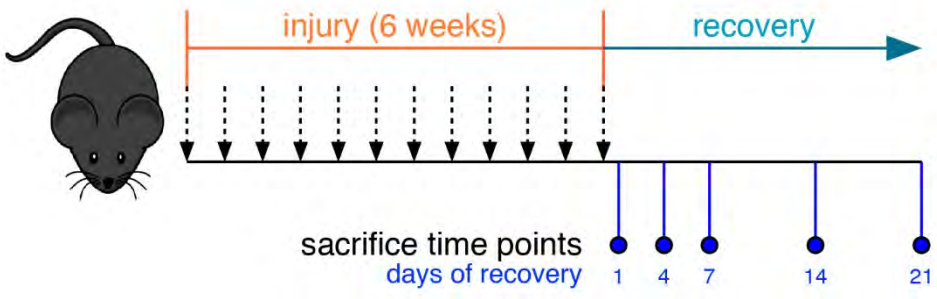

Figure 3-2: Schematic of IP CCl_4 chronic hepatic injury (low dose) and resolution

Age-matched male C57Bl/6 mice were injected IP (dashed vertical arrows) with CCl_4 diluted in mineral oil (1:3) at a dose of 1µl/g 12 times over 6 weeks (twice per week). Six mice were euthanised on each of indicated recovery time points (blue circles) after the last IP injection for tissue and serum analysis.

I undertook a time course experiment to delineate peak fibrosis and natural resolution after injury cessation using a modified version of a previously established protocol at the University of Birmingham liver laboratories (Figure 3.2)[154]. All mice survived the protocol, with none showing significant signs of distress or prohibitive weight loss (Figure 3.3).

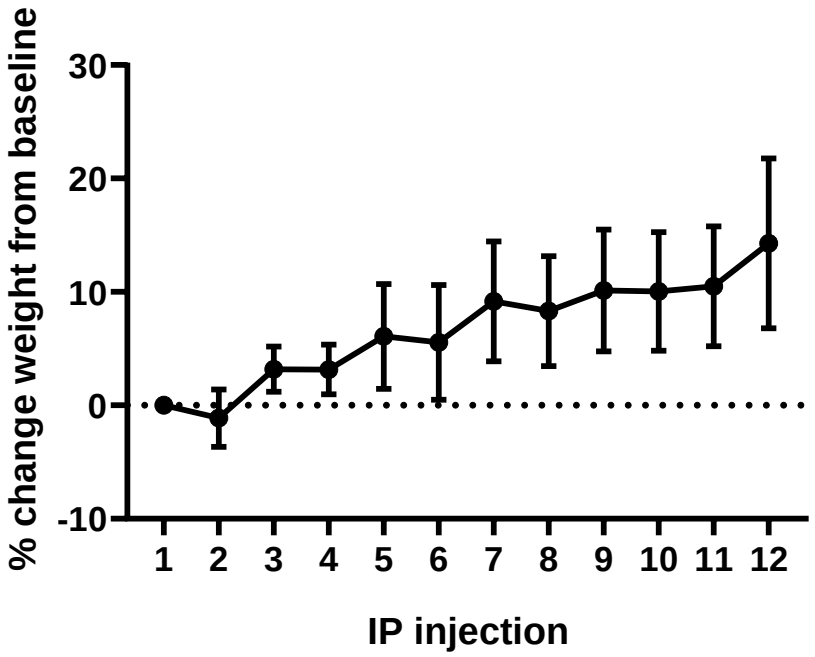

Figure 3-3: Mouse weight changes; IP CCl_4 chronic hepatic injury (low dose)

Mice in experiment described in Figure 3.2 were weighed and assessed for signs of distress prior to each IP dose of CCl_4. Summary bars: Standard deviation and mean value.

The peak fibrosis as shown in figure 3.4 (panel A), was readily reproducible across the test mice, but with a wide range, which was evident in both the PSR (peak CPA, median 2.14%, interquartile range (IQR) 0.60%) and Hyp outputs (peak Hyp, median 276µg/g, IQR 381µg/g) (Figure 3.5). There was clear evidence of natural resolution over the 21 days after injury cessation (nadir PSR median 1.33%, IQR 0.91%; nadir median Hyp 229 µg/g, IQR 101µg/g), but the fibrosis persisted above the levels of the control injections with mineral oil (Figure 3.4, panel F) (median PSR 0.47%, IQR 0.33%, p=0.004; median Hyp 122µg/g, IQR 47µg/g, p=0.002).

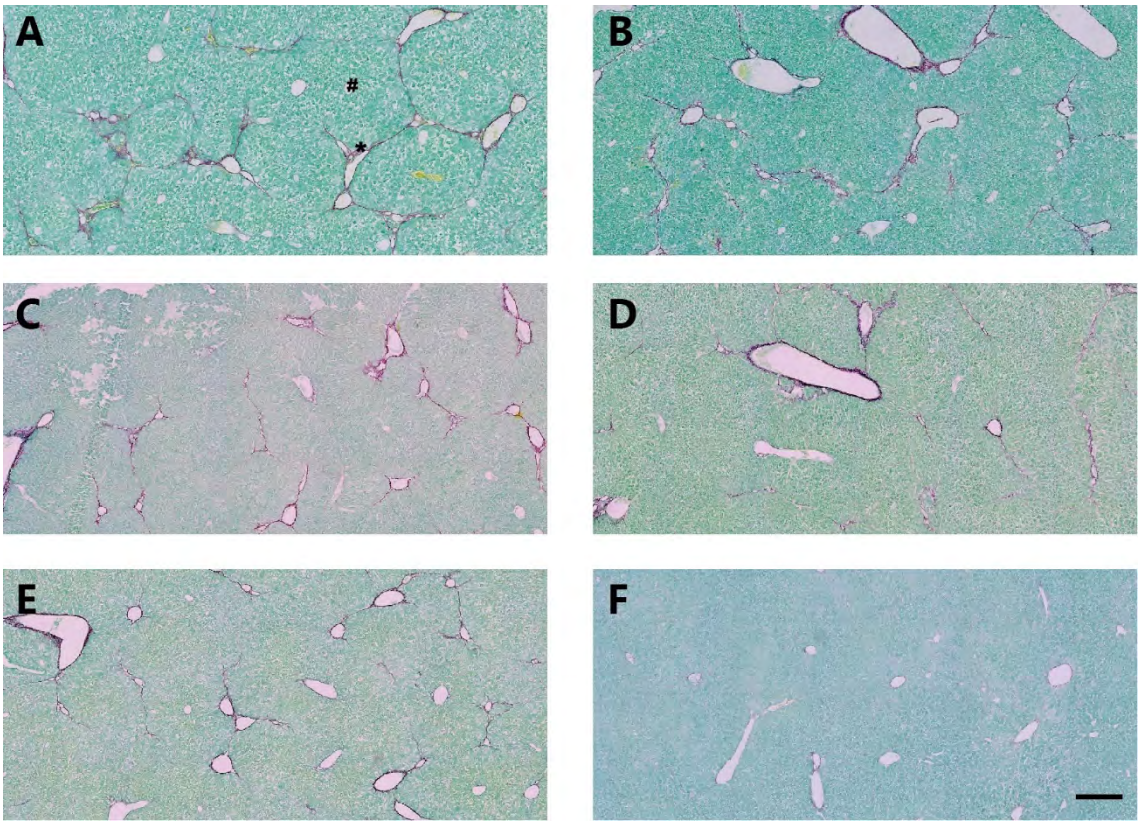

Figure 3-4: Staining of collagen deposition by PSR; IP CCl_4 chronic hepatic injury (low dose) and resolution

Mice were euthanised for tissue analysis on days 1 (A), 4 (B), 7 (C), 14 (D) and 21 (E) of recovery after chronic hepatic injury as described in Figure 3.2. Paraffin-embedded tissue (left hepatic lobe) cut to a thickness of 8µm were stained for collagen by picrosirius red (PSR) and fast green as described in section 2.11.3. Red areas demarcate collagen. Figure F shows PSR staining from a mouse subject to iterative IP injections of mineral oil (control). Scale bar (–) measures 200µm. Examples of the centrilobular vein (#) and portal tract (*) are illustrated.

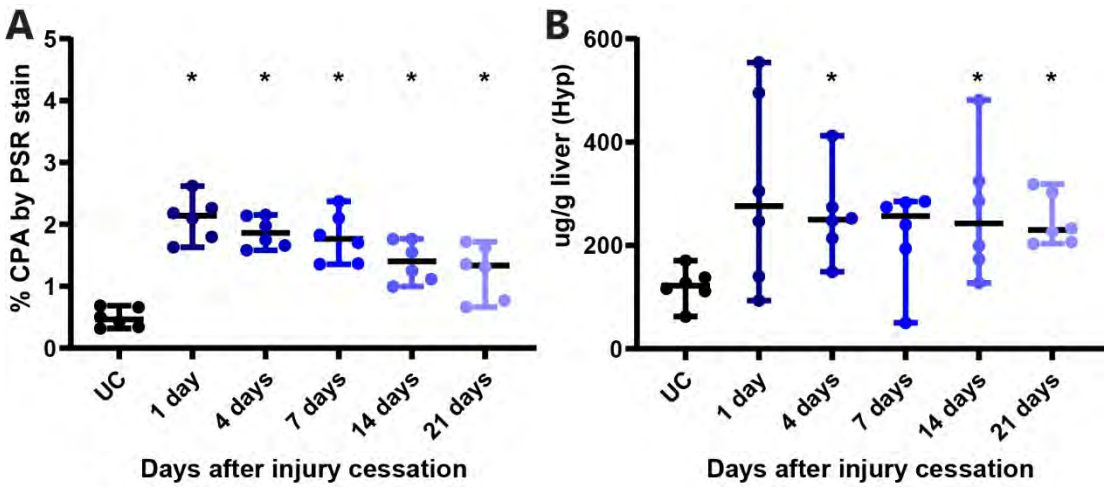

Figure 3-5: Quantitative analysis of collagen deposition; IP CCl4 chronic hepatic injury (low dose), and resolution

Morphometric analysis of collagen proportionate area (CPA) following picrosirius red (PSR) staining of paraffin-embedded sections as described in Figure 3.4 (A). The caudate & quadrate lobes were used for hepatic hydroxyproline assay (B) (section 2.10). Summary bars: 95% confidence interval and median value. The Mann-Whitney test was used to compare values in the injured mice euthanised at different time points against uninjured control (UC) mice; $p<0.05$ (*) were deemed statistically significant.

3.3.2. Fibrosis and resolution model: High dose CCl_4

As the protocol was well tolerated, I undertook another time course experiment (Figure 3.6) with a view to achieving a greater peak fibrosis, thereby allowing a more established scar on which an intervention could work. I chose a higher dose over the same duration to maintain the ease of protocol completion.

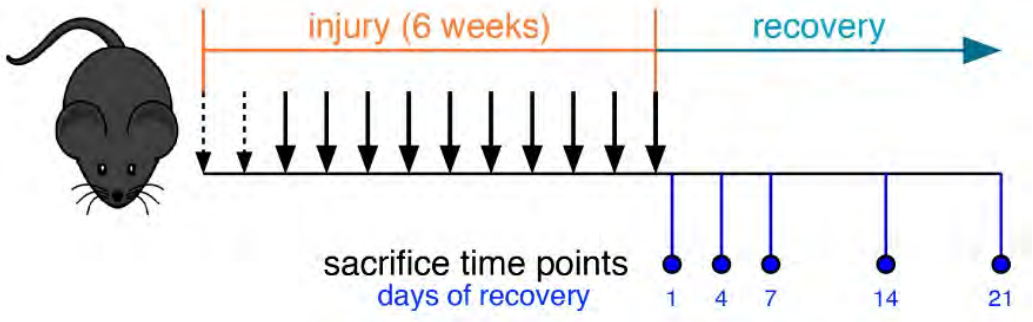

Figure 3-6: Schematic of IP CCl_4 chronic hepatic injury (high dose) and resolution

Age-matched male C57Bl/6 mice were twice injected IP with CCl_4 diluted in mineral oil (1:3) at a dose of 1 μl/g (dashed vertical arrows), followed by 10 injections of 2µl/g (blocked vertical arrows) over 6 weeks (twice per week). Ten mice were euthanised at the indicated time points (blue circles) after the last IP injection for tissue and serum analysis.

The protocol was well tolerated with no deaths or dropouts for ill health or weight loss (Figure 3.7).

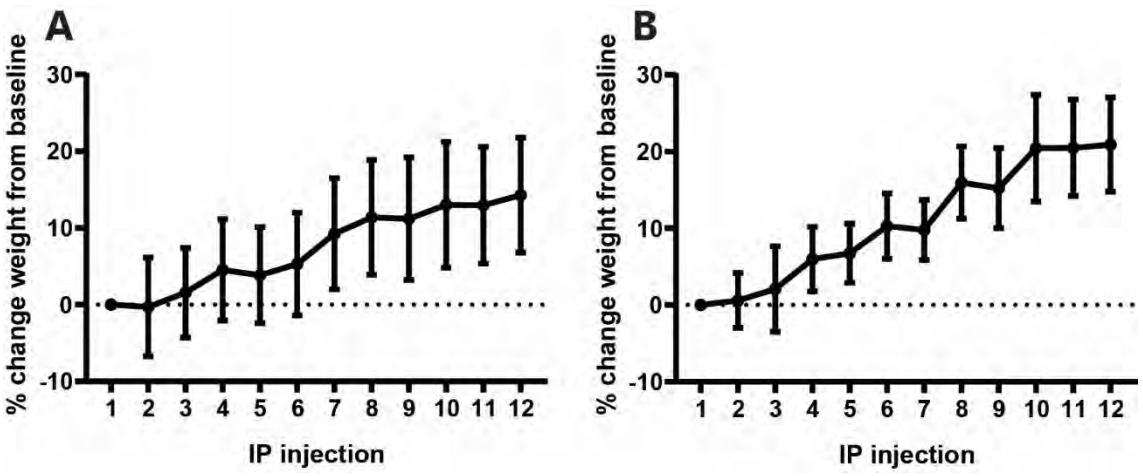

Figure 3-7: Mouse weight changes; IP CCl_4 chronic hepatic injury (high dose)

Mice subject to chronic hepatic injury as described in Figure 3.6 were weighed and assessed for signs of distress prior to each IP dose of CCl_4 (A) or mineral oil (B). Summary bars: standard deviation and mean value.

The fibrosis as measured by median PSR CPA (Figure 3.8, panel A & 3.9) was markedly higher than that achieved with the lower dose protocol at peak (2.85%, IQR 0.97%, p=0.011), and nadir (1.79%, IQR 0.72%, p=0.042). The hydroxyproline assay yielded crude results to suggest that fibrosis was greater in the mice injured with a higher dose, though the difference did not reach statistical significance (peak, 385 µg/g, IQR 179µg/g, p=0.368; nadir, 266µg/g, IQR 89µg/g, p=0.427) owing largely to the imprecision of the test.

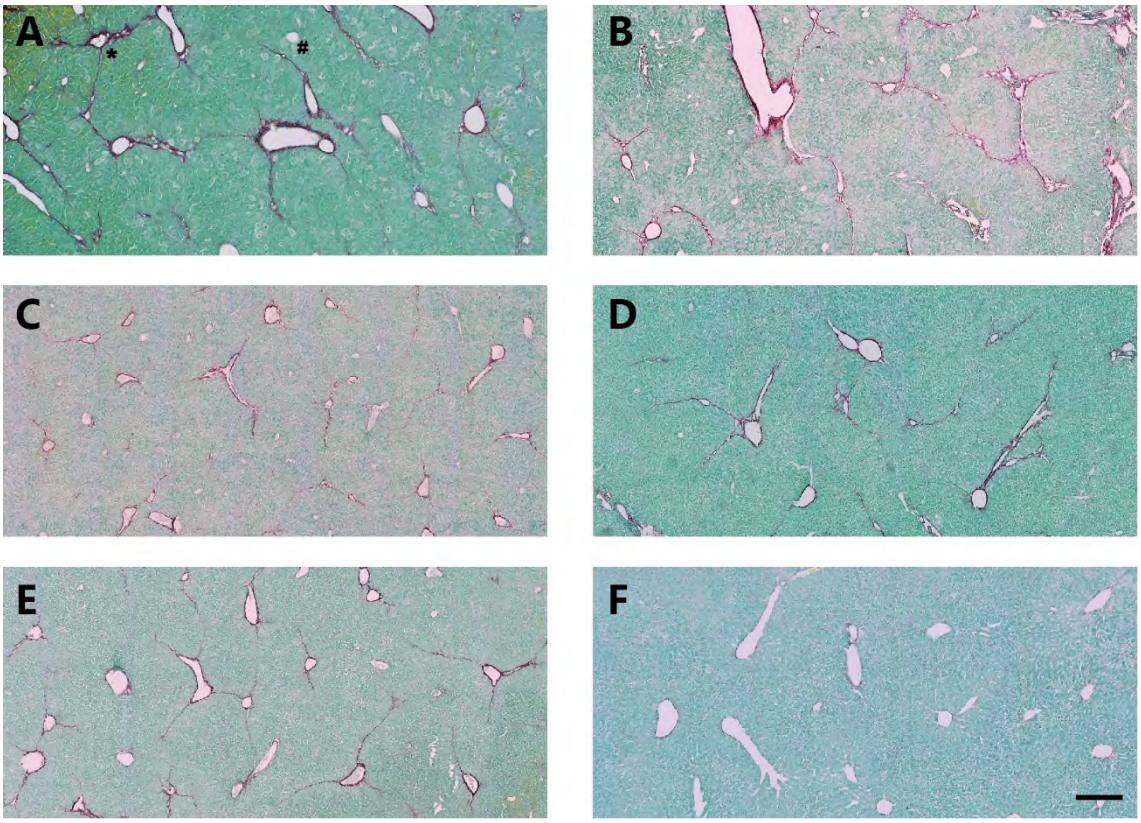

Figure 3-8: Staining of collagen deposition by PSR; IP CCl_4 chronic hepatic injury (high dose), and resolution

Mice were euthanised for tissue analysis on days 1 (A), 4 (B), 7 (C), 14 (D) and 21 (E) of recovery after chronic hepatic injury as described in Figure 3.6. Paraffin-embedded tissue (left hepatic lobe) cut to a thickness of 8µm were stained for collagen by picrosirius red (PSR) and fast green as described in section 2.11.3. Red areas demarcate collagen. Figure F shows PSR staining from a mouse subject to iterative IP injections of mineral oil (control). Scale bar (–) measures 200µm. Examples of the centrilobular vein (#) and portal tract (*) are illustrated.

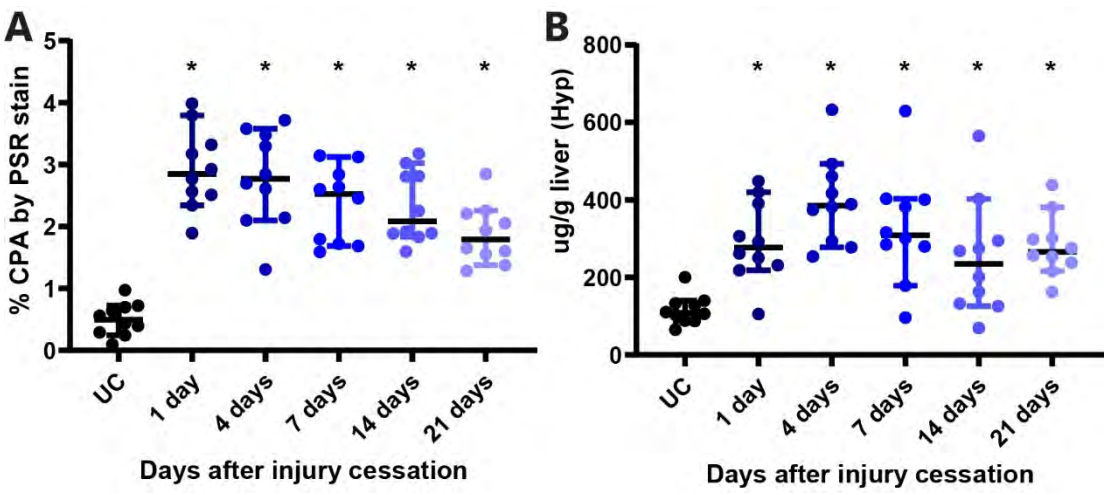

Figure 3-9: Quantitative analysis of collagen deposition; IP CCl_4 chronic hepatic injury (high dose), and resolution

Morphometric analysis of collagen proportionate area (CPA) following picrosirius red (PSR) staining of paraffin-embedded sections as described in Figure 3.8 after chronic hepatic injury as described in Figure 3.6 (A). The caudate and quadrate lobes of the extracted livers were used for hepatic hydroxyproline assay (B) as described in section 2.10. Summary bars: 95% confidence interval and median value. The Mann-Whitney test was used to compare values in the injured mice euthanised at different time points against uninjured control (UC) mice; $p<0.05$ (*) were deemed statistically significant.

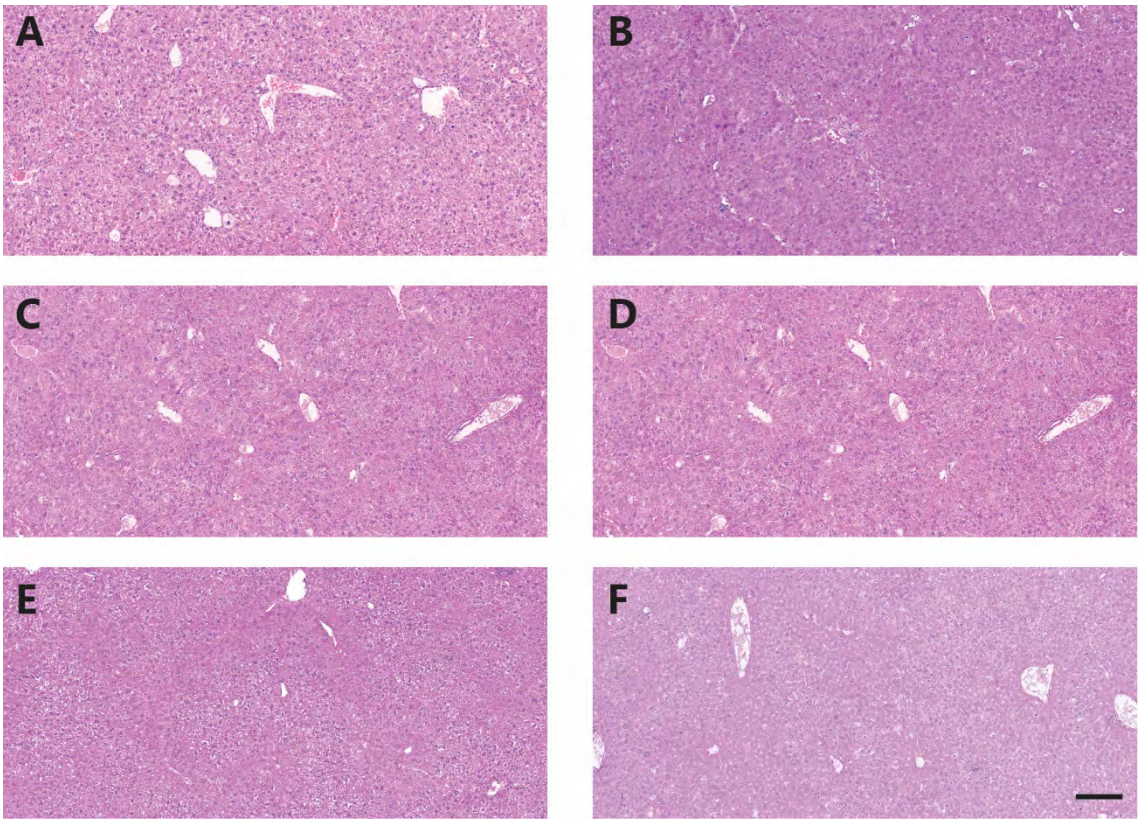

Figure 3-10: Gross histopathological assessment of hepatic tissue by H&E staining; IP CCl_4 chronic hepatic injury (high dose), and resolution

Mice were euthanised for tissue analysis on days 1 (A), 4 (B), 7 (C), 14 (D) and 21 (E) of recovery after chronic hepatic injury as described in Figure 3.6. Paraffin-embedded sections (left hepatic lobe) cut to a thickness of 3µm were stained with H&E to assess overall morphological changes. Figure F shows H&E staining from a mouse subject to iterative IP injections of mineral oil (control). Scale bar (–) measures 200µm.

Gross morphometric analysis of the liver tissue by H&E (Figure 3.10), shows relatively healthy lobules with periportal mild inflammation (Panels A & B) which dissipated with time from last injury. The fibrous strands were not obvious.

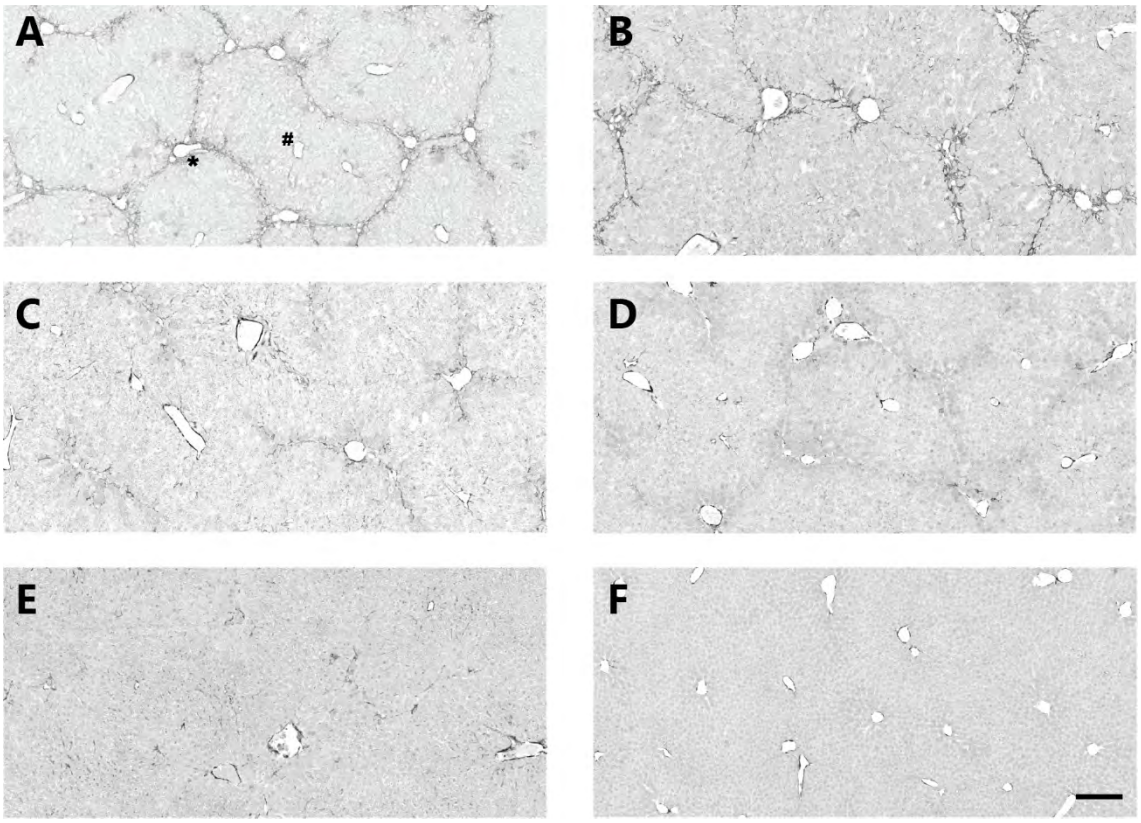

Figure 3-11: Staining for activated myofibroblasts by αSMA; IP CCl_4 chronic hepatic injury (high dose), and resolution

Mice were euthanised for tissue analysis on days 1 (A), 4 (B), 7 (C), 14 (D) and 21 (E) of recovery after chronic injury as described in Fig 3.6. Paraffin-embedded sections (left hepatic lobe) cut to 3µm thickness were stained for alpha smooth muscle actin (αSMA) as described in section 2.11.2. Figure F shows αSMA staining from a mouse subject to iterative IP injections of mineral oil (control). Dark areas indicate positive staining. Scale bar (–) measures 200µm. Examples of the centrilobular vein (#) and portal tract (*) are illustrated.

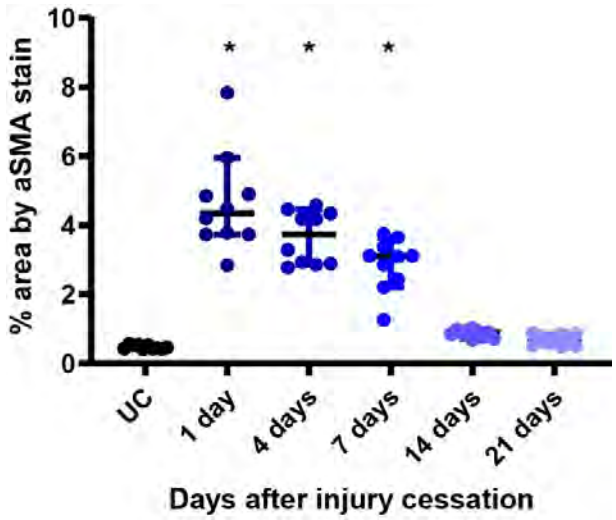

Figure 3-12: Quantitative analysis of myofibroblast activation; IP CCl_4 chronic hepatic injury (high dose), and resolution

Morphometric analysis of positive-stained areas following α SMA (alpha smooth muscle actin) staining of paraffin-embedded sections as described in Figure 3.11 after chronic hepatic injury as described in Figure 3.6. Summary bars: 95% confidence interval and median value. The Mann-Whitney test was used to compare values in the injured mice euthanised at different time points against uninjured control (UC) mice; $p<0.05$ (*) were deemed statistically significant.

The higher dose protocol yielded a greater fibrotic residue without compromising feasibility or mouse safety. Similarly, the higher-dose protocol demonstrated a clear persistence of scar-associated myofibroblasts expressing αSMA for 7 days after injury cessation (median 3.10%, IQR 1.06%; UC median 0.46%, IQR 0.12%, $p<0.001$) (Figure 3.11 & 3.12). They were visibly diminished from the 14th day of resolution onwards, despite a persistent scar. It is noteworthy that there was a significant statistical difference of the αSMA-stained areas between each of the injured cohorts and the uninjured controls. However, as stated, the difference in magnitude of positive area between the injured and uninjured mice was negligible beyond the 7th day of recovery (Day 14, median 0.90%, IQR 0.22% vs UC, $p<0.001$; Day 21, median 0.67%, IQR 0.33% vs UC, $p=0.003$).

The expression of a panel of fibrosis-related genes were examined (Figure 3.13). The expression of each of the genes was significantly elevated at peak injury (day 1 of recovery) (Table 3.1), and the expression of all diminished with time from injury cessation. The expression of *Col3a1* (median 2.07-fold, IQR 1.63-fold, $p=0.005$), *Mmp2* (median 2.62-fold, IQR 1.12-fold, $p=0.003$), and *Timp1* (median 2.45-fold, IQR 1.48-fold, $p=0.004$) were still significantly elevated on day 21 of recovery compared to the uninjured control. The expression of *Col1a1*, *Tgfb1* and *Mmp9* diminished to the levels of the uninjured control by day 14 of recovery.

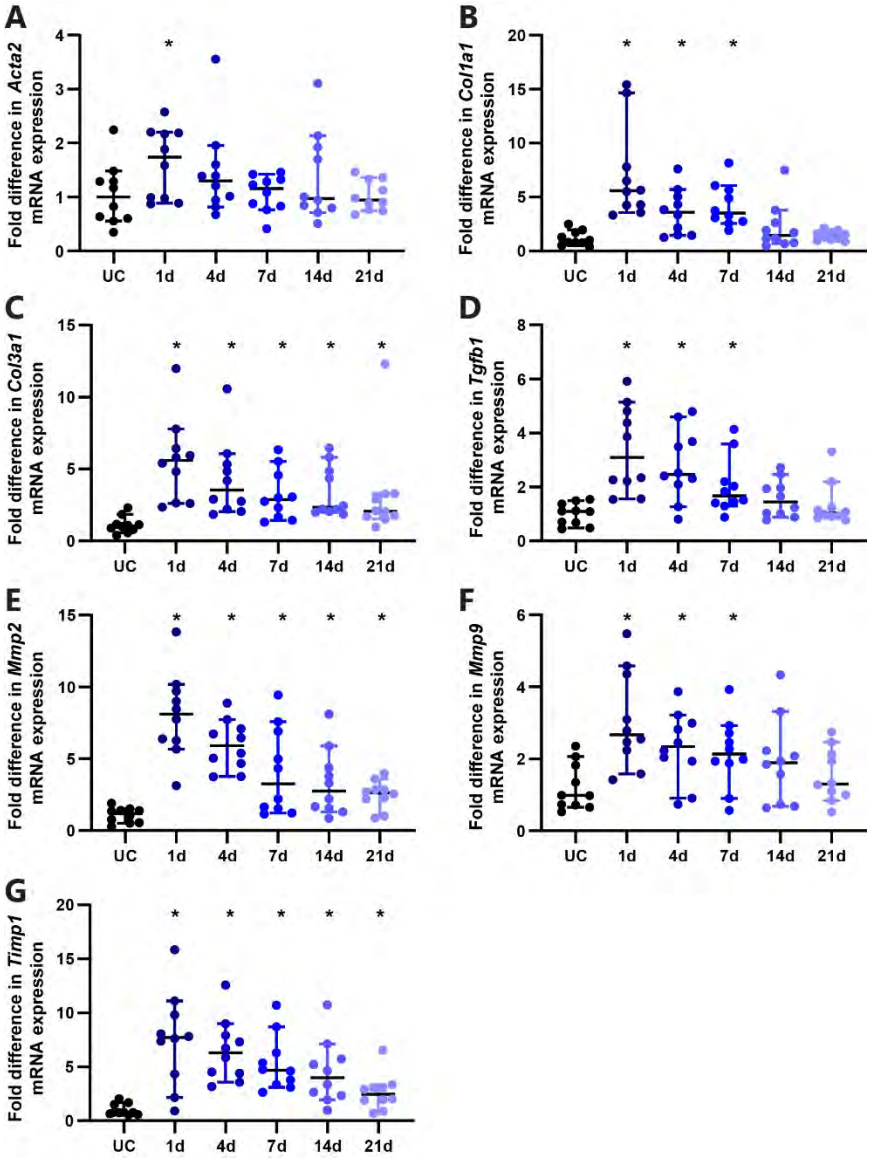

Figure 3-13: Gene expression analysis by qPCR of fibrosis-associated genes; IP CCl_4 chronic hepatic injury (high dose), and resolution

Mice were euthanised for tissue analysis on days 1, 4, 7, 14 and 21 of recovery after chronic injury as described in Fig 3.6. Expression of fibrosis-associated genes (A: *Acta2*, B: *Col1a1*, C: *Col3a1*, D: *Tgfb1*, E: *Mmp2*, F: *Mmp9*, G: *Timp1*) was assessed by qPCR of homogenised and disrupted hepatic tissues (caudate and quadrate lobes) as described in section 2.14. Summary bars: 95% confidence interval and median value. The Mann-Whitney test was used to compare values in the injured mice euthanised at different time points against uninjured control (UC) mice; $p<0.05$ (*) were deemed statistically significant. *Acta2*, actin; *Col1a1*, collagen-1; *Col3a1*, collagen-3; *Mmp*, matrix metalloproteinase; *Timp1*, tissue inhibitor of matrix metalloproteinase-1; *Tgfb1*, transforming growth factor beta-1.

3.3.3. Determining period of continued inflammation and hepatocyte injury after toxin-cessation: High dose CCl_4 model

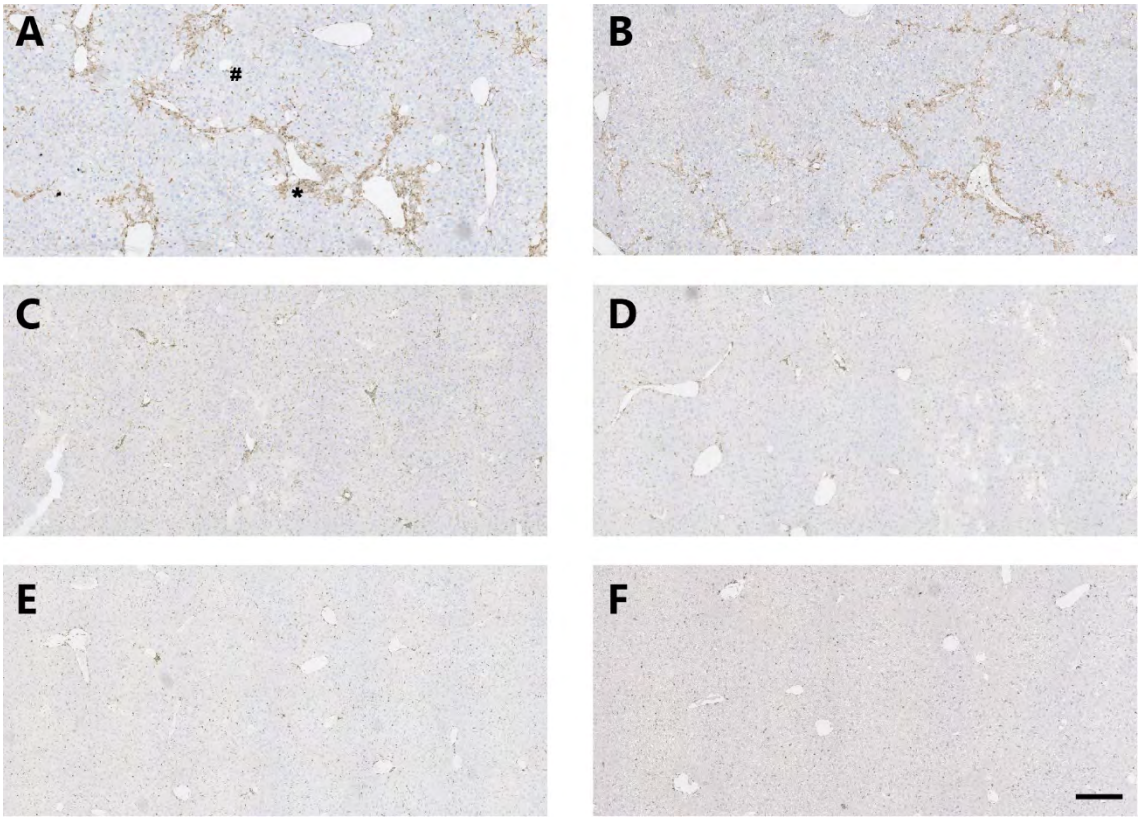

Figure 3-14: Assessment of inflammatory infiltrate by CD45 staining; IP CCl_4 chronic hepatic injury (high dose), and resolution

Mice were euthanised for tissue analysis on days 1 (A), 4 (B), 7 (C), 14 (D) and 21 (E) of recovery after chronic hepatic injury as described in Figure 3.6. Paraffin-embedded sections (left hepatic lobe) cut to a thickness of 3µm were stained for CD45 as described in section 2.11.2. Figure F shows staining from a mouse subject to iterative IP injections of mineral oil (control). Sections were counterstained with haematoxylin to demarcate background nuclei. Brown areas indicate positive staining. Scale bar (–) measures 200µm. Examples of the centrilobular vein (#) and portal tract (*) are illustrated.

IHC for CD45 facilitated qualitative and quantitative assessment of inflammatory cell infiltrate (Figure 3.14 & 3.15). This demonstrated an increase in inflammatory cell density concentrated around the portal tracts; this was most prominent at 24 hours (Panel A; median positive area 4.98%, IQR 1.34% vs. UC 2.64%, IQR 0.44%, $p<0.001$) after the last CCl_4 injection, but still obvious on day 4 (Panel B; area 4.72%, IQR 1.32% vs. UC, $p<0.001$) of recovery. By day 7 and beyond, the infiltrate has dispersed from the portal areas, though the morphometric analysis of positive-stained area was significantly elevated above the uninjured control until day 14 (day 7, area 3.66%, IQR 1.41%, $p=0.012$; day 14 area, 3.27%, IQR 0.85%, $p=0.019$).

ALT is a serum marker of hepatocyte damage or membrane instability (Figure 3.16). Serum ALT was significantly raised for the first 24 hours after injury cessation (median 776IU/L, IQR 514IU/L vs UC median 15IU/L, IQR 15IU/L, $p<0.001$), and was only marginally raised by the 4^{th} day (median 30IU/L, IQR 34.5IU/L, $p=0.006$). Levels settled to equivalence with the uninjured control by day 7.

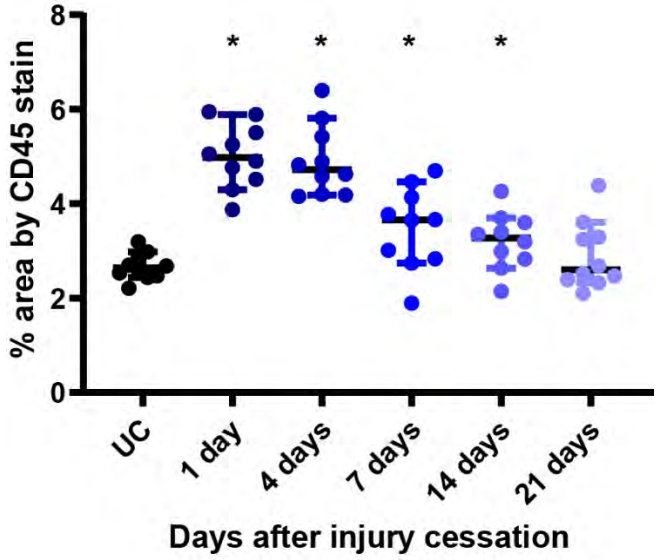

Figure 3-15: Quantitative analysis of inflammatory infiltrate by CD45 staining; IP CCl_4 chronic hepatic injury (high dose), and resolution

Morphometric analysis of positive-stained areas following CD45 staining of paraffin-embedded sections as described in Figure 3.14. Summary bars: 95% confidence interval and median value. The Mann-Whitney test was used to compare values in the injured mice euthanised at different time points against uninjured control (UC) mice; $p<0.05$ (*) were deemed statistically significant.

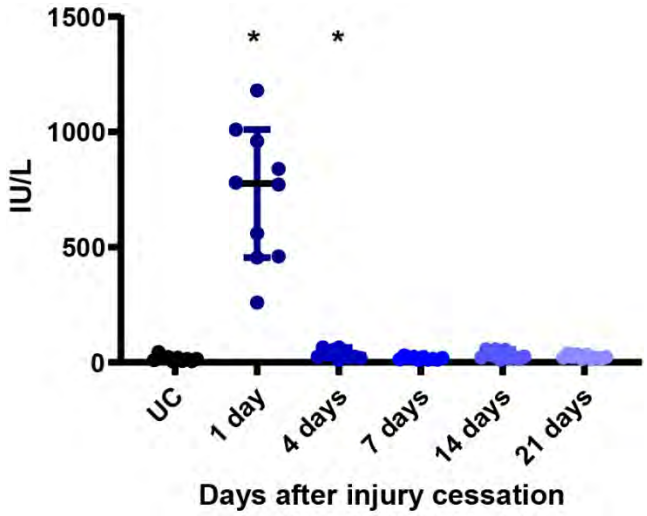

Figure 3-16: Serum ALT as a marker of hepatocyte injury; IP CCl_4 chronic hepatic injury (high dose), and resolution

Sera from each euthanised mouse as described in Figure 3.6 were analysed for ALT as a surrogate for hepatocyte injury or cell membrane instability using a clinical biochemistry analyser. Summary bars: 95% confidence interval and median value. ALT, alanine aminotransferase; IU, international units. The Mann-Whitney test was used to compare values in the injured mice euthanised at different time points against uninjured control (UC) mice; $p<0.05$ (*) were deemed statistically significant.

3.4. Establishing models of liver fibrosis and resolution: TAA

The Birmingham Biomedical Services Unit (BMSU) and our laboratory have some experience of using CCl_4 as both an acute and chronic hepatotoxic agent[154]. However, the TAA model had not been utilised prior; as such, experimentation required early low-volume feasibility and safety experiments before embarking on establishing a fibrosis and resolution model.

3.4.1. Feasibility and safety of IP TAA protocol

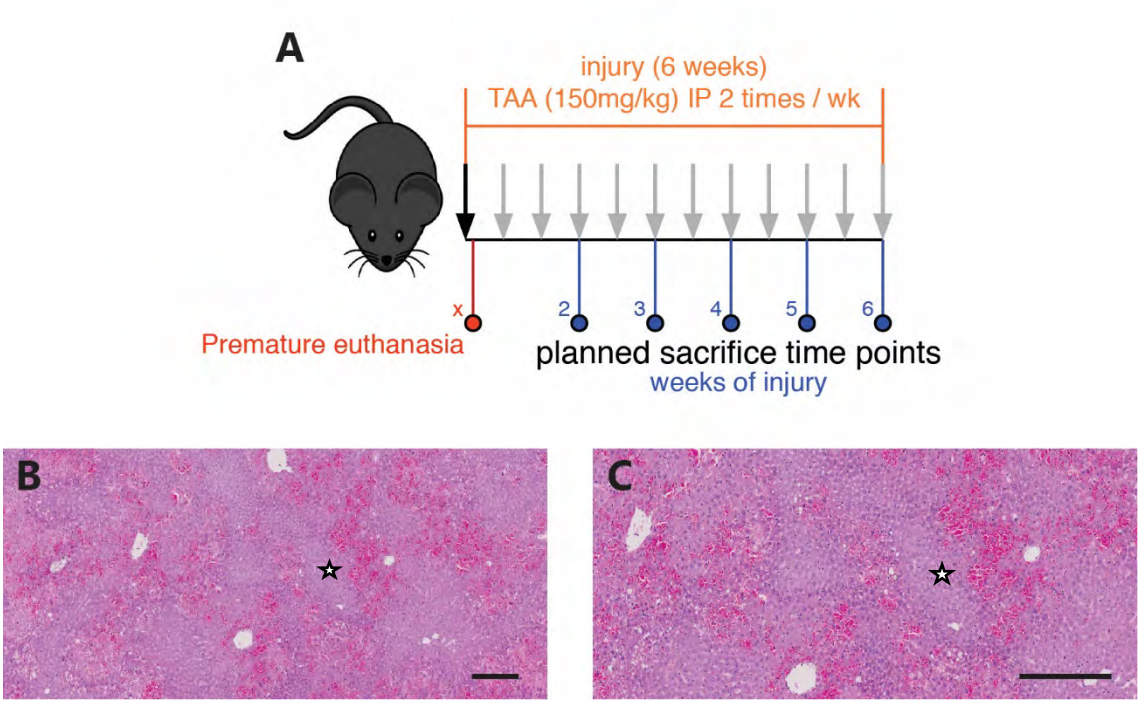

Figure 3-17: IP TAA chronic hepatic injury feasibility experiment

Age-matched male C57Bl/6 mice were injected IP with 150mg/kg TAA diluted in mineral oil, with a plan to euthanise two mice at each of the indicated time points (blue circles) for tissue and serum analysis (A). However, the experiment was prematurely terminated 24 hours after the first IP injection of three mice due to evidence of severe physical distress in the mice. The mice were euthanised after cardiac puncture under terminal anaesthesia. H&E staining of paraffin-embedded tissue (B, C; left hepatic lobe) showed continuous peri-centrilobular necrosis (eosinophilic hot pink areas) surrounding islands of surviving peri-portal hepatocytes (star). Scale bar (–) measures 200µm.

A feasibility experiment was conducted to examine the safety and efficacy of a chronic model of hepatic injury by the iterative delivery of IP TAA. A protocol was produced by reference to peer-reviewed and published standard operating procedures and a literature search[53,60,167,169]. The protocol was submitted as an amendment to our project licence and ratified by the Birmingham BMSU and named animal care and welfare officer (NACWO). We trialled a conservative starting dose of 150mg/kg, with a plan to titrate over 6 weeks depending on physical response[40] (Figure 3.17, panel A). 24 hours after the initial dose, the mice were observed to be obtunded, lacking a postural righting response and showing clear signs of physical distress with tachypnoea and grimacing. Under the advice of the supervising NACWO, the mice were sacrificed after cardiac puncture under terminal anaesthesia, and tissue was collected post-mortem for analysis. Serum transaminase levels for all three mice were over 4000IU/L, suggesting massive hepatic injury. H&E staining (panels B & C) showed a widespread and profound zonal necrosis, with islands of surviving hepatocytes around portal tracts. As a consequence of this catastrophic hepatic necrosis, the IP TAA approach to chronic hepatic injury was abandoned.

3.4.3. Feasibility and safety of oral TAA protocol

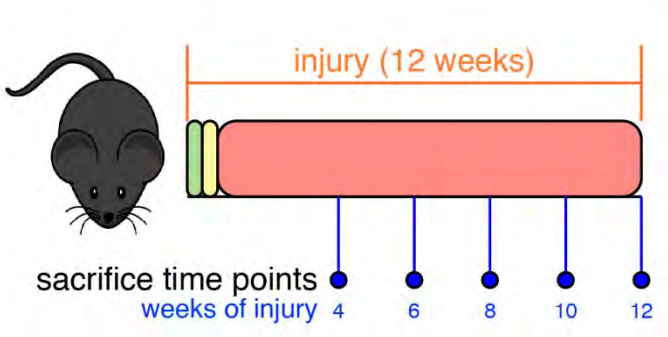

Figure 3-18: Schematic of oral TAA chronic hepatic injury - feasibility experiment

Age-matched male C57Bl/6 mice were subject to hepatic injury by substituting their drinking water with TAA diluted in fruit squash (1:5) to be taken *ad libitum*. A starting dose of 100mg/L (three days - green block) was sequentially increased to 300mg/L (three days - yellow block) and 600mg/L (pink block) for the remainder of the 12-week experiment. Two mice were euthanised on each of indicated time points (blue circles) during injury for tissue and serum analysis.

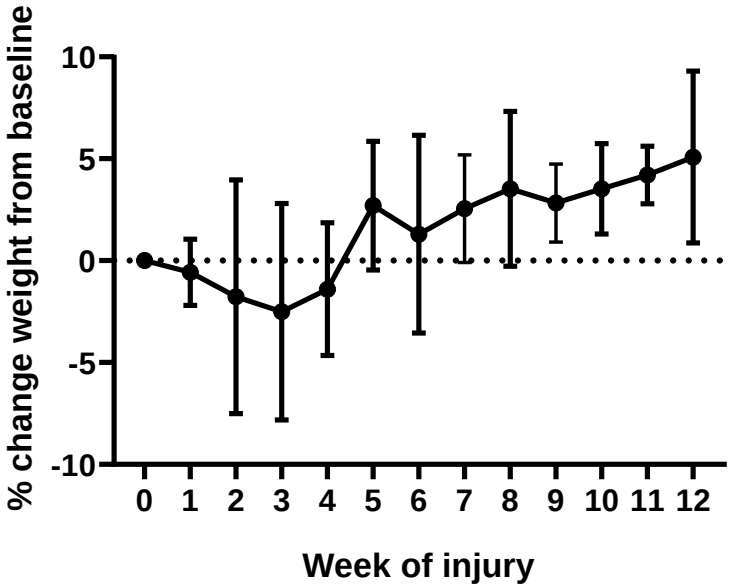

Figure 3-19: Mouse weight changes; oral TAA chronic hepatic injury model – feasibility experiment

Mice were weighed and assessed for signs of distress every week whilst on oral TAA as described in Figure 3.18. Summary bars: range and mean value.

An experiment to examine the feasibility and safety of an oral TAA-induced hepatic fibrosis model followed. An externally validated operating protocol was acquired from Professor Henderson's laboratory and modified (MRC Centre for Inflammation Research, Edinburgh, UK)[60]. Ten mice were subject to the protocol as described in section 2.5.3.2, and depicted in figure 3.18. Mice were weighed and examined for signs of distress daily for two weeks, every 48 hours for another two weeks, and bi-weekly thereafter. The mice were noted to lose weight in the first four weeks but never below the threshold of 80% of their starting weight, before regaining and maintaining an acceptable weight for the remainder of the injury period (Figure 3.19). Despite the initial weight loss, the mice did not exhibit signs of distress, and were healthy throughout. All mice survived until their intended euthanasia date.

Nevertheless, there were evidence of significant hepatic injury by week 4 as evidenced by bridging necrosis between portal tracts, and hepatocyte vacuolization on H&E staining (Figure 3.20, Panel A)[167]. By week 10 and 12, the areas of necrosis were being replaced by pale pink bands of thick fibrosis (Panels C – E). IHC for CD45 cells reflected the area of cellular damage, but the infiltrate was comparatively modest, and seemed to increase with the fibrotic burden in weeks 10 and 12 of injury (Figure 3.21 & Figure 3.22, Panel A). As has been previously published, hepatocyte damage was persistent throughout but the ALT rise was modest (<100IU/L for 10 weeks, upper limit of normal 50IU/L)[167], before apparently spiking at week 12 (Figure 3.22, Panel B).

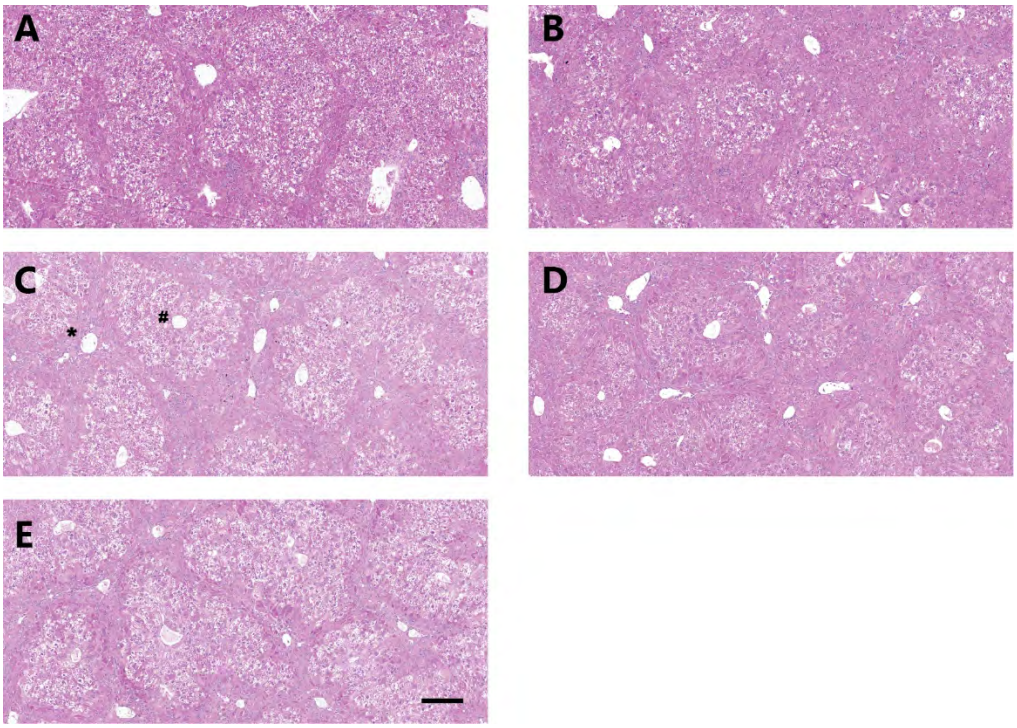

Figure 3-20: Gross histopathological assessment of hepatic tissue by H&E staining; oral TAA chronic hepatic injury - feasibility experiment

Mice were euthanised for tissue analysis after 4 (A), 6 (B), 8 (C), 10 (D) and 12 (E) weeks of chronic hepatic injury as described in Figure 3.18. Paraffin-embedded sections (left hepatic lobe) cut to a thickness of 3µm were stained with H&E to assess overall morphological changes. Scale bar (–) measures 200µm. Examples of the centrilobular vein (#) and portal tract (*) are illustrated.

Fibrosis occurred in a dose / duration dependent manner (Figure 3.23 & 3.24), and manifested as thick septa of portal-portal bridging surrounding islands / nodules or apparently normal tissue by weeks 10 and 12. Deposition of collagen as revealed by PSR was temporally congruent with scar-associated myofibroblast activation as evidenced αSMA IHC (Figure 3.25), and the increased expression of fibrosis related genes (Figure 3.26). The model was deemed not only to be safe and feasible, but delivered a significant scar by week 12, that resembled early cirrhosis. Allied fibrosis outputs also increased, affording good reason to pursue a time-course experiment to delineate peak fibrosis and resolution in recovery.

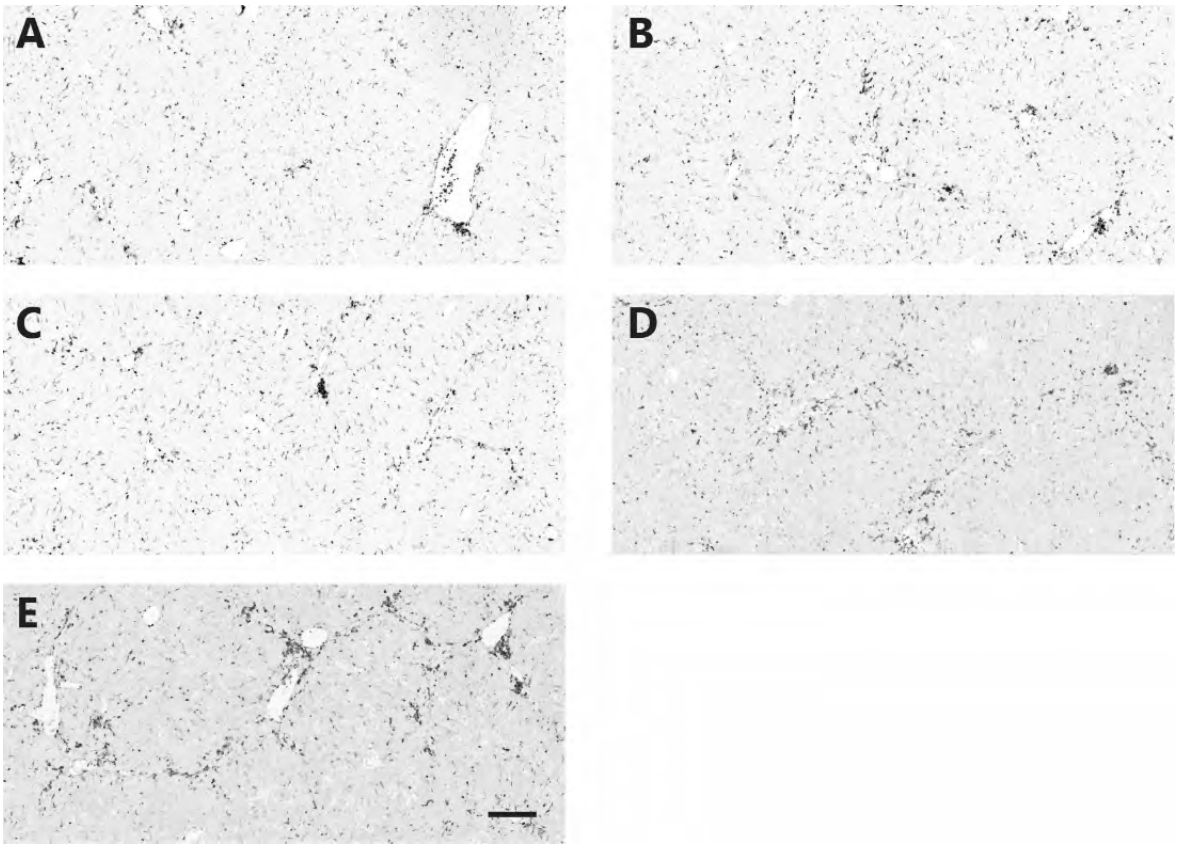

Figure 3-21: Assessment of inflammatory infiltrate by CD45 staining; oral TAA chronic hepatic injury - feasibility experiment

Mice were euthanised for tissue analysis after 4 (A), 6 (B), 8 (C), 10 (D) and 12 (E) of chronic hepatic injury as described in Figure 3.18. Paraffin-embedded sections (left hepatic lobe) cut to a thickness of 3µm were stained for CD45 as described in section 2.11.2. Dark areas indicate positive staining. Scale bar (–) measures 200µm. Examples of the centrilobular vein (#) and portal tract (*) are illustrated.

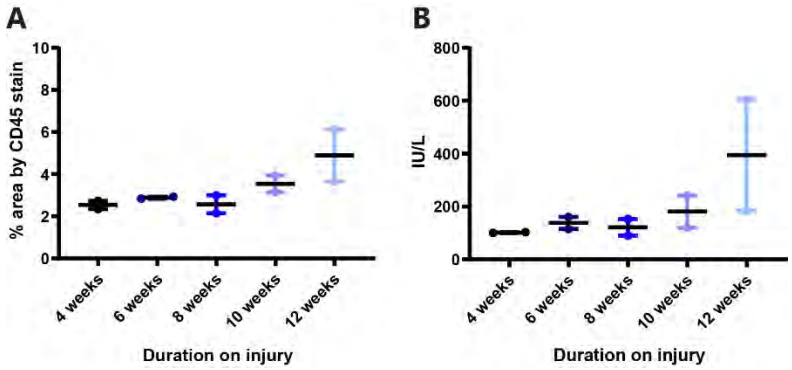

Figure 3-22: Quantitative analysis of inflammatory infiltrate by CD45 staining and hepatocyte injury by serum ALT measurements; oral TAA - feasibility experiment

Morphometric analysis of positive-stained areas following CD45 staining as described in Figure 3.21. Sera from each euthanised mouse after chronic hepatic injury as described in Figure 3.18 were analysed for alanine aminotransferase (ALT) as a surrogate for hepatocyte injury or cell membrane instability using a clinical biochemistry analyser. IU, international units

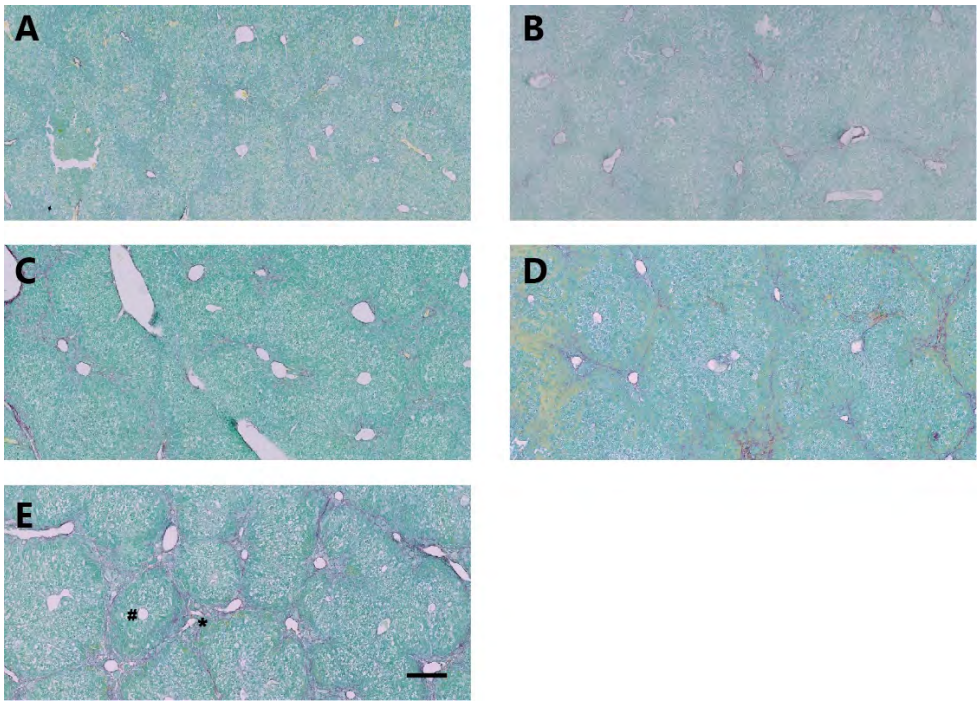

Figure 3-23: Staining of collagen deposition by PSR; oral TAA chronic hepatic injury - feasibility experiment

Mice were euthanised for tissue analysis after 4 (A), 6 (B), 8 (C), 10 (D) and 12 (E) weeks of chronic hepatic injury as described in Figure 3.18. Paraffin-embedded tissue (left hepatic lobe) cut to a thickness of 8µm were stained for collagen by picrosirius red (PSR) and fast green as described in section 2.11.3. Red areas demarcate collagen. Scale bar (–) measures 200µm. Examples of the centrilobular vein (#) and portal tract (*) are illustrated.

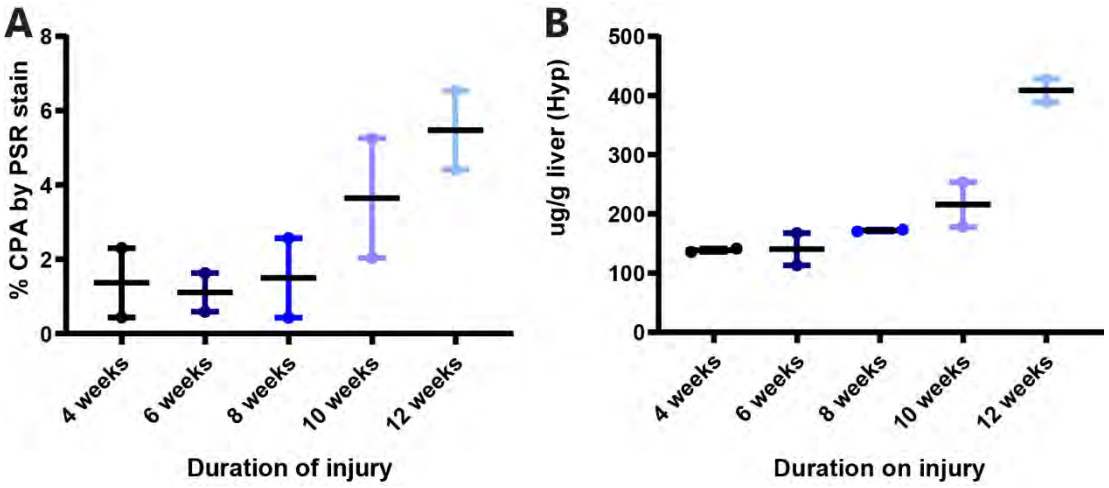

Figure 3-24: Quantitative analysis of collagen deposition; oral TAA chronic hepatic injury - feasibility experiment

Morphometric analysis of collagen proportionate area (CPA) following picrosirius red (PSR) staining of paraffin-embedded sections as described in Figure 3.23 after chronic hepatic injury as described in Figure 3.18 (A). The caudate and quadrate lobes of the extracted livers were used for hepatic hydroxyproline assay (B) as described in section 2.10. Summary bars: range and mean value.

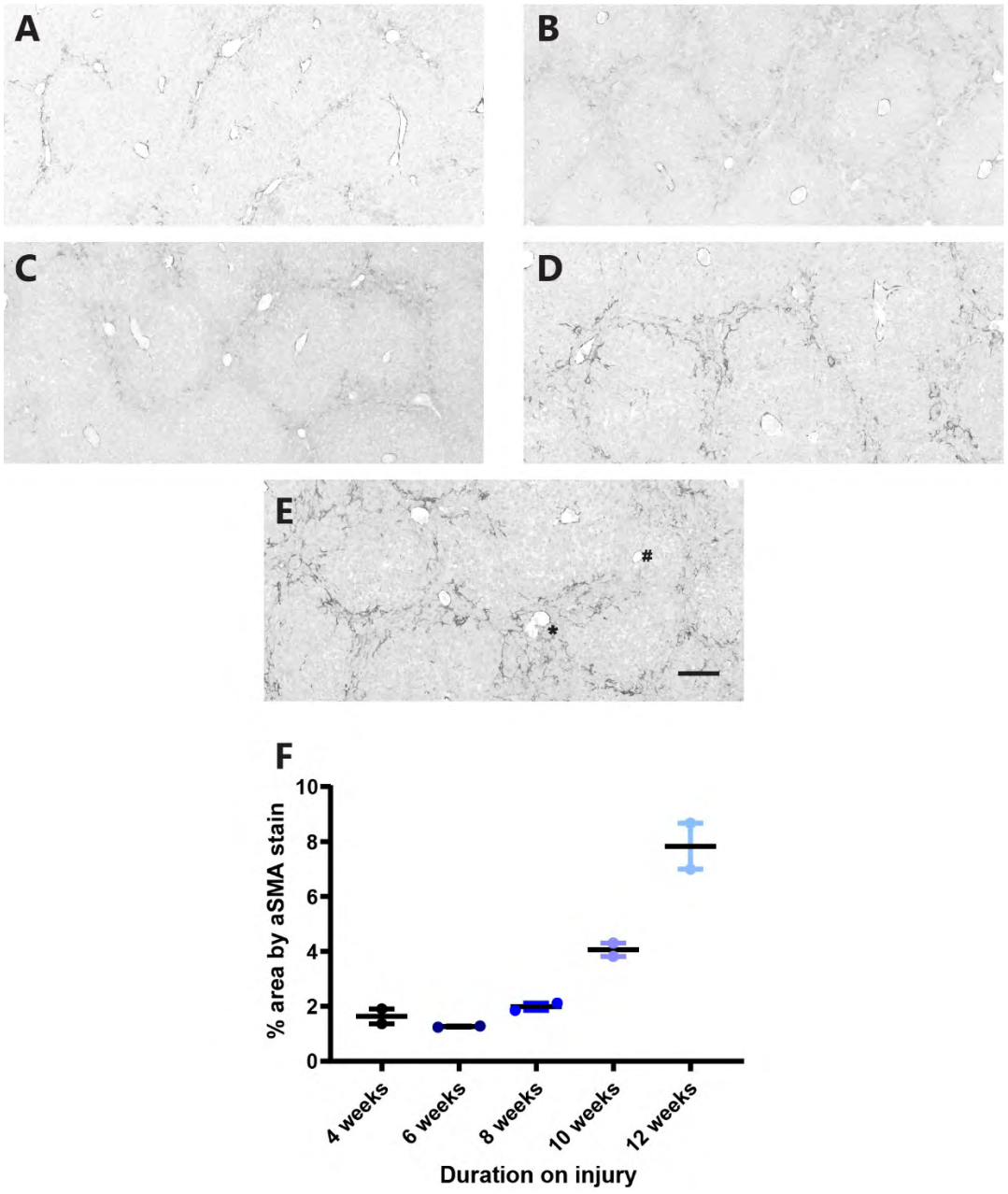

Figure 3-25: Staining for activated myofibroblasts by αSMA; oral TAA chronic hepatic injury - feasibility experiment

Mice were euthanised for tissue analysis after 4 (A), 6 (B), 8 (C), 10 (D) and 12 (E) weeks of chronic hepatic injury as described in Figure 3.18. Paraffin-embedded sections (left hepatic lobe) cut to a thickness of 3µm were stained for alpha smooth muscle actin (α SMA) as described in section 2.11.2. Dark areas indicate positive staining. Scale bar (–) measures 200µm. Morphometric analysis of positive-stained areas is graphically represented in Figure F. Summary bars: range and mean value. Examples of the centrilobular vein (#) and portal tract (*) are illustrated.

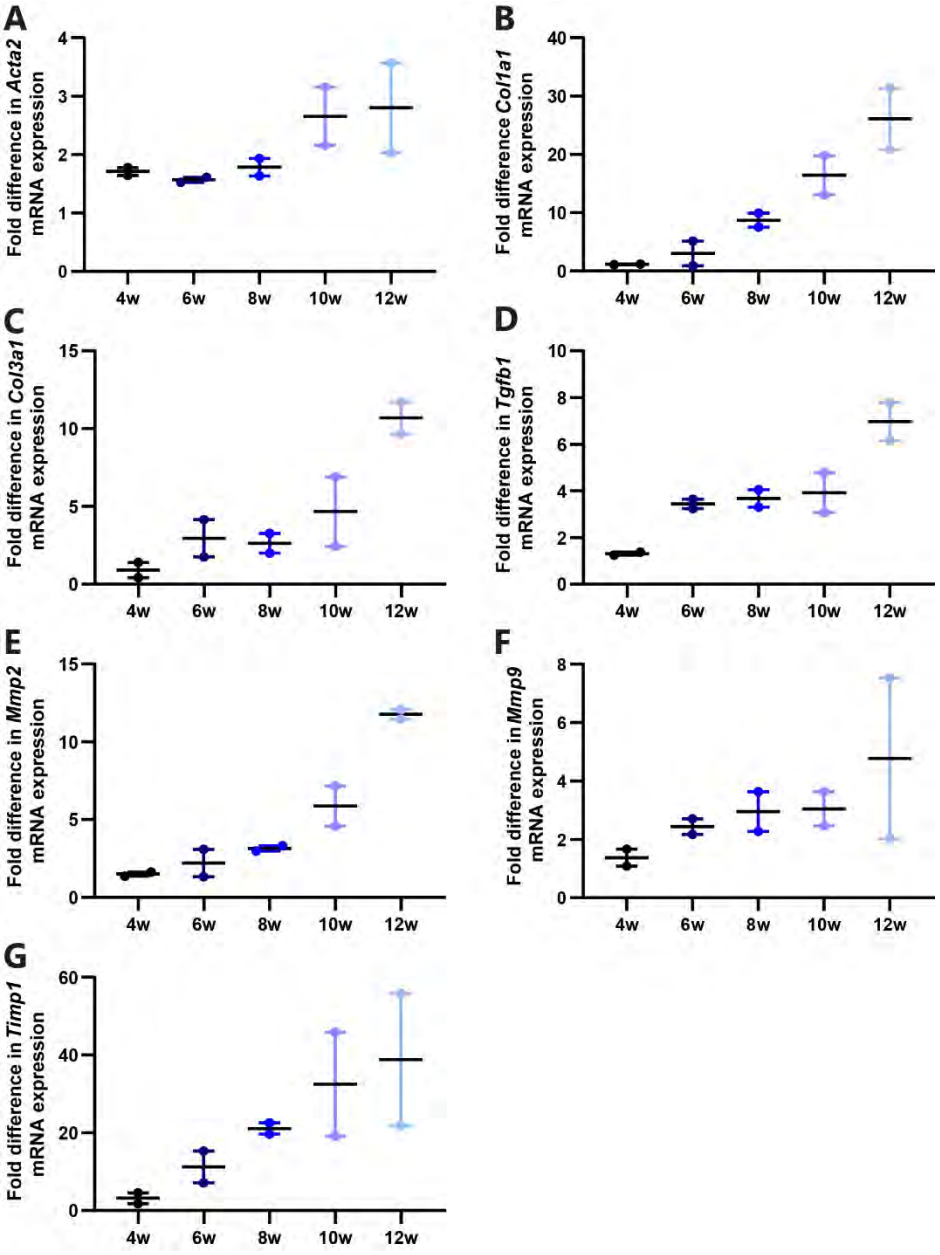

Figure 3-26: Gene expression analysis by qPCR of fibrosis-associated genes; oral TAA chronic hepatic injury - feasibility experiment

Mice were euthanised for tissue analysis after 4, 6, 8, 10 and 12 weeks of chronic hepatic injury as described in Figure 3.18. Expression of fibrosis-associated genes (A: *Acta2*, B: *Col1a1*, C: *Col3a1*, D: *Tgfb1*, E: *Mmp2*, F: *Mmp9*, G: *Timp1*) was assessed by qPCR of homogenised and disrupted hepatic tissues (caudate and quadrate lobes) as described in section 2.14. Summary bars: range and mean value. *Acta2*, actin; *Col1a1*, collagen-1; *Col3a1*, collagen-3; *Mmp*, matrix metalloproteinase; *Timp1*, tissue inhibitor of matrix metalloproteinase-1; *Tgfb1*, transforming growth factor beta-1

3.4.4. Fibrosis and resolution model: oral TAA

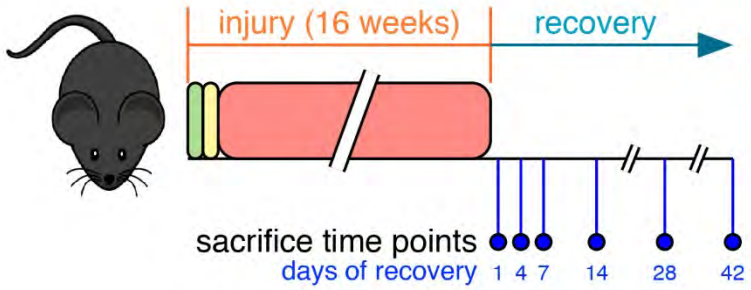

Figure 3-27: Schematic of oral TAA chronic hepatic injury model and resolution

Mice were subject to hepatic injury as described in Figure 3.18 by substituting their drinking water with TAA diluted in fruit squash (1:5), at increasing concentrations. The TAA was replaced by standard drinking water after 16 weeks. Ten mice were euthanised on each of indicated recovery time points (blue circles) for tissue and serum analysis.

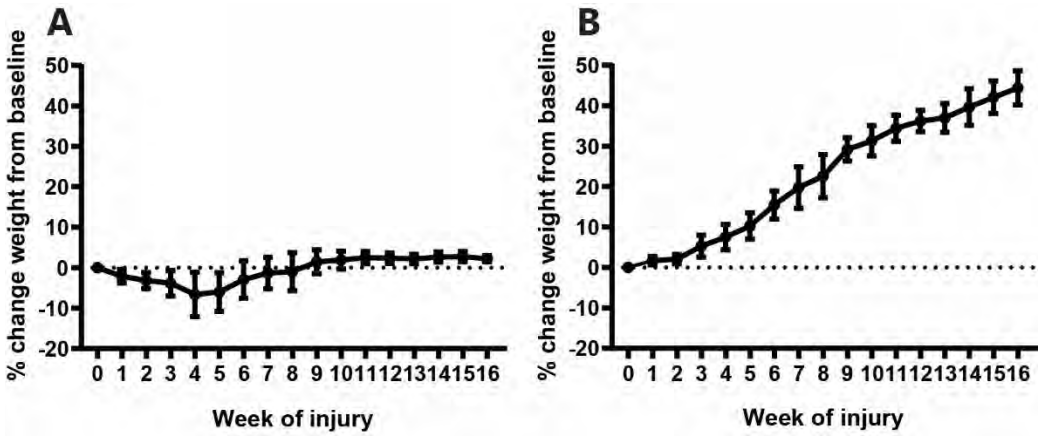

Figure 3-28: Mouse weight changes; oral TAA chronic hepatic injury model and resolution

Mice were weighed and assessed for signs of distress every week whilst on oral TAA (Fig 3.27) (A), or on fruit squash without TAA (Control – B). Summary bars: standard deviation and mean value.

For the purposes of the time course experiment we extended the injury for 16 weeks with the intent of depositing a resolute scar (Figure 3.27). As in the feasibility experiment, all mice survived the protocol, with none showing significant signs of distress or prohibitive weight loss (Figure 3.28).

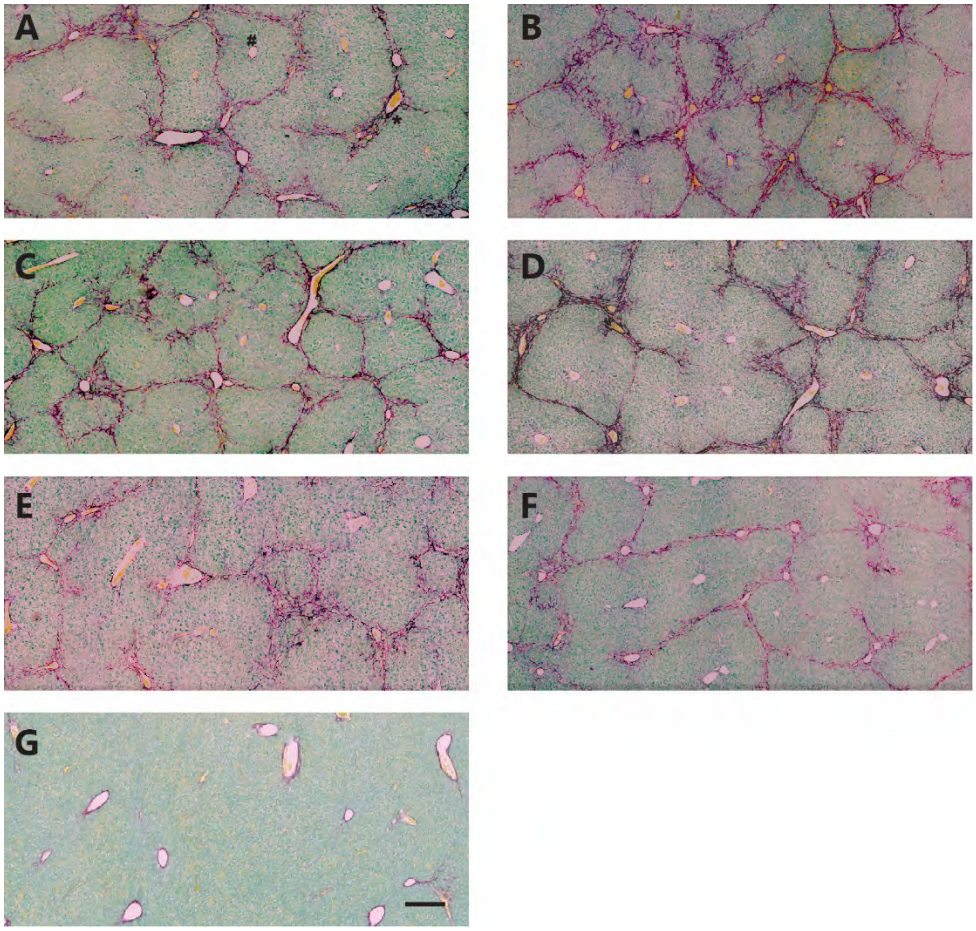

Figure 3-29: Staining of collagen deposition by PSR; oral TAA chronic hepatic injury model and resolution

Mice were euthanised for tissue analysis after 1 (A), 4 (B), 7 (C), 14 (D), 28 (E) and 42 (F) days of recovery following 16 weeks of chronic hepatic injury as described in Figure 3.27. Paraffin-embedded tissue (left hepatic lobe) cut to a thickness of 8μm were stained for collagen by picrosirius red (PSR) and fast green as described in section 2.11.3. Figure G shows staining from a mouse euthanised after drinking fruit squash without TAA for 16 weeks, and normal drinking water for 1 day (control). Red areas demarcate collagen. Scale bar (–) measures 200μm. Examples of the centrilobular vein (#) and portal tract (*) are illustrated.

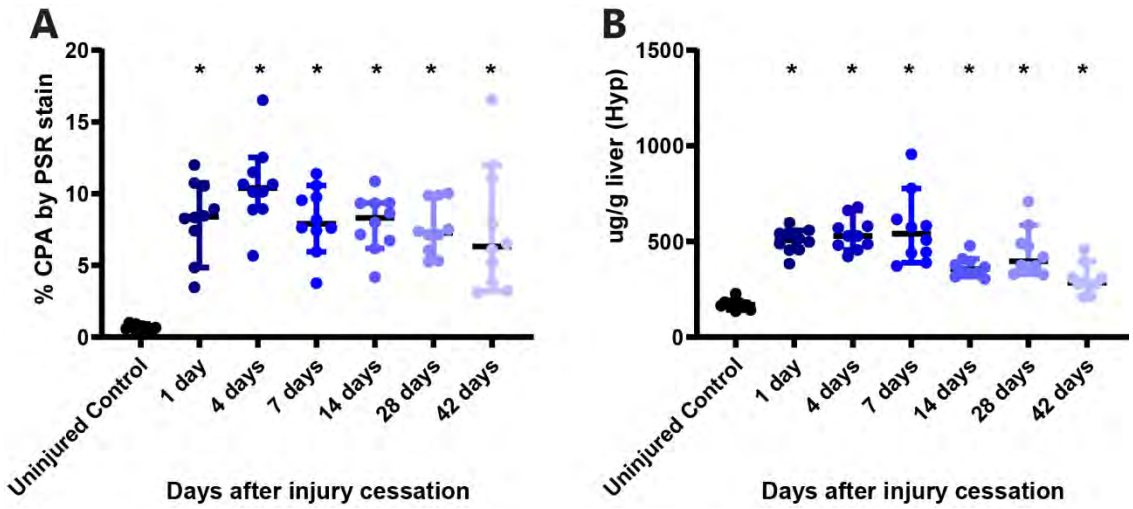

Figure 3-30: Quantitative analysis of collagen deposition; oral TAA chronic hepatic injury model and resolution

Morphometric analysis of collagen proportionate area (CPA) following picrosirius red (PSR) staining of paraffin-embedded sections as described in Figure 3.29 (A). The caudate and quadrate lobes of the extracted livers were used for hepatic hydroxyproline assay (B) as described in section 2.10. Summary bars: 95% confidence interval and median value. The Mann-Whitney test was used to compare values in the injured mice euthanised at different time points against uninjured control (UC) mice; $p<0.05$ (*) were deemed statistically significant.

The model resulted in a reproducible thick scar (Figure 3.29 & 3.30), which continued to progress and reach peak fibrosis 4 days after injury cessation (median PSR 10.39%, IQR 2.82%; median Hyp 529µg/g, IQR 125µg/g). The scar was resolute and persisted for 42 days after cessation of injury (median PSR 6.32%, IQR 7.63%; median Hyp 284µg/g, IQR 77µg/g). However, the persistence of fibrosis was not consistent after 42 days of recovery, with a wide range of residual scar as measures by PSR.

αSMA-expressing scar associated myofibroblasts persisted for 14 days (median area 3.17%, IQR 1.85% vs. UC median 0.11%, IQR 0.10%, $p<0.001$), after which the expression diminished to the

levels seen in uninjured controls (day 28 median area 0.15%, IQR 0.23%, p=0.09) (Figure 3.31 & 3.32).

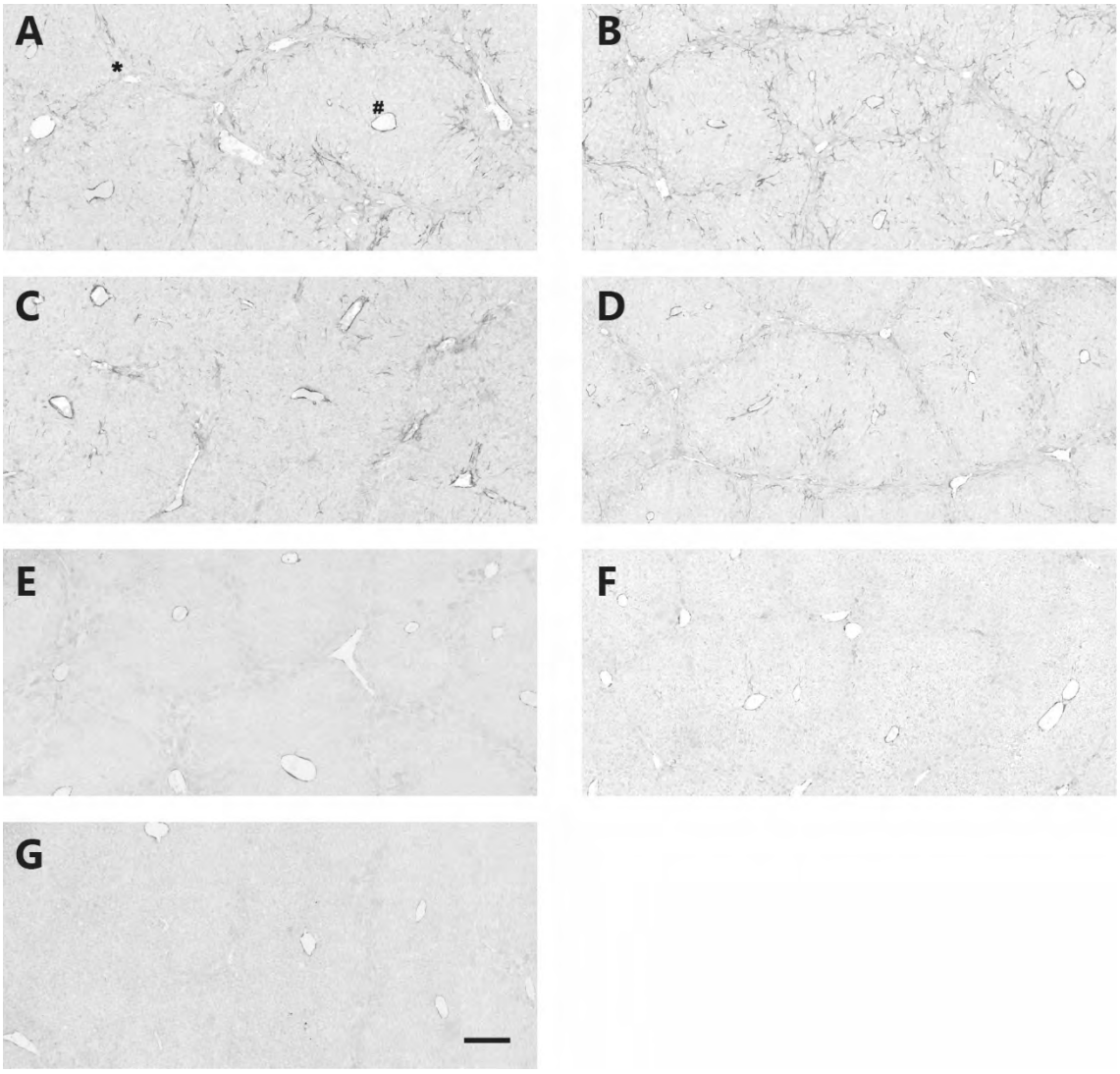

Figure 3-31: Staining for activated myofibroblasts by αSMA; oral TAA chronic hepatic injury model and resolution

Mice were euthanised for tissue analysis after 1 (A), 4 (B), 7 (C), 14 (D), 28 (E) and 42 (F) days of recovery following 16 weeks of chronic hepatic injury as described in Figure 3.27. Paraffin-embedded sections (left hepatic lobe) cut to a thickness of 3μm were stained for alpha smooth muscle actin (α SMA) as described in section 2.11.2. Figure G shows α SMA staining from a mouse euthanised after drinking fruit squash without TAA for 16 weeks, and normal drinking water for 1 day (control). Dark areas indicate positive staining. Scale bar (–) measures 200μm. Examples of the centrilobular vein (#) and portal tract (*) are illustrated.

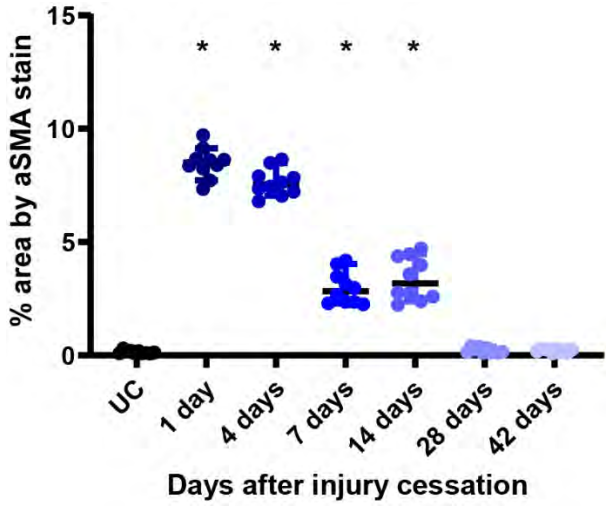

Figure 3-32: Quantitative analysis of myofibroblast activation; oral TAA chronic hepatic injury model and resolution

Morphometric analysis of positive-stained areas following alpha smooth muscle actin (αSMA) staining of paraffin-embedded sections as described in Figure 3.31. Summary bars: 95% confidence interval and median value. UC, uninjured control

The resolution of the expression of fibrosis-related genes is described in figure 3.33. The expression of all the genes were elevated throughout the 42 days of recovery, except for *Acta2* (the expression on day 4 and 28 of recovery were not statistically different to the UC). The expression of *Col1a1, Col3a1, Tgfb1, Mmp2,* and *Timp1* peaked within the first week of recovery before diminishing to a lower level elevation (Table 3.1). By comparison, the expression of *Acta2* and *Mmp9* persisted around 2-3 fold that of the uninjured control cohort throughout recovery. The difference between the expression at day 1 and day 42 of recovery were statistically insignificant in both genes (*Acta2*, p=0.248; *Mmp9*, p=0.353)

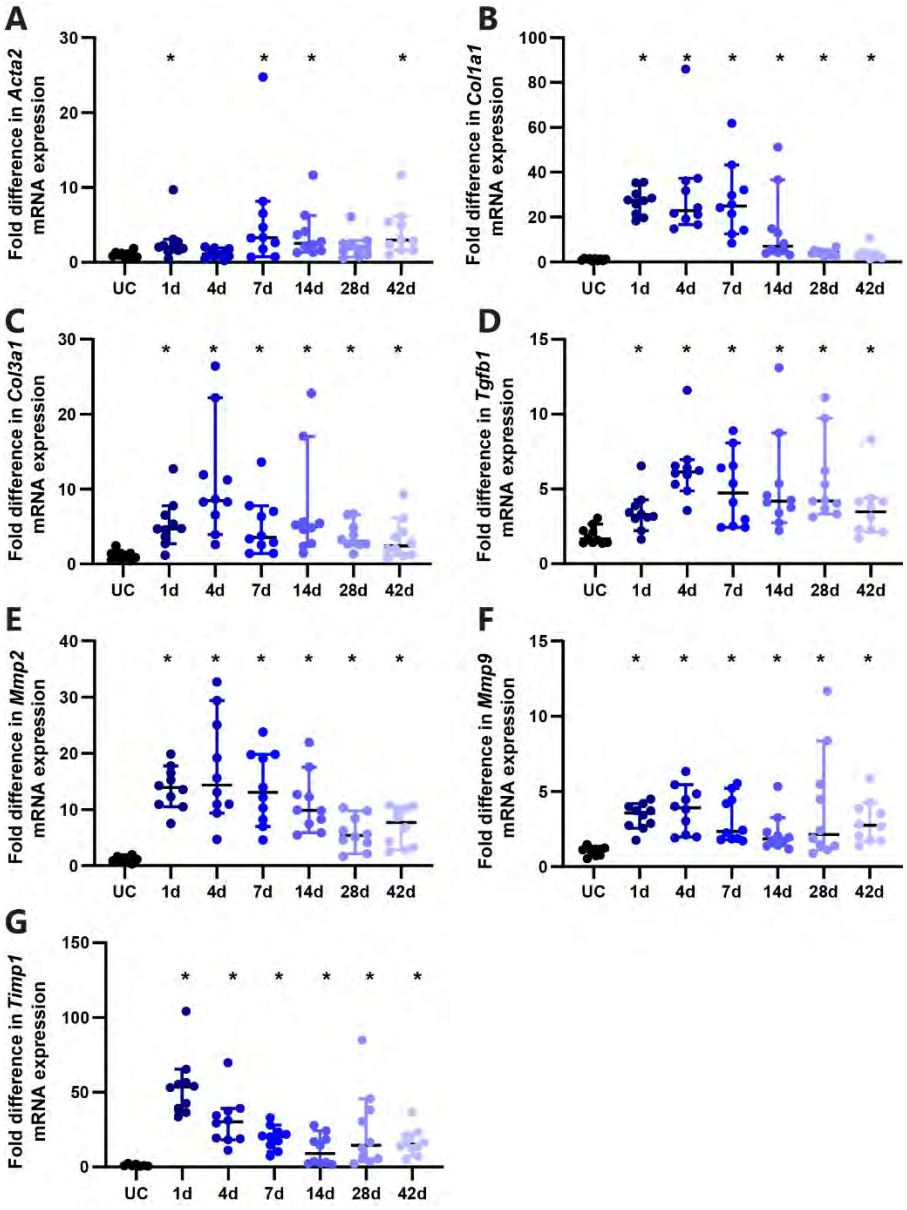

Figure 3-33: Gene expression analysis by qPCR of fibrosis-associated genes; oral TAA chronic hepatic injury model and resolution

Mice were euthanised for tissue analysis after 1, 4, 7, 14, 28 and 42 days of recovery following 16 weeks of chronic hepatic injury as described in Figure 3.27. Expression of fibrosis-associated genes (A: *Acta2*, B: *Col1a1*, C: *Col3a1*, D: *Tgfb1*, E: *Mmp2*, F: *Mmp9*, G: *Timp1*) was assessed by qPCR of homogenised and disrupted hepatic tissues (caudate and quadrate lobes) as described in section 2.14. Summary bars: 95% confidence interval and median value. The Mann-Whitney test was used to compare values in the injured mice euthanised at different time points against uninjured control (UC) mice; $p<0.05$ (*) were deemed statistically significant. *Acta2*, actin; *Col1a1*, collagen-1; *Col3a1*, collagen-3; *Mmp*, matrix metalloproteinase; *Timp1*, tissue inhibitor of matrix metalloproteinase-1; *Tgfb1*, transforming growth factor beta-1.

3.4.5. Determining the profile of inflammation and hepatocyte injury after toxin-cessation: oral TAA model

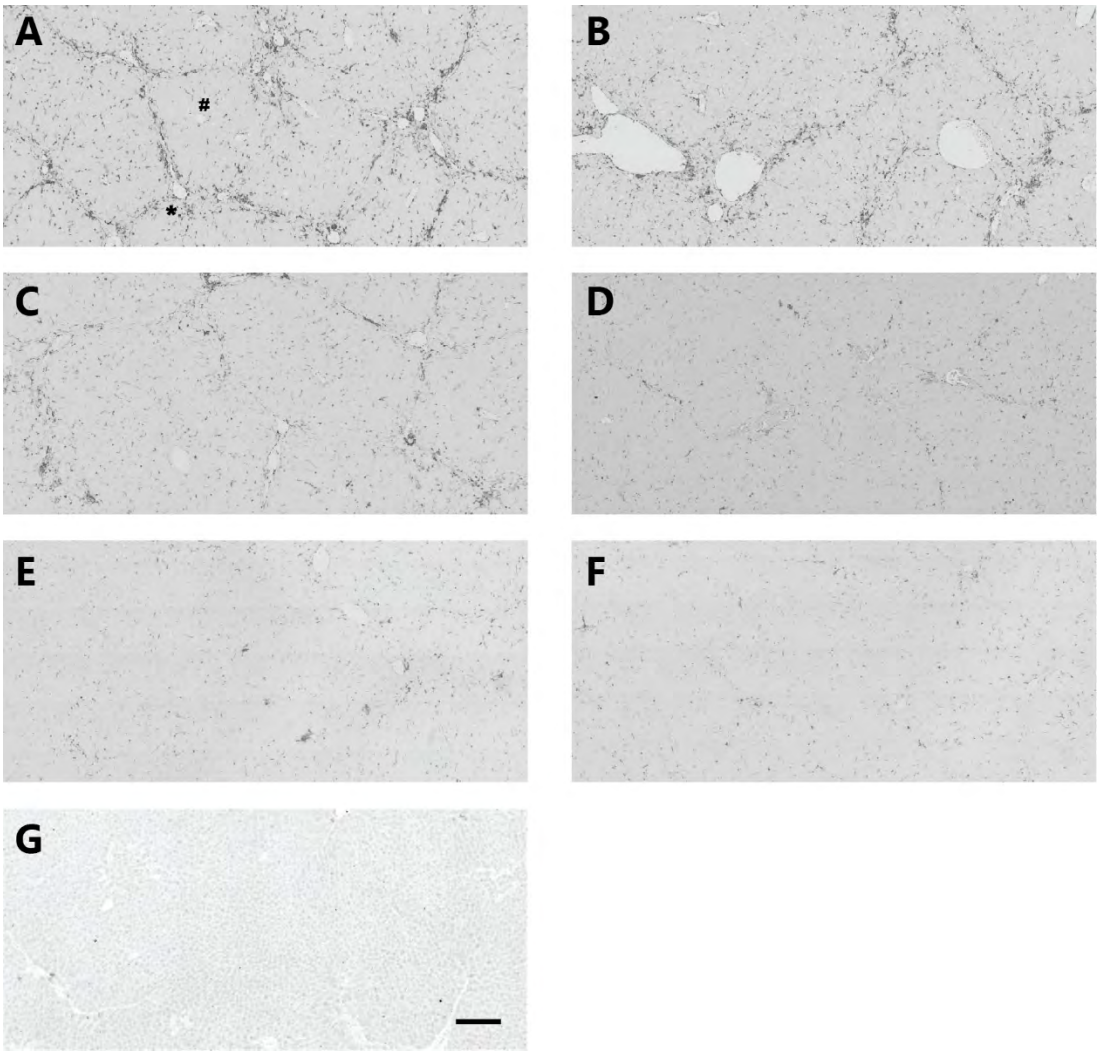

Figure 3-34: Assessment of inflammatory infiltrate by CD45 staining; oral TAA chronic hepatic injury model and resolution

Mice were euthanised for tissue analysis after 1 (A), 4 (B), 7 (C), 14 (D), 28 (E) and 42 (F) days of recovery following 16 weeks of chronic hepatic injury as described in Figure 3.27. Paraffin-embedded sections (left hepatic lobe) cut to a thickness of 3μm were stained for CD45 as described in section 2.11.2. Figure G shows CD45 staining from a mouse euthanised after drinking fruit squash without TAA for 16 weeks, and normal drinking water for 1 day (control). Dark areas indicate positive staining. Scale bar (–) measures 200μm. Examples of the centrilobular vein (#) and portal tract (*) are illustrated.

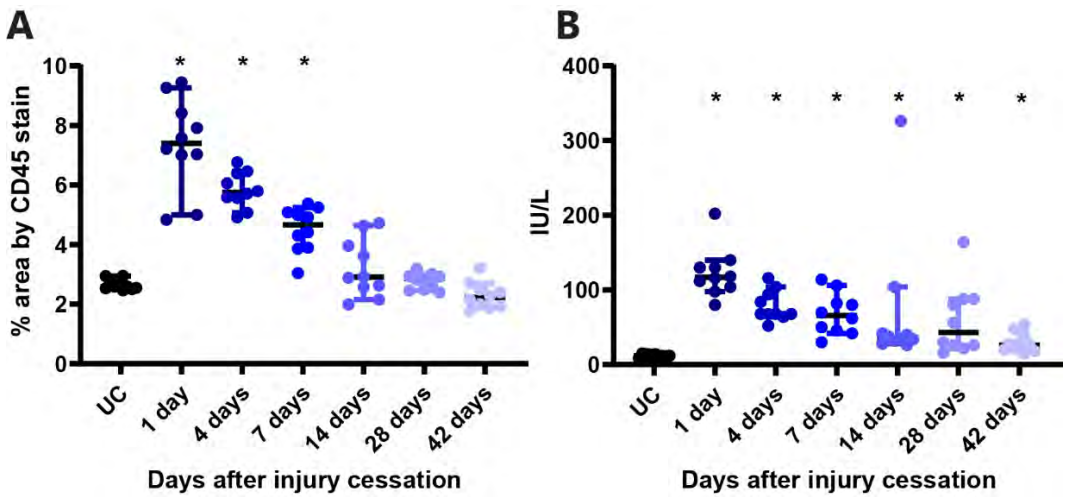

Figure 3-35: Quantitative analysis of inflammatory infiltrate by CD45 staining and hepatocyte injury by serum ALT measurements; oral TAA chronic hepatic injury model and resolution

Morphometric analysis of positive-stained areas following CD45 staining of paraffin-embedded sections as described in Figure 3.34. Sera from each euthanised mouse as described in Figure 3.27 were analysed for ALT as a surrogate for hepatocyte injury or cell membrane instability using a clinical biochemistry analyser. ALT, alanine aminotransferase; IU, international units. The Mann-Whitney test was used to compare values in the injured mice euthanised at different time points against uninjured control (UC) mice; $p<0.05$ (*) were deemed statistically significant.

The inflammatory infiltrate settled along the fibrotic scar and around the portal tracts (Figure 3.34). The infiltrate progressively dispersed and partially diminished (Figure 3.35, panel A) through the first week of recovery. By day 14 the level of inflammatory infiltrate equated to the uninjured controls ($p=0.248$). Serum ALT was modestly elevated at the cessation of injury (median ALT 117IU/L, compared to 776IU/L in the CCl_4 after the 1st day of recovery) reflecting the persistent low-level hepatocyte damage observed in the feasibility study (Figure 3.35, panel B). The low-level rise of serum ALT remained significantly elevated after 42 days of recovery. However, the median values fell below the clinical upper limit of normal (50IU/L) by the 14th day of recovery (median 36IU/L), in congruence with the dissipation of the inflammatory infiltrate.

3.5. Discussion

3.5.1. Feasibility and safety

The IP CCl_4 chronic hepatic injury model has already been established and used at the Birmingham BMSU[170]. Nevertheless, the study confirmed that it could be completed safely, at a higher dose than previously trialled. The 16-week oral TAA model was introduced to the Birmingham BMSU following a small volume feasibility experiment over 12 weeks. The mice were healthy throughout, with no dropouts or deaths over the 16-week injury period.

However, IP TAA, used at previously published safe doses to induce liver fibrosis[171], caused a catastrophic hepatic injury as a consequence of widespread acute zonal necrosis after a single dose. I considered trialling the IP route again at a lower dose[172], but it was deemed more reasonable to trial the oral regimen which had proven safety and efficacy at another UK institute[60].

3.5.2. Peak fibrosis and resolution

CPA after PSR staining is, on balance, a better test than hepatic hydroxyproline for quantifying extant tissue ECM, in that it provides a direct and accurate representation of microscopically visible collagen deposition, which has been shown to have excellent clinical prognostic value[173]. Moreover, bias was minimised in this study by using a slide-scanner to measure the CPA across the largest lobe of liver (>80% of available area) to ensure fidelity to standardised guidelines requiring truly "representative morphometric analysis"[73] (as described in section 2.11.5).

Peak fibrosis as measured by CPA in both the CCl_4 and the TAA models were comparable to published data[60,154,165]. TAA delivered a greater fibrotic scar than the CCl_4 model (Table 3.1). The fibrosis persisted to the investigated recovery time points in both but was more pronounced in the TAA model. The decrease of the mRNA expression of fibrosis-related genes in resolution is in the same order of magnitude as has been published in similar models of fibrosis[165,172]. The findings as summarised in table 3.1 would suggest the chronic TAA model to be a better fit to the "ideal" scenario as graphically described in figure 3.1, but both were nevertheless suitable to test the therapeutic intervention (Chapter 5).

Table 3-1: Summary comparison of fibrosis at peak and after recovery in the IP CCl_4 and oral TAA model

Fibrosis readout	Peak			After recovery		
	CCl_4 Day 1	**TAA Day 4**	**P**	**CCl_4 Day 21**	**TAA Day 28**	**p**
% CPA of PSR ***(median, IQR; %)***	2.85, 0.97	10.39, 2.82	**<0.001**	1.79, 0.72	7.27, 1.02	**<0.001**
Hepatic hydroxyproline ***(median, IQR; µg/g liver)***	385, 179	529, 125	**0.005**	266, 89	397, 155	**0.002**
% area αSMA staining ***(median, IQR; %)***	4.37, 1.43	7.54, 0.87	**<0.001**	0.62, 0.33	0.15, 0.23	***<0.001***
PCR: *Acta2* ***(median, IQR; fold)***	1.74, 1.23	1.09, 1.12	0.123	0.94, 0.58	1.88, 1.66	**0.043**
PCR: *Col1a1* ***(median, IQR; fold)***	5.58, 5.43	22.92, 17.88	**<0.001**	1.48, 0.75	4.19, 17.88	**<0.001**
PCR: *Col3a1* ***(median, IQR; fold)***	5.60, 4.15	8.46, 8.56	**0.035**	2.07, 1.63	3.05, 2.69	0.190
PCR *Tgfb1* ***(median, IQR; fold)***	3.10, 2.84	6.14, 1.43	**<0.001**	1.04, 0.58	4.21, 3.50	**<0.001**
PCR: *Mmp2* ***(median, IQR; fold)***	8.10, 3.70	14.33, 15.66	**0.007**	2.62, 1.12	5.38, 5.19	**0.009**
PCR: *Mmp9* ***(median, IQR; fold)***	2.67, 2.34	3.92, 2.91	0.393	1.30, 1.26	2.15, 4.88	0.105
PCR: *Timp1* ***(median, IQR; fold)***	7.71, 6.36	30.31, 19.08	**<0.001**	2.45, 1.48	14.50, 34.88	**<0.001**

Differences in fibrosis readouts at peak, and after a designated duration of recovery after last hepatic injury in the CCl_4 and TAA models. Comparisons between outputs were undertaken by a Mann-Whitney test (nonparametric) and deemed statistically significant if $p<0.05$ (**bold**). ***Bold italics*** were assigned to statistically significant differences whereby CCl_4 > TAA. αSMA, alpha smooth muscle actin; *Acta2*, actin; *Col1a1*, collagen 1; *Col3a1*, collagen 3; IQR, interquartile range; *Mmp*, matrix metalloproteinase; *Tgfb1*, transforming growth factor 1; *Timp1*, tissue inhibitor of matrix metalloproteinase 1; CPA, collagen proportionate area; PSR, picrosirius red.

3.5.3. Defining a time frame for intervention

The data was used to inform the timing of the intervention (MSCs) in the primary experiment (in Chapter 5) in the absence of continuing evidence of active hepatocyte injury and inflammatory reaction. This scenario was chosen to ensure any observed therapeutic effect on fibrosis was independent of a dampening of immune-mediated injury and was primarily anti-fibrotic. Furthermore, it was thought to be analogous (though imperfectly so) to the intended beneficiaries – patients with persistent fibrosis or cirrhosis in the absence of ongoing aetiological injury (i.e. abstinent patients with ARLD, treated viral hepatitis related cirrhosis, controlled autoimmune hepatitis, etc.).

ALT had near normalised by day 4, and CD45 cell infiltration had dispersed from the portal tracts, and dissipated to low levels by day 7 in the chronic CCl_4 model. As such, day 7 of recovery was deemed an appropriate time point to intervene on established fibrosis in the CCl_4 model.

Day 14 of recovery was selected as an appropriate intervention time point for the chronic TAA model, based on CD45-positive cells dissipating to levels equivalent to the uninjured controls, and serum ALT level normalisation.

3.5.4. Variation in fibrosis despite identical injury

One of that the major shortcoming of both models is an inadequate reproducibility of fibrosis as primarily measured by CPA and Hyp at peak and during resolution. Though the vagaries of the Hyp assay could attribute to some of the variance (as described in Section 2.10), the CPA assay

was a representation of what could be microscopically seen, and bias was limited by using an automated slide scanner and measuring CPA from >80% of each paraffin section of the largest lobe of the liver. Moreover, the variance was also evident in the PCR of fibrosis-related genes.

Age and sex-matched mice were bought from a common supplier and the experimental conditions including the timing of dosing for mice were identical for each experiment. As for the CCl_4 model, the study employed an IP weight-based dosing strategy that is preferred by many investigators for excellent reproducibility, ease of performance and safety[162]. Whereas some investigators have abandoned the IP route of administration due to peritoneal adhesions, I found minimal complications in any of the mice at the time of tissue extraction[165]. Moreover, having previously completed a similar IP-dosed chronic injury model, the experiment was not a victim of my own personal learning curve[154]. It was not possible to accurately determine whether the mice took comparable doses of TAA *ad libitum* throughout their 16-week injury period. However the model is well established and preferred by other laboratories[60,167]. Moreover, the mice self-governed their intake and maintained good hydration throughout, and a very narrow variation on weight over the 16-week period suggesting their fluid intake was appropriate for their needs (Figure 3.28). Nevertheless, I concede a variation in dosing may have contributed to the variation in fibrosis in the oral TAA model.

Having controlled for obvious variables, the variation may be attributable to natural inter-mouse differences that other investigators and experiments would also be subject to. It is difficult to ascertain the true reproducibility of fibrosis in the available published data, as few clearly represent

the variance of their data, and fewer still undertake power calculations to necessitate such granularity. Furthermore, investigators rarely employ identical injury strategies. Scholten's standard operating manual for the CCl_4 model have used their internal data to approximate a 25% variance within each group of *Col1* mRNA expression, but have not declared the expected variance for other outputs[162]. Trautwein's guidelines for *in vivo* pre-clinical experimentation suggested group sizes of 8-15 but did not qualify on what measured output or power this was based. Nevertheless, for the purposes of this study, it was necessary to base sample size calculation on a change in established fibrosis – extant ECM. We elected to use CPA based on the earlier discussion about representative sampling and limitation of bias.

Table 3-2: Sample size calculations for intervention experiment based on time course experiments in both models

	CPA (PSR)			
	CCl_4 Day 1	**CCl_4 Day 21**	**TAA Day 4**	**TAA Day 28**
Mean (%)	2.92	1.87	10.55	7.56
Standard deviation	0.62	0.44	2.64	1.73
Minimal sample size / group	16	20	20	18

Sample size calculations based on peak fibrosis and resolution data to achieve a Δ of 25% to a statistical power of 90% with a specific α error probability of 0.05. The data was presumed to be parametrically distributed for the purposes of the calculation and a two-tailed test was performed. CPA, collagen proportionate area; PSR, picrosirius red

Mr James Hodson (Statistician at the Institute of Translational Medicine, University Hospital Birmingham, UK) checked and verified the sample size calculations.

3.5.5. Summary

In summary, the work in this chapter has established the safety and feasibility of 2 hepatic fibrosis and resolution models, 1) 12 IP injections of CCl_4 over 6 weeks, followed by 3 weeks of recovery, 2) 16 weeks of oral TAA in drinking squash given *ad libitum* followed by up to 6 weeks of recovery. The results also highlighted the potential toxicity of IP TAA.

Fibrosis attenuated with recovery but persisted to the final investigated recovery time points in both models. Fibrosis was variably reproducible despite identical injury conditions, which in turn informed the sample size for subsequent intervention experiments as described in Chapter 5. Moreover, delineation of changes to the inflammatory cell infiltrate and serum ALT informed an ideal time point for intervention in both models.

Chapter 4

Characterising MSCs

4.1. Background and context

MSCs were classically defined as BM cells that adhered to plastic[75]. This yielded heterogeneous unsorted cells that varied both phenotypically and functionally from batch to batch, rendering it difficult to establish a true picture of efficacy and comparability. To rectify this, the ISCT agreed standards by which to uniformly characterise MSCs[81,82]. Further to their ability to adhere to plastic, MSCs needed to readily transdifferentiate down different mesodermal lineages and express CD73, CD90 and CD105, but not express CD14, CD34, CD45 and class-II MHC.

Pre-clinical experimentation with MSCs should report their isolation techniques, enrichment, cell surface marker profiles with respect to the aforementioned ISCT guidance, mesogenic differentiation[174,175], and cell preparation information[45]. This will inform the translatability of *in vitro* and *in vivo* studies to clinical trials.

I have chosen to use human MSCs for this study with a view to shortening the bridge to translate any pre-clinical findings to clinical application. Furthermore, our laboratory has close professional links with commercial partners, OTL (Galway, Ireland), who have developed a novel method to isolate and purify MSCs for use in human therapy. OTL allogeneic MSC therapies are currently being trialled for a number of clinical conditions including autoimmune hepatitis and primary sclerosing cholangitis (MERLIN, ClinicalTrials.gov identifier: NCT02997878). They have kindly provided MSCs for this body of work.

4.1.1. Mesenchymal stromal cell selection by prospective enrichment

To date, MSC isolation from tissue has relied on their functional capacity to adhere to tissue culture plastic. According, the mononuclear cells are left to incubate for 10-14 days in which time the MSCs will attach and form colonies at a recognised frequency of 1/80,000. At 10-14 days these colony forming units are harvested by trypsin digest and re-plated in serum-rich or platelet lysate-rich media at a density of up to 8,000 MSCs per cm^2. These MSCs proliferate *in vitro* until sufficient cell numbers are obtained to permit biochemical and cytological assessment. This plastic adherent MSC isolation technique was developed in the 1960s and has several limitations[75]. The co-expansion of other adherent cells standardly delivers a very impure population and low yield: only ~1/80,000 BM-MNC plated are MSC. This is reflected in guidelines from the European Medicines Agency Committee for Advanced Therapies, including a proposal for rigorous and prospective characterisation in order to deliver a purer, more defined cell population[176,177], to supplement existing standards.

Even at the time of publication, the ISCT definition for characterising MSCs was recognised as being limited because CD 105, CD73 and CD90 are expressed on many different cells, and selecting on these grounds still yielded intra-population heterogeneity[178]. Prospective isolation was seen as a step towards greater precision in isolating a purer MSC population[179]. It relies on the identification, and subsequent isolation and enrichment of the MSCs by their expression of a discriminatory cell surface antigen. However, identifying a single cell surface marker to discriminate MSCs from other mononuclear cells has proved challenging. Attempts to advance prospective isolation of MSC began in the late 1980s when Simmons and Torok-Storb identified

the first reagent that was used to prospectively isolate MSC from BM, an IgM antibody called Stro1[180]. However, the Stro1 antigen was never identified, and proved to be poorly discriminatory for MSCs amongst other mononuclear cells. McGonagle and Jones identified antibodies to CD271 as a marker to capture all MSC from human BM[181]. Likewise, two groups in Germany and Australia identified two different antibodies that bind and isolate the same antigen on all MSC within human BM. Bühring and colleagues identified an antibody to tissue non-specific alkaline phosphatase (ALP) called W8B2[182] whereas Gronthos identified the antibody, Stro3 that also binds ALP[183]. Anti-Stro-3 (or W8B2) antibody-coated magnetic bead reagents can be used to positively select cells displaying the ALP surface antigen. This magnetic assisted cellular sorting (MACS) approach can process a high number (10^9) of BM-MNC in a few hours, but the resulting product output is still a heterogeneous mixture of cells because of the single parameter (one antibody/one-bead) selection. That said, MACS separation of BM-MSC using anti-CD271 or anti-ALP antibodies (W8B2/Stro3) can enrich the MSC/MNC ratio to from 1:80,000 seen in PA-MSC preparations to ~1:300[184]. This MACS-based prospective isolation of $Stro3^+$MSC is a proprietary method used by Mesoblast (Australia) to manufacture their MSC therapeutics, NeoFuse™ and Revascor™. The Mesoblast Stro3 technology represents the only commercial advanced MSC prospective isolation technology and is protected by Mesoblast intellectual property filings. A plotted summary of the progress of isolation techniques has been reviewed elsewhere[185].

OTL have identified CD362/Syndecan-2 (S2) as a cell surface marker that can be used to prospectively isolate MSC from different tissues, that is conserved across species. In collaboration with Miltenyi Biotec, OTL has developed a Good Medical Practice (GMP)-grade anti-S2 antibody

that is bound to Miltenyi proprietary Microbead technology. This anti-S2-microbead reagent is proprietary technology that permits MACS-based enrichment of S2-MSC using the Miltenyi CliniMACS Prodigy device from several adult tissues. It provides a 300-fold enrichment of S2-MSC over other current MSC isolation technologies (Data from OTL, Ireland).

4.1.2. Umbilical-cord tissue derived mesenchymal stromal cells

Umbilical cord tissue is an attractive source of MSCs and has many practical advantages over other potential sources. Procurement from UCT removes the risk and morbidity of donors undergoing BM harvest or procurement from other tissue. Furthermore, the abundance of potential donors extends the translational potential of pre-clinical work. UCT is obtained from donors of roughly similar age. This may confer a favourable batch variability profile. Data from OTL indicates homogeneity with less than 10% variability on CCL2 secretion and less than 5% variability in IL-6 secretion in contrast to the 50% difference in CCL2 secretion and 40% variability in IL-6 secretion observed with plastic adherent BM MSC. Other investigators have found human UCT-MSC to persist longer in mouse models than human BM MSCs[186].

OTL has developed an enriched S2-MSC isolated from human UCT, ORBCEL-C™. ORBCEL-C™ has a narrow batch variability profile, greater proliferative capacity and enhanced immunomodulation compared to bone marrow derived cells in different pre-clinical experimental models (data from OTL, and the MERLIN consortium).

4.1.3. Syndecan-2

Syndecan-2 has a role in prospective isolation of MSCs and is of undoubted commercial value to OTL, but its biological significance on MSCs is less certain. *In vitro* and *in vivo* data using S2-selected MSCs from OTL have shown them to influence inflammatory processes more effectively than unselected MSCs. These include their effect on the hepatic inflammatory infiltrate and modifying macrophage polarity in a mouse model of biliary injury. Preliminary data in our laboratory suggest S2-MSC may be biologically distinct from un-enriched MSC in their ability to suppress CD4 T-cell proliferation *in vitro* (personal communication with Dr. Ashnila Janmohamed, 2018, Newsome laboratory, University of Birmingham). However, it is unclear whether S2 is a participant in the biological processes or whether it is an inert bystander. There are no published data investigating this yet.

Syndecans are a family of four members of transmembrane heparin sulfate proteoglycans found in mammalian cells[187]. Since their discovery in 1989, there has been a relative paucity of data to explain what their exact functions in disease and health are. They reportedly perform a wide range of tasks, with some investigators theorising that they may be intrinsically disordered proteins that lack a unique tertiary structure in isolation, but acquire it only after interacting with a partner, thereby enabling them to activate disparate intracellular and extracellular pathways[188]. S2 interacts with ECM and has a role in matrix interactions and assembly at the cell surface, cell-signalling and migration. S2 may be crucial during embryonic neurogenesis and angiogenesis[189], and may play a part in the pathogenesis of colorectal and lung cancer[190–192]. There are data to suggest S2 may have a role in fibrosis, yet in keeping with the pleiotropic nature of syndecans, it is unclear whether

the effect if pro-[193–195] or anti-fibrotic[196,197]. Moreover, cleaved/shed S2 and membrane-bound S2 may have contrasting functions[194], reflecting a possible role in context-dependent homeostasis.

Nevertheless, for this study, the primary function of syndecan-2 is as a cell surface marker of MSCs that facilitate the prospective enrichment of MSCs by the project's industry collaborators, OTL.

OTL generously provided human UCT-derived MSCs as described in section 2.1, and undertook the S2 enrichment process by their own proprietary technology. This project used S2-selected (D1/S2) and unselected MSCs (D1/US) from a matched donor (from herein described as donor 1 (D1)), and S2-selected MSCs (D2/S2) from another donor (donor 2 (D2)).

4.2. Aims of the chapter

The aims of the work in this chapter were to:

- Characterise S2-selected MSCs from two different donors, and unselected MSC from a matched donor by ISCT guidelines
- Evaluate the expression of S2 from donor-matched S2-selected and unselected MSCs
- Evaluate the expression of S2 at different cellular confluences *in vitro*

4.3. Morphology and plastic adherence of MSCs

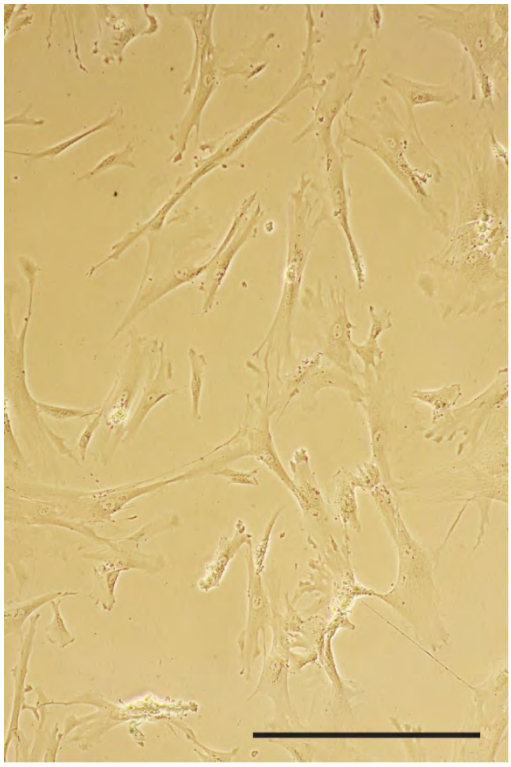

Figure 4-1: Bright field image of human UCT-derived MSCs

S2-selected MSCs plated on un-coated plastic. The image is representative of S2-selected and unselected MSCs from different donors. Scale bar (–) measures 100µm.

D1/S2, D1/US, and D2/S2 MSCs were all plastic adherent under standard culture conditions as described in section 2.2. MSCs spread their processes and exhibited a classic "fibroblast-like" morphological phenotype within 6 hours of seeding on uncoated plastic (Figure 4.1). Between passages 1-4, the cells reached confluence from a seeding density of 30-50% within 4-5 days (Figure 4.2)

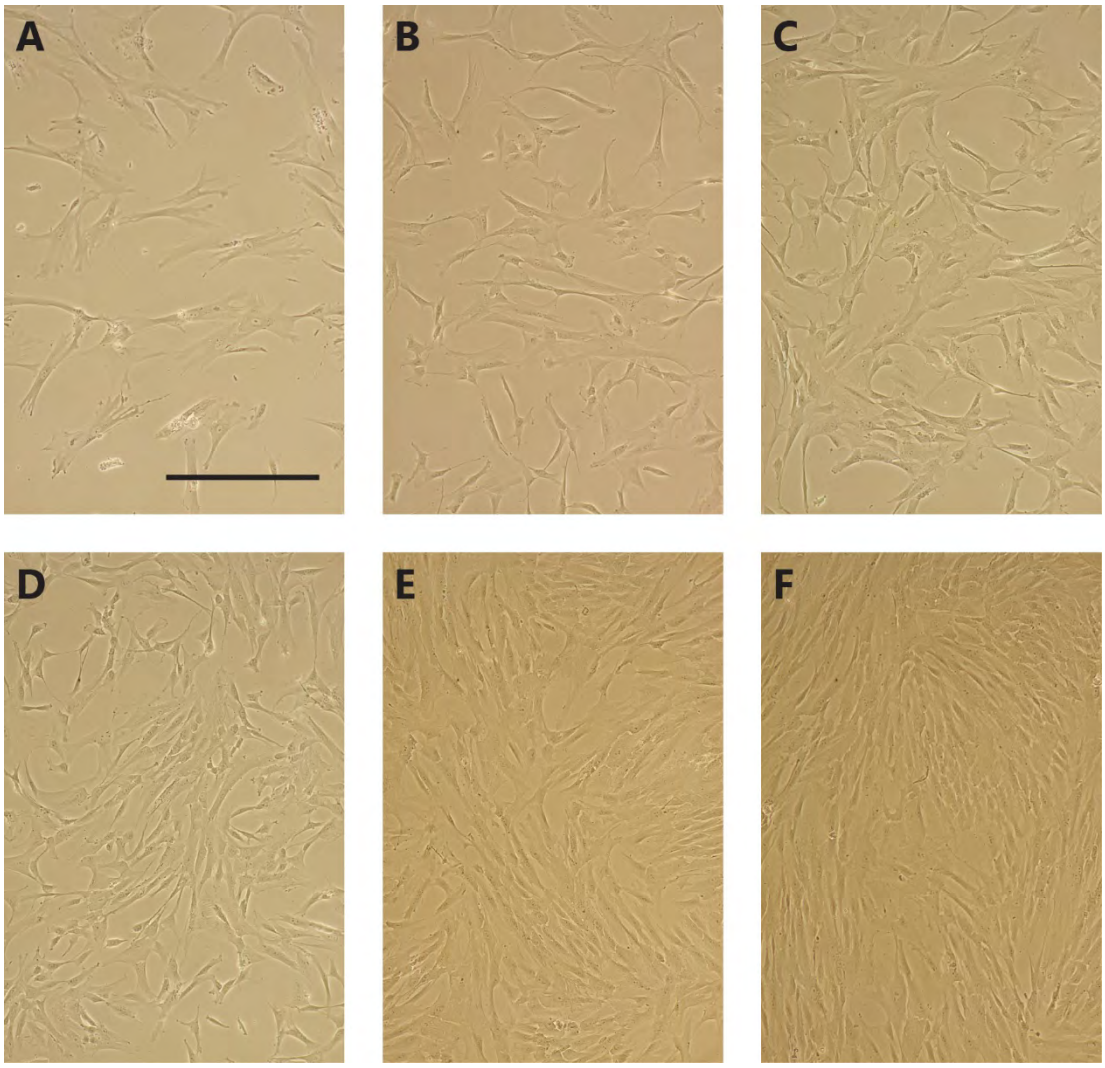

Figure 4-2: Bright field images of human UCT-derived MSCs at different confluences

MSCs plated on un-coated plastic at 30% (**A**), 40% (**B**), 50% (**C**), 60% (**D**), 70-80% (**E**), and 90-100% (**F**) confluence. Scale bar (**–**) measures 200µm.

4.4. The mesogenic process – mesodermal differentiation of MSCs

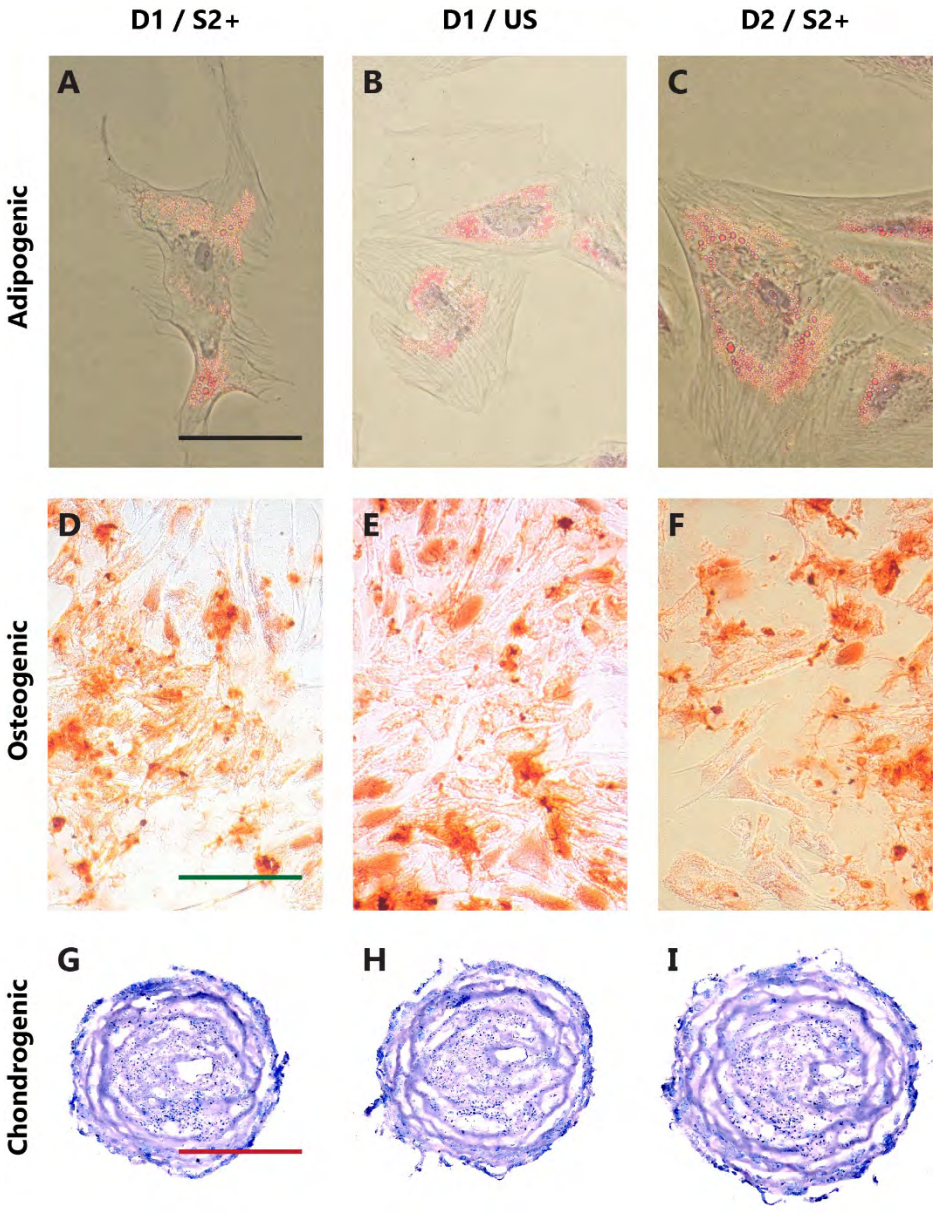

Figure 4-3: Tri-lineage differentiation of human UCT-derived MSCs

Adipogenic (Section 2.3.2, panels A, B, C), osteogenic (Section 2.3.4, panels D, E, F) and chondrogenic (Section 2.3.3, panels G, H, I) differentiation was stimulated in human UCT-derived MSCs from donor 1 (D1/S2+, syndecan-2 selected: panels A, D, G; D1/US, unselected: panels B, E, H) and donor 2 (D2/S2+, syndecan-2 selected: panels C, F, I). Lipid vacuoles in plastic-adherent MSCs were confirmed by Oil Red O staining (A, B, C). 1% Alizarin Red S solution was used to stain and confirm osteogenesis on plastic-adherent MSCs (D, E, F). Chondrogenesis was confirmed by staining frozen sections of the chondrocyte bullet with 0.1% toluidine blue (G, H, I). Black scale bar measures 20µm, green scale bar measures 100 µm, red scale bar measures 500µm.

Both selected (D1 and D2) and unselected MSCs (D1) underwent the mesogenic process when appropriately stimulated *in vitro* as described in Figure 4.3. There were no qualitative differences in the ease by which the MSCs underwent mesodermal transdifferentiation.

4.5. Cell-surface marker analysis

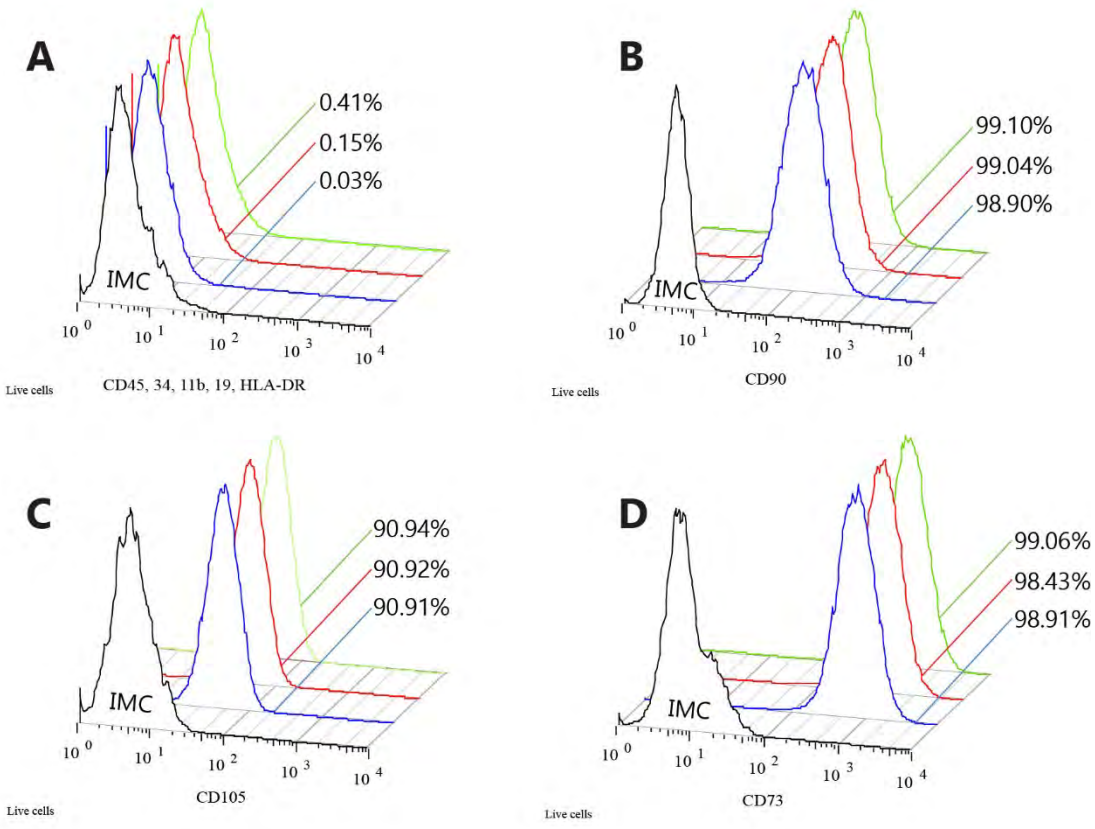

Figure 4-4: Flow-cytometric analysis of human UCT-derived MSCs by the expression of MSC-defining markers

Syndecan-2-selected MSCs from Donor 1 (green histogram) and 2 (blue histogram), and unselected MSCs from Donor 1 (red histogram) were labelled and prepared for flow cytometry using a the BD Stemflow™ Human MSC Analysis Kit as described in section 2.3.1. MSCs were shown to not express CD45, CD34, CD11b, CD19 and HLA-DR (PE fluorochrome) (A). They did express CD90 (FITC-conjugated, panel B), CD105 (PerCP-Cy™5.5- conjugated, panel C) and CD73 (APC-conjugated, panel D). Differences between test histograms and control histograms was calculated using the absolute Overton subtraction method. There were no statistically significant differences in the expression of MSC markers between donors, and between syndecan-2 selected and unselected MSCs.

All the MSCs expressed the requisite cell surface markers to satisfy the ISCT guidance. There were no statistically significant differences in the expression of specific markers between the MSC groups (Figure 4.4).

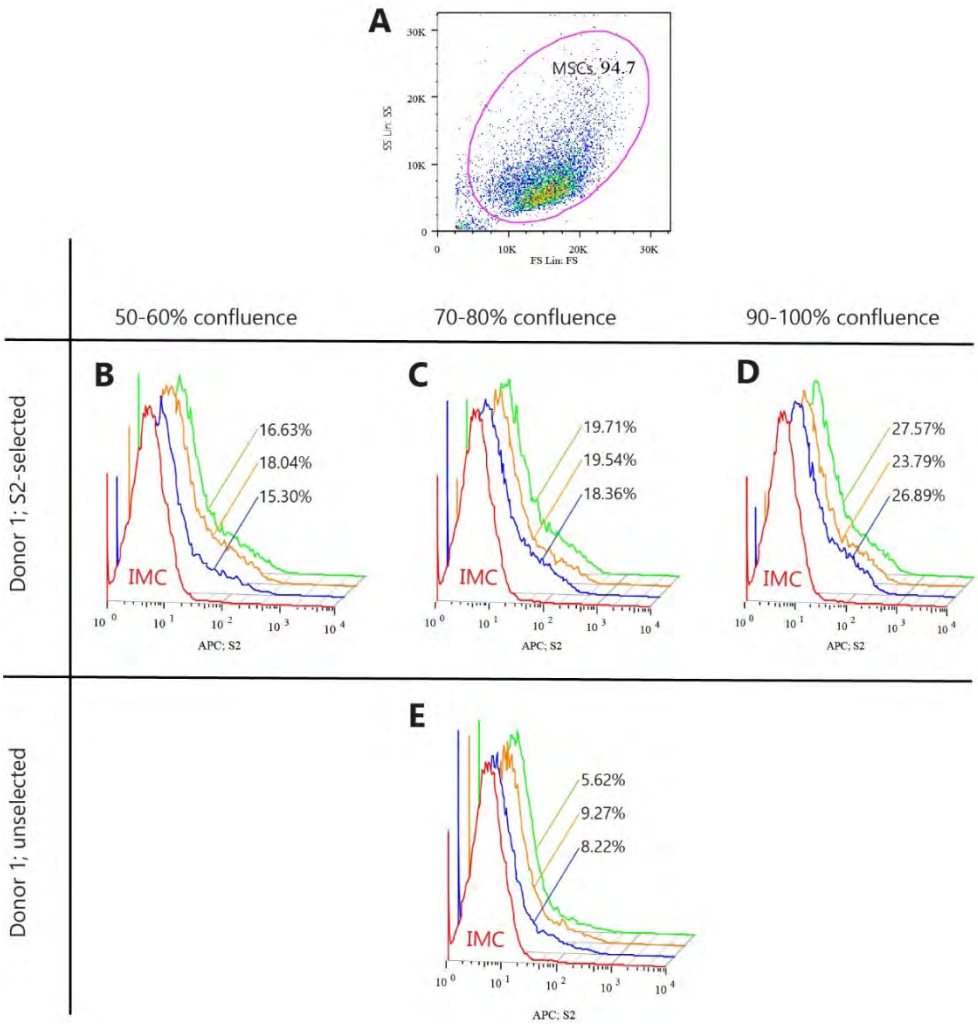

Figure 4-5: Flow-cytometric analysis of syndecan-2 expression in human UCT-derived MSCs by their mode of selection and cellular confluence *in-vitro*

MSCs were selected by an appropriate flow cytometry gate (A). S2-selected (B-D) and unselected (E) MSCs were either labelled with APC-conjugated S2 antibody (blue, orange and green), or an IMC (red histogram). S2 expression on MSCs increased with in-vitro cellular confluence (B-D). Differences between test histograms and control histograms was calculated using the absolute Overton subtraction method. There was a significant difference in S2-expression in MSCs enriched by S2-MACS (C), and unselected MSCs (E) at 70-80% confluence (Student's t, $p<0.001$). Cellular confluence had a significant effect on cell-surface S2 expression (Panels B-D, ordinary one-way ANOVA, $p<0.001$).

A flow-cytometric comparison of S2 expression between MSCs that had either undergone S2-selection (Section 2.1, Panel C, mean 19.2%) or not (Panel E, mean 7.7%) revealed a significant enrichment of S2-expressing MSCs in the cells that had undergone the MACS cellular sorting process (Student's t-test, $p<0.001$). The MSCs were from the same donor (D1) and matched for *in vitro* cellular confluence at the time of removal from culture.

Cellular confluence had a significant effect on cell-surface S2 expression, with a statistically greater expression noted at higher confluences (50-60% confluence; 16.7%, 70-80% confluence, 19.2%; 90-100% confluence, 26.1%; ordinary one-way ANOVA, $p<0.001$).

4.6. Discussion

4.6.1. The characterisation of MSCs

We confirmed that the MSCs we subsequently used in our *in vivo* and *in vitro* experiments reached the minimum threshold to be characterised as MSCs as decreed by the ISCT. The results were consistent between different donors, and the OTL proprietary MACS-enrichment process does not affect the baseline defining characteristics of the cells. We also confirmed that the MACS-enrichment process certainly selects an S2-enriched population, and we went on to investigate whether the enriched MSCs (S2-selected MSCs, S2-MSC), were functionally distinct in their ability to affect fibrosis in Chapters 5.

4.6.2. Moving goal posts – finessing the characterisation of MSCs

The 2006 ISCT MSC minimum characterisation guidelines did not incorporate their immunomodulatory properties. In 2014, the committee published a proposal to stimulate the field to discuss the incorporation of immunological/functional features to the baseline definitive characterisation of MSCs for clinical use[198]. It should follow, that immunological characterisation of MSCs be expected for pre-clinical experimentation as well. Primary to the proposals were incorporating functional potency assays (qPCR / protein based assays of secretome / flow cytometric analysis) to provide mechanistic insights on clinical response[198,199]. Interrogating the IDO response was proposed as an assay to describe the immunomodulatory potency of MSCs. Colleagues in the Newsome laboratory have pursued this line of interrogation using the OTL human UCT-MSCs, including T-cell suppression assays, which further adds to the fuller

characterisation of the cells used in this study (personal communication, Dr. Ashnila Janmohamed, 2018, Newsome laboratory, University of Birmingham). However, functional assays need to be function-specific; although the ISCT have proposed assays for the well-characterised immunomodulatory effects of MSCs, assays to reflect poorly characterised functions such as fibrolysis will require more exploration.

4.6.3. The effect of *in vitro* confluence on MSC biology

MSCs clearly increase their expression of cell surface S2 with increasing confluence; the biological relevance of this remains unclear. Published data suggests that other phenotypic characteristics of MSCs are unchanged at different cellular confluences[200]. Other investigators have found that increasing confluence, especially when close to 100%, may affect some biological functions (pro-angiogenesis), whilst sparing others (immunomodulation)[201]. Nevertheless, one cannot escape the potential confounding nature of changing S2 expression with confluence, especially in the absence of knowledge of what S2 actually does on MSCs. The issue of ensuring a fixed confluence for different experiments highlights the need for controlling other potential confounders when preparing MSCs (or any cellular therapy) *in vitro*. Other members of the Newsome laboratory have explored the utility of controlling cellular passage (Alfaifi M, 2018, PhD thesis, University of Birmingham), though even the effect of cellular aging on function remains a contentious one[153].

4.6.4. Summary

In summary, human UCT-derived MSCs donated by OTL from different donors were fully characterised as MSCs by ISCT guidelines. The proprietary MACS process by which S2 cells are enriched certainly increases the relative number of cells expressing S2. *In vitro* confluence also has a significant effect on S2 expression on MSCs. It is unclear whether these confluence-related changes affect MSC function, but the findings focus the investigator's requirement to ensure cells are harvested from culture at a set confluence, and that *in-vitro* culture conditions do not divagate to avoid any unintended confounding changes.

Chapter 5

The therapeutic effect of systemic human UCT-MSC therapy on liver fibrosis in murine models

5.1. Background and context

The overall aim of this body of work is to examine the therapeutic effect of mesenchymal stromal cells on liver fibrosis.

Healthcare systems in the western world have made progress in arresting the primary disease aetiology for a number of the major causes of liver cirrhosis. Improving public health and preventative measures tackle ARLD and NASH and effective antiviral therapy can control or cure hepatitis B and C respectively[3]. However, though some patients experience a reversal of their liver fibrosis upon stopping the iterative aetiological injury, others, often those with more advanced disease, can be left with a resistant hepatic scar, and the sequelae that follow including the risk of hepatocellular carcinoma, decompensation and death. It is for these patients that an anti-fibrotic agent may be most impactful.

Chapter 1 discusses the existing published data that explores the therapeutic effect of MSC on liver fibrosis. The pre-clinical data (Table 1.2) have been blighted by being underpowered, using poorly defined populations of MSCs, and at times failing to apply appropriate methodological rigour. However, the over-arching conclusions have been that MSCs seem to prevent fibrogenesis, but it remains unclear if they act to resolve established fibrosis[45]. Thus, MSCs given during injury seem to lessen the fibrotic response, but there remains equipoise as to whether MSCs given after fibrosis enhance resolution. The preclinical data sits alongside a body of published MSC clinical trial data (Table 1.1), including four randomised clinical trials, one of which explored the use of

MSC in abstinent patients with ARLD, in whom autologous MSCs given via the hepatic artery decreased fibrosis and biochemical surrogate scores of disease severity (MELD score)[100].

To model the clinical scenario of established liver fibrosis without continuing active injury, I established two models of toxin-induced liver fibrosis as described in Chapter 3. Both models delivered an appreciable scar, which persisted upon cessation of injury. The oral TAA model produced a more profound and persistent scar than the IP CCl_4 model. However, the wide natural variation in the fibrosis as measured by PSR CPA morphometric analysis necessitates sample sizes of 20 in the treatment and control groups to discern a 25% decrease in fibrosis (Table 3.2) in either model. The data identified a time point at which there were no evidence of significant continuing hepatic injury or inflammation in both models.

S2-selected UCT-MSC are prospectively enriched MSCs that are already under assessment for the treatment of inflammatory liver disease (autoimmune hepatitis and primary sclerosing cholangitis) in a Phase 2a clinical trial (MERLIN: http://fp7merlin.eu/project/). Chapter 4 described the ISCT characterisation of the MSCs that were donated for the interventional aspects of this study by OTL, and the need to control for cellular confluence at the point of detachment from *in vitro* expansion.

Three trial arms were tested against controls in this chapter. These included S2-selected MSCs from 2 different donors (D1/S2+; D2/S2+), thereby examining whether any effects (or absence

thereof) were donor-specific. Donor matched MSCs that had not undergone the S2 enrichment process were also tested (D1/US), to assess whether effects were consequent on S2 selection.

5.2. Aims of the chapter

The aims of the work in this chapter were to:

- Examine the effect of systemic human UCT-MSC therapy on fibrosis resolution in the absence of ongoing hepatic injury or inflammation in 2 murine models
- To also examine the effect of systemic human UCT-MSC therapy on fibrogenesis

5.3. Intervention to enhance fibrosis resolution in the absence of ongoing hepatocyte injury or inflammation

5.3.1. The effect of human UCT-MSCs on established CCl_4-induced liver fibrosis

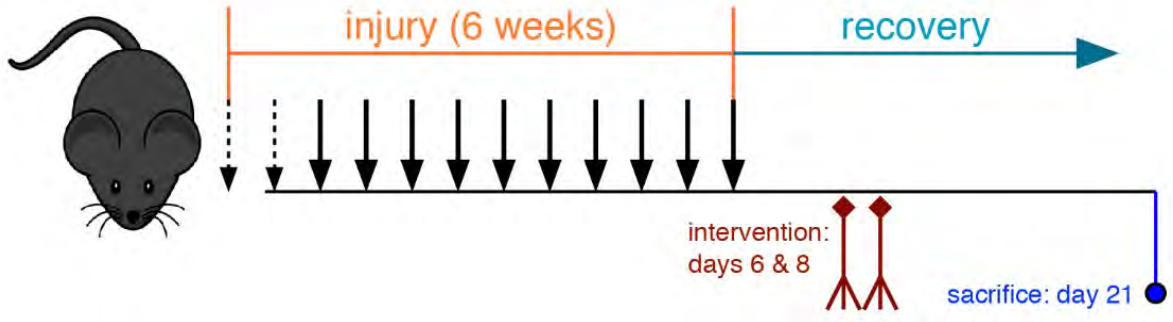

Figure 5-1: Schematic of experiment to explore the effect of MSC therapy on the resolution of established liver fibrosis using the IP CCl_4 chronic hepatic injury model: Experiment 1

Age-matched male C57Bl/6 mice were twice injected with CCl_4 diluted in mineral oil (1:3) at a dose of 1µl/g bodyweight (dashed vertical arrows) IP, followed by 10 injections at a dose of 2µl/g bodyweight (blocked vertical arrows) over 6 weeks. Mice were injected with $0.75x10^6$ MSCs in 200µL of sterile 0.9% saline carrier (test) or just carrier (control) by tail-vein on days 6 and 8 of recovery (total dose = $1.5x10^6$ cells) – EXPERIMENT 1. Mice were euthanised on day 21 of recovery (after last IP injection) for tissue and serum analysis. Syndecan-2-selected MSC were tested from two donors (D1/S2+ and D2/S2+), and unselected MSC from donor 1 (D1/US) (N=20 each test arm, N=20 control arm). Primary analyses in this experiment were between the each of the test arms and the control arm.

The time course experiments delineating peak hepatic fibrosis and resolution following 6 weeks of high dose IP CCl_4 (Section 3.3.2), revealed that hepatic inflammatory cells as assessed by CD45 IHC, had dispersed from portal areas and hepatocyte damage as measured by serum ALT had normalised by day 7 of recovery. As such, intervention was given as 2 doses at day 6 and 8 (Figure 5.1). A dose of $0.75x10^6$ MSC was selected as a maximum for a single bolus due to mice on occasion suffering immediate post injection fatal thromboembolic phenomena (cerebrovascular

event or pulmonary embolus) using doses above this threshold (preliminary tests – results not shown). A total of $1.5x10^6$ MSCs was chosen to be similar to doses that have been trialled in mice before in chronic models (Table 1.2), and was cumulatively greater than doses trialled in acute liver injury models in the Newsome laboratory[202].

The time point for assessment was chosen based on the time-course experiments that showed persistent scar at day 21 of recovery. Moreover, natural resolution takes days (as shown in Chapter 3), and any therapeutic enhancement would likely require days to manifest – therefore a 14 day interval was deemed reasonable.

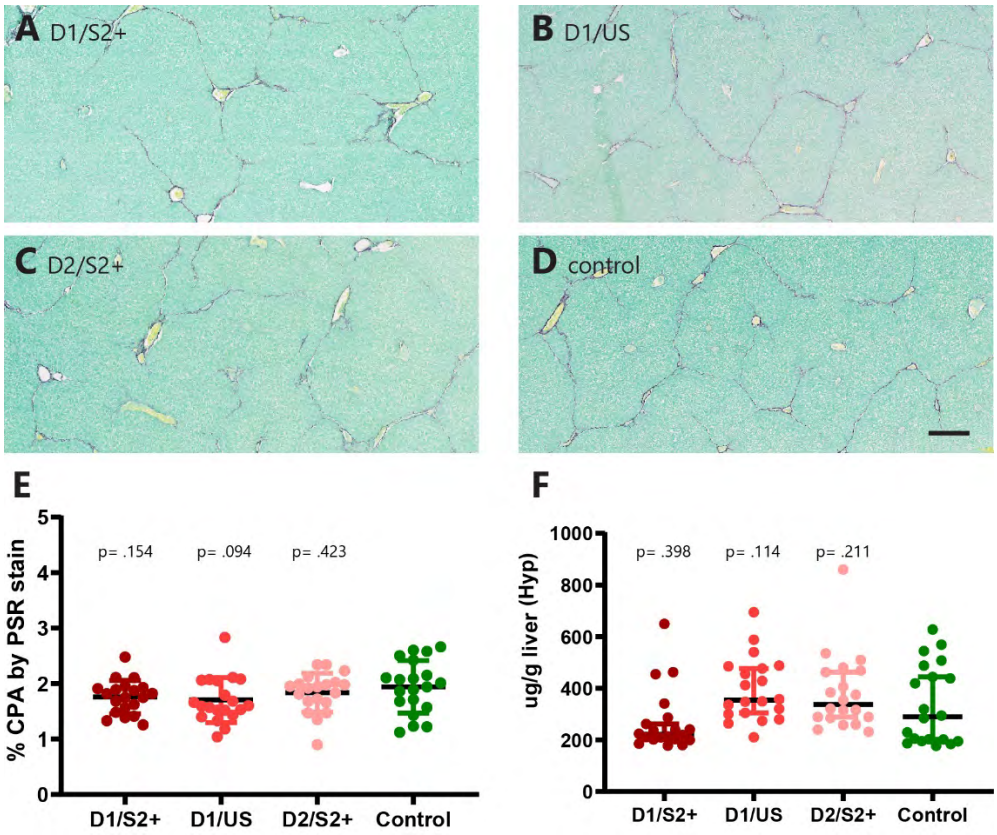

Figure 5-2: Analysis of collagen deposition in Experiment 1

Following injury, mice were injected with MSCs (donor 1, S2-selected [D1/S2+] - A; donor 1, unselected [D1/US] – B; donor 2, S2-selected [D2/S2+] – C) or control (D) as described in Figure 5.1 and euthanised on day 21 of recovery. Paraffin-embedded tissue were stained for collagen by PSR and fast green as described in section 2.11.3. Red areas demarcate collagen. Scale bar (–) measures 200µm. Morphometric analysis of collagen proportionate area (CPA) (E) and assessment of hepatic hydroxyproline (F) as described in section 2.10 allowed comparison between the treatment groups and the control group by the use of the unpaired Student's t-test (E) and Mann-Whitney test (F); $p<0.05$ was deemed significant. Summary bars: standard deviation and mean value for figure E; 95% CI and median value for figure F

Human UCT-MSCs had no significant effect on the resolution of IP CCl_4-induced liver fibrosis when administered in the absence of ongoing hepatic injury or inflammation (Figure 5.2). By day 21 of recovery, αSMA-positive scar-associated myofibroblasts were inactivated in natural resolution (Figure 3.11, 3.12), and the results in Figure 5.3 and Panel A of Figure 5.4 suggest MSC administration has no effect on αSMA expression.

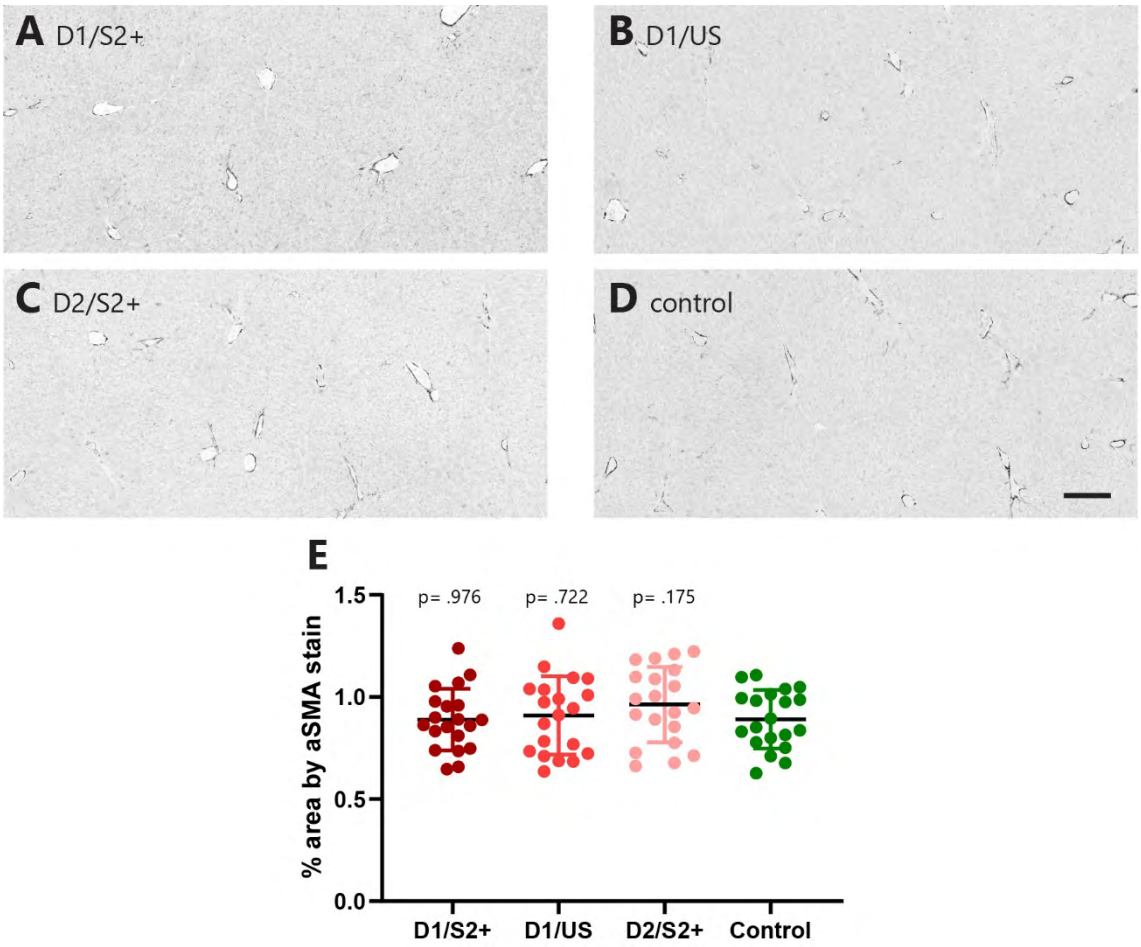

Figure 5-3: Analysis of myofibroblast activation in Experiment 1

Following injury, mice were injected with MSCs (donor 1, S2-selected [D1/S2+] - A; donor 1, unselected [D1/US] – B; donor 2, S2-selected [D2/S2+] – C) or control (D) as described in Figure 5.1 and euthanised on day 21 of recovery. Paraffin-embedded tissue were stained for αSMA as described in section 2.11.2. Dark areas indicate positive staining. Scale bar (–) measures 200μm. Morphometric analysis of positive stained area (E) allowed quantitative comparison between treatment groups and the control group by the use of the unpaired Student's t-test; $p<0.05$ was deemed significant. Summary bars: standard deviation and mean value

Overall, MSC intervention had little effect on the expression of fibrosis-related gene mRNA expression (Figure 5.4). However, S2-selected MSCs (but not unselected MSCs) from 2 donors increased the expression of *Col1a1, Col3a1* and *Tgfβ1*. The significance of these isolated adverse findings is questionable without any lasting effect on myofibroblast activation or gross scar deposition (PSR and hydroxyproline assays).

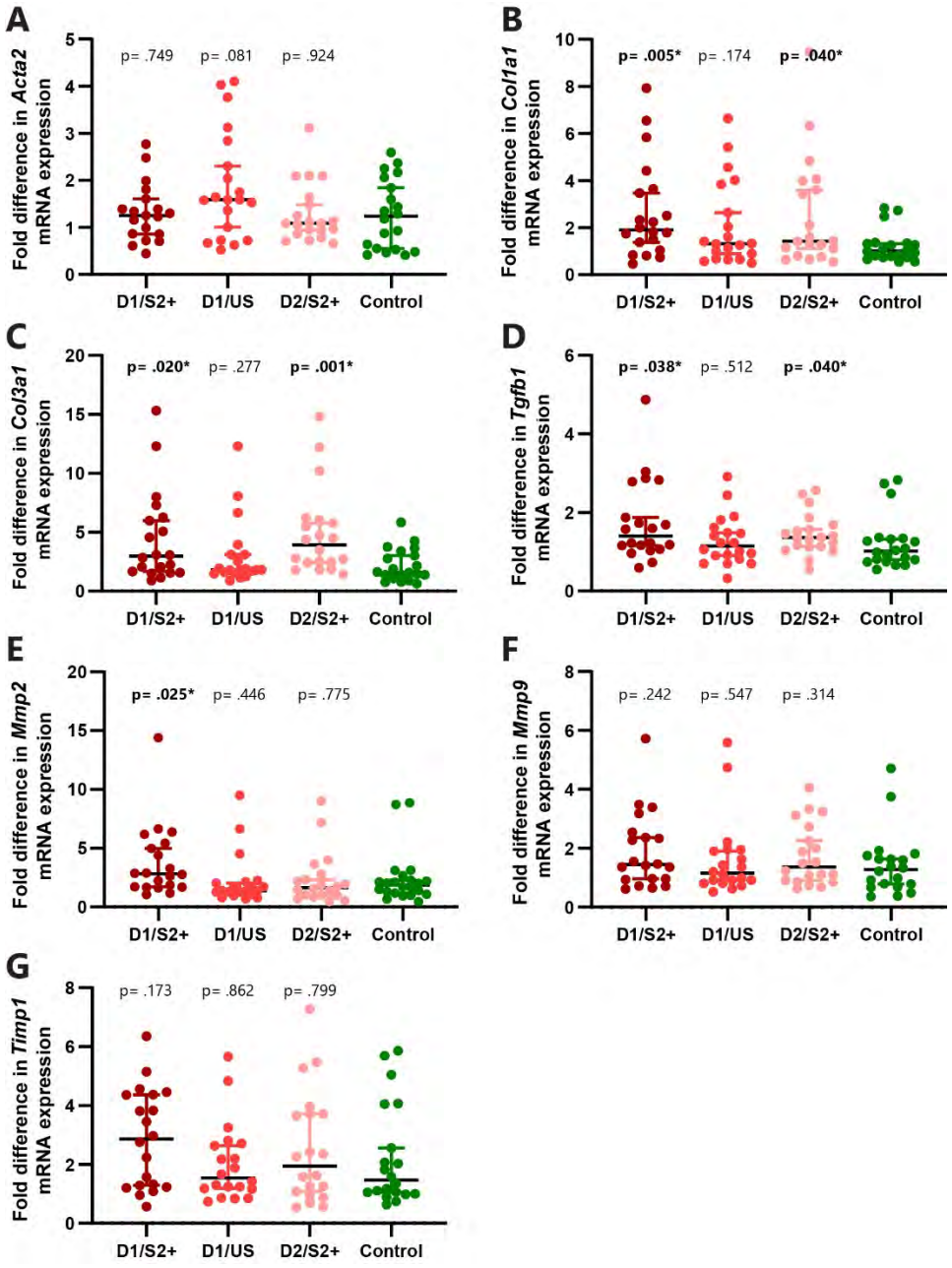

Figure 5-4: Gene expression analysis by qPCR of fibrosis-associated genes in Experiment 1

Following injury, mice were injected with MSCs (donor 1, S2-selected [D1/S2+]; donor 1, unselected [D1/US]; donor 2, S2-selected [D2/S2+]) or control as described in Figure 5.1 and euthanised on day 21 of recovery. Expression of fibrosis-associated genes (A: *Acta2*, B: *Col1a1*, C: *Col3a1*, D: *Tgfb1*, E: *Mmp2*, F: *Mmp9*, G: *Timp1* versus. Housekeeping gene *Gapdh*) were assessed by qPCR of hepatic tissues as described in section 2.14. The Mann-Whitney test was used to compare expression in treatment groups and control group; $p<0.05$ was deemed significant and highlighted in bold. Summary bars: 95% CI and median value

In knowledge of the immunomodulatory effect of MSC, I went on to examine whether the MSC administration had any effect on the myeloid inflammatory infiltrate. Members of the Newsome laboratory using the same MSCs had shown an MSC-induced change of macrophage polarity in a murine biliary injury model, which may have relevance to fibrotic pathways[202].

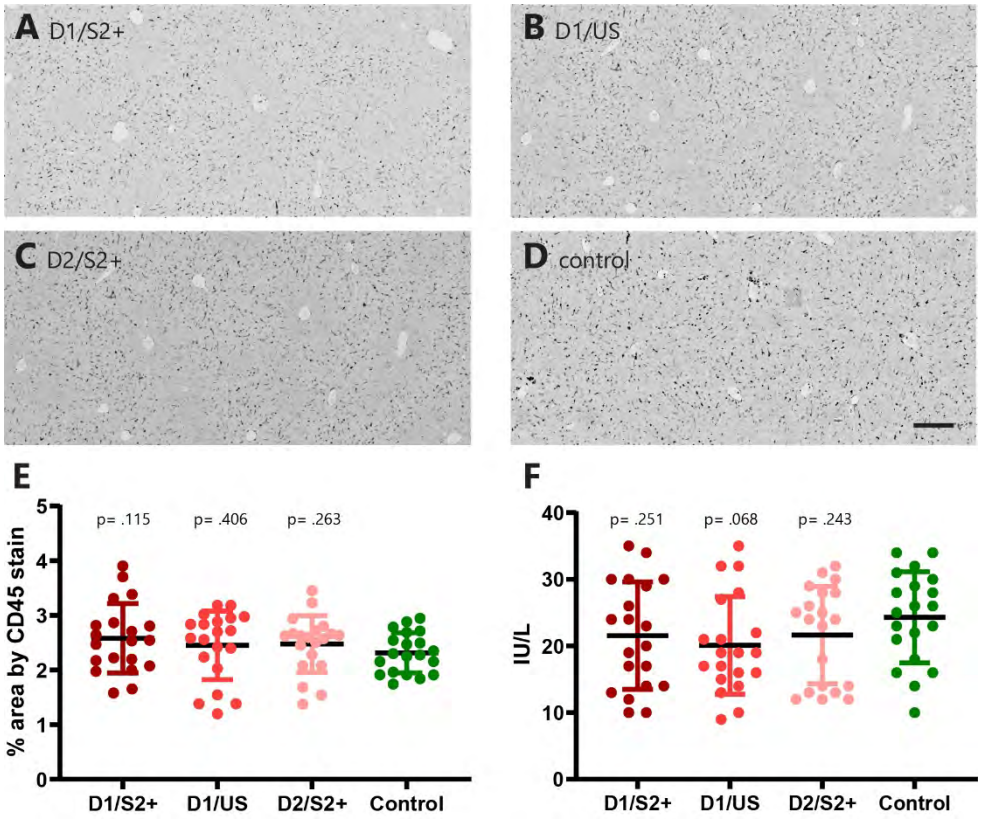

Figure 5-5: Analysis of inflammatory infiltrate by CD45 staining and hepatocyte injury by serum ALT measurements and in Experiment 1

Following injury, mice were injected with MSCs (donor 1, S2-selected [D1/S2+] - A; donor 1, unselected [D1/US] – B; donor 2, S2-selected [D2/S2+] – C) or control (D) as described in Figure 5.1 and euthanised on day 21 of recovery. Paraffin-embedded sections were stained for CD45 for assessment of inflammatory-cell infiltrate as described in section 2.11.2. Dark areas indicate positive staining. Scale bar (–) measures 200μm. Morphometric analyses of positive stained area were used for quantitative comparisons (E). Sera from each euthanised mouse were analysed for ALT as a surrogate for hepatocyte injury or cell membrane instability (F). The unpaired Student's t-test was used to compare values in treatment groups and control group; $p<0.05$ was deemed significant. Summary bars: standard deviation and mean value

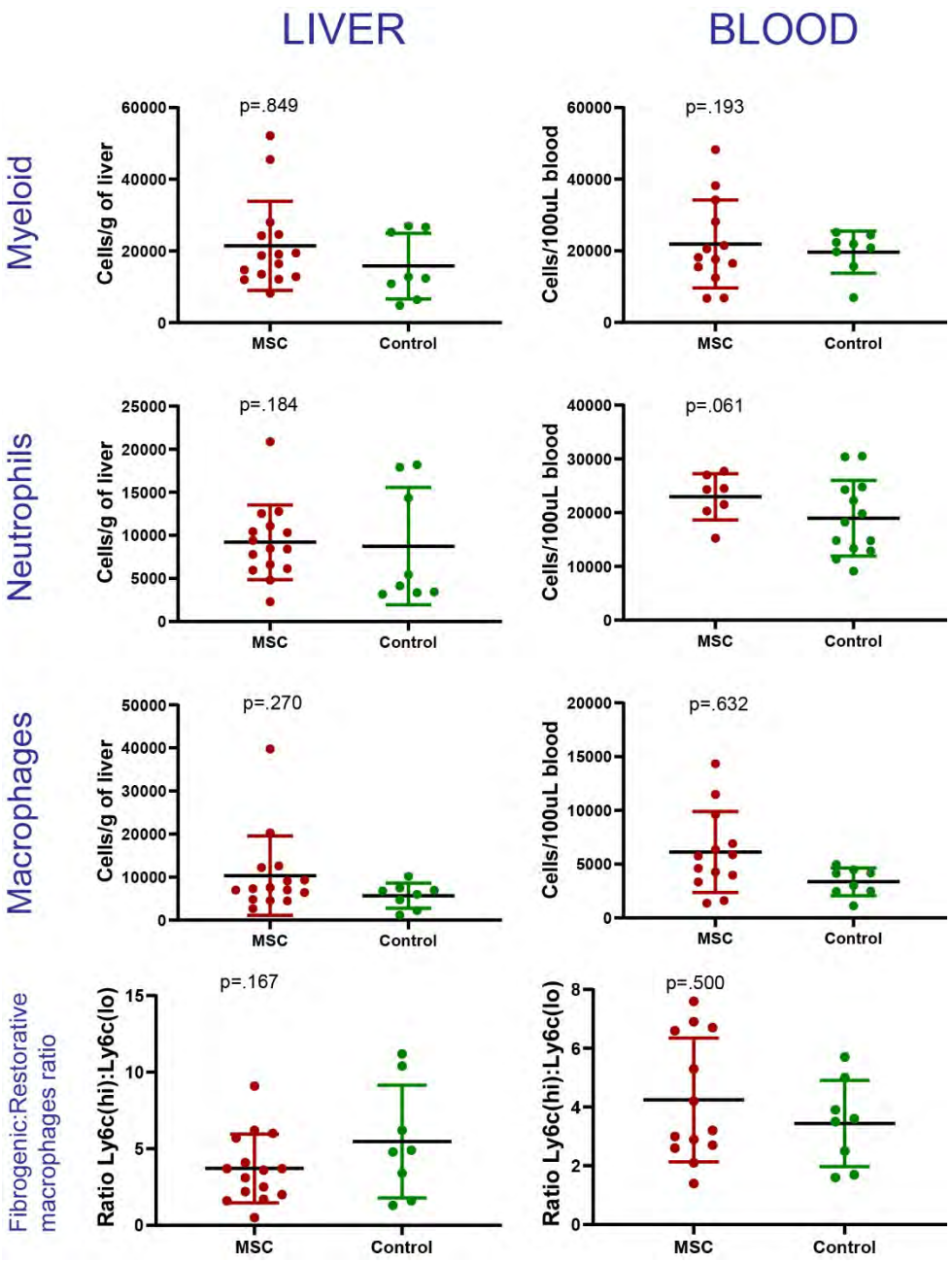

Figure 5-6: Flow cytometric analysis of myeloid cells from hepatic tissue and sera in Experiment 1

Following injury, mice were injected with MSCs or control as described in Figure 5.1 and euthanised on day 21 of recovery. Hepatic tissue and sera were processed for flow cytometric analysis as described in section 2.8. The gating strategy as described in section 2.8.4 was used to determine the number of myeloid cells ($CD11b^+$, $CD11c^-$), neutrophils ($CD11b^+$, $CD11c^-$, $F4/80^-$, Gr^+), macrophages/monocytes ($CD11b^+$, $CD11c^-$, $F4/80^+$), fibrogenic macrophages ($CD11b^+$, $CD11c^-$, $F4/80^+$, $Ly6c^{hi}$), and restorative macrophages ($CD11b^+$, $CD11c^-$, $F4/80^+$, $Ly6c^{lo}$). The unpaired Student's t-test was used to compare mean values the treatment and control groups; $p<0.05$ was deemed significant. Summary bars: standard deviation and mean value

MSC administration had no significant measured effect on surrogates on hepatocyte injury (ALT – Figure 5.5, Panel F), the gross inflammatory infiltrate (Figure 5.5, Panel E), or myeloid inflammatory subsets (Figure 5.6) in the IP CCl_4 model.

5.3.2. The effect of human UCT-MSCs on established TAA-induced liver fibrosis

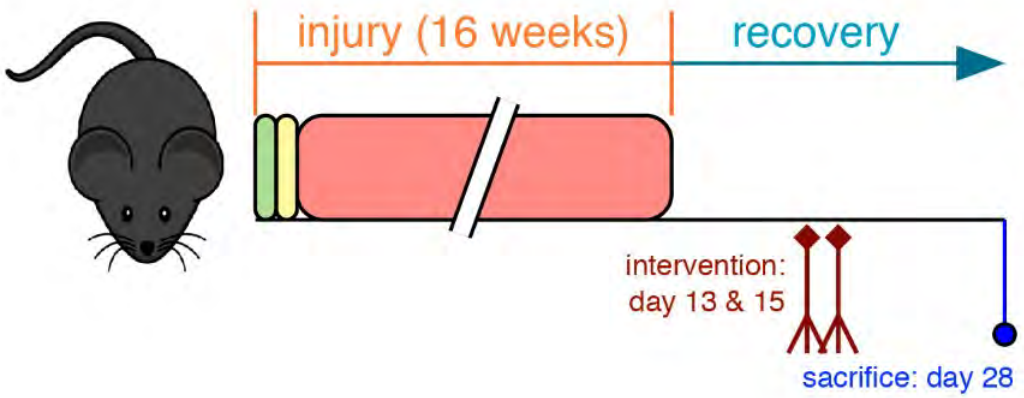

Figure 5-7: Schematic of experiment to explore the effect of MSC therapy on the resolution of established liver fibrosis using the oral TAA chronic hepatic injury model: Experiment 2

Age-matched male C57Bl/6 mice were subject to hepatic injury by substituting their drinking water with TAA diluted in fruit squash (1:5) to be taken *ad libitum*. A starting dose of 100mg/L (three days - green block) was sequentially increased to 300mg/L (three days - yellow block) and 600mg/L (pink block). The TAA solution was replaced by standard drinking water after 16 weeks. Mice were injected with $0.75x10^6$ S2-selected MSCs (from a single donor) in 200uL of sterile 0.9% saline carrier (test, N = 20) or just carrier (control, N = 20) by tail-vein on days 13 and 15 of recovery (total dose = $1.5x10^6$ cells) – EXPERIMENT 2. Mice were euthanised on day 28 of recovery (after oral TAA removed) for tissue and serum analysis. Primary analyses in this experiment were between the test arm and the control arm.

The time point at which inflammation and hepatic injury had settled after the cessation of oral TAA (protocol as described in Section 3.4.4), was determined after examination of fibrosis and resolution time course experiments (Figure 3.35). As such, intervention was given as 2 doses at day 13 and 15 (Figure 5.7) of recovery following oral TAA-induced hepatic fibrosis, when the ALT had normalised and the CD45 inflammatory infiltrate had dispersed. A persistent scar was evident to day 42 of natural recovery (Figure 3.30); however, there was a wide variation in the morphometric analysis of CPA by PSR staining at day 42, which was not evident at day 28 of recovery. Moreover, as explained in section 5.3.1, 14 days was deemed long enough for MSCs to

have an effect on fibrosis resolution. As such, day 28 of recovery was chosen as the time point for assessment of the effect of MSC administration.

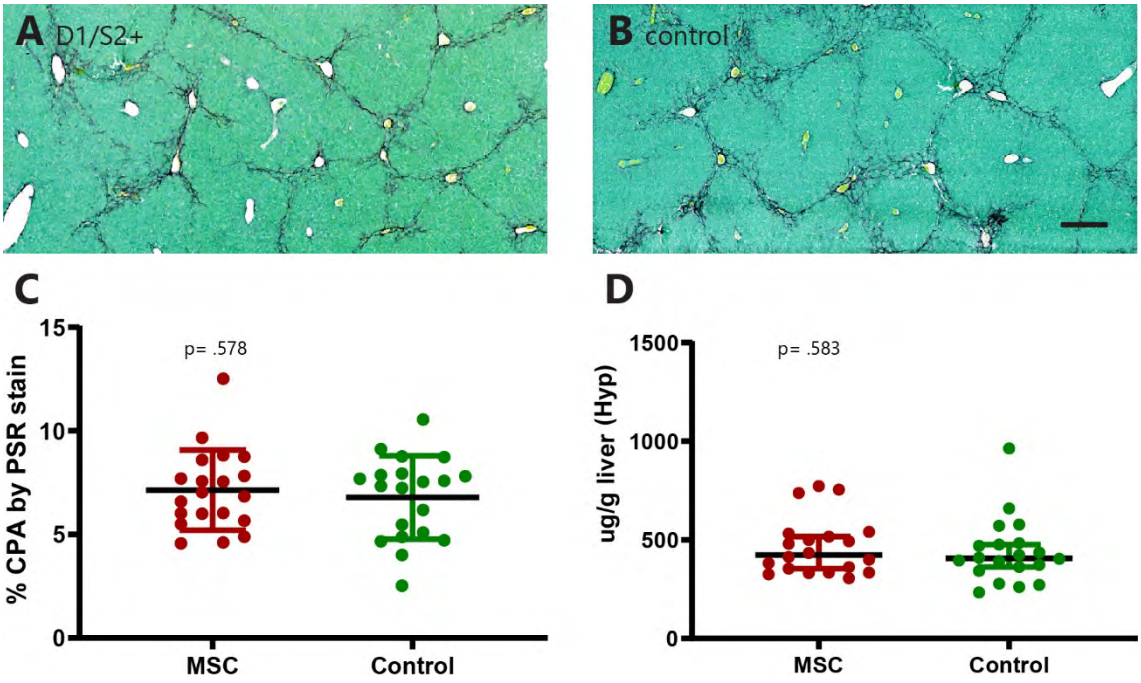

Figure 5-8: Analysis of collagen deposition in Experiment 2

Following injury, mice were injected with S2-selected MSCs from a single donor (A) or control (B) as described in Figure 5.7 and euthanised on day 28 of recovery. Paraffin-embedded tissue were stained for collagen by PSR and fast green as described in section 2.11.3. Red areas demarcate collagen. Scale bar (–) measures 200μm. Morphometric analysis of collagen proportionate area (CPA) (C) and assessment of hepatic hydroxyproline (D) as described in section 2.10 allowed comparison between the treatment group and control group by the unpaired Student's t-test (C) and Mann-Whitney test (D); $p<0.05$ was deemed significant. Summary bars: standard deviation and mean value for figure C; 95% CI and median value for figure D

Human UCT-MSCs had no significant effect on the resolution of oral TAA-induced liver fibrosis when administered in the absence of ongoing hepatic injury or inflammation (Figure 5.8). Moreover, as was seen in the IP CCl_4 model, MSC administration had no effect on *αSMA* expression (Figure 5.9 and Panel A of Figure 5.10), and had no effect on the mRNA expression of other fibrosis-related genes (Figure 5.10).

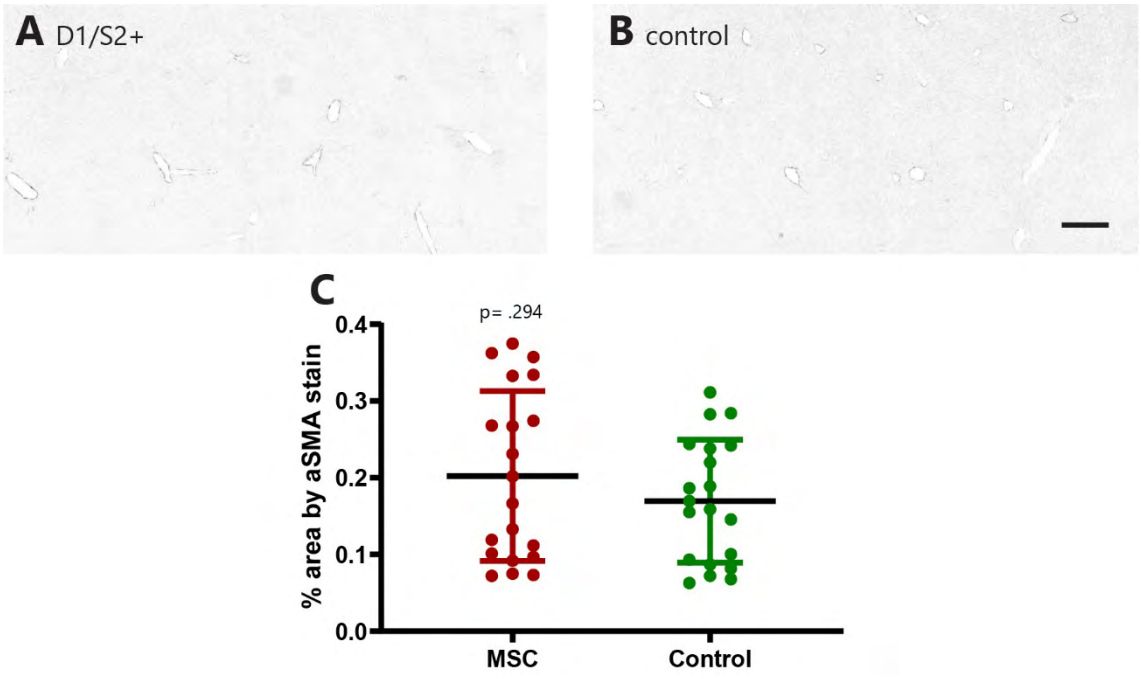

Figure 5-9: Analysis of myofibroblast activation in Experiment 2

Following injury, mice were injected with S2-selected MSCs from a single donor (A) or control (B) as described in Figure 5.7 and euthanised on day 28 of recovery. Paraffin-embedded tissue were stained for αSMA as described in section 2.11.2. Dark areas indicate positive staining. Scale bar (–) measures 200μm. Morphometric analysis of positive stained area (C) allowed quantitative comparison between the treatment group and control group by the unpaired Student's t-test; $p<0.05$ was deemed significant. Summary bars: standard deviation and mean value

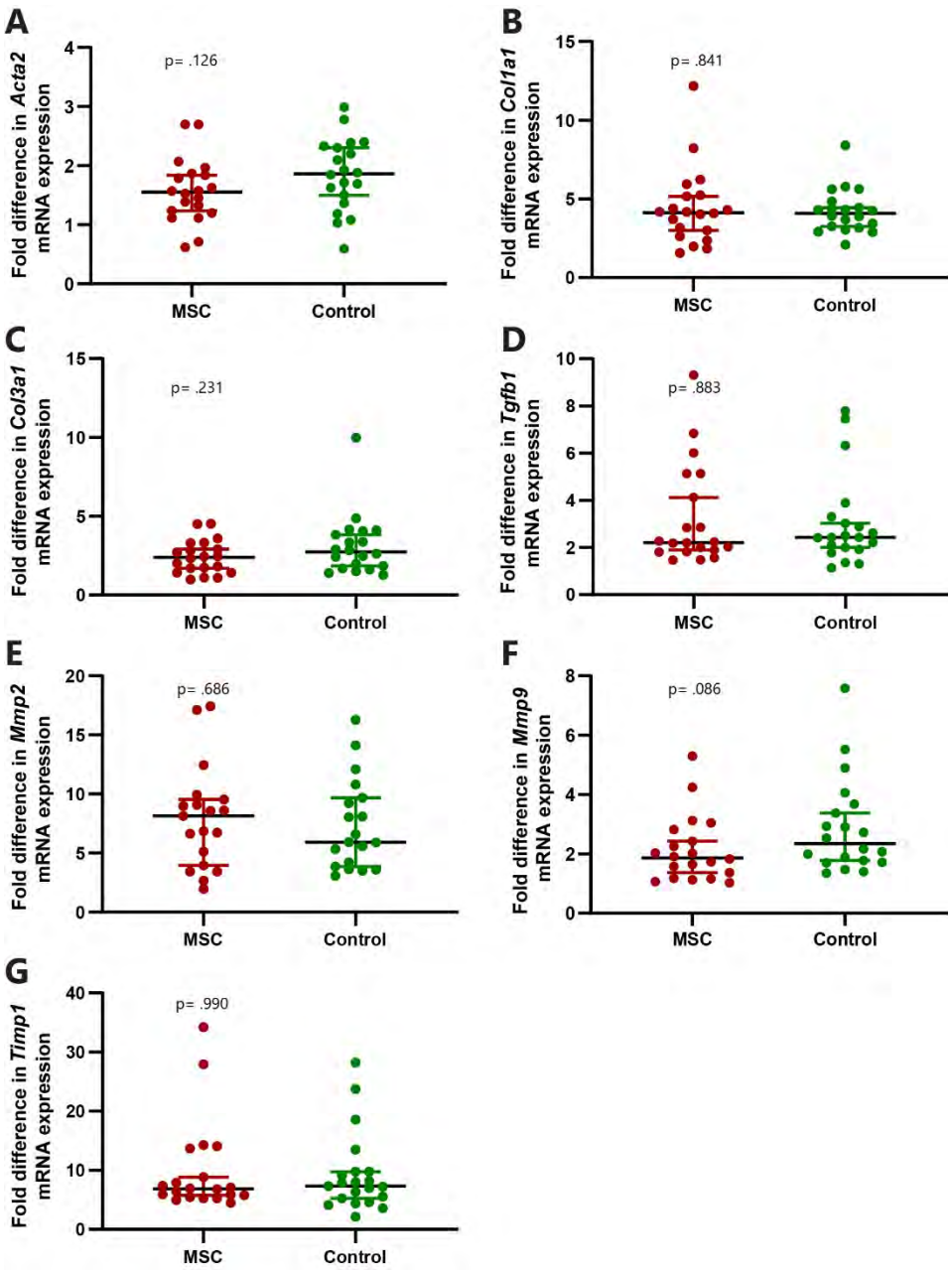

Figure 5-10: Gene expression analysis by qPCR of fibrosis-associated genes in Experiment 2

Following injury, mice were injected with S2-selected MSCs from a single donor or control as described in Figure 5.7 and euthanised on day 28 of recovery. Expression of fibrosis-associated genes (A: *Acta2*, B: *Col1a1*, C: *Col3a1*, D: *Tgfb1*, E: *Mmp2*, F: *Mmp9*, G: *Timp1* versus. housekeeping gene *Gapdh*) was assessed by qPCR of hepatic tissues as described in section 2.14. Comparison between the treatment group and control group was done by the Mann-Whitney test; $p<0.05$ was deemed significant. Summary bars: 95% CI and median value.

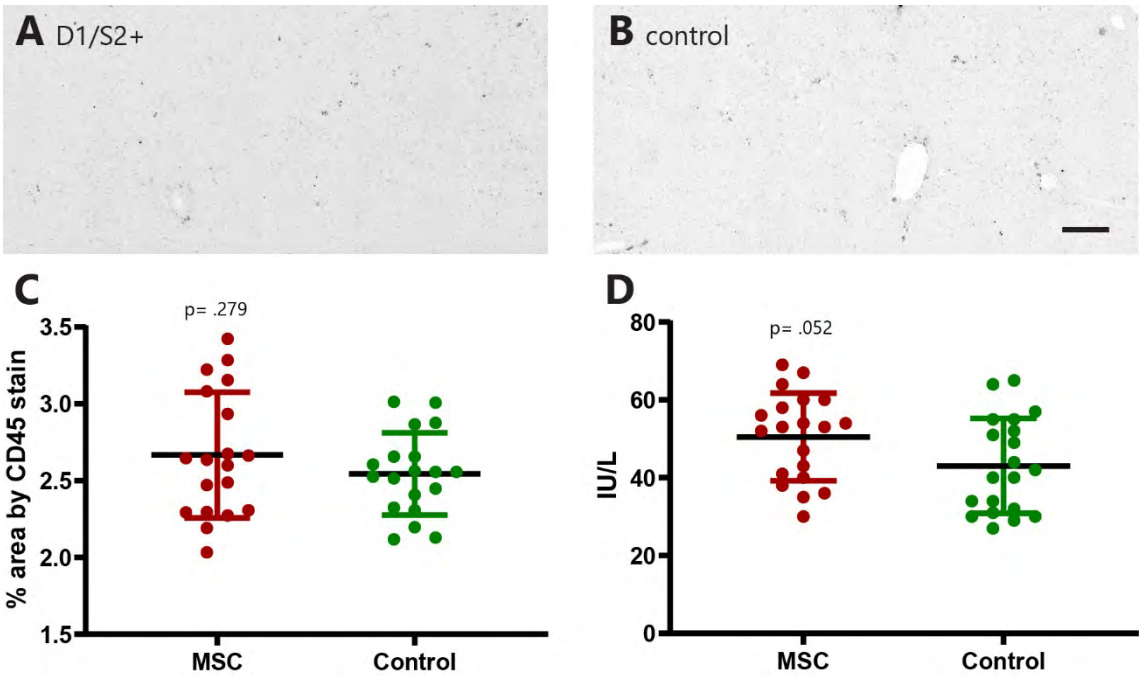

Figure 5-11: Analysis of inflammatory infiltrate by CD45 staining and hepatocyte injury by serum ALT measurements and in Experiment 2

Following injury, mice were injected with S2-selected MSCs from a single donor (A) or control (B) as described in Figure 5.7 and euthanised on day 28 of recovery. Paraffin-embedded sections were stained for CD45 for assessment of inflammatory-cell infiltrate as described in section 2.11.2. Dark areas indicate positive staining. Scale bar (–) measures 200μm. Morphometric analyses of positive stained area were used for quantitative comparisons (C). Sera from each euthanised mouse were analysed for ALT as a surrogate for hepatocyte injury or cell membrane instability (D). Comparison between the treatment group and control group was done by the unpaired Student's t-test; $p<0.05$ was deemed significant. Summary bars: standard deviation and mean value.

As in the IP CCl_4 model, MSC administration in the absence of ongoing hepatic injury had no measured effect on surrogates on hepatocyte injury (ALT – Figure 5.11, Panel D), and the gross inflammatory infiltrate (Figure 5.11, Panel C).

5.4. Intervention to enhance fibrosis resolution in the presence of ongoing hepatocyte injury or inflammation

Human UCT-MSC therapy did not resolve established fibrosis in the setting of a no ongoing hepatic injury or inflammation in either the IP CCl_4 or oral TAA model.

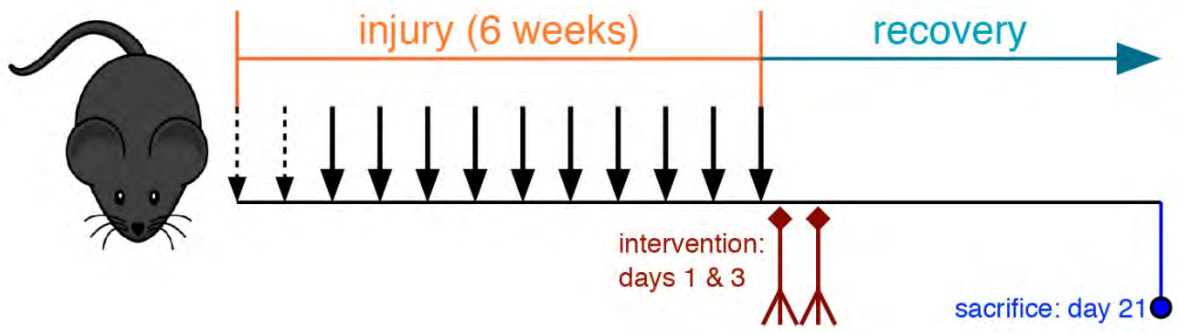

Figure 5-12: Schematic of experiment to explore the effect of MSC therapy on the resolution of established liver fibrosis in the presence of on-going inflammation using the IP CCl_4 chronic hepatic injury model: Experiment 3

Age-matched male C57Bl/6 mice were twice injected with CCl_4 diluted in mineral oil (1:3) at a dose of 1µl/g bodyweight (dashed vertical arrows) IP, followed by 10 injections at a dose of 2µl/g bodyweight (blocked vertical arrows) over 6 weeks. Mice were injected with $0.75x10^6$ S2-selected MSCs (from a single donor) in 200uL of sterile 0.9% saline carrier (test, N = 20) or just carrier (control, N = 20) by tail-vein on days 1 and 3 of recovery (total dose = $1.5x10^6$ cells) – EXPERIMENT 3. Mice were euthanised on day 21 of recovery (after last IP injection) for tissue and serum analysis. Primary analyses in this experiment were between the test arm and the control arm.

There are evidence to suggest that MSCs require *in vivo* interaction with an inflammatory milieu (licencing) to effect a function[203]. This is particularly true for MSC-mediated immunomodulation in the setting of graft-versus host disease, where MSCs have a clear benefit when given in severe steroid-refractory disease, but not in more quiescent disease[204,205]. Therefore, I subsequently sought to examine whether the timing of therapy may influence outcome. I used the shorter 6-

week IP CCl_4 protocol rather than the longer 16-week oral TAA protocol, and administered MSC therapy after injury had ceased, but at a time when there was still residual hepatocyte injury and hepatic inflammation; days 1 & 3 of recovery (Figure 5.12).

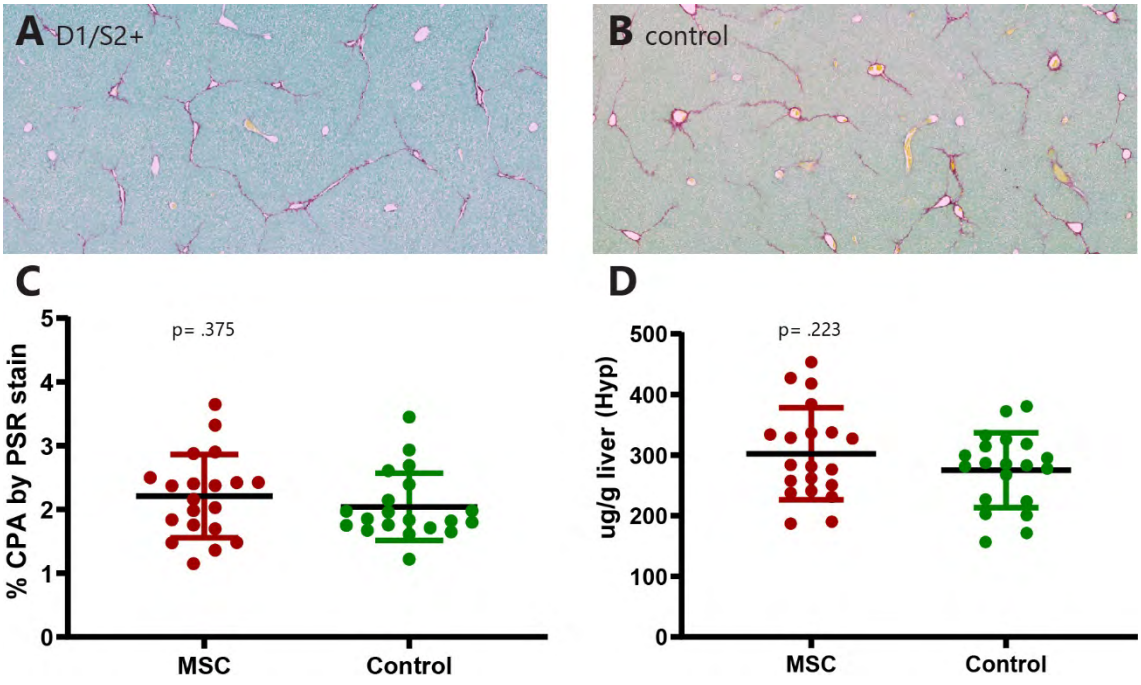

Figure 5-13: Analysis of collagen deposition in Experiment 3

Following injury, mice were injected S2-selected MSCs from a single donor (A) or control (B) as described in Figure 5.12 and euthanised on day 21 of recovery. Paraffin-embedded tissue were stained for collagen by PSR as described in section 2.11.3. Red areas demarcate collagen. Scale bar (–) measures 200μm. Morphometric analysis of collagen proportionate area (CPA) (C) and assessment of hepatic hydroxyproline (D) as described in section 2.10 allowed comparison between the treatment groups and the control group by the use of the unpaired Student's t-test. $p<0.05$ was deemed significant. Summary bars: standard deviation and mean value

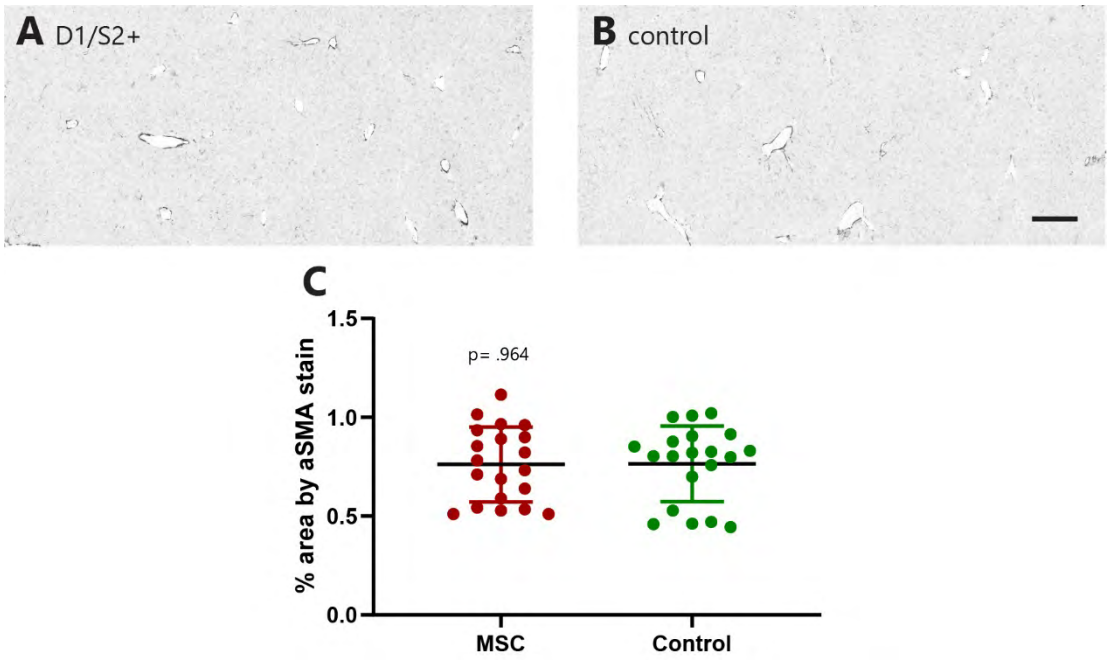

Figure 5-14: Analysis of myofibroblast activation in Experiment 3

Following injury, mice were injected with S2-selected MSCs from a single donor (A) or control (B) as described in Figure 5.12 and euthanised on day 21 of recovery. Paraffin-embedded tissue were stained for αSMA as described in section 2.11.2. Dark areas indicate positive staining. Scale bar (–) measures 200μm. Morphometric analysis of positive stained area (C) allowed comparison between treatment groups and the control group by the use of the unpaired Student's t-test; $p<0.05$ were deemed significant. Summary bars: standard deviation and mean value

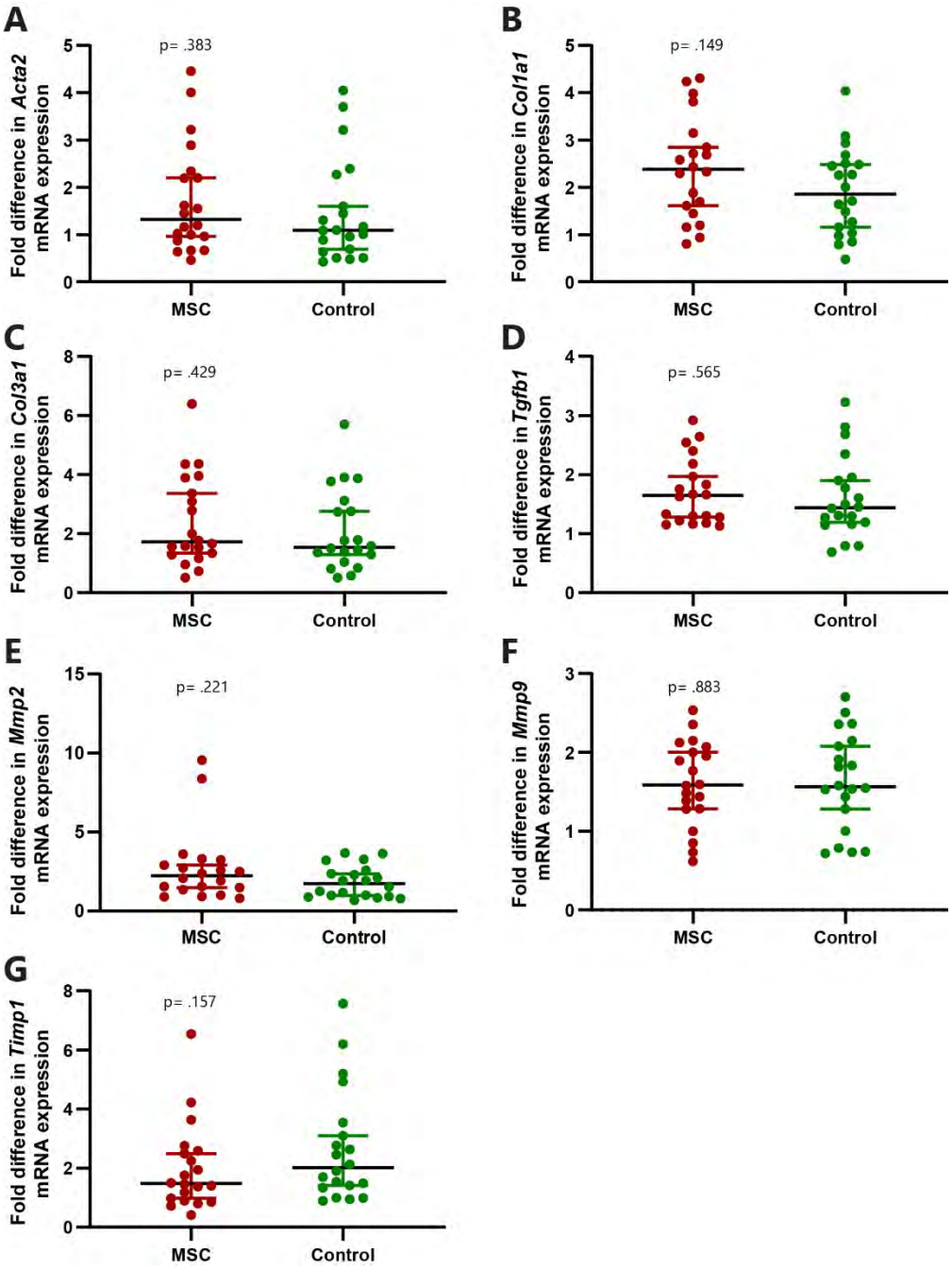

Figure 5-15: Gene expression analysis by qPCR of fibrosis-associated genes in Experiment 3

Following injury, mice were injected with S2-selected MSCs from a single donor or control as described in Figure 5.12 and euthanised on day 21 of recovery. Expression of fibrosis-associated genes (A: *Acta2*, B: *Col1a1*, C: *Col3a1*, D: *Tgfb1*, E: *Mmp2*, F: *Mmp9*, G: *Timp1* versus. housekeeping gene *Gapdh*) were assessed by qPCR of hepatic tissues as described in section 2.14. The Mann-Whitney test was used to compare expression in treatment groups and control group; $p<0.05$ was deemed significant. Summary bars: 95%CI and median value.

Changing the timing of MSC administration did not change the effect of their administration. Human UCT-MSCs had no significant effect on the resolution of IP CCl_4-induced liver fibrosis when administered in the setting of ongoing hepatic injury and inflammation, whether measured by extant collagen (Figure 5.13), myofibroblast activation (Figure 5.14) or the expression of fibrosis-related genes (Figure 5.15).

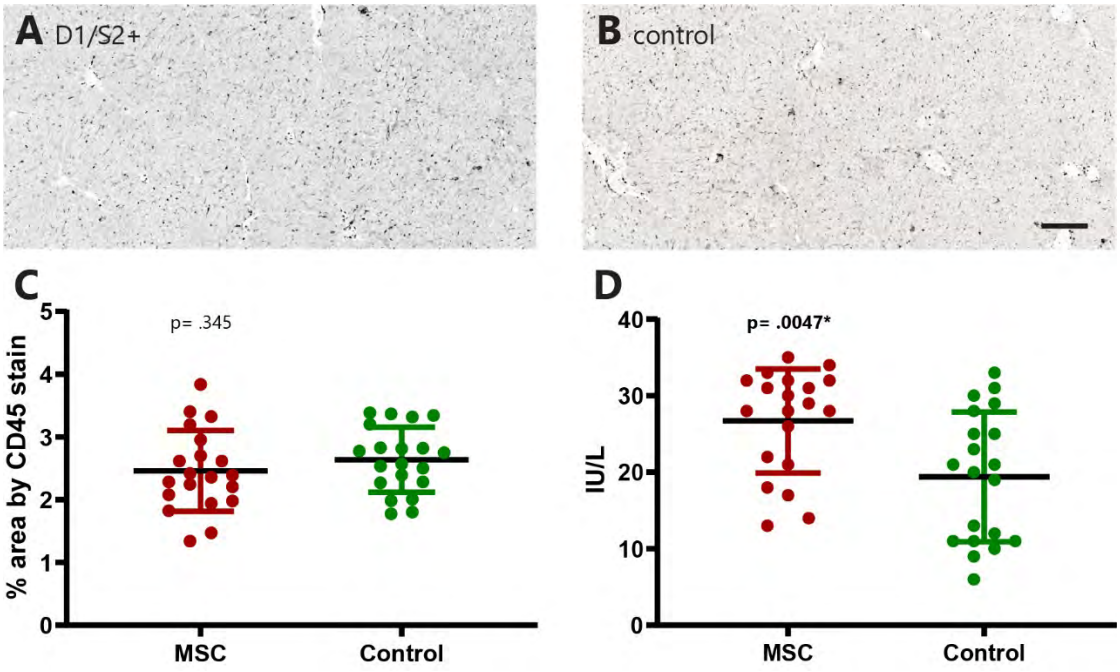

Figure 5-16: Analysis of inflammatory infiltrate by CD45 staining and hepatocyte injury by serum ALT measurements and in Experiment 3

Following injury, mice were injected with S2-selected MSCs from a single donor (A) or control (B) as described in Figure 5.12 and euthanised on day 21 of recovery. Paraffin-embedded sections were stained for CD45 for assessment of inflammatory-cell infiltrate as described in section 2.11.2. Dark areas indicate positive staining. Scale bar (–) measures 200μm. Morphometric analyses of positive stained area were used for quantitative comparisons (C). Sera from each euthanised mouse were analysed for ALT as a surrogate for hepatocyte injury or cell membrane instability (D). The unpaired Student's t-test was used to compare expression in treatment groups and control group; $p<0.05$ was deemed significant and *-marked. Summary bars: standard deviation and mean value

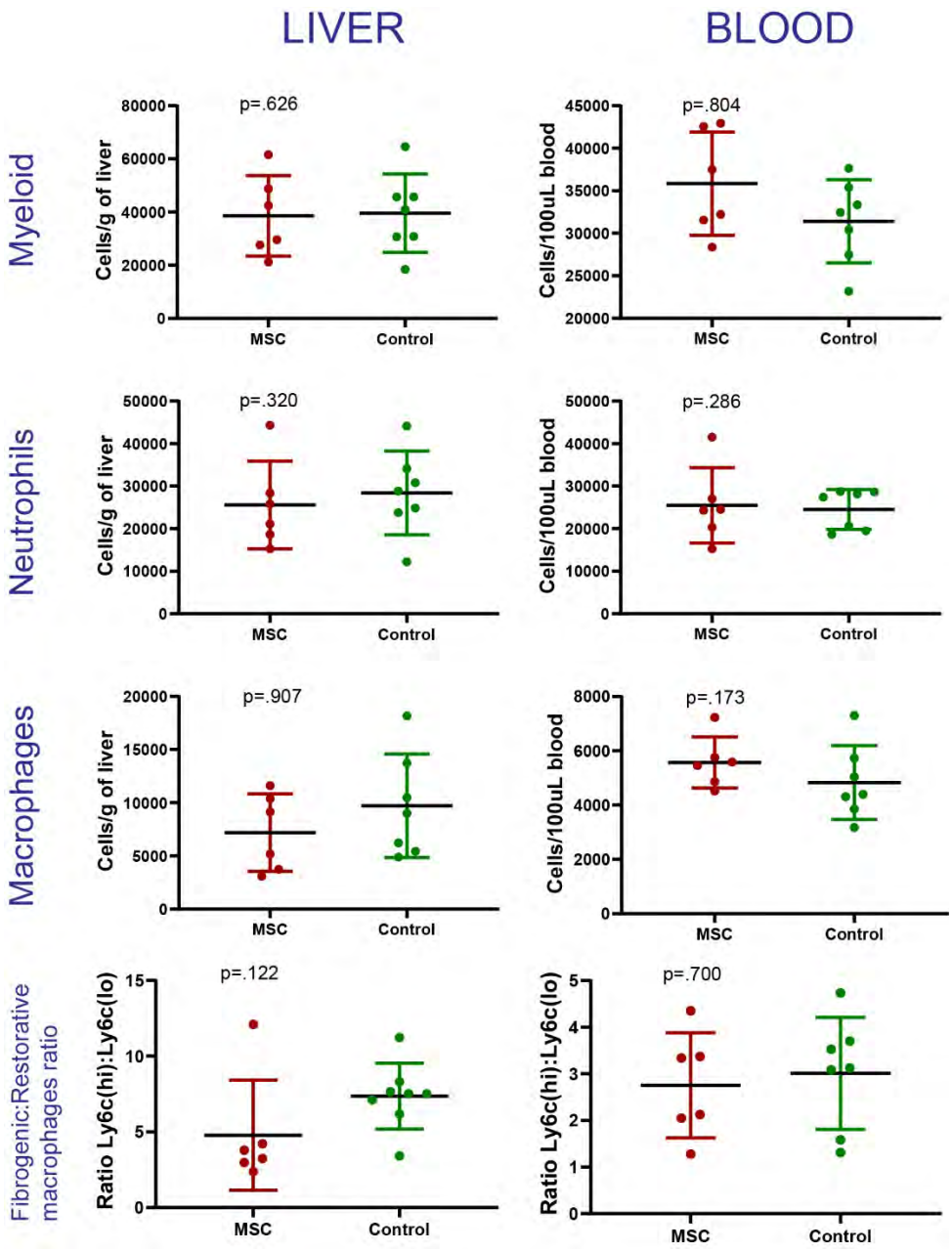

Figure 5-17: Flow cytometric analysis of myeloid cells from hepatic tissue and sera in Experiment 3

Following injury, mice were injected with MSCs or control as described in Figure 5.12 and euthanised on day 21 of recovery. Hepatic tissue and sera were processed for flow cytometric analysis as described in section 2.8. The gating strategy as described in section 2.8.4 was used to determine the number of myeloid cells ($CD11b^+$, $CD11c^-$), neutrophils ($CD11b^+$, $CD11c^-$, $F4/80^-$, Gr^+), macrophages/monocytes ($CD11b^+$, $CD11c^-$, $F4/80^+$), fibrogenic macrophages ($CD11b^+$, $CD11c^-$, $F4/80^+$, $Ly6c^{hi}$), and restorative macrophages ($CD11b^+$, $CD11c^-$, $F4/80^+$, $Ly6c^{lo}$). The unpaired Student's t-test was used to compare mean values the treatment and control groups; $p<0.05$ was deemed significant. Summary bars: standard deviation and mean value

Moreover, MSC administration had no significant effect on hepatic inflammation as measured by CD45 IHC (Figure 5.16, Panel A-C), or flow cytometry of myeloid inflammatory substrates (Figure 5.17). A statistically significantly raised ALT in the MSC treatment arm (Figure 5.16, Panel D) is unlikely to be biologically significant as the mean values and range are still under the upper limit of normal (ALT upper limit of normal = 50IU/L). Moreover, a qualitative comparative assessment of the H&E staining between the treatment and control arms yielded no significant differences (images not shown).

5.5. Intervention to reduce fibrogenesis during ongoing hepatic injury

Human UCT-MSC therapy did not resolve established fibrosis in the presence or absence of ongoing inflammation and hepatocyte injury in either the IP CCl4 or oral TAA model.

The published data overwhelmingly suggests MSCs given during the fibrogenic process (whilst injury is ongoing) can reduce the final burden of fibrosis. This has been shown in multiple rodent fibrosis models, and using both syngeneic and xenogeneic (including human) MSCs (Table 1.2).

As such, I sought to examine whether intervening during injury can reduce fibrosis in both the IP CCl_4 (Figure 5.18) and oral TAA models (Figure 5.24) in a statistically powered experiment.

5.5.1. The effect of human UCT-MSCs during CCl_4-induced liver fibrosis

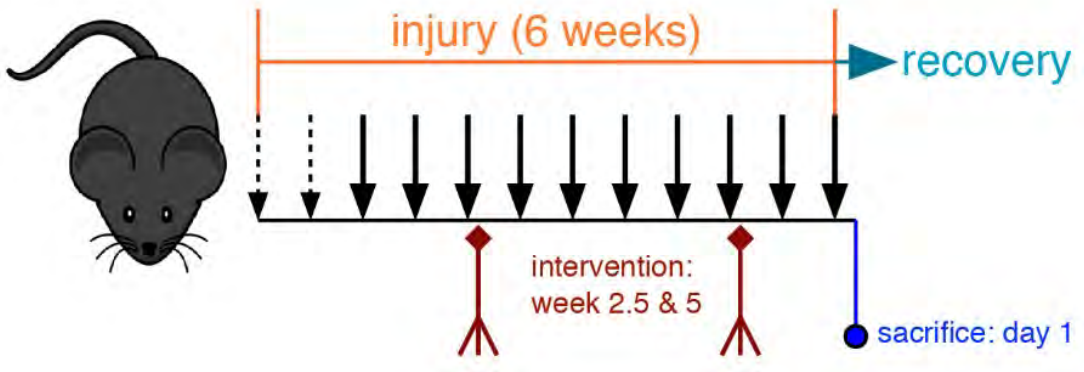

Figure 5-18: Schematic of experiment to explore the effect of MSC therapy on fibrogenesis using the IP CCl_4 chronic hepatic injury model: Experiment 4

Age-matched male C57Bl/6 mice were twice injected with CCl_4 diluted in mineral oil (1:3) at a dose of 1µl/g bodyweight (dashed vertical arrows) IP, followed by 10 injections at a dose of 2µl/g bodyweight (blocked vertical arrows) over 6 weeks. Mice were injected with $0.75x10^6$ MSCs in 200uL of sterile 0.9% saline carrier (test) or just carrier (control, N = 20) by tail-vein 24 hours after the 5th and 10th IP injections (total dose = $1.5x10^6$ cells) – EXPERIMENT 4. Mice were euthanised 24 hours after the last IP injection for tissue and serum analysis. Syndecan-2-selected MSC were tested from two donors (D1/S2+ and D2/S2+), and unselected MSC from donor 1 (D1/US) (N=20 each test arm). Primary analyses in this experiment were between the test arms and the control arm.

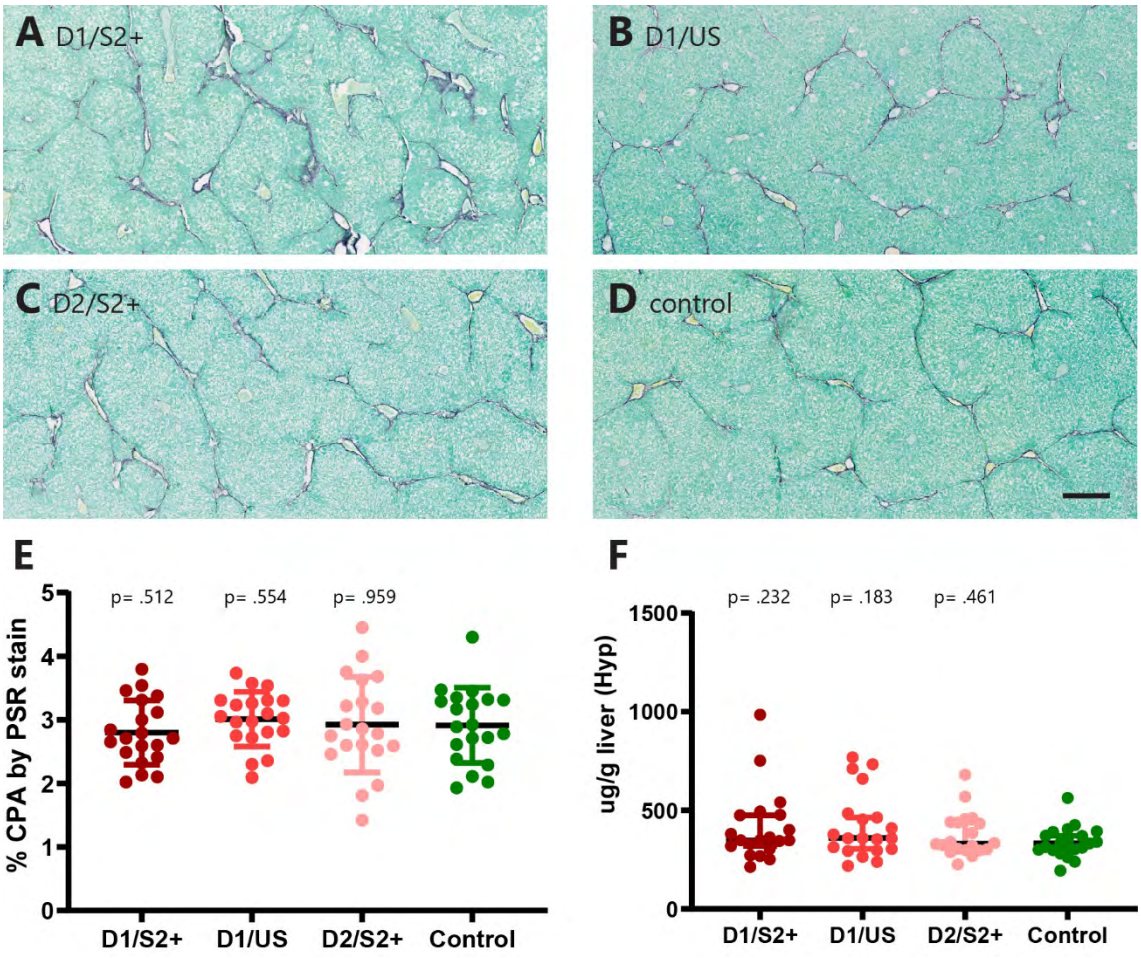

Figure 5-19: Analysis of collagen deposition in Experiment 4

During injury, mice were injected with MSCs (donor 1, S2-selected [D1/S2+] - A; donor 1, unselected [D1/US] – B; donor 2, S2-selected [D2/S2+] – C) or control (D) as described in Figure 5.1 and euthanised on day 21 of recovery. Paraffin-embedded tissue were stained for collagen by PSR and fast green as described in section 2.11.3. Red areas demarcate collagen. Scale bar (–) measures 200μm. Morphometric analysis of collagen proportionate area (CPA) (E) and assessment of hepatic hydroxyproline (F) as described in section 2.10 allowed comparison between the treatment groups and the control group by the use of the unpaired Student's t-test (E) and Mann-Whitney test (F); $p<0.05$ was deemed significant. Summary bars: standard deviation and mean value for figure E; 95% CI and median value for figure F

Human UCT-MSCs had no significant effect on the fibrogenesis of IP CCl_4-induced liver fibrosis, whether measured by extant collagen (Figure 5.19), myofibroblast activation (Figure 5.20) or the expression of fibrosis-related genes (Figure 5.22).

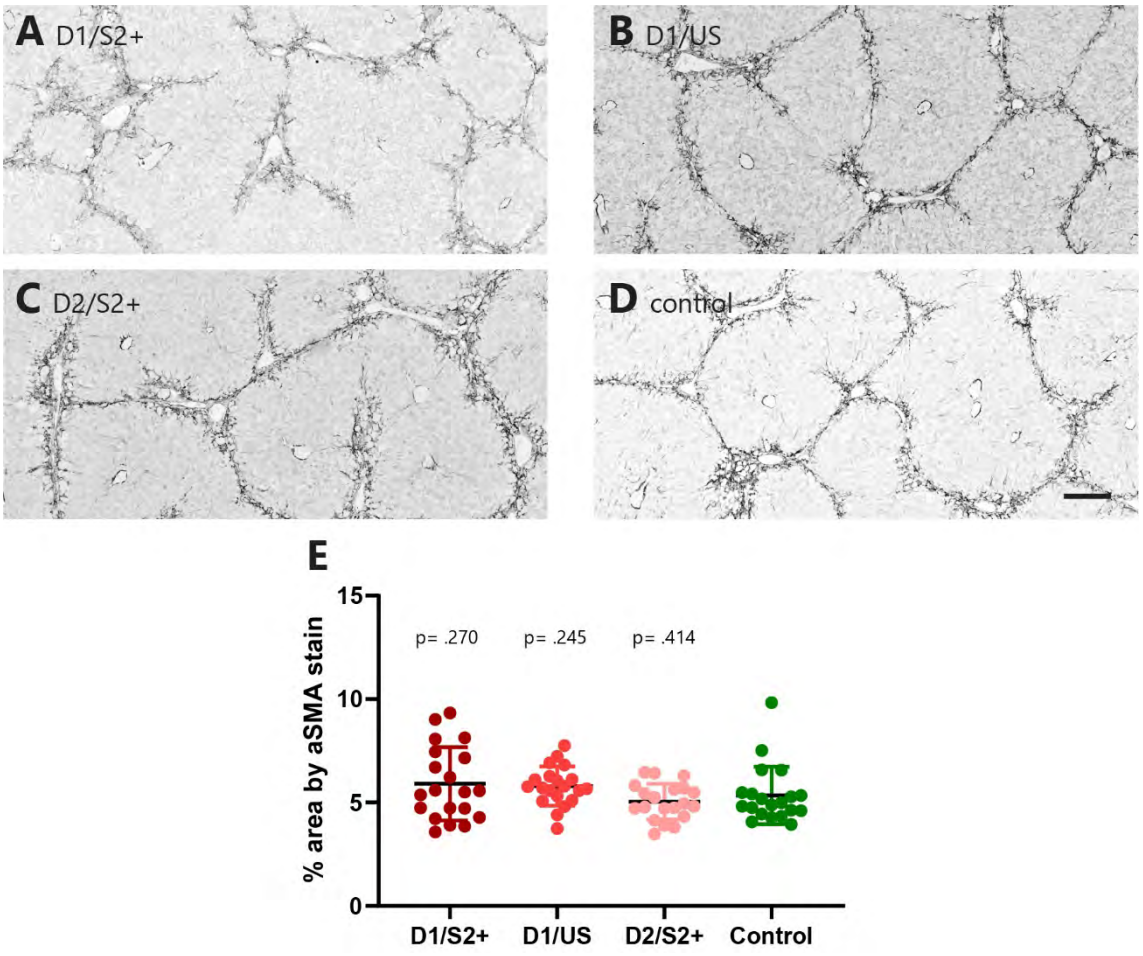

Figure 5-20: Analysis of myofibroblast activation in Experiment 4

During injury, mice were injected with MSCs (donor 1, S2-selected [D1/S2+] - A; donor 1, unselected [D1/US] – B; donor 2, S2-selected [D2/S2+] – C) or control (D) as described in Figure 5.18 and euthanised 24 hours after the last IP injection. Paraffin-embedded tissue were stained for αSMA as described in section 2.11.2. Dark areas indicate positive staining. Scale bar (–) measures 200μm. Morphometric analysis of positive stained area (E) allowed comparison between the treatment group and control group by the unpaired Student's t-test; $p<0.05$ was deemed significant. Summary bars: standard deviation and mean value

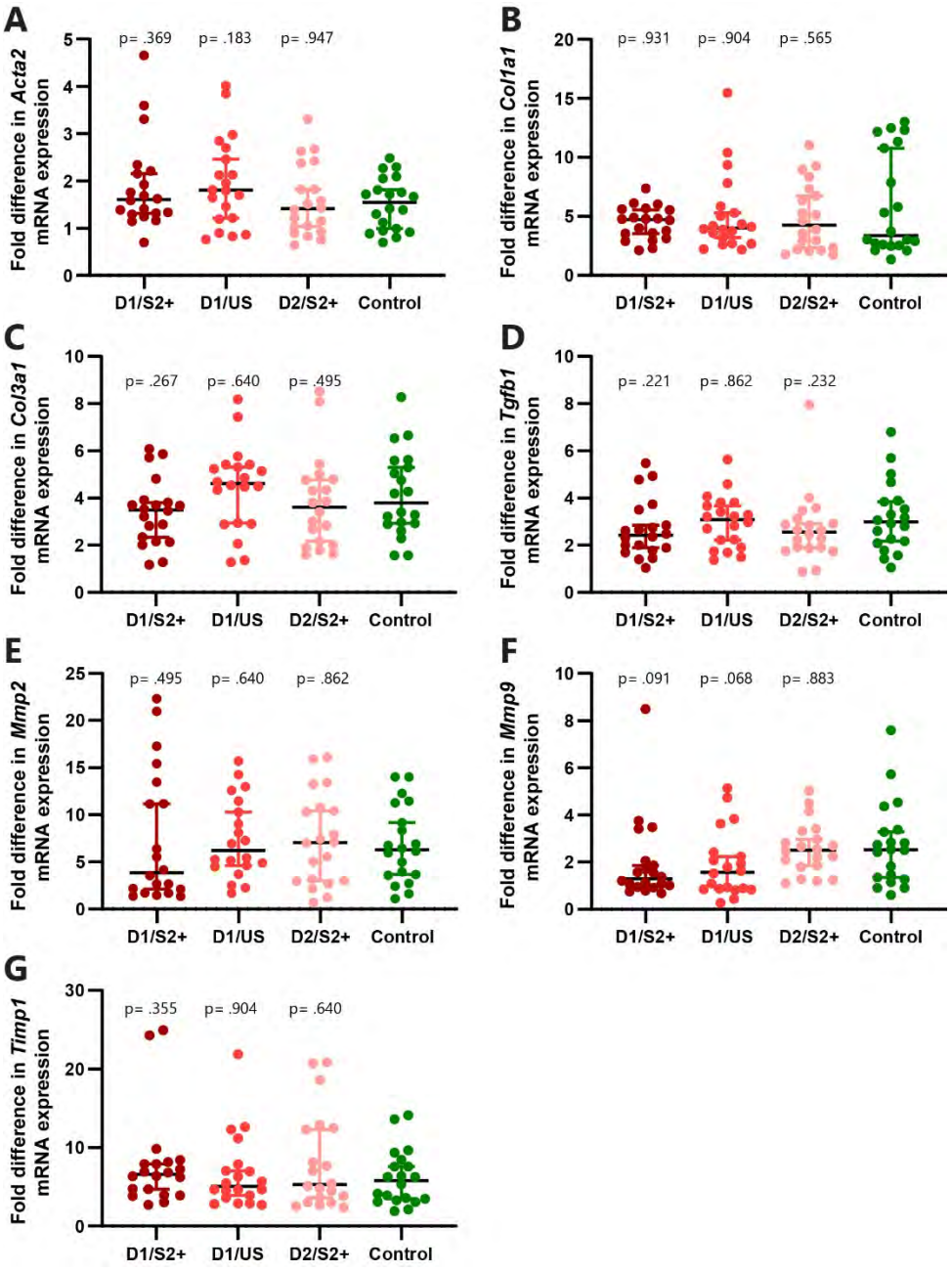

Figure 5-21: Gene expression analysis by qPCR of fibrosis-associated genes in Experiment 4

During injury, mice were injected with MSCs (donor 1, S2-selected [D1/S2+]; donor 1, unselected [D1/US]; donor 2, S2-selected [D2/S2+]) or control as described in Figure 5.18 and euthanised 24 hours after the last IP injection. Expression of fibrosis-associated genes (A: *Acta2*, B: *Col1a1*, C: *Col3a1*, D: *Tgfb1*, E: *Mmp2*, F: *Mmp9*, G: *Timp1* versus housekeeping gene *Gapdh*) was assessed by qPCR of hepatic tissues as described in section 2.14. The Mann-Whitney test was used to compare expression in treatment groups and control group; $p<0.05$ was deemed significant. Summary bars: 95%CI and median value.

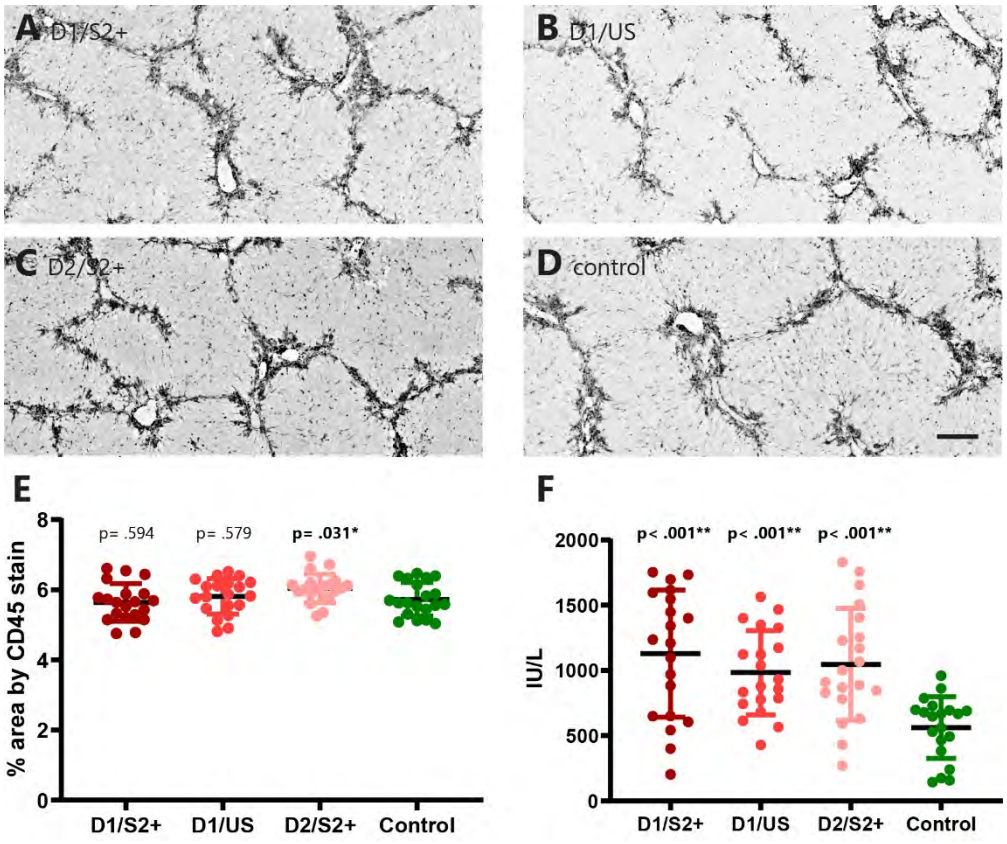

Figure 5-22: Analysis of inflammatory infiltrate by CD45 staining and hepatocyte injury by serum ALT measurements and in Experiment 4

During injury, mice were injected with MSCs (donor 1, S2-selected [D1/S2+] - A; donor 1, unselected [D1/US] – B; donor 2, S2-selected [D2/S2+] – C) or control (D) as described in Figure 5.18 and euthanised 24 hours after the last IP injection. Paraffin-embedded sections were stained for CD45 for assessment of inflammatory-cell infiltrate as described in section 2.11.2. Dark areas indicate positive staining. Scale bar (–) measures 200µm. Morphometric analyses of positive stained area were used for quantitative comparisons (E). Sera from each euthanised mouse were analysed for ALT as a surrogate for hepatocyte injury or cell membrane instability (F). The unpaired Student's t-test was used to compare expression in treatment groups and control group; $p<0.05$ was deemed significant. Summary bars: standard deviation and mean value

MSC administration resulted in a higher serum ALT than control saline administration (Figure 5.29, Panel F). The effect was independent of MSC donor or the S2 selection process. There were no obvious qualitative differences in the gross morphological pathology between the treatment and control groups when assessed by H&E staining (images not shown).

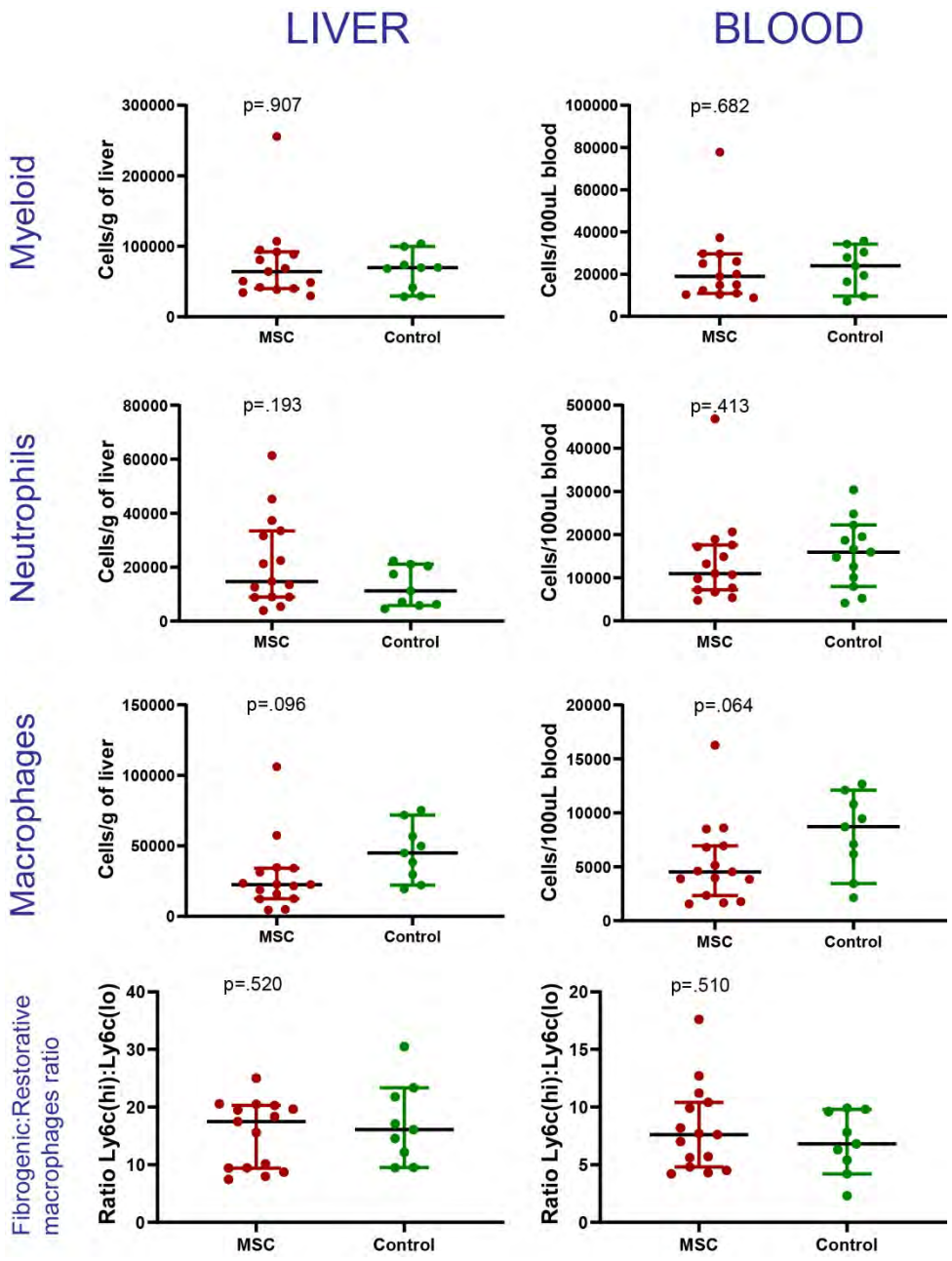

Figure 5-23: Flow cytometric analysis of myeloid cells from hepatic tissue and sera in Experiment 4

Following injury, mice were injected with MSCs or control as described in Figure 5.18 and euthanised on day 21 of recovery. Hepatic tissue and sera were processed for flow cytometric analysis as described in section 2.8. The gating strategy as described in section 2.8.4 was used to determine the number of myeloid cells ($CD11b^+$, $CD11c^-$), neutrophils ($CD11b^+$, $CD11c^-$, $F4/80^-$, Gr^+), macrophages/monocytes ($CD11b^+$, $CD11c^-$, $F4/80^+$), fibrogenic macrophages ($CD11b^+$, $CD11c^-$, $F4/80^+$, $Ly6c^{hi}$), and restorative macrophages ($CD11b^+$, $CD11c^-$, $F4/80^+$, $Ly6c^{lo}$). The Mann-Whitney was used to compare mean values the treatment and control groups; $p<0.05$ was deemed significant. Summary bars: 95% CI and median value

An evaluation of the gross inflammatory infiltrate by CD45 IHC (Figure 5.22, Panels A-E) showed a dense peri-portal and scar-associated infiltrate with a statistically significant elevation CD45 stained area in mice injected with S2-selected MSCs from donor 2, but not the other treatment groups. The effect was small, and a statistical evaluation of inter-treatment arm differences yielded no significant variance (one-way ANOVA >0.05). A subsequent analysis of myeloid inflammatory subsets by flow cytometry demonstrated no significant effect of MSC administration (Figures 5.23).

5.5.3. The effect of human UCT-MSCs during TAA-induced liver fibrosis

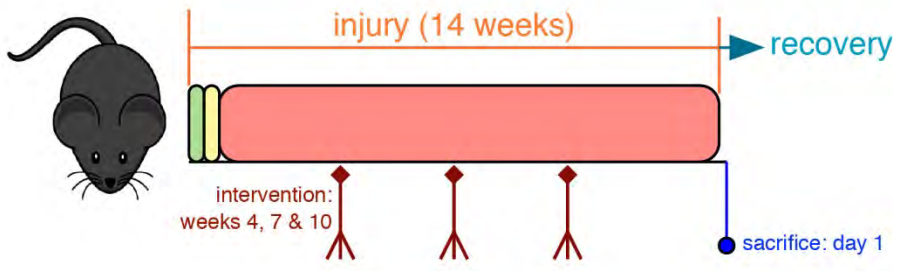

Figure 5-24: Schematic of experiment to explore the effect of MSC therapy on fibrogenesis using the oral TAA chronic hepatic injury model: Experiment 5

Age-matched male C57Bl/6 mice were subject to hepatic injury by substituting their drinking water with TAA diluted in fruit squash (1:5) to be taken *ad libitum*. A starting dose of 100mg/L (three days - green block) was sequentially increased to 300mg/L (three days - yellow block) and 600mg/L (pink block). The TAA solution was replaced by standard drinking water after 14 weeks. Mice were injected with $0.75x10^6$ S2-selected MSCs (from a single donor) in 200uL of sterile 0.9% saline carrier (test, N = 20) or just carrier (control, N = 20) by tail-vein after 4, 7 and 10 weeks of injury (total dose = $2.25x10^6$ cells) – EXPERIMENT 5. Mice were euthanised 24 hours after TAA was removed for tissue and serum analysis. Primary analyses in this experiment were between the test arm and the control arm.

The oral-TAA protocol was shortened for the purposes of testing the effect of MSC administration during continuing injury. The feasibility experiment for the model (Figure 3.23), demonstrated that fibrosis was not evident at week 4 of the protocol, and significant fibrosis and myofibroblast activation only manifest from week 12. As such, we selected an injury duration of 14 weeks to ensure the uninterrupted protocol could deliver a significant scar. We chose to start intervention at a time when there was no significant fibrosis, but there was evidence of hepatic injury (week 4, ref H&E staining Figure 3.20). We delivered three MSC doses to ensure any effect they have was not lost with continuing injury over the 14-week protocol. Therefore, a greater total dose of MSCs was given in the treatment arm in experiment 5, compared to the other intervention experiments in this chapter.

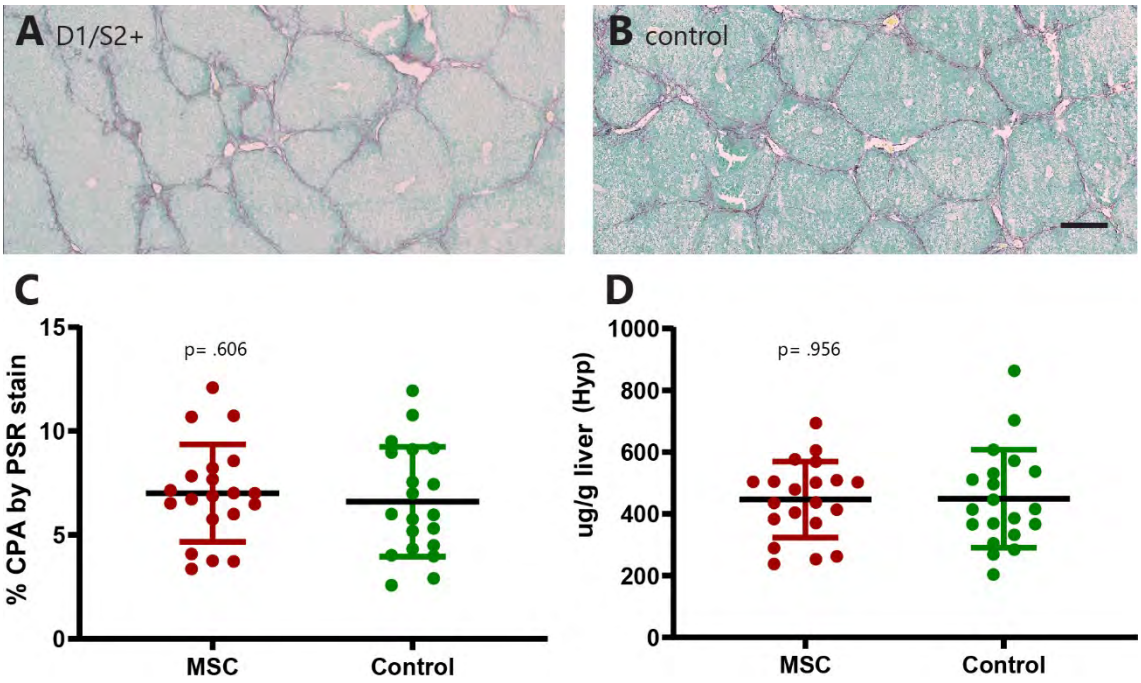

Figure 5-25: Analysis of collagen deposition in Experiment 5

During injury, mice were injected with S2-selected MSCs from a single donor (A) or control (B) as described in Figure 5.24 and euthanised 24 hours after TAA was removed. Paraffin-embedded tissue were stained for collagen by PSR and fast green. Red areas demarcate collagen. Scale bar (–) measures 200µm. Morphometric analysis of collagen proportionate area (CPA) (C) and assessment of hepatic hydroxyproline (D) as described in section 2.10 allowed comparison between the treatment group and control group by the use of the unpaired Student's t-test. $p<0.05$ was deemed significant. Summary bars: standard deviation and mean value

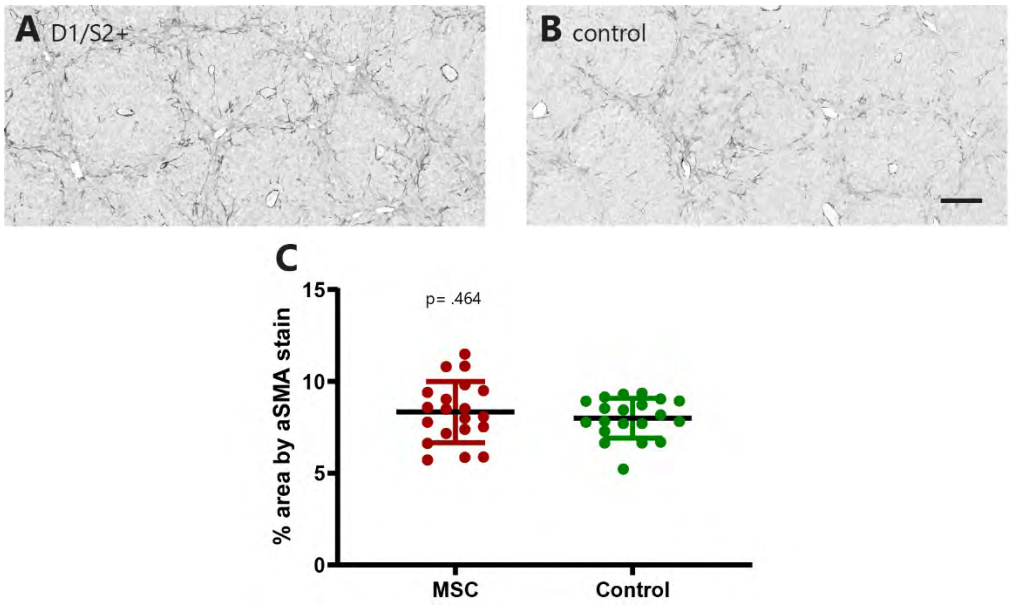

Figure 5-26: Analysis of myofibroblast activation in Experiment 5

During injury, mice were injected with S2-selected MSCs from a single donor (A) or control (B) as described in Figure 5.24 and euthanised 24 hours after TAA was removed. Paraffin-embedded tissue were stained for αSMA. Dark areas indicate positive staining. Scale bar (–) measures 200μm. Morphometric analysis of positive stained area (C) allowed comparison between the treatment group and control group by the unpaired Student's t-test; $p<0.05$ was deemed significant. Summary bars: standard deviation and mean value

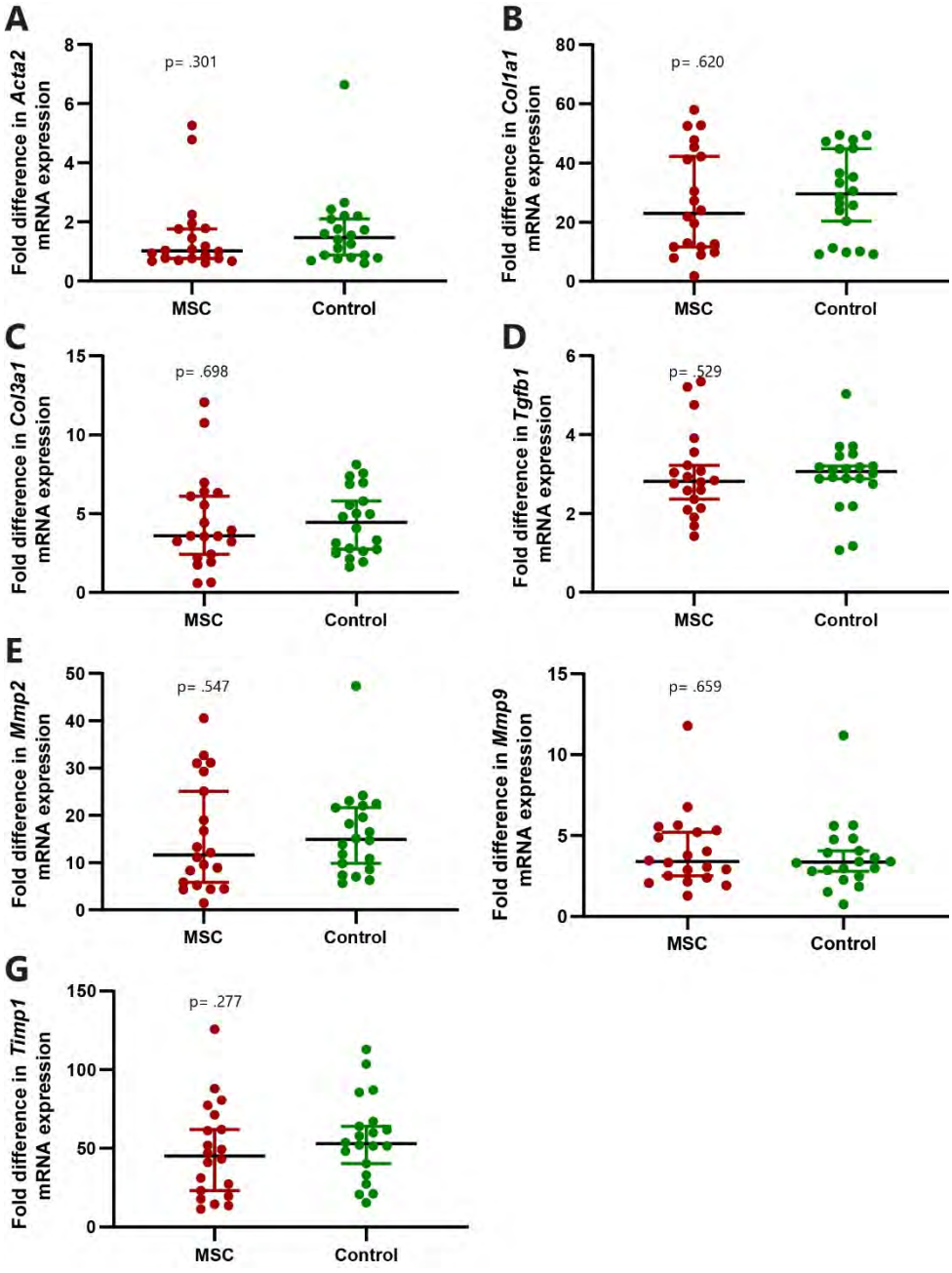

Figure 5-27: Gene expression analysis by qPCR of fibrosis-associated genes in Experiment 5

During injury, mice were injected with S2-selected MSCs from a single donor or control as described in Figure 5.24 and euthanised 24 hours after TAA was removed. Expression of fibrosis-associated genes (A: *Acta2*, B: *Col1a1*, C: *Col3a1*, D: *Tgfb1*, E: *Mmp2*, F: *Mmp9*, G: *Timp1* versus housekeeping gene *Gapdh*) was assessed by qPCR of hepatic tissues as described in section 2.14. The Mann-Whitney-test was used to compare expression in treatment groups and control group; $p<0.05$ were deemed significant. Summary bars: 95% CI and median value

Much like intervention during the chronic IP CCl_4 protocol in experiment 4, MSCs had no effect on fibroplasia when given during oral TAA-induced fibrosis (Figure 5.25-5.27).

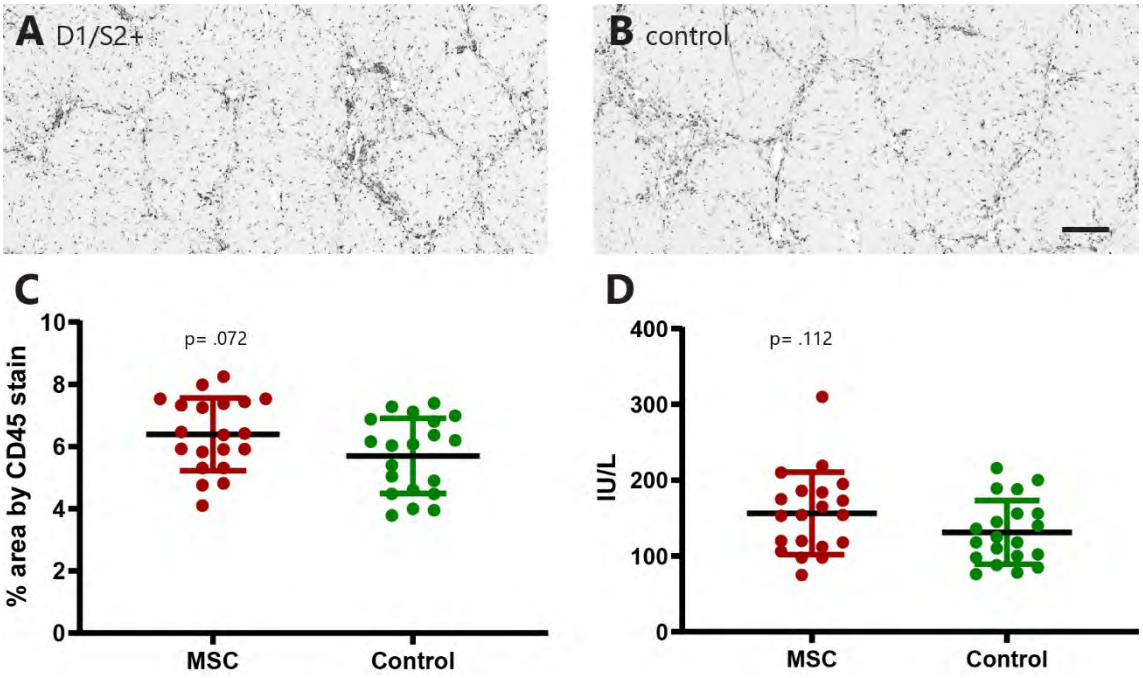

Figure 5-28: Analysis of inflammatory infiltrate by CD45 staining and hepatocyte injury by serum ALT measurements and in Experiment 5

During injury, mice were injected with S2-selected MSCs from a single donor (A) or control (B) as described in Figure 5.24 and euthanised 24 hours after TAA was removed. Paraffin-embedded sections were stained for CD45 for assessment of inflammatory-cell infiltrate as described in section 2.11.2. Dark areas indicate positive staining. Scale bar (–) measures 200µm. Morphometric analyses of positive stained area were used for quantitative comparisons (C). Sera from each euthanised mouse were analysed for ALT as a surrogate for hepatocyte injury or cell membrane instability (D). The unpaired Student's t-test was used to compare expression in treatment groups and control group; $p<0.05$ was deemed significant. Summary bars: standard deviation and mean value

Moreover, MSC administration during oral TAA induced injury had no effect on serum ALT, or gross hepatic inflammatory infiltrate (Figure 5.28).

5.6. Discussion

The work in this chapter has comprehensively demonstrated that human UCT-MSCs given via tail-vein in two well-characterised murine models of liver fibrosis has no effect of fibrosis as measured by extant collagen, the expression of αSMA as a marker of activated myofibroblasts, and fibrosis-related gene expression. The experiments were statistically powered to show a meaningful difference in the most reliable output measure of extant ECM – morphometric analysis of collagen proportionate area. As such, the data is robust, and the methodology reflects standardised guidelines that have been proposed to overcome the shortfalls of much of the published data in the field (Table 5.1) [73,162,206]:

Table 5-1: Application of standardised guidelines to improve reliability of outputs from animal experimentation to explore liver fibrosis

Guidance[73,206]	**Action in this study**
Selection of animals of defined adult age and sex	Male C57Bl/6 mice aged 8-10 weeks at injury onset
Group sizes of 8-15	Group sizes of 20 based on variance noted on preliminary data (Chapter 3, Table 3.2)
Optimised route and dose of toxin application	Route of application chosen based on translatability of peripheral systemic injection – discussed further in Chapter 6
Analysis of liver samples of sufficient size (5-10%)	Hyp assay performed using 100µg sample (approximately 7.5% of total mouse liver weight)
Representative morphometric analysis	Use of slide scanner to acquire images of whole of left lobe of liver – using >80% of each available image to almost nullify image selection bias.
Use of representative spectrum of quantitative fibrosis and fibrolysis readouts	Broad use of fibrosis output measures, all of which well established in literature.

It is unlikely that the non-effect was due to a resistant scar, as both models had exhibited the ability to naturally and progressively resolve in the absence of continuing injury in Chapter 3.

However, before declaring strong conclusions, one must consider methodological aspects that may have obstructed an effect being realised. The main considerations are:

1) Inadequate dose
2) Inadequate delivery method
3) MSC heterogeneity
4) Xenogeneic effect (human MSCs in a mouse model)

0.75×10^6 cells was chosen as the maximum safe single bolus in the fibrotic models, based on preliminary work during which tail-vein injections of 1×10^6 cells would occasionally lead to catastrophic embolic phenomena (pulmonary emboli or cerebrovascular events) immediately after injection (death in less than 2 minutes) in approximately 1 in 10 cases. This never happened with 0.75×10^6 cells. The published data suggests that very few investigators had trialled human cells via the tail-vein of mice to ameliorate fibrosis (Table 1.1)[45]. The total doses have ranged from 1×10^6 to 3×10^6 in chronic liver injury models[207], though a greater range have been trialled in the setting of acute liver injury[208]. Existing data has not adequately examined the optimal dosing regimen to deliver a desired therapeutic effect, and comparisons between studies will be confounded by variations in model of injury, timing of dose, type of MSC and outcome measures. Hong *et al* transplanted human UCT-MSC into rats with dimethylnitrosamine-induced liver injury (0.01% supplemented diet given *ad libitum* for 4 weeks) at varied doses, either as single infusions or as split dosing. They found that the anti-fibrotic effect was dose dependent, but probably not enhanced by split infusions[209]. Higher doses of single infusions (3 and 6×10^6) led to a significant reduction of collagen-1 gene expression compared to the lowest dose (1×10^6) ($p<0.05$). There was

a trend to a dose-dependent reduction of fibrosis as measured by PSR CPA, although this was not statistically significant: $1x10^6$ - 1.45%; $3x10^6$ - 0.8%; $6x10^6$ -0.1%. However, Hong's study was in rats, not mice. Miryounesi *et al* highlighted the possible benefits of split dosing over single infusions by infusing $3x10^6$ human BM-MSC in a murine CCl_4 injury model (IP twice per week for 9 weeks in NMRI mice)[207]. This was administered as a single infusion at week four or as a split dose of $1x10^6$ MSC on three occasions at weeks 4, 5 and 6 of a 9-week injury protocol. Mice were sacrificed for assessment at the end of injury and the single treatment arm showed no significant reduction in fibrosis versus the untreated arm as measured by CPA, although there was a significant reduction in the expression of *Col1α1* ($p<0.05$). The staggered treatment arm produced a significantly reduction in fibrosis as measured by CPA (2.5% vs 6%), and *Col1α1* gene expression (both $p<0.05$) compared to the untreated control and the single-treatment arm. It is plausible that earlier MSC infusions make the injured environment more tolerable for later MSC infusions by inducing the down-regulation of cytotoxic T-cell, and up regulation of regulatory T-cells, thus making it less likely that they will succumb to cytotoxic lysis[108]. Early MSC infusions may dampen the IFN-γ signal[108], thereby removing the stimulus for MSC to express MHC-antigens[210], and allowing their continued immune-privileged state. However, this was a speculative conclusion by the authors with no data to support their claim.

Intertwined with the dosing issue, is the mode of delivery. Systemic infusion provides the least invasive and most practical mode of cell therapy delivery in humans. Direct access to the liver is difficult, and is associated with complications. The risks are compounded in those with established liver disease. Therefore, to be able to translate the preclinical findings in this study, we chose to

evaluate the efficacy of tail-vein systemic injection of MSCs in our mouse models. This study goes on to explore and discuss the bio-distribution and persistence of systemically injected MSCs in Chapter 6.

As already discussed in Chapter 4, the term mesenchymal stromal cell describes a very heterogeneous cell population. MSCs from different tissue sources are likely to have very different biological effects, as they are known to have vastly different biological functions, differential potential and transcriptomic signatures[211–214]. The ISCT accept this as a critical shortcoming of the field, and therefore expect only that MSCs are clearly defined by their source, mesogenic potential, cell surface markers, culture conditions, and any relevant functional assays[178,215]. For this reason, it is difficult to compare and generalise conclusions from experiments using MSCs, and one can only safely deduce that S2-selected and unselected MSCs from the 2 donors trialled in this study do not affect liver fibrosis in the models that have been tested. Only one study to date has examined the effect of MSCs from different tissue sources on liver fibrosis. Briquet *et al.* compared the effect of well characterised human bone marrow, umbilical cord and liver MSCs on an IP CCl_4 model of liver fibrosis in mice, and found no difference in fibrosis as measured by CPA when injected by tail-vein after the cessation of injury[114].

Testing human MSCs in a xenogeneic model is a critical limitation of this study[216]. Xenogeneic MSCs may be subject to accelerated immune clearance. However, there are little data to support that notion. MSCs are considered to be immuno-privileged as they do not express class II[217] major histocompatibility complex (MHC) molecules, very low levels of class-I MHC molecules and or co-

stimulatory antigens CD80 and CD86 *in vitro*, which forms the basis of their allogeneic use[175]. However, the immuno-privilege of allogeneic MSC is a contentious issue, as in the presence of an inflammatory milieu (especially one containing high concentrations of IFN-γ), the expression of MHC-I and -II antigens are increased, rendering MSC susceptible to cytotoxic lysis[210,218]. However, this is in-part countered by their ability to induce an increase in regulatory T-lymphocytes, and suppress $CD4^+$ and $CD8^+$ memory and cytotoxic cells[219–221], in areas of injury. Nevertheless, adoptively transferred syngeneic and xenogeneic MSC are readily cleared within days both in pre-clinical and clinical settings, despite benefit out-lasting their presence[175]. Moreover, the clinical relevance of human MSCs having (or not having) an effect in animal model systems is debatable, as it assumes a requisite homology of disease and homeostatic pathways between the model and the human. For example, human MSCs use indoleamine 2,3-dioxygenase to suppress T-cells, whereas mouse MSCs utilise nitric oxide[219,222]. Similarly, the well characterised dichotomy of pro-inflammatory and fibrogenic Ly-$6c^{hi}$ monocyte derived macrophages and "restorative" Ly-$6c^{lo}$ macrophages are critical modulators of fibrosis in mice[58]; however, the human counterparts are less well characterised, and a similar differentiation of fibrogenic and restorative macrophages has not yet been described. Human $CD14^+16^+$ tissue macrophages share functional similarities with the pro-fibrogenic Ly-$6c^{hi}$ macrophages in mice, whilst also possessing high phagocytic activity akin the restorative Ly-$6c^{lo}$ macrophages[223,224]. Therefore even though human MSCs have been shown to have significant effects of murine pathology by other investigators, including pathways that may be relevant to fibrosis[202], the relevance in humans remains foggy. Using humanised animal models may be a way to bridge the understanding[214].

The data in this chapter suggests that MSCs given during the injurious phase neither prevented fibrosis, nor influenced chronic hepatic inflammation. As described in Chapter 3, the fibrogenic pathways of both the CCl_4 and TAA models are driven by hepatocyte death, oxidative stress and inflammation. Data from others in the Newsome laboratory have shown that the same MSCs used in this study can abrogate oxidative stress in an acute CCl_4 injury model (Alfaifi M, 2018, PhD Thesis, University of Birmingham) and immunomodulate to increase hepatic T-helper cell populations and polarise macrophages from M1 to M2 in the inflammatory biliary injury model[202] (MDR2 knockout mice). It is plausible, that the alleviation of oxidative stress is short-lived (72 hours) after infusion, and overwhelmed in the setting of continuing injury. Moreover, the immunomodulatory effects may again be short lived and not be critical to the fibrotic pathways, as MSC infusions were not seen to affect fibrosis readouts in the MDR2 model. The isolated rise in serum ALT noted when MSCs were administered during CCl_4-induced injury may represent a flux in oxidative stress, especially in the absence of finding any changes in inflammatory infiltrate. As such, it would be worth a further exploration, but others in the Newsome laboratory are focussing on the effect of MSC therapy on redox homeostasis, and the focus of my study is fibrosis. In the absence of any significant effect on fibrosis, I chose not to pursue this angle any further.

5.6.1. Summary

The work in this chapter is a robust, statistically powered analysis of the effect of human UCT-MSCs on fibroplasia and fibrosis resolution in two well characterised models of murine liver fibrosis. The absence of any effect is not MSC donor specific, and not a function of prospective enrichment for syndecan 2. Notwithstanding the potential limitations of using a xenogeneic

model, and the possibility that MSCs from other tissue sources may have a different effect, it is safe to recommend that future investigators require a significant deviation in methodology or proven mechanism-of-action-based hypothesis before pursuing this line of research again.

Chapter 6

Bio-distribution and persistence of human MSCs injected by tail-vein in mice with established liver fibrosis

6.1. Background and context

Systemic infusion provides the least invasive and most practical mode of cell therapy delivery. Direct access to the liver is difficult and is associated with complications. The risks are compounded in those with established liver disease due to coagulopathy and portal hypertension. Therefore, we chose to evaluate the efficacy of tail-vein systemic injection of MSCs in our mouse models.

In the absence of eliciting any substantial effect of human UCT-MSC therapy on fibrosis regression or resolution, we sought to examine the bio-distribution and persistence of MSCs following tail-vein injection.

6.1.1. Cryoviz™ imaging of nanocrystal labelled MSCs

The Qtracker® Cell Labeling Kits (Q25001MP; Life technologies, Invitrogen, UK) aggregates Qdot® nanocrystals into the cytoplasm and organelles of intact cells within an hour of incubation, by an enzyme-independent mechanism. The technology avoids degradation and photo bleaching[225,226]. The nanocrystals are inherited by daughter cells for at least six generations, and offer long-term photo-stability and fluorescence for up to a week when tested in a number of cell lines according to the manufacturers product specification; this retention facilitates cell migration to be tracked *in vivo*[227]. Other investigators have demonstrated no impact of Qdot® labeling on MSC proliferation and DNA damage for up to 120 hours[228]. However, a dose dependent effect on cytokine release and apoptosis was seen, though not at the concentrations recommended by the

manufacturer. Few labelling techniques have demonstrated such stability without affecting cellular function or viability. One exception is the novel ^{89}Zr labelling method which exhibits a half-life of nearly 80 hours, thereby enabling high resolution *in vivo* tracking for up to 3 weeks[229].

Cellular aggregation of nanocrystals registers as a fluorescent unit that can be detected by the Cryoviz™ technology. The Cryoviz™ or cryomicrotome imaging system requires cryopreserved tissues to be sectioned at 20μm thickness to acquire high-resolution bright field and fluorescence images. The 2D planar images can then be reformatted to produce 3D renderings and thereby enable 3D interrogation[230]. This resulting cellular-level resolution of tagged cells *in vivo* in an "intact" mouse can facilitates a high throughput and highly granular assessment of tagged-cell distribution[231]. The technology quantifies the number of cells distributed throughout the whole body, and provides a considerably greater resolution of cellular tracking than other whole-body imaging methods such as positron emission tomography of radiolabelled MSCs[229], or even magnetic resonance imaging of MSCs loaded with supermagnetic particles[232]. The major disadvantage of the Cryoviz™ system is that it requires mice to be euthanised prior to imaging, whereas the other methods permit imaging in live animals and thereby open the potential for serial imaging over time within the same mouse.

Ex vivo histological assessment is the most common approach to localise labelled MSCs, whether it be via basic IHC (using Qdots®, vital dyes or green-fluorescent protein)[233,234] or *in situ* hybridisation in sex or species-mismatched samples[233]. Though these techniques can provide *in situ* visualisation within the context of tissue structure, they require the cells to be abundant

enough to be detected. Contemporary PCR-based techniques including RT-PCR can overcome some of the issues of sensitivity with an estimated threshold for detection as low as one human MSC in 600,000 murine cells[235]. Nevertheless, tissue collection from different organ compartments throughout the body is highly intensive, invasive, and susceptible to sampling bias. Cryoviz™ overcomes each of these issues and provides the state-of-the-art *ex vivo* imaging option (Figure 6.1).

Industry collaborators BioInVision Inc. (Cleveland, USA) kindly provided the images and crude quantification of the labelled MSCs in frozen mice using Cryoviz™, following the *in vivo* experiments that I conducted myself in Birmingham.

6.2. Aims of the chapter

The aims of the work in this chapter were to:

- Map the bio-distribution of Qdot® nanocrystal labelled human UCT-MSCs injected by the tail-vein of immunocompetent mice with established liver fibrosis.
- Determine the persistence of the cells in vivo through 8 days after injection.

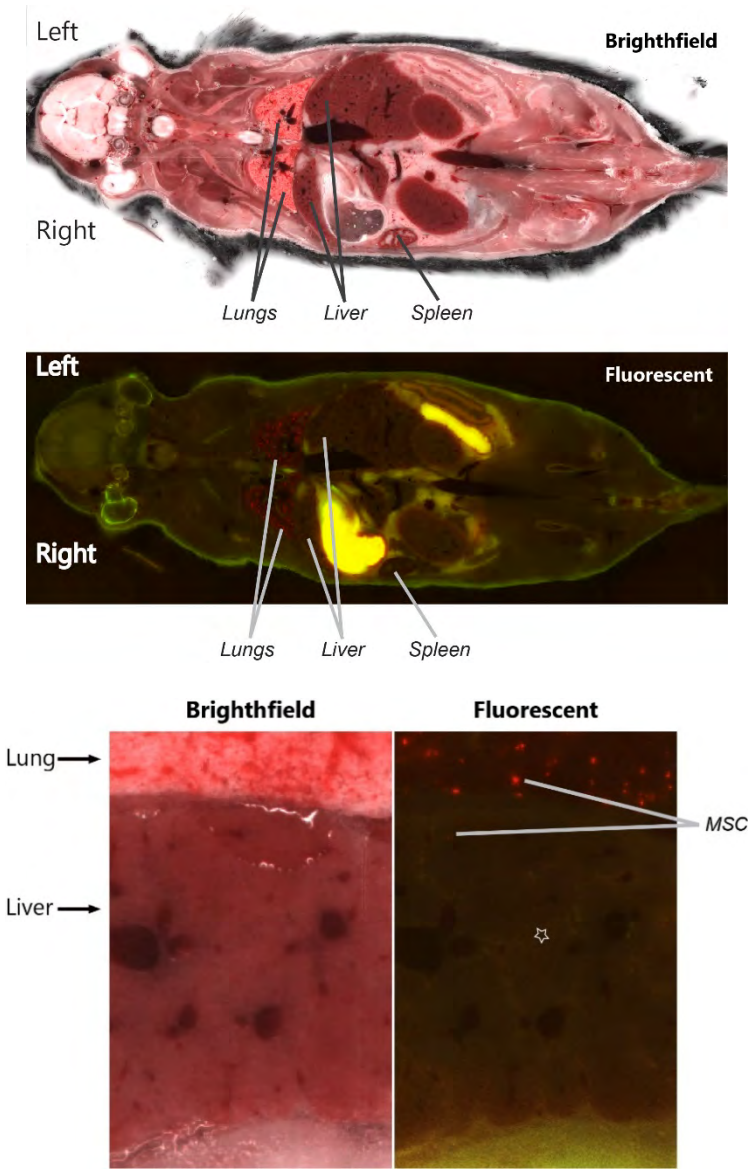

Figure 6-1: Image acquisition using Cryoviz™ technology: localising MSCs

The technology and software provided 20µm sections through a fixed plane (coronal) of the cryopreserved whole mice, which were subsequently rendered in to three-dimensional maps for localisation of fluorescently labelled cells. The top (bright field) and bottom (fluorescent) images of the whole mouse show corresponding coronal sections through a frozen mouse using the Cryoviz™ technology and software. The fluid-filled gut can be seen to be auto fluorescent (yellow) and fluorescently labelled MSCs can be seen to aggregate in the lungs (speckled red distribution) in the middle image. The bottom left (bright field) and right (fluorescent) images are magnified corresponding sections from the whole mouse. The fluorescent bright-red aggregated MSCs are easily seen in the lungs, but are more sparse in the liver. Of interest, the band-like pink auto-fluorescence (highlighted by star) are likely to demarcate bands of fibrosis or inflammatory infiltrate, which are not obviously evident in the bright field images. Images provided by BioInVision Inc. (Cleveland, USA).

6.3. Qdot® nanocrystal labelling of human UC MSCs

6.3.1. Labelling uptake efficacy

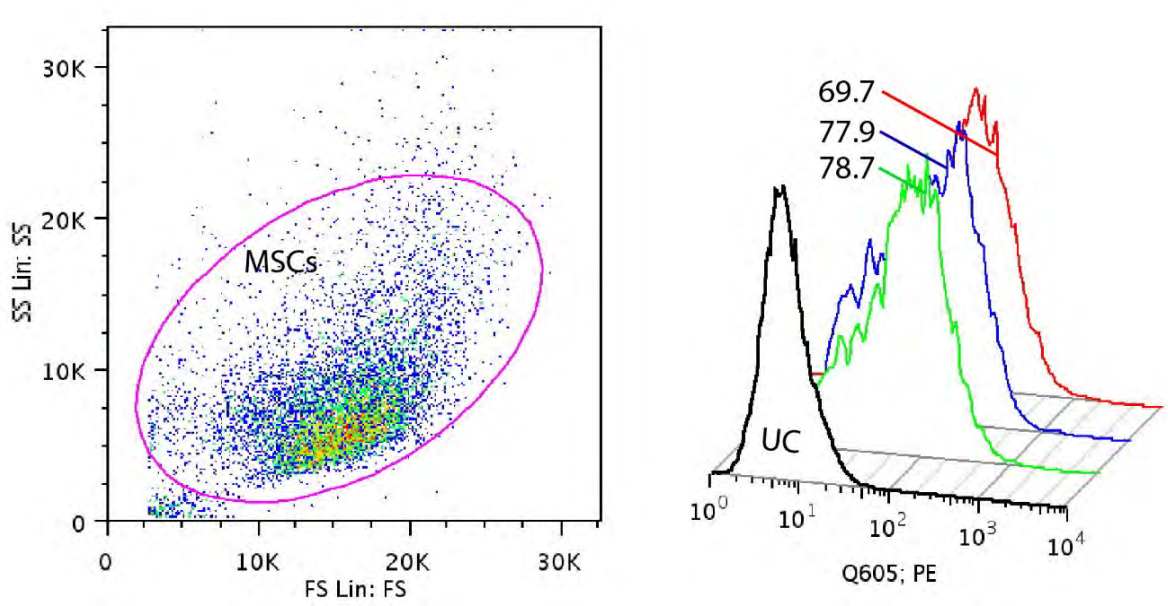

Figure 6-2: Flow cytometric analysis of Qdot® uptake by MSCs in culture

Human UCT-MSCs were expanded in culture to passage 3 and enzymatically detached from the tissue culture flasks at a confluence of 70-80%. $1x10^6$ cells from each of three tissue culture flasks (green, blue and red histograms) were labelled with Qdot®-605 nanocrystals as per manufacturer's instructions. The labelled cells were examined for fluorescence on the PE channel using a Cyan ADP flow cytometer. The proportion of labelled cells were determined using the Overton subtraction technique (percentages above the histograms) against the histogram of unlabelled cells (UC)).

The Qtracker® cell tagging protocol labelled 75.4±4.1% (mean ± standard deviation) of human UCT-MSCs after triplicate testing using MSCs from different starting vials. The consistency of percentage uptake reassured me that the numbers detected *in vivo* would be faithfully comparable between mice.

6.3.2. The effect of label uptake on cellular viability

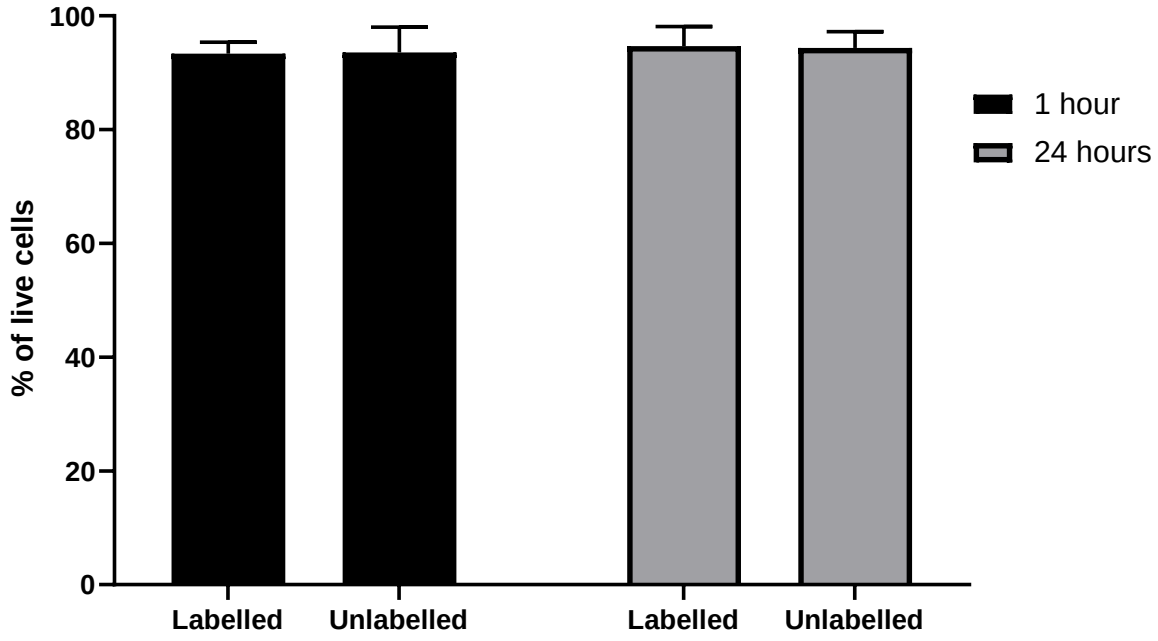

Figure 6-3: Cell viability of Q-dot®-labelled and unlabelled MSCs

3 sets of $1x10^6$ MSCs were labelled with Q-dot®-605 nanocrystals as per manufacturers instructions and assessed for cellular viability after 1 and 24 hours in culture medium by the Trypan-blue exclusion method using a haemocytometer. The percentage of viable cells (unstained) were charted. 3 sets of a matched number of unlabelled MSCs were similarly examined as a control. Data summary bars represent the mean and range. There were no significant difference in cell viability between the two groups.

The Qtracker® cell tagging protocol did not affect cell viability both in the immediate aftermath of incubating with the nanocrystals, and after 24 hours of further *in vitro* culture.

6.4. Bio-distribution and persistence of Qdot® labelled UC MSCs

We injected 1x10^6 MSC Qdot® -605 labelled MSCs via tail-vein in to ten mice with established hepatic fibrosis as described in Figure 6.4. Two mice were euthanised by a Schedule 1 approved CO_2 asphyxiation technique at each of the five time points after injection.

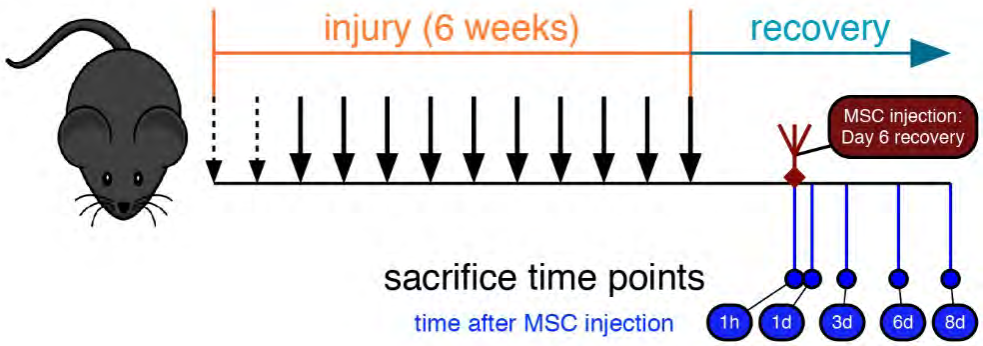

Figure 6-4: Schematic of experiment to explore the bio-distribution tail-vein-injected MSCs in a model of liver fibrosis

Age-matched male C57Bl/6 mice were twice injected with CCl_4 diluted in mineral oil (1:3) at a dose of 1 μ l/g bodyweight (dashed vertical arrows) IP, followed by 10 injections at a dose of 2µl/g bodyweight (blocked vertical arrows) over 6 weeks. Mice were injected with 1x10^6 S2-selected MSCs (labelled using Qdot®-605) in 200uL of sterile 0.9% saline carrier on day 6 of recovery after the last IP injection. Two mice were euthanised by CO_2 asphyxiation on each of indicated time points (blue circles) after the last MSC injection, and prepared for whole-body bio-distribution analysis by Cryoviz™ technology. In brief, the carcasses were submerged and embedded in PolyFreeze Tissue Freezing Medium (SHH0026; Sigma, UK), and rapidly frozen on a bed of dry ice. They were then stored at -80°C until shipment to BioInVision Inc. (Cleveland, USA).

At 1 hour after injection, a mean of 88.3% of MSCs were in the lung, with 5.9% in the liver. The mean number of detected cells at 1 hour (7.43x10^5) was used as the baseline for subsequent calculations.

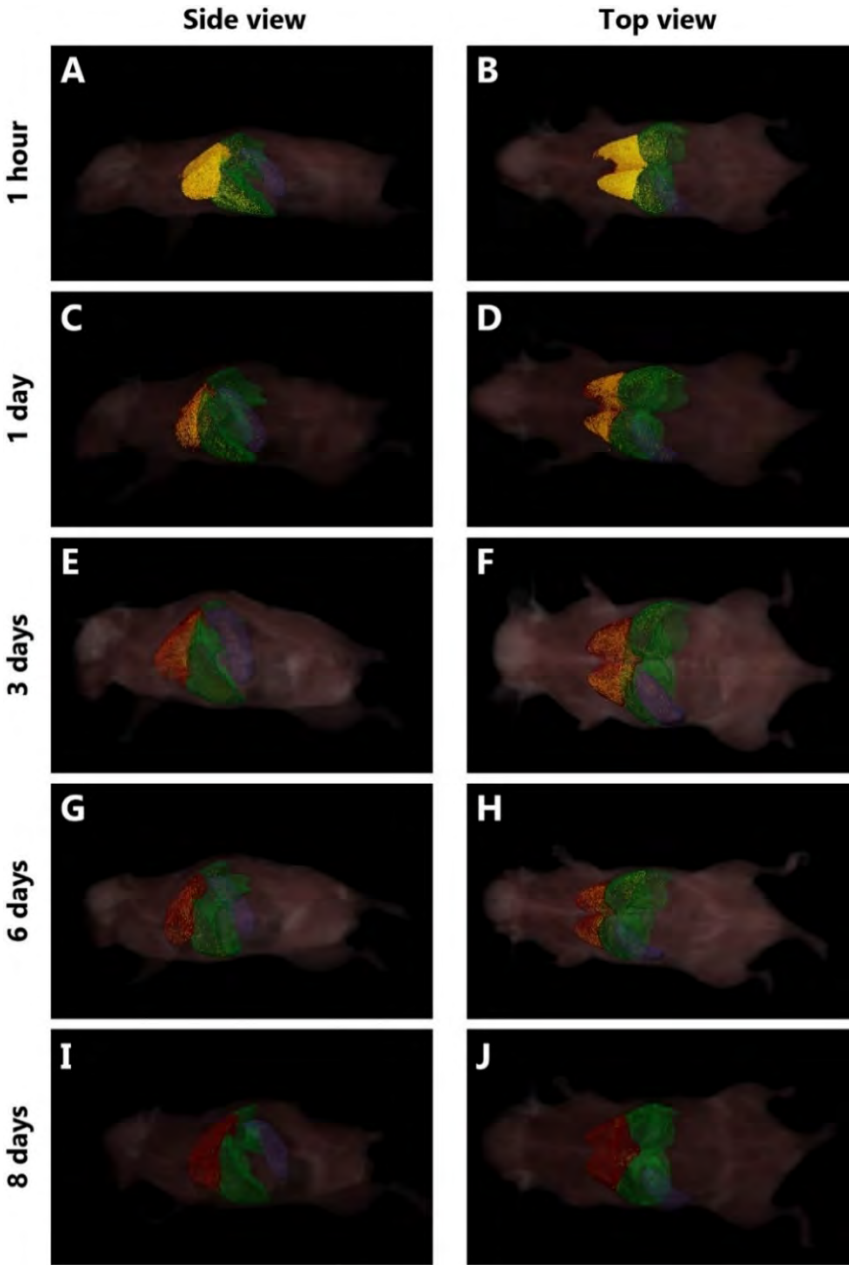

Figure 6-5: 3-dimensional rendering of Cryoviz™ images to illustrate the distribution of MSCs in the injected CCl_4-injected mice at advancing time points after tail-vein injection

The images represent 3-dimensional reconstructions of 2-dimensional sections constructed by the Cryoviz™ software viewed along the sagittal (A, C, E, G, I) and coronal (B, D, F, H, J) planes. The bright yellow dots denote MSCs in the ghost-like representations of the underlying organs (red – lungs; green – liver; purple - spleen). Mice were euthanised for analysis 1 hour (A, B), 1 day (C, D), 3 days (E, F), 6 days (G, H) and 8 days (I, J) after tail-vein injection of fluorescently labelled cells as described in Figure 6.4. Images provided by BioInVision Inc. (Cleveland, USA).

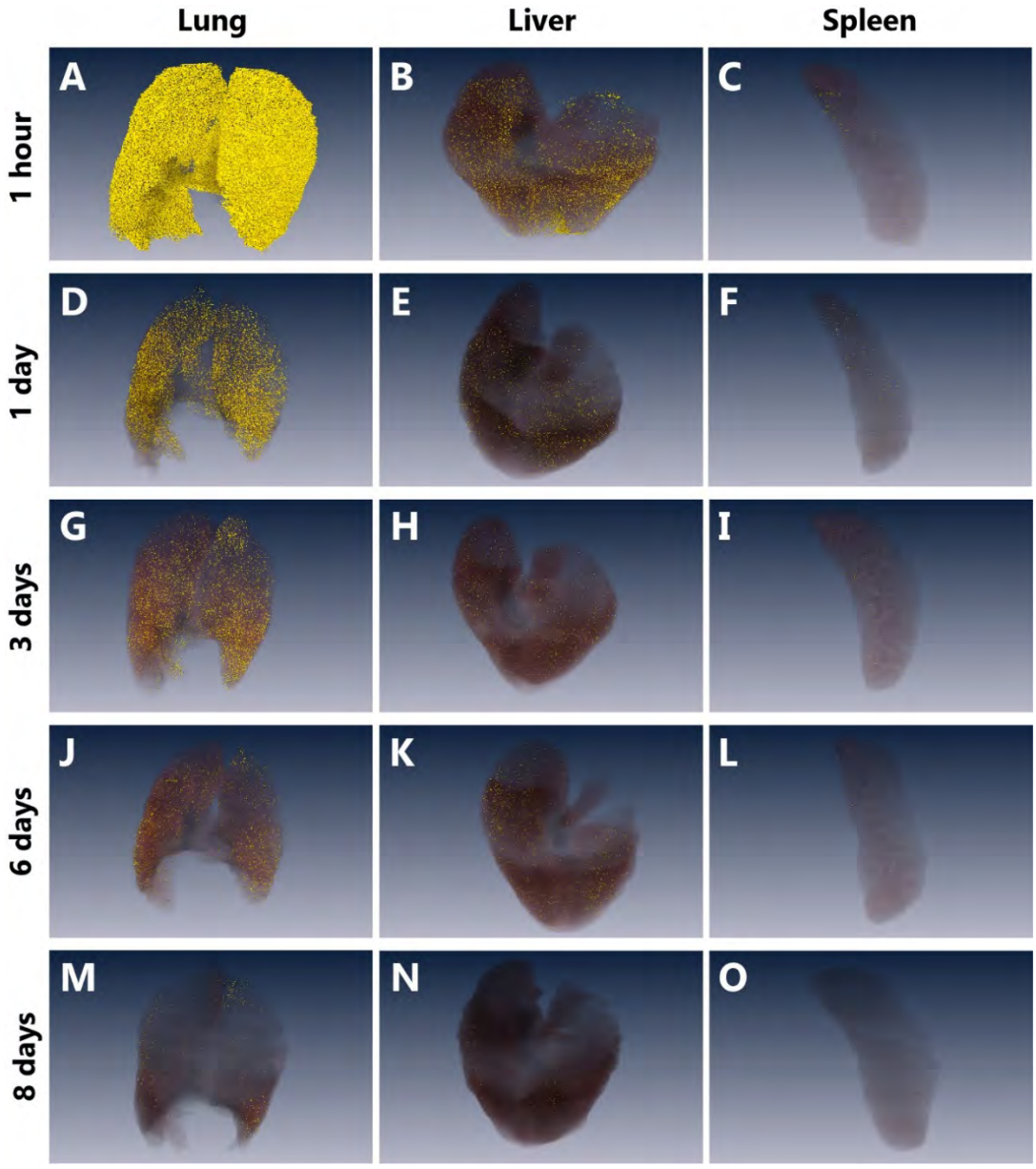

Figure 6-6: 3-dimensional rendering of Cryoviz™ images to illustrate the distribution of MSCs in the lungs, liver and spleen at advancing time points after tail-vein injection

The images are 3-dimensional reconstructions of 2-dimensional sections constructed by the Cryoviz™ software. The bright yellow dots represent MSCs in the brown ghost-like representations of the underlying organs (A, D, G, J, M – lungs; B, E, H, K, N – liver; C, F, I, L, O - spleen). Mice were euthanised for analysis 1 hour (A – C), 1 day (D – F), 3 days (G – I), 6 days (J – L) and 8 days (M – O) after tail-vein injection of fluorescently labelled cells as described in Figure 6.4. Images provided by BioInVision Inc. (Cleveland, USA).

A correction of this value using the estimated proportion of cells that take up Qdot® nanocrystal labelling (75.4%) suggests a very faithful cell preparation and injection protocol with minimal loss of cells in the process ($9.85x10^5$ cells compared to the intended $1x10^6$).

The majority of cells were cleared rapidly, with only 17.6% of the average baseline number of cells being detectable after 24 hours. The total rate of clearance subsequently slowed with 6.9% of cells still detectable after 3 days. 4.8% after 6 days and 1.8% after 8 days (Figure 6.5-6.7).

The rate of clearance was more rapid from the lung than in is the liver (Figure 6.8). The change in the relative proportions of cells in the liver and lung may reflect cells moving from the lung to the liver between day 1 and day 6 after injection, though it is not possible to know for sure without repeated tracking of cells within the same mouse, and correcting for rates of proliferation and death in each organ compartment. This is not possible using the available means in this experiment. The relative proportion of cells in the spleen throughout was negligible.

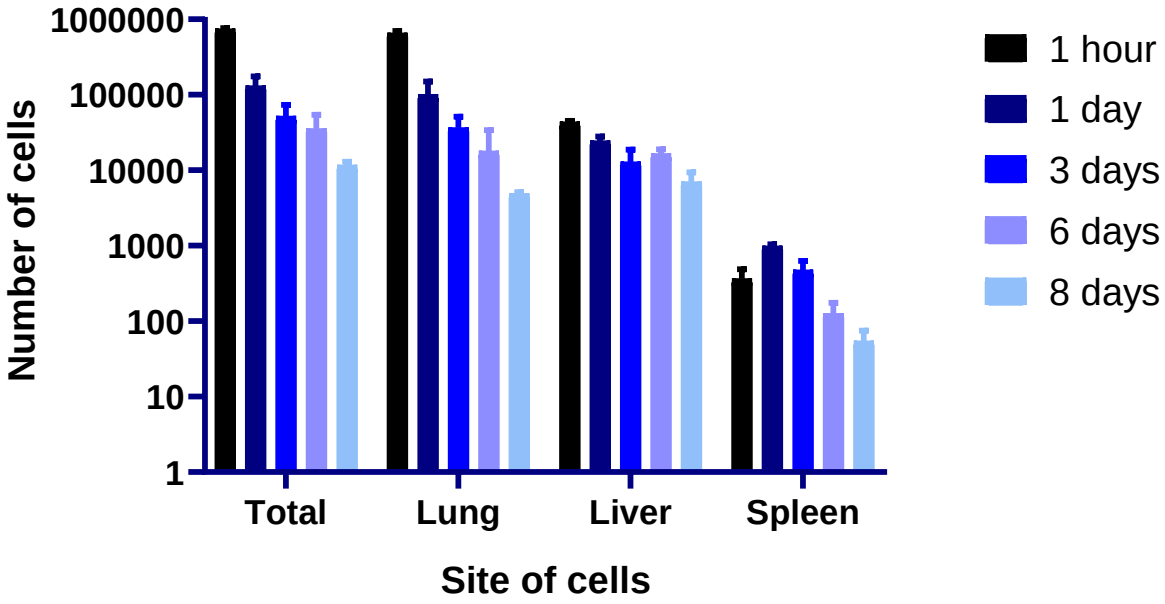

Figure 6-7: Analysis of MSC numbers in the lungs, liver and spleen at advancing time points after tail-vein injection

The charts depict the numbers of detectable cells in the different organ compartments with advancing time after tail-vein injection of human UCT-MSCs in mice with established fibrosis as described in Figure 6.4. Cells were labelled with Qdot®-605 nanocrystals and detected using the aforementioned Cryoviz™ system. Data summary bars represent the mean and range. The y-axis depicts the number of cells using a $\log_{10}$ scale.

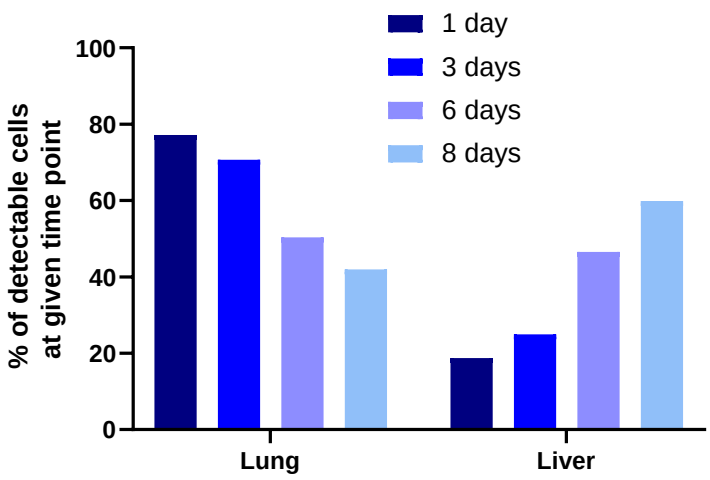

Figure 6-8: Changes in relative proportions of detectable cells in the liver in lung with advancing time

The analyses depict the change in the proportion of the total number of detectable cells in the liver and lung with advancing time following the tail-vein injection of Qdot®-labelled human UCT-MSCs in mice with established liver fibrosis as described in Figure 6.4.

6.5. Discussion

6.5.1. MSC labelling efficiency is consistent

Approximately 75% of the MSCs were labelled by the Qdots® on each of the incubation runs with little variance. It is unclear why the label uptake efficiency differs from other investigators. For example, Auletta managed a 70% uptake using human BM-MSCs[236], Rak-Raszewska showed an 85% uptake in two different murine stem cell populations[225], and Alfaifi, using the same human UCT-MSCs in the same laboratory as this body of work, reported a 92% labelling efficiency (Alfaifi M, 2018, PhD thesis, University of Birmingham). However, differences in how uptake efficiency was calculated may account for the different reported values; Alfaifi and Rak-Raszewska used manual counts of positively stained cells after fluorescent imaging, whereas this study used flow cytometry, and was therefore subject to less user bias. Nevertheless, the vital finding was consistency – repeated labelling yielded consistent uptake efficiency, which provided assurance and confidence that the numbers detected *in vivo* would be faithfully comparable between mice. Moreover, the adjusted cell numbers an hour after injection were very close to the intended injection number of $1x10^6$, suggesting very little cell loss in the preparation phase, and a consistent and reliable preparation protocol. The labelling protocol had no effect on cell viability, in keeping with published data[225], and the persistence of fluorescent cell detection to day 6 and 8 in vivo were very much in keeping with the advertised photo-stability of a week. However, one must be mindful of data suggesting that Qdots® may deplete from some *in vitro* cell cultures (mouse embryonic stem cells and mouse tissue-specific stem cells), with a drop from 80-90% cellular labelling on day 0, down to 10-40% by day 3 in culture[225]. Though this drop was not reported in

all cell types, it would have been prudent to determine the labelling efficiency over time *in vitro* using the cells I used for the *in vivo* cell tracking experiments. One must interpret the results of this chapter in knowledge of this limitation.

6.5.2. The pulmonary "first-pass" effect – Big round pegs don't fit through small square holes

The findings in this study are not novel[237], though they are the first to confirm the bio-distribution and persistence of systemically injected MSCs in a murine liver fibrosis model using the Qdot® and Cryoviz™ system. After systemic injection, MSCs get trapped in the first small-calibre capillary bed the encounter; in the case of peripherally injected MSCs, the first capillary bed is in the lungs[238]. This "passive entrapment" is a primarily consequence of the cells being too big to traverse narrower vessels. Though endogenous, inactivated BM derived MSCs are small (~10μm), *ex-vivo* expanded MSCs grow, reaching sizes greater than 30μm in diameter by the 7th day of culture[239]. However, in health, the estimated diameter of both human and murine pulmonary capillaries is approximately 8μm, a terminal arteriole 10μm, and venule is 20μm[237,240]. There are physical limits to how much cellular deformability can overcome this disparity without compromising cellular viability or vascular patency[241].

6.5.3. Changing the bio-distribution of systemically injected MSCs

Having identified the issue of pulmonary trapping as a critical roadblock for intravenous MSC therapy, a logical next step to investigate whether MSC therapy affects fibrosis would be to

increase the delivery of MSCs to the liver. The most effective way to do this would be inject MSCs via the portal vein or hepatic artery to facilitate passive "hepatic entrapment". This would facilitate an examination of MSC distribution and persistence via a more direct route, but one could again examine the effect of MSC therapy on fibrosis. If a dose-dependent effect was observed, then one could examine modes of enhancing the delivery of systemically injected MSCs to the liver, to replicate the effect of the much more invasive portal vein or hepatic artery injection. This mode of deliver is technically difficult requiring a procedure under anaesthesia in mice, and practical clinical translation is less feasible and less attractive.

A number of investigators have developed *ex vivo* culture protocols to yield smaller MSCs[239,242–244], with an increased capacity to traverse the lung unimpeded[243]. Similarly, pulmonary vasodilators have been used to good effect[245]. Other investigators have utilised cytokine pre-treatment or "licensing" to reduce pulmonary sequestration in the immediate aftermath of systemic injection with different cytokine mono-treatments and cocktails eliciting different effects[246]. This allies to an observed effect on *in vivo* longevity after different licencing techniques[45], including the pre-incubation of MSCs with organic compounds such as hyperosmolaric hydroxyethyl starch, which was shown to both decrease MSC size, change bio-distribution and increase the viability of systemically injected MSCs[247]. Alternative cell detachment techniques of *in vitro* preparations have changed the bio-distribution of systemically injected cells. Pronase detachment markedly increased the relative proportion of cells in the liver in the first 15 hours after tail-vein infusion[248]. However, the analysis was of proportional radioactivity at different sites after infusing radiolabelled cells, so it is unclear how the pronase affected the total number of cells.

6.5.4. MSC homing to areas of injury

MSC homing has been described as active or passive arrest of MSCs within the vasculature followed by transmigration across the endothelium[249]. We know from many dedicated mechanistic studies that MSCs migrate to sites of injury, like leukocytes, often in response to chemotactic cues[39], attach the endothelium[250], and have the capacity for diapedesis[251].

Unfortunately, this part of the study was not designed to examine a difference in migration and homing to the injured livers versus uninjured livers, as no uninjured age matched control mice were infused with labelled cells. Colleagues in the Newsome laboratory found no difference between the percentage of detectable cells in the liver 24 hours after labelled MSC injection in an acute CCl_4 model of hepatic injury versus an uninjured control (Alfaifi M, 2018, PhD thesis, University of Birmingham). However, one would envisage that cells engrafting to the liver after 1st pass pulmonary retention[238] would respond to chemotactic cues, and differences in the relative percentages of detectable cells between the liver and lung in the following 3-5 days may be more informative in the chronic setting.

The phenomenon of label detection in the liver in preference to the lung after the initial pulmonary sequestration, as seen in Figure 6.8, is not necessarily a function of hepatic injury. Bansal *et al.* documented a similar finding in uninjured mice injected with ^{89}Zr-labelled human MSCs[229]. 7 days after injection, there was proportionately greater radioisotope reading from the liver (50% of the injected dose) than the lung (27% of the injected dose). The liver has been repeatedly shown to

be the preferred destination for injected MSCs after the lung following systemic intravenous injection[252,253]. It is unclear whether the inverse proportional relationship between the cells in the lung and liver are a consequence of migration, or a differential in the cell death rates in the two organ compartments (i.e. is the pulmonary environment more hostile than the hepatic environment?). Certainly, the increase in measured number of cells in the liver between days 3 and 6 after injection may suggest migration to the liver, or a greater proliferative index than cell death.

6.5.5. The fate of MSCs after systemic injection

One must be mindful of the possibility of a false positive signal. Label detection, by whichever means including Cryoviz™ as described in the introduction to this chapter, is subject to false positive input as a result of label redistribution by phagocytic monocytes following uptake of cellular debris from dying MSCs[237]. The relevance of this becomes apparent when considering contemporary data that has demanded a re-examination of some fundamental assumptions about MSC therapy. Upon injection, MSCs quickly lose cellular integrity, start to fragment and become apoptotic[247]. Moreover, the MSC fragments are subject to opsonisation, and start falling victim to phagocytosis by circulating monocytes and tissue macrophages[254]. Upon efferocytosis, they induce changes in the macrophage polarisation, by which they can effect immunomodulation, whether it be by the PGE_2-dependent[255], or IDO-dependent pathways[204]. These data would, in part, start to explain the paradox that MSCs seem to be therapeutically efficacious despite a lack of engraftment and rapid clearance[256], in that they act via a surrogate. Moreover, amongst patients with GvHD, only those with high cytotoxic activity against MSCs

responded to MSC infusions[204]. If, in fact, MSC apoptosis is critical to their downstream clinical effect, perhaps efforts to enhance MSC survival *in vivo* should be redirected to predisposing MSCs to apoptosis[257]. Other work in the Newsome laboratory has shown MSC therapy has induced macrophage polarity changes in murine models of PSC without exploring interim MSC apoptosis[202]. However, the work in Chapter 5 did not reveal an MSC-therapy induced change in macrophage polarity in either the resolution of fibrogenic phases.

6.5.6. Summary

The data from this chapter describes the pulmonary sequestration and subsequent rapid clearance of human UCT-MSCs administered by tail-vein injection in mice with established liver fibrosis. A negligible proportion of MSCs persist globally after a week (1.8%), and less than 3.5% of the injected cells (positive labelled units) are in the liver at 24 hours. The findings are in keeping with existing data that describe the pulmonary first pass phenomenon. Bypassing pulmonary entrapment by portal vein or hepatic artery injection in chronic hepatic fibrosis models may inform of any direct effect MSCs have on fibrosis, but the experiments are technically very difficult. As such, in Chapter 7, this study proceeds to examine whether MSCs have any direct effect on the primary lynchpin of fibrosis and its resolution – myofibroblasts.

Chapter 7

The effect of MSC conditioned media on LX2 cell biology

7.1. Background and context

A complex interplay between cells and the local microenvironment governs hepatic fibrosis and its regression[63,206], but the lynchpin around which the complexity is interwoven is the myofibroblast. Upon activation, hepatic stellate cells transdifferentiate to become myofibroblasts that secrete ECM, and TIMP to maintain the matrix. With continuing injury, they proliferate in response to mitogens like PDGF, and become increasingly resistant to inactivation and apoptosis. However, regression is marked by myofibroblast inactivation, senescence or apoptosis[51]. The diminished effect of myofibroblasts enables restorative macrophages to effect the dissolution of ECM by the unopposed action of MMPs (Figure 1.1). This is a simplified version of events which are more completely described in Chapter 1, and in dedicated review articles[63].

Systemic MSC administration had no effect on liver fibroplasia or fibrosis regression (Chapter 5). A possible reason could be an inadequate delivery of MSCs to the site of the pathology due to pulmonary entrapment[238], though this theory makes assumptions about the mechanism of action by which MSCs may act to disrupt fibrosis – that being the need for proximity and persistence as discussed in Chapter 6. To explore this further, I chose to examine the direct effect of MSC conditioned medium on stellate cell biology. I chose not to explore the direct cell-cell induced effects of MSCs on HSCs as the work in Chapter 6 has already shown how sparsely MSCs locate in the liver. Even if MSCs were injected via the portal vein, one would have to demonstrate that MSCs could migrate across the capillarised sinusoidal endothelium in cirrhotic livers in to the Space of Disse to make it a worthwhile exercise[258].

Primary isolated stellate cells would have been an ideal substrate upon which to test the action of MSC conditioned medium. They retain their *in vivo* state and exhibit the plasticity required to realise an effect of therapy[259]. However, despite my own previous success in using a protocol of enzymatic and mechanical disruption and digestion followed by density gradient centrifugation to isolate murine hepatic stellate cells[154], the yield and purity was extremely variable, with a significant burden of non-parenchymal cell contamination (results not shown). Moreover, isolating human primary stellate cells was hindered by infrequent and unpredictable access to human tissue, with concerns of inter-batch cell heterogeneity[260].

With a view to maintaining substrate homogeneity, I chose to utilise LX2 cells. Of all the human HSC cell lines, LX cells have been most extensively characterised[260,261], and tested upon. LX cells are generated by plasmid transfection of primary stellate cells conferring SV40 T antigen immortalisation, with LX2 cells undergoing clonal expansion under low-serum (1-2% FBS) conditions[260]. They have a reported phenotype that is closest to activated HSCs *in vivo*, and are known to express a catalogue to genes typically expressed in activated stellate cells including PDGFβ, TGFβ, collagen types I and IV, vimentin, desmin, and αSMA[261]. For this reason they are regarded as first choice when modelling activated human HSCs[262].

7.2. Aims of the chapter

The aims of the work in this chapter were to:

- Examine the effect of MSC conditioned medium on LX2 cell biology

7.3. Characterising LX2 cells

LX2 cells were obtained from Dr. Scott Friedman (Mount Sinai Hospital, New York, USA), and stored between in liquid nitrogen at a concentration of $1x10^6$ in 1mL of serum with 10% dimethyl sulfoxide (DMSO). For use, cells were plated in low-serum (2% FBS) LX2 complete medium as described in section 2.13.1 for 8 hours, and serum-starved (supplemented with 0.1% BSA) for 24 hours prior to experimentation.

This part of the study characterised the behaviour of LX2 cells in low-serum (2% FBS), high-serum (10% FBS) and serum-free conditions (0.1% BSA). It was critical to assess the baseline phenotype of LX2 cells in 10% FBS as it would form the negative control for the intervention experiments using MSC conditioned media (CM). Attempts to culture MSCs at lower serum concentrations (2% FBS) led to considerably attenuated proliferation. As such, MSC-CM was collected using standard MSC culture media (10% FBS), but without FGF (Section 2.2.1).

Regardless of the culture medium, LX2 cells adopted an activated contracted fibroblastic appearance on uncoated plastic (Figure 7.1, Panel A). All cells expressed the intermediate cytoskeletal filament vimentin that is typical of cells of mesenchymal origin. Magnified images clearly demonstrate the cytoplasmic reticular pattern of a cytoskeletal framework highlighted by vimentin staining (Figure 7.1, Panels E-G). Moreover, as has been previously shown in the landmark papers that originally characterised LX2 cells[260], and in keeping with a partially activated phenotype, all LX2 cells express αSMA in a similar cytoskeletal pattern (Figure 7.1, Panels E-G) regardless of the culture medium they were incubated in.

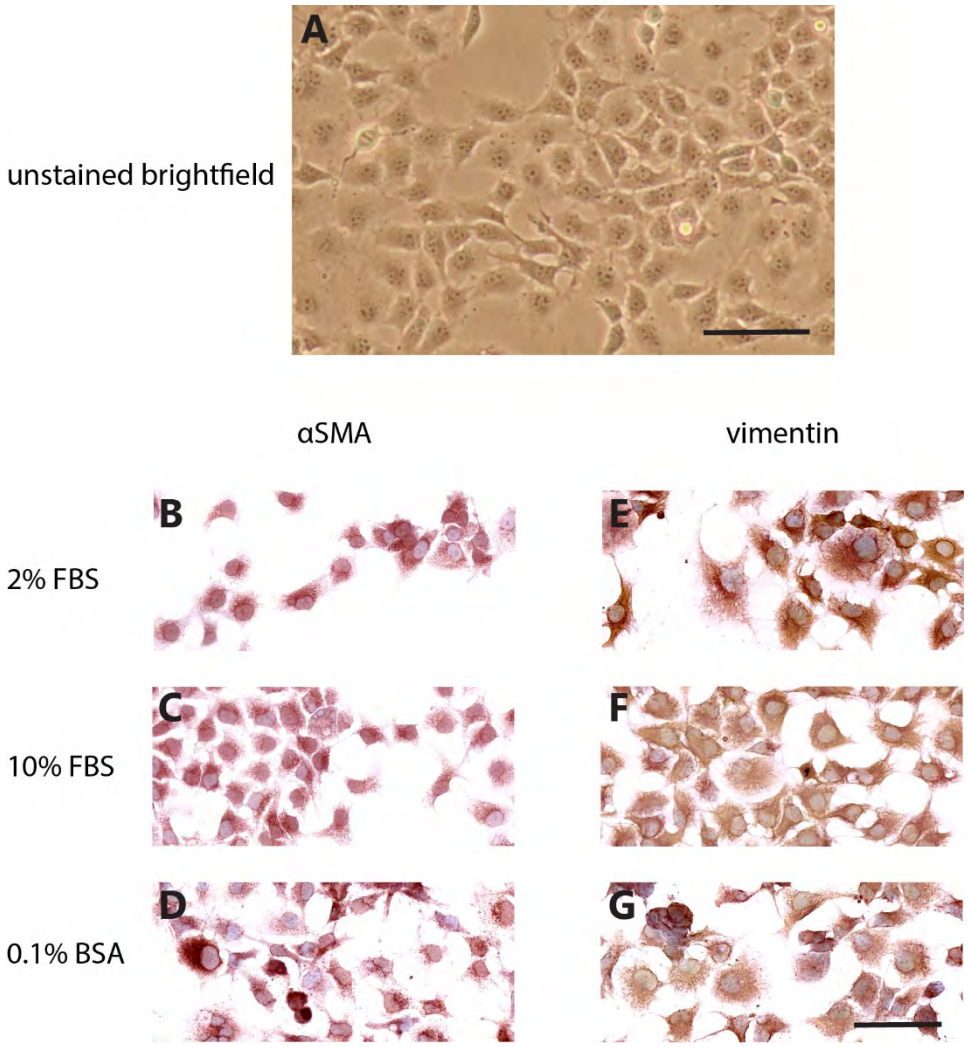

Figure 7-1: Expression of intermediate filaments by LX2 cells in different culture media

LX2 cells adopted a contracted fibroblastic appearance (A) upon *in vitro* culture. They were expanded (see Section 2.13.1) in low-serum media containing 2% foetal bovine serum (FBS) (B & E), serum-free media supplemented with 0.1% bovine serum albumin (BSA) (C & F), and high-serum conditions containing 10% FBS (D & G). Upon immunocytochemical examination (Section 2.13.2) the cells universally expressed cytoskeletal proteins α smooth muscle actin (αSMA) (B-D), a marker of stellate cell activation and vimentin (E-G), a marker of cells of mesenchymal origin in all culture media. Scale bar (–) measures 100μm.

Nevertheless, an examination of the mRNA expression (Figure 7.2) of αSMA (*ACTA2*) and *COL1A1* revealed that cells cultured in media containing 10% FBS adopt a more activated phenotype in having significantly greater expression of both than cells grown in low-serum conditions (*ACTA2*,

4.3-fold mean difference, p<0,.001; *COL1A1*, 2.0-fold mean difference, p=0.002). Conversely, serum-starved cells express less *COL1A1* (0.5-fold mean difference, p<0.001) than cells grown in low-serum conditions, suggesting a less fibrogenic phenotype. However, neither media containing 10% FBS, nor serum starved media affected the expression of *PPAR-gamma* – a marker of both primary stellate and LX2 cells quiescence[48]. It is likely that the cells are activated enough in all three culture conditions to suppress the expression of *PPAR-gamma* which is typically expressed in quiescent cells that return to a fat-storing and flattened phenotype which was not seen in these experiments.

In keeping with the more activated phenotype, LX2 cells in 10% FBS expressed 1.6-fold more *PDGFR-B* mRNA (p<0.001) than cells grown in low-serum conditions. Conversely, serum-starved cells expressed significantly less *PDGFR-B* (0.6-fold difference, p<0.001), but the cells were still mitotically responsive to PDGF-BB ligand – a defining characteristic of activated stellate cells[260]. Ki67 (a marker of proliferating cells), seemed to be positive regardless of PDGF-BB response which may suggest that Ki67 was a poor proliferative marker in LX2 cells and is constitutively expressed (Figure 7.3).

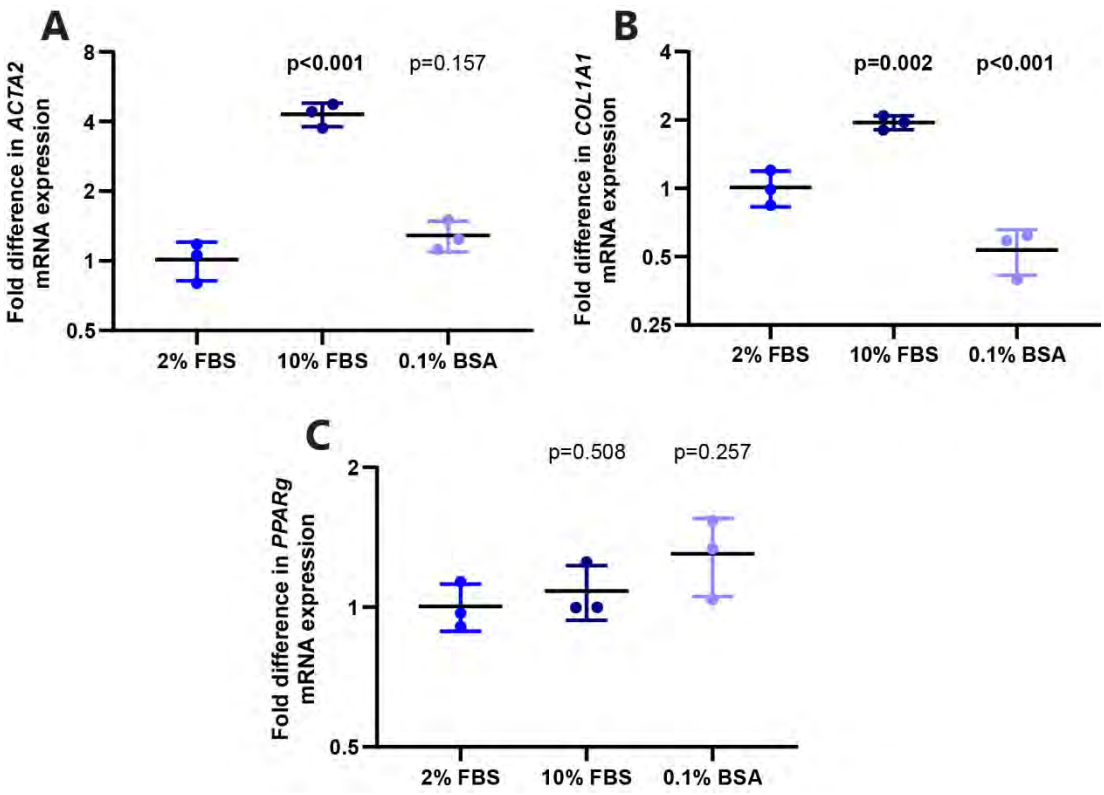

Figure 7-2: mRNA expression of genes related to stellate cell activation in different culture media

Expression of activation-associated genes in unstimulated LX2 (A: *ACTA2*, B: *COL1A1*, C: *PPARg*, against housekeeping gene *SRSF4*) was assessed by qPCR as described in section 2.14. Expression was analysed in cells from three different vials (N=3). Cells were cultured in low-serum (2% foetal bovine serum (FBS)) conditions, serum-free media supplemented with 0.1% bovine serum albumin (BSA), or high-serum media (10% FBS) for 72 hours. Each data point represents the average of technical triplicates. Data were summarised by mean and standard deviation and compared against cells in low-serum media; $p<0.05$ were deemed significant.

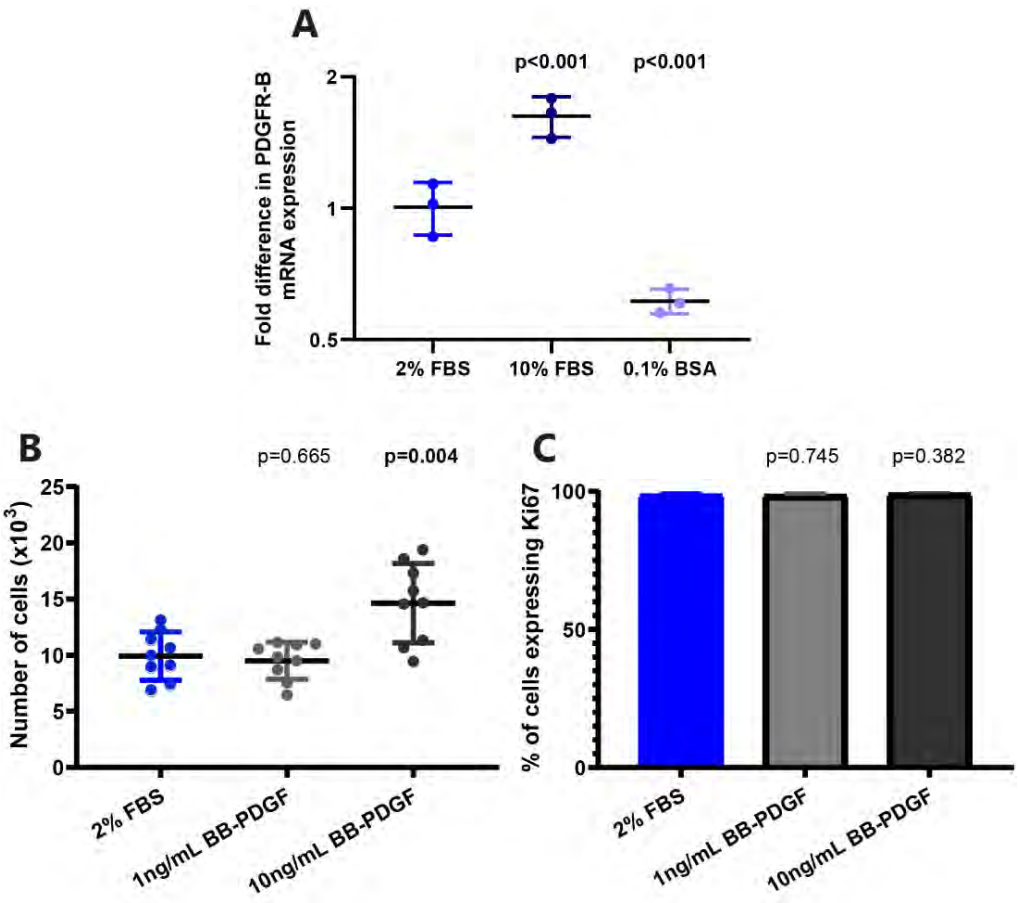

Figure 7-3: Response of LX2 cells to PDGF-BB

Expression of *PDGFR-B* in LX2 cells (against housekeeping gene *SRSF4*) was assessed by qPCR as described in section 2.14 (A). Expression was analysed in cells from three different vials (N=3). Cells were cultured in low-serum (2% foetal bovine serum (FBS)) conditions, serum-free media supplemented with 0.1% bovine serum albumin (BSA) and high-serum media (10% FBS) for 72 hours. Each data point represents the average of technical triplicates. LX2 cells were stimulated with platelet derived growth factor-BB (PDGF-BB) at a concentration of either 1ng/mL or 10ng/mL in low-serum (2%FBS) media. CyQUANT® analysis was used to determine the number of cells after 24 hours (Section 2.13.4) (B). Immunocytochemical analysis with ki67 for proliferating cells (C) (Section 2.13.2). The proportion of proliferating cells (N=3 plates for each growth condition) were compared after analysing 500 cells in each plate. Data were summarised by mean and standard deviation and compared against cells in low-serum media; $p<0.05$ were deemed significant.

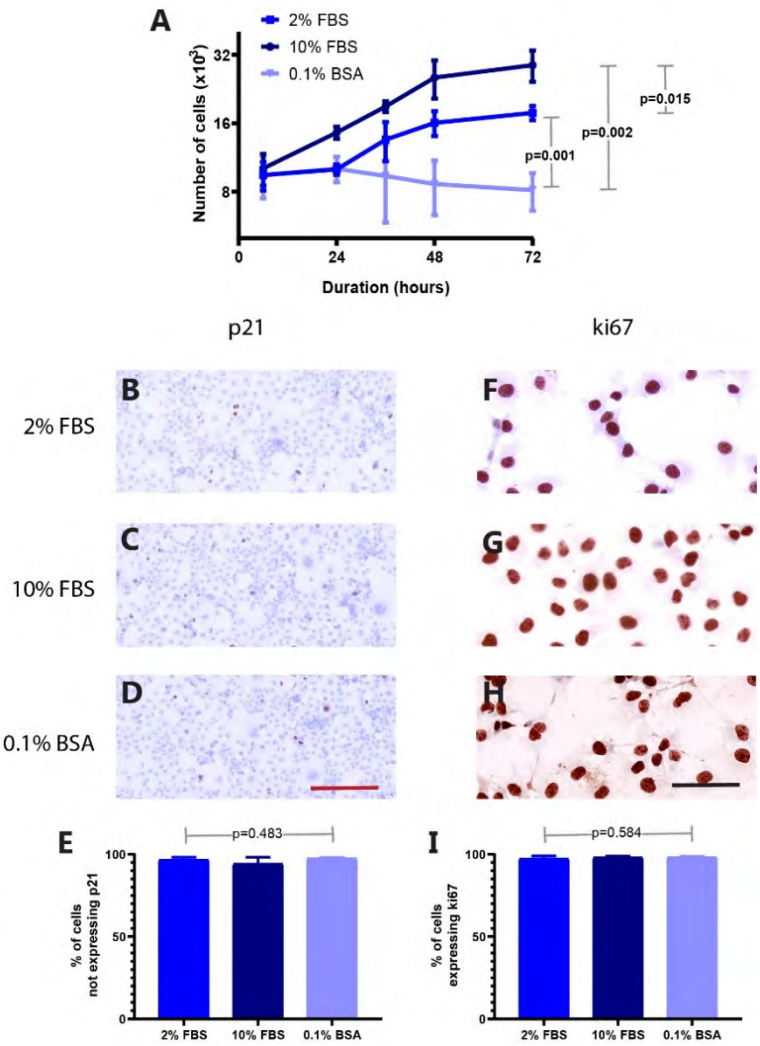

Figure 7-4: Proliferation and senescence of LX2 cells in different culture media

Following *in vitro* expansion, the numbers of LX2 cells were analysed at serial time points (1, 24, 36, 48 and 72 hours) in different growth media conditions using CyQUANT® analyses (Section 2.13.4) (A). Cells were cultured in low-serum media containing 2% foetal bovine serum (FBS) (B & F), serum free media supplemented with 0.1% bovine serum albumin (BSA) (C & G), and high-serum conditions containing 10% FBS (D & H). Data from the CyQUANT® tests were summarised by mean and standard deviation of the numbers of cells at 72 hours; groups were compared by Student's t-test. The experiment was repeated thrice, and each data point represents the mean of technical triplicates on each plate. Immunocytochemical analysis with p21 (B-D) was used as a surrogate for identifying senescent cells, and ki67 for proliferating cells (F-H) (Section 2.13.2), using haematoxylin to identify nuclei. The proportion of non-senescent cells (E) and proliferating cells (I) in different culture conditions (N=3 plates for each growth condition) were compared between groups after analysing 500 cells in each plate. Data were summarised by mean and standard deviation and all groups compared by one-way ANOVA; $p<0.05$ were deemed significant. Red scale bar (–) measures 500µm, black scale bar measures 100µm

LX2 cells were more numerous in media with 10% FBS at 24, 36, 48 and 72 hours ($p<0.05$ at each time point) than cells in low-serum conditions as measured by CyQUANT® analysis (Figure 7.4, Panel A). There were no differences in senescence as assessed by p21 IHC (Figure 7.4, Panels B-E), or apoptosis as measured by Annexin-V flow cytometry (Figure 7.5). Ki67 seemed to be constitutively expressed in all growth media to support that it seems an unreliable marker of proliferation in LX2 cells (Figure 7.4, Panels F-I). In the absence of differences in senescence and apoptosis it seems likely that LX2 cells in 10% FBS media may have had a proliferative advantage over cells in 2% FBS.

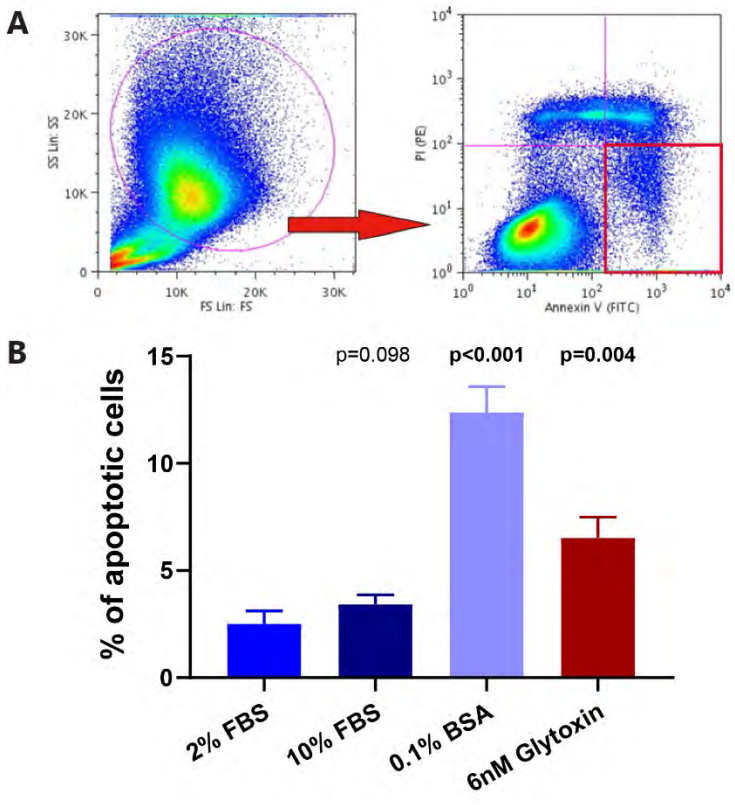

Figure 7-5: Apoptosis of LX2 cells in different culture media

After seeding and serum-starving LX2 cells in culture, they were grown in low-serum conditions containing 2% foetal bovine serum (FBS), 10% FBS or serum-free media supplemented with 0.1% bovine serum albumin (BSA) for 48 hours (Section 2.13.1). A positive control was designed by culturing cells in low-serum media for 44 hours, and adding 6nM Glytoxin for the final 4 hours. Cells were then assessed for apoptosis using a commercially available Annexin-V apoptosis detection kit whereby cells were stained for FITC-conjugated Annexin-V as a marker for apoptosis, and PE-conjugated propidium iodide (PI) as a marker for necrosis and examined by a flow cytometer for FITC-positive / PE-negative events – apoptotic cells, as demarcated by the red box (A). Data were summarised by mean and standard deviation. Mean proportions of apoptotic cells were compared against results in the low-serum group by Student's t-test (B); $p<0.05$ were deemed significant

Cells in serum-free conditions were less numerous than cells in 2% and 10% FBS, despite no differences in Ki67 and P21 staining. They were more prone to apoptosis which at least in part accounted for the differences in cell numbers, though I am not able to reliably comment on proliferative differences with this selection of tests. Dye dilution assays (using next-generation CellTrace fluorescent stains) may have overcome this unforeseen limitation of Ki67 staining.

Overall, these findings suggest that the different growth media conditions affect LX2 cell biology in nuanced ways, and reinforce the need to clearly define the culture conditions and activation phenotype before undertaking an intervention experiment. The results also reflect the bi-directional plasticity of LX2 cells on uncoated plastic; despite a naturally semi-activated state, they have the capacity to express a more and less fibrogenic phenotype in different conditions. This is critical for the assessment on an intervention on their biology. This is particularly pertinent, as previous examinations of MSC therapy on stellate cell biology have shown conflicting results, with some authors demonstrating fibrogenic attenuation[132,137], whilst others showing fibrogenic accentuation[118]. Thus, I chose not to further activate the LX2 cells with TGFβ treatment[132], as I did not want to mask a potential pro-fibrotic response to MSC-CM.

7.4. The effect of MSC conditioned media on LX2 cell activation

In the absence of S2-selection related or donor related variations in the effect of MSCs *in vivo* (Chapter 5), I chose to examine the effect of S2-selected MSCs from a single donor. CM was prepared as stated above, and described in section 2.2.1.

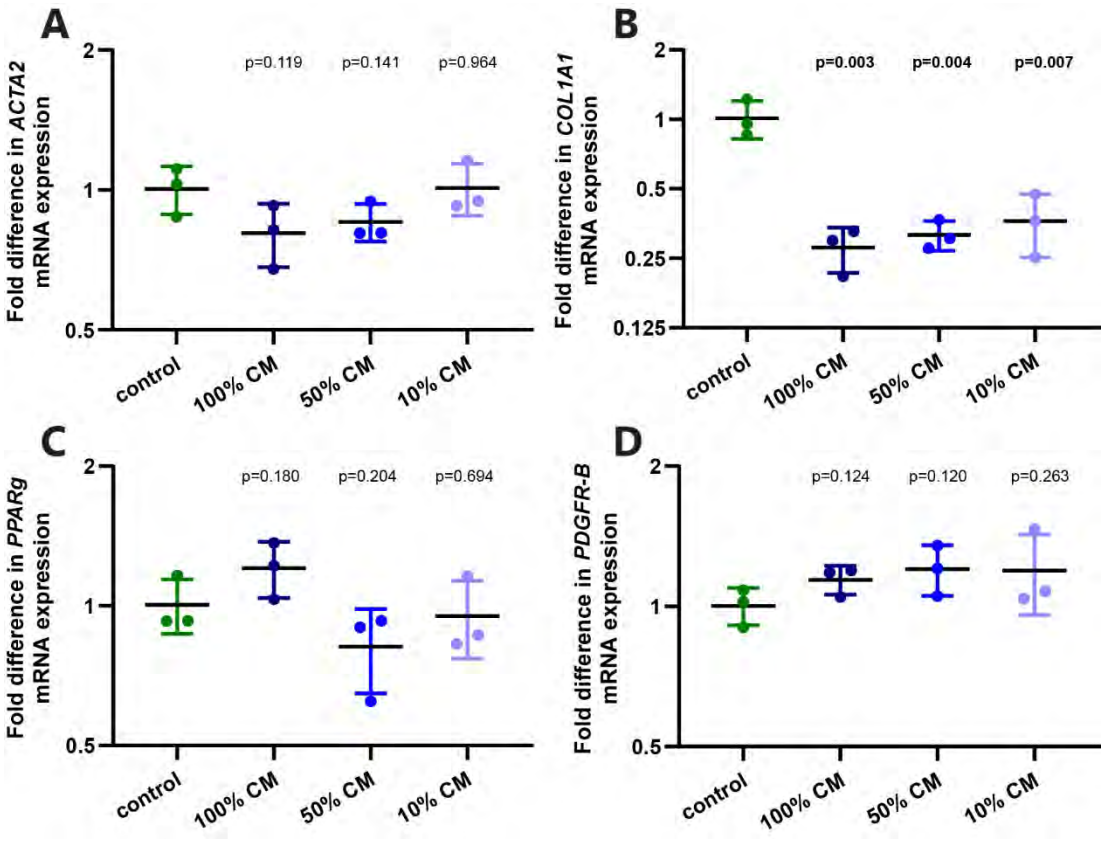

Figure 7-6: mRNA expression of genes related to stellate cell activation in MSC conditioned media

MSC conditioned media (CM) was collected after 24 hours of culture with syndecan-2 selected MSCs at a starting confluence of 60-80% as described in section 2.2.1. The CM was then diluted in fresh complete media (containing 10% foetal bovine serum) to an end-dilution of either 50% or 10% CM. Expression of activation-associated genes in LX2 cells cultured in CM for 72 hours (A: *ACTA2*, B: *COL1A1*, C: *PPARg*, D: *PDGFR-B*; against housekeeping gene *SRSF4*) was assessed by qPCR as described in section 2.14. Each experiment had an N=3, and each data point represents the average of technical triplicates. Data were summarised by mean and standard deviation and test samples (those with CM) were compared against cells in complete medium containing 10% FBS (control); $p<0.05$ were deemed significant

The CM partially suppressed the fibrogenic phenotype of LX2 cells by significantly attenuating the mRNA expression of *COL1A1* (100% CM, 0.3-fold mean difference, p=0.003; 50% CM, 0.3-fold mean difference, p=0.004; 10% CM, 0.4-fold mean difference, p=0.007)), but had no effect on the expression of *ACTA2*, *PPAR-gamma*, or *PDGFR-B* (Figure 7.6). The absence of effect of *ACTA2* mRNA expression was mirrored by the ICC examination of αSMA expression in CM and control (Figure 7.7).

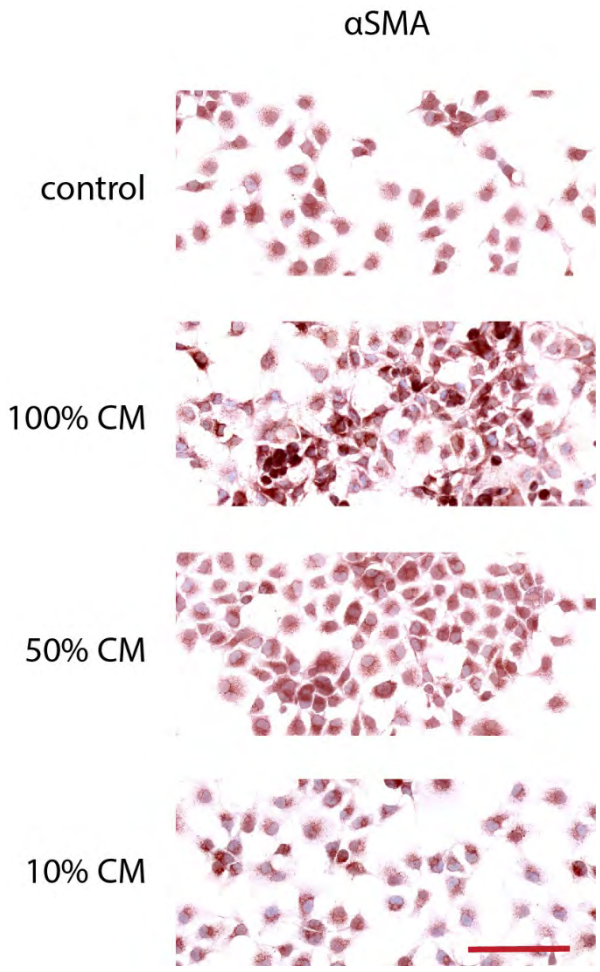

Figure 7-7: Expression of α SMA in LX2 cells in MSC conditioned media

MSC conditioned media (CM) was collected after 24 hours of culture with syndecan-2 selected MSCs at a starting confluence of 60-80% as described in section 2.2.1. The CM was then diluted in fresh complete media (containing 10% foetal bovine serum) to an end-dilution of either 50% or 10% CM. Upon immunocytochemical examination (Section 2.13.2) the cells universally expressed α smooth muscle actin (α SMA), a marker of stellate cell activation in CM and in control medium. Scale bar (–) measures 250μm.

7.5. The effect of MSC conditioned media on LX2 senescence, proliferation and viability

MSC-CM did not affect LX2 cell senescence as examined by p21 ICC or senescence associated β-galactosidase activity (Figure 7.8). However, the CM did have a dose-dependent effect on LX2 cell apoptosis as measured by Annexin-V flow cytometry, without apparently affecting cell proliferation (notwithstanding the aforementioned limitations of Ki67 ICC as a proliferative index in LX2 cells) (Figure 7.9).

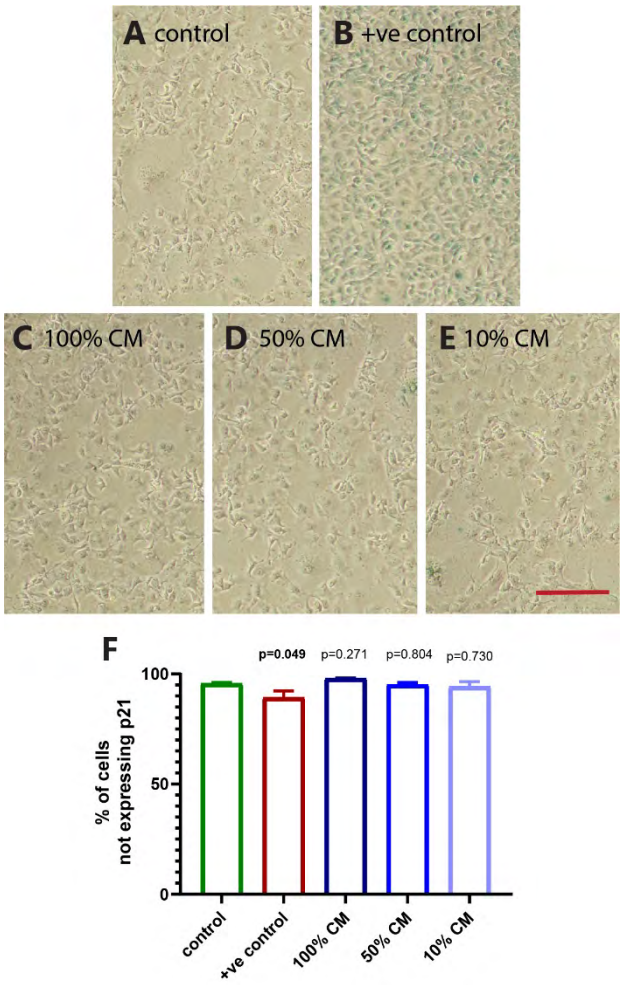

Figure 7-8: LX2 cell senescence in MSC conditioned media

MSC conditioned media (CM) was collected after 24 hours of culture with syndecan-2 selected MSCs at a starting confluence of 60-80% as described in section 2.2.1. The CM was then diluted in fresh complete media (containing 10% foetal bovine serum) to an end-dilution of either 50% or 10% CM. Senescence associated β-galactosidase activity (Section 2.13.3) was assessed after 48 hours of culture in negative-control media (A), a positive control (100ng/mL IGF-1) (B), or CM (Panels C-E); blue staining indicated the presence of β-galactosidase. Scale bar (–) measures 250µm. Upon immunocytochemical examination (Section 2.13.2) the percentage of cells not expressing p21 (a surrogate marker of senescence) were calculated after analysing 500 cells on each plate (N=3 for each group). Data were summarised by mean and standard deviation and test samples (those with CM and positive control) were compared against cells in complete medium containing 10% FBS (negative control); $p<0.05$ were deemed significant.

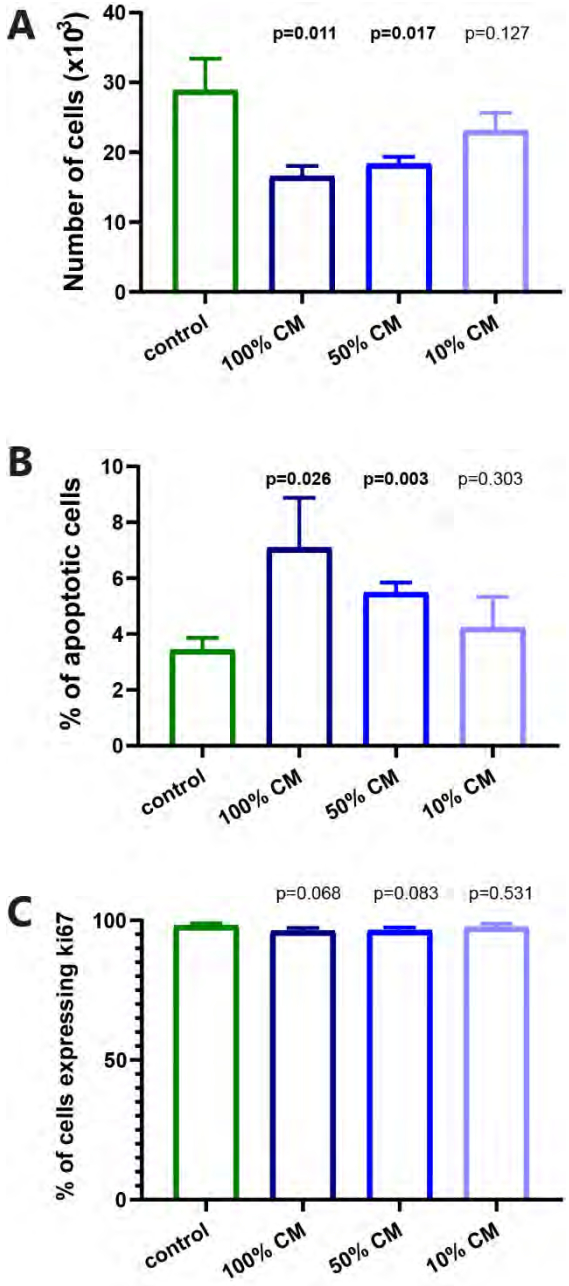

Figure 7-9: LX2 cell proliferation and viability in MSC conditioned media

MSC conditioned media (CM) was collected after 24 hours of culture with syndecan-2 selected MSCs at a starting confluence of 60-80% as described in section 2.2.1. The CM was then diluted in fresh complete media (containing 10% foetal bovine serum) to an end-dilution of either 50% or 10% CM. The total number of LX2 cells after 48 hours of growth in different culture conditions was examined using the CyQUANT® technique as described in section 2.13.4 (A). The percentage of apoptotic LX2 cells in different culture conditions after 48 hours was assessed by staining with FITC-conjugated Annexin-V and PE-conjugated propidium iodide (PI) and examined by a flow cytometer for FITC-positive / PE-negative events – apoptotic cells (B) (Section 2.13.5). The percentage of proliferating cells following 48 hours in different culture conditions were assessed by immunocytochemical analysis with ki67 (C) (Section 2.13.2) and analysing 500 cells in each plate. Each experiment had an N=3 in each group. Data were summarised by mean and standard deviation and test samples (those with CM) were compared against cells in complete medium containing 10% FBS (control); $p<0.05$ were deemed significant.

7.6. Discussion

MSC-derived soluble molecules carried by the CM, partially attenuated the fibrogenic phenotype of LX2 cells in decreasing the transcription of *COL1A1*, and significantly promoted LX2 cell apoptosis in a dose-dependent fashion. The results support a primary anti-fibrotic effect of agents within the MSC secretome, which seems to be independent of *in-vitro* priming. A number of available strategies can be utilised to interrogate the cellular secretome, and downstream analysis can hypothesise and interrogate putative anti-fibrotic agents[263]. One could speculate the possibility that the dose-dependent effect of CM may reflect nutrition depletion from the growth medium. A further *in vitro* examination using a Transwell co-culture system (MSCs separated from LX2 cells seeded at different densities) would answer this question.

7.6.1. Aligning the findings to the existing literature

Parekkadan *et al*. undertook a robust *in-vitro* analysis by indirect Transwell co-culture of human BM-MSCs and a different immortal human stellate cell line – TWNT-4[137,264]. As with the results in this chapter, the authors demonstrated a MSC dose-dependent reduction of procollagen type I, inhibition of stellate cell proliferation, and induction of stellate cell apoptosis. Neutralising antibodies against IL-10 and TNF-α negated the MSC-induced effects on HSCs. The authors demonstrated that the secretion of IL-10 by MSCs to be a dynamic response to TNF-α and HSC-derived IL-6. The concentrations of TNF-α required to induce the secretion of IL-10 were not readily achieved by co-culture, but may hint to the need for *in vivo* priming in an injured milieu where the cytokine concentrations are higher. However, this chapter's results suggest that MSC-CM acts to suppress LX2 cells independent of MSC priming. The authors also demonstrated

antibody-neutralisation of HGF led to a reduction in SC apoptosis back to baseline levels. However, these results fail to acknowledge the extremely short half-life of HGF *in vivo* of less than 5 minutes, limiting its utility as a paracrine agent, unless the source is producing large quantities and is in close proximity to the stellate cells[265,266]. Nevertheless, the half-life may depend of how the HGF is transported; exosomes (which I will go on to discuss) can package a membrane-bound "pay-load" for delivery at distant sites in protected conditions, and may overcome this issue[267].

More recently, An *et al.* explored the effect of human UCT-MSC secretome on primary human HSCs and immortalised cell lines, including LX2 cells[268]. The authors demonstrated that TGFβ-induced primary HSC activation as evidenced by the expression of *αSMA , COL1A1* and *COL1A2* was suppressed by the MSC-secretome, and this was in-part replicated to statistical significance in LX2 cells. However, unlike the results in this chapter and Parekkadan's study, the secretome had no effect on LX2 apoptosis or senescence. The authors went on to identify anti-fibrotic candidates in the secretomes using nanochip liquid chromatography / quadrupole time-of-light mass spectrometry. Enriched proteins in the secretomes were loaded in to a pathway analysis database (GeneGo), and MetaCore mapping tools focussing on proteins involved in fibrogenic pathways. The authors identified candidate proteins, of which only milk fat globule-EGF factor 8 (MFGE8) was noted to diminish TGFβ-induced αSMA expression in primary HSCs in a dose-dependent fashion; it worked via down-regulating TGFβ-receptor type I. Of note, the authors went on to describe MFGE8 in the secretome of MSCs from many different tissue sources.

Meier *et al*. demonstrated a down-regulation of *αSMA* translation in LX2 cells by MSC-CM, but did not comment on *COL1A1* expression[132]. Subsequent MSC-CM cytokine array analysis revealed elevated levels of insulin-like growth factor binding protein-2 (IGFBP-2), IL-6, IL-1Ra, and monocyte chemotactic protein-1 (MCP-1). IGFBP-2 regulates insulin-like growth factor-I, which is a potent cytoprotective and anabolic hormone produced by the liver; up-regulated IGF-I was shown to promote resolution during experimental liver fibrosis[269]. IL-6 has well-recognised cytoprotective functions[270]. IL-1Ra inhibits pro-inflammatory IL-1[271], whilst MCP-1 is a pro-inflammatory cytokine that attracts macrophages – which are critical to the resolution of fibrosis[35], and may account for the elevated levels of MMP-9 the authors demonstrated *in vivo* after injecting micro-encapsulated MSCs IP to attenuate CCl_4-induced liver fibrosis in mice. However, the authors did not examine whether these agents were critical for the observed *in vitro* effect.

An assessment of the direct effect of MSC or MSC-CM on HSCs or ECM bypasses the possibility that MSCs may work via trophic mediators[174] – agents that facilitate an effector change in an intermediate cell to induce it to secrete a biologically active agent or change in function that in turn has an indirect effect on the desired outcome. An interrogation of such an effect would respect the complex interaction of multiple cell lines *in vivo* that govern fibroplasia and its regression. Moreover, such effects are attractive to investigate as MSC therapy has been shown to effect a biological change that outlives their persistence *in vivo* in multiple different pathologies including cerebrovascular events and ischaemic heart disease[175]. With respect to liver fibrosis, MSC-derived trophic factors such as FGF2 have been shown to indirectly regulate HSC activation

and persistence by interfering with the secretion of hepatocyte-derived cytokine Dlk1 which was shown to be critical for HSC activation and persistence[138].

Based on the findings in this chapter, and allied to existing published data, one may conclude it reasonable to pursue an approach to enhance the delivery of MSCs to the liver (discussed in Chapter 6), thereby enhancing whatever effect it may have via their secretome, directly or indirectly on myofibroblasts. On the other hand, one could trial the therapeutic potential of MSC-derived secreted agents, to overcome the pulmonary sequestration. In fact, the aforementioned study by An *et al.* examined the effect of injecting the secretome from human UCT-MSCs in to mice with TAA-induced and CCl_4-induced established liver fibrosis[268]. Having identified MFGE8 as a putative direct anti-fibrotic from their *in vitro* work, the authors demonstrated an anti-fibrotic action of the whole secretome and isolated recombinant MFGE8. The effects of both were abrogated by the use of a neutralising antibody. Other authors have examined other characteristics and components of the secretome. Exosomes and microvesicles are membrane-bound extracellular vesicles (ECV) that are critical to intercellular communication and the modulation and mediation of a number of cellular processes[267]. MSC-ECVs carry a complex cargo of lipids, nucleic acids and proteins, which in all may contain > 850 unique gene products and > 150 miRNAs[272,273]. Upon release ECVs can either be taken up by target cells, or be carried to distant sites, and protect their load until they reach their target site[267]. As such, the therapeutic potential of MSC-ECVs have become a target of research interest, including their utility in liver fibrosis. Li *et al.* published data to demonstrate an UCT-MSC exosome-induced reversal of TGFβ-induced activation of a human HSC line – HL7702, but did not interrogate the contents of the ECVs any

further[133]. Another study has implicated MSC-ECV-microRNAs in the suppression of HSC activation via inhibition of the Hedgehog pathways[274].

However, as eluded to earlier, not all examinations of the effect of MSC on stellate cells *in vitro* have demonstrated a favourable effect. Baligar *et al.* demonstrated activation and increased proliferation of primary HSCs *in vitro* upon incubation with murine AT-MSC-CM, which was attributed to MSC-derived TGFβ – an agent widely accepted as critical to the immunomodulatory functions of MSCs[118]. This finding was at odds with their subsequent *in vivo* findings of a reduction of established fibrosis with decreased hepatic TGFβ, following intra-splenic injection of syngeneic AT-MSC. The study is an example of the many that have failed to replicate *in vitro* mechanisms with *in vivo* findings in the field.

7.6.2. *In vitro* models need to improve

As with the results of this chapter, the discordance between results found *in vitro* and *in vivo* is ubiquitous in life sciences, and in particular in liver fibrosis research, owing largely to how inadequate the models are[45,118,259,275]. The data by An *et al.* sits apart in marrying robust *in vitro* analysis of standard 2D monoculture experiments to an *in vivo* mechanism of action.

One must be cognisant of the strengths and limitations of widely used *in vitro* models of liver fibrosis. 2D monolayer stellate cell cultures are easy to set up and reproducible; primary stellate cells and immortalised cell lines adopt an activated myofibroblast-like phenotype when plated on uncoated tissue-culture plastic in the presence of serum, with the potential for further activation

and reversion upon manipulation and drug testing[73]. However, the spontaneous activation and maintenance of a myofibroblastic phenotype on plastic does not recapitulate the *in vivo* counterpart. Though the archetypal hallmarks of activation are conserved (e.g. ACTA2, COL1A1), there is only a 25% overlap of differential gene expression between myofibroblasts *in vivo* and *in vitro*[276]. Notwithstanding the absence of cell-cell and cell-ECM interactions, myofibroblasts on plastic adopt an unnatural elongated shape, with a large proportion of the cell covered in plastic that provides a tensile force of over 10,000kPA[277]. Comparatively, the environment of a normal liver exerts approximately 0.5kPA, and a fibrotic liver up to 20kPA[278]. Environmental stiffness has been shown to be a critical fibrogenic stimulus for stellate cell activation[279].

A number of strategies have been developed to improve cell culture models for liver fibrosis. The use of low elastic modulus Matrigel® provides a commercially available, soft ECM base upon which to culture stellate cells; it has been shown to encourage a quiescent phenotype in cell lines and primary stellate cells[260,280]. 2D co-culture with other cells (e.g. hepatocytes) recapitulate cellular aspects of the natural environment of stellates *in vivo*, and have been shown to influence stellate cell behaviour (promote quiescence) *in vitro*[281]. More recent efforts to improve *in vitro* systems have responded to the call for 3D structure and the expression of a physiological framework of ECM[73,282,283]. The most accessible example of this would be the use of 3D co-culture spheroids. A number of different techniques have been utilised to develop and maintain 3D spheroids[275] whereby typically (though not exclusively) a core of hepatic stellate cells are surrounded by a sheet of hepatocytes[284,285]. Individual laboratories have developed their own techniques, but commercially available hanging drop culture systems (e.g. InSphero) has made the technology

more accessible and enabled standardisation of protocols[286]. The culture system has been shown to be phenotypically stable for up to 5 weeks, and can be engineered to include other important cell types including Kupffer cells[287]. However, the spheroids are small (<200μm) and technically challenging to manipulate. The technology is expensive, labour intensive and outputs require proteomic or mRNA analysis. Another approach taken by researchers is to preserve native tissue architecture by the extraction of precision cut liver slices. They are acquired by cutting explanted liver (from animal or human) to a thickness of up to 250μm by the use of vibratome. The slices can be subsequently cultured for up to a week, but researchers are still ascertaining the phenotypic flux of different components of the tissue over prolonged incubation. Few investigators have yet used this technology for a base for fibrosis research owing largely to a lack of accessibility[288]. Recellularisation of decellularised liver scaffolds perhaps represent the current state-of-the-art of *in vitro* modelling of the liver. Healthy or diseased liver can be stripped to a framework of native ECM and vasculature, and repopulated with cells that behave more naturally in a familiar 3D environment[289]. This represents the future, as the technology is yet to be used as a model to test fibrotic pathways and intervention.

The apparent improvements of the *in vitro* models has not yet translated to routine use. Many of the techniques have not been fully characterised as fibrotic models and unfamiliarity breeds suspicion and doubt. Moreover, they remain inaccessible for most. However, the field should be encouraged to embrace contemporary technologies and knowledge, especially in appreciation of how sub-optimally the standard 2D *in vitro* models perform. They may be reproducible and easy

to use, but one must reconcile the current lack of effective translation from bench to clinic with the failure of the *in vitro* systems to adequately model.

7.6.3. Summary

MSC-derived soluble molecules carried by the CM, partially attenuated the fibrogenic phenotype of LX2 cells and significantly promoted LX2 cell apoptosis in a dose-dependent fashion. Notwithstanding the limitations of the *in vitro* modelling platform, the findings demand a further assessment of the utility of MSCs *in vivo*. Injection of the secretome would be the most direct approach to determine an *in vivo* effect on established liver fibrosis. An effect would implicate MSC access (Chapter 6) to the diseased site as the reason for the *in vivo* failure in Chapter 5.

Chapter 8

Conclusions and Discussion

8.1. Summary of findings

The research arc described in this thesis was set out to explore the effect of MSC therapy on liver fibrosis. Intravenously injected MSCs from human UCT neither resolved established liver fibrosis, nor abrogated fibrogenesis in two well-characterised murine models of toxin-mediated chronic hepatic injury. Tail-vein injected MSCs were subject to the pulmonary "first-pass" effect with few MSCs homing to the liver. However, MSC conditioned medium had a direct anti-fibrotic effect on human stellate cell line, LX2 cells, by attenuating the expression of *COL1A1* mRNA and promoting LX2 apoptosis. The findings of this robust and statistically powered set of experiments strongly support a recommendation that the anti-fibrotic effects of human UCT-MSCs given via tail-vein should not be tested in murine models without a significant deviation in protocol to overcome a documented barrier from this study (i.e. pulmonary entrapment).

8.2. Strengths and limitations

The strengths and limitations of each of the study parts were described in each of the results chapters, whilst delineating the context of the findings within the extant published literature, and unpublished data from our own laboratory. The key strengths were as follows:

- I described the feasibility and safety of two limitable models of liver fibrosis
- The peak fibrosis, especially in the chronic TAA model, showed features consistent with advanced scarring akin to cirrhosis, with dense fibrous bands, bridging fibrosis and nodule formation. This afforded greater parallels to human disease.
- I delineated the in-house variability of relevant fibrosis outputs in each of our fibrosis models, thereby allowing appropriate statistically powered tests.
- I used a breadth of different readouts for both the *in vivo* and *in vitro* experiments to test the effect of the intervention on fibrosis, adding validity to the findings, and was in keeping with ideal recommendations[73]. Moreover, efforts were made to reduce user bias, by examining as much of the available tissue as possible rather than using representative sampling.
- The use of two fibrosis models confirmed that the experimental findings were not model-specific.
- I clearly defined the MSCs used in the experiments in line with ISCT recommendations. This is critical in a field plagued by cell identity heterogeneity.
- I used state-of-the-art cell tracking technology to determine the bio-distribution and persistence of human MSCs injected by tail vein in mice subjected to a chronic hepatic injury. The Cryoviz™ technology allowed quantitative analysis of cell numbers in 3D-

rendered representations of whole mice; it avoided highly intensive, invasive techniques of detection that are subject to a high degree of sampling error.

The conclusions drawn from the research in this thesis were made in knowledge of the limitations that have been extensively described throughout the results chapters. The key limitations are summarised as follows:

- Murine models have low fidelity to the human counterpart, in that the mode of chronic injury by which fibrosis is achieved in both chronic CCl_4 and TAA is not replicated in human disease. However, the end fibrotic scar itself is thought to have parallels to human hepatic scar, thereby offering high discrimination.
- There was high variability in the end fibrotic burden in the mice despite identical injury conditions. Though this may have been attributable in part to not actively controlling for the dose in the TAA model (given *ad libitum*), the variation in the CCl_4 model (in which the dosing was weight-based) was presumably a consequence of an unmeasured variable. This limitation was addressed in the power calculations mentioned above.
- It is possible that an anti-fibrotic effect of MSCs was not realised as a consequence of inadequate dosing. However, as described in the Discussion section of Chapter 5, my single bolus dosing was limited by fatal thromboembolic events at higher doses. Moreover, the cumulative doses used were in the range of previously published positive results. Nevertheless, I would only know this for sure by delivering a greater cumulative dose by more regular dosing throughout either resolution or injury.

- Tail-vein cell-therapy seems to be universally limited by the pulmonary first pass phenomenon – as was the case in Chapter 6. However, other investigators have demonstrated an effect on end organs (immunomodulatory effect) despite this. It is unclear whether enhancing MSC delivery to the liver would unmask a therapeutic effect; I have discussed this at length in Chapter 7, and later in this discussion.
- Moreover, I have discussed the questionable validity of xenogeneic cell therapy testing (human MSCs in murine models); biological pathways may not be analogous.
- The bio-distribution experiments were not designed to examine whether the MSCs preferentially homed to areas of injury (fibrotic liver), as an uninjured control was not used.
- LX2 cells were chosen for ease-of-use and presumed homogeneity as isolation of primary stellate cells proved to be inconsistent. It would have been useful to demonstrate an effect of MSC-CM on primary murine stellate cells, as well as human cells, to further bridge the findings in this experiment from bench to clinic.
- 2D cell-centric *in vitro* models have a number of limitations, which I have described in Chapter 7, and later in this discussion. Primary to these limitations are the artificial mode of HSC activation, and the absence of interaction with ECM and other cell types that are integral to the interplay that govern fibrotic homeostasis.

8.3. Further experiments

Notwithstanding the limitations of the 2D "cell-centric" *in vitro* model used, the discordance between the *in vitro* and *in vivo* findings demand further attention. An *et al.* performed a series of elegantly designed tests to interrogate the cellular secretome for putative anti-fibrotic candidates using liquid chromatography and mass-spectrometry allied to pathway analysis databases[268]. A similar approach could be taken to interrogate the secretome of the MSCs donated by OTL for this body of work. However, it would be prudent to acknowledge the evidence-based interest in ECVs within the secretome. For reasons already described in chapter 7, ECVs provide a more realistic and believable therapeutic unit than free cytokines and growth factors, in that they carry a "pay-load" of multiple agents including proteins, mitochondria and nucleic acids which may have a context-dependent pleiotropic effect when working in concert. Moreover, the load is membrane-bound, thereby not only protecting it from degradation, but also influencing the way it is utilised at the effector site[134]. The therapeutic effect of ECVs, the secretome, or even selected agents within the secretome could be examined in models of liver fibrosis following tail-vein injection; a favourable therapeutic effect would then marry the *in vitro* findings to *in vivo* utility. This would inform the subsequent investigative pathway.

A more complete examination of the effect of MSCs in murine models of liver fibrosis would require an exploration of the effects of MSCs from different tissue sources, and syngeneic MSCs. The existing data is explored in Chapter 1, in which I have laid out the need for further exploration before firm conclusions are drawn.

8.4. Commentary on broader aspects of MSC research

Beyond their use in liver fibrosis, there remain fundamental issues with MSC therapy that need to be addressed before the scientific and clinical communities can expect robust and reproducible translation of laboratory findings to clinical benefit[45]. MSCs as identified by the International Society for Cellular Therapy guidelines, still represent a heterogeneous population of cells and the definition of MSC would benefit from further refinement, as described in chapter 4. In conjunction with this, another major challenge for allogeneic MSC therapy is inter-batch variability[290]. Donor-to-donor functional variability will only be apparent if relevant functional assays are carried out on a sample-by-sample basis; however, the functional assay used should be specific to the intended action of the MSCs, rather than universal to all MSC therapy[45]. Furthermore, future exploration of MSC biology needs to tackle the impact of MSC preparation on functionality. Most pre-clinical studies use continuous culture-expanded MSC, whereas clinical studies often use off-the-shelf freshly thawed cryopreserved MSC, which may have a profound effect of MSC immunomodulatory action[290,291]. These details need to be considered when translating preclinical studies to clinical study design. In light of these issues, studies should include details of isolation techniques, any prospective enrichment, cell surface marker profile with respect to the International Society for Cellular Therapy guidance, all functional assays including mesodermal lineage differentiation and cell preparation information including culture conditions, passage number and any licensing[45]. A growing body of work has challenged the fundamental assumptions about how MSCs exert a biological effect *in vivo*[227,257]. MSC survival and persistence may not be desirable; instead, their apoptosis, and subsequent efferocytosis by host phagocytic cells may induce an effector phenotype in the engulfing cell[257]. This has been shown to be the likely

mechanism by which MSCs act in GvHD. The limitations of our understanding of some of the core fundamentals describe some of the broad challenges that need to be addressed as MSC-based therapies continue to be investigated for a number of different indications[256]. The difficulties of acquiring relevant pre-clinical data to explore mechanisms of actions are discussed earlier and also elsewhere[178]. It has driven some investigators to pursue clinical trials in the absence of reproducible and relevant preclinical evidence of mechanisms of actions. After all, the clinical efficacy of MSCs in clinical trials to treat GvHD could not be predicted based on the immunosuppressive activity of donor MSCs evaluated *in vitro*[292].

At the time of writing this report, there are 59 MSC-based clinical trials currently recruiting patients and registered with clinicaltrials.gov. However, it remains a challenge to draw conclusions about MSC therapy from the trials for a number of reasons[178]: heterogeneity of cells between laboratories, unclear MSC identity, a failure to demonstrate dose-dependent effects and an inability to readily reproduce findings are but a few examples. The commercialization of MSCs may have a number of scientific advantages in terms of speed, but unfortunately a number of industry sponsored trials are not published – thereby skewing the available public knowledge base. It highlights the importance of establishing and maintaining international registries of MSC based therapies, so that investigators do not work in silos, but collaborate.

8.5. Commentary on broader aspects of pre-clinical fibrosis research

The inadequacy of preclinical models of liver fibrosis is a crippling barrier to meaningful translational science. The absence of an effective anti-fibrotic therapy after 30 years of research is testament to that fact. I have described the need to interrogate the potential of contemporary modelling techniques including 3D co-culture spheroids, recellularised liver scaffolds and precision-cut liver slices to move the field of meaningful *in vitro* modelling forward in chapter 7. I am mindful not to draw strong conclusions based on the results of chapter 7 in light of the known infidelity of the *in vitro* modelling system used.

Moreover, *in-vivo* models are not as predictable and reproducible as advertised[168]. There is significant heterogeneity within controlled experiments as demonstrated by the results in chapter 3. Existing recommendations to increase the statistical validity of animal research fall short in not recommending statistically powered tests based on meaningful outcomes[73,206] (Table 5.1). Considering the heterogeneity of results conducted by one investigator in one unit in this study, one can assume that results between units are not uniformly comparable, thereby necessitating in-house exploration of outcome variability. Though cumbersome, it provides necessary rigour and is in line with the ethical *Principles* laid out by Russell and Burch 70 years ago[159]:

> *The other great progressive human activity is art, which is so closely related to science as to be virtually the same activity. Thus it comes that the greatest scientific experiments have always been the most humane and the most aesthetically*

attractive, conveying that sense of beauty and elegance which is the essence of science at its most successful'[159].

Russell and Burch's seminal text – The principles of Humane Experimental Technique – was published 70 years ago, and still acts as a cornerstone of ethical scientific research. The excerpt above distils much of foundation of the 3Rs principle for the more ethical use of animals in scientific research. Slow adoption prompted the *Principles* to be transcribed to law by the implementation of EU Directive 2010/63 – a collection of 66 restrictive articles that decree that wherever possible, alternative scientific methods that do not need the use of live animals, should be applied in experimental research[162].

The variability of fibrosis amongst individuals subjected to the same chronic injury protocol focuses the need to track the burden of fibrosis and its regression within individuals. The limitations of serial histological assessment in clinical trials are well recognised and is not a viable option in small animal studies. Therefore, the development of a non-invasive biomarker of fibrosis or resolution would not only facilitate serial assessments to determine a meaningful response to therapy in an individual subject (animal model or human), but also profoundly reduce the number of animals required per experiment in alignment with the 3Rs principles. Detlef Schuppan described the desired characteristics of a non-invasive marker of liver fibrosis in 2008[206]:

- The marker should be liver-specific
- The levels should not be affected by alterations of liver, renal or reticuloendothelial function

- Results should be reproducible
- Levels should predict disease progression or regression
- Levels should provide a measurement of stage of fibrosis, activity of matrix deposition, or activity of matrix removal.

Unfortunately, as of yet, none of the available advances in biomarkers have been sufficiently validated to become the staple of pre-clinical or clinical experimentation[293–296]. Many of the available non-invasive markers are summarised in a recent review article[73]. Validating a bio-marker would go a long way to "squaring the circle" of finding the elusive effective anti-fibrotic agent to serve a growing population in need.

To reiterate some of the discussion in chapter 3, experimental biologists must by cognisant of the limitations of the rodent models they use. The chronic CCl_4 and TAA models deliver fibrosis with pre-dominant HSC activation; yet neither recapitulate mechanisms of fibrogenesis in human disease[45]. They do not reflect the time course or scale of human cirrhosis, and are driven by mechanisms that have no common human counterpart[166]. The advent of humanised animal models promised to shorten the bridge from animal experimentation to clinical translation[45]. A series of experiments by Bility *et al.* demonstrated the recapitulation of fibrotic responses from long-term viral hepatitis infection[297]. However, they represent a poor mimic of human disease with a limited anti-viral immune response. Nevertheless, they provide a proof-of-concept, and advances in this field may overcome many of the concerns of applicability of xenogeneic cell therapy animal experimentation[298,299].

The emerging technologies afford a great deal of hope and optimism. Characterisation of contemporary *in vitro* and *in vivo* models will continue to shorten the gap between the models and human disease, enhance our understanding of the complex interplay of different aspects of disease pathways, and facilitate the discovery of an effective anti-fibrotic armamentarium.

Chapter 9

References

1. Williams R, Aspinall R, Bellis M, et al. Addressing liver disease in the UK: a blueprint for attaining excellence in health care and reducing premature mortality from lifestyle issues of excess consumption of alcohol, obesity, and viral hepatitis. Lancet 2014;384:1953–97.
2. Pimpin L, Cortez-Pinto H, Negro F, et al. Burden of liver disease in Europe: Epidemiology and analysis of risk factors to identify prevention policies. J Hepatol 2018;69:718–735.
3. Williams R, Alexander G, Armstrong I, et al. Disease burden and costs from excess alcohol consumption, obesity, and viral hepatitis: fourth report of the Lancet Standing Commission on Liver Disease in the UK. Lancet 2018;391:1097–1107.
4. Williams R. Liver disease in the UK: Startling findings & urgent need for action. J Hepatol 2015;63:297–299.
5. Public Health England, NHS Right Care. The 2nd Atlas of variation in risk factors and healthcare for liver disease in England. 2017.
6. Department of Health. 2012 Annual Report of the Chief Medical Officer. 2012:1–78.
7. All-Party Parliamentary Hepatology Group. Liver disease: today's complacency, tomorrow's catastrophe. The All-Party Parliamentary Hepatology Group (APPHG) Inquiry into improving outcomes in liver disease. 2014.
8. Williams R, Ashton K, Aspinall R, et al. Implementation of the Lancet Standing Commission on Liver Disease in the UK. Lancet 2015;386:2098–2111.
9. Williams R, Alexander G, Aspinall R, et al. New metrics for the Lancet Standing Commission on Liver Disease in the UK. Lancet 2017;389:2053–2080.
10. Verne J. Liver disease: a preventable killer of young adults (accessed June 2018). https://publichealthmatters.blog.gov.uk/2014/09/29/liver-disease-a-preventable-killer-of-

young-adults 2014.

11. Mokdad AA, Lopez AD, Shahraz S, et al. Liver cirrhosis mortality in 187 countries between 1980 and 2010: a systematic analysis. BMC Med 2014;12:145.
12. Asrani SK, Devarbhavi H, Eaton J, et al. Burden of liver diseases in the world. J Hepatol 2019;70:151–171.
13. Rehm J, Samokhvalov A V., Shield KD. Global burden of alcoholic liver diseases. J Hepatol 2013;59:160–168.
14. Younossi Z, Anstee QM, Marietti M, et al. Global burden of NAFLD and NASH: trends, predictions, risk factors and prevention. Nat Rev Gastroenterol Hepatol 2017.
15. Burnet FM. Immunological recognition of self. Science 1961;133:307–11.
16. Medawar PB. Immunological tolerance. Science 1961;133:303–6.
17. Starzl TE. The long reach of liver transplantation. Nat Med 2012;18:1489–1492.
18. Calne RY. "It can't be done." Nat Med 2012;18:1493–1495.
19. Eurotransplant. Eurotransplant - Statistics (accessed June 2017). http://statistics.eurotransplant.org/index.php.
20. Friedman SL. Reversibility of hepatic fibrosis and cirrhosis--is it all hype? Nat Clin Pract Gastroenterol Hepatol 2007;4:236–7.
21. Wynn TA. Common and unique mechanisms regulate fibrosis in various fibroproliferative diseases. J Clin Invest 2007;117:524–529.
22. Liaw Y-F. Reversal of cirrhosis: an achievable goal of hepatitis B antiviral therapy. J Hepatol 2013;59:880–1.
23. Liaw Y-F, Sung JJY, Chow WC, et al. Lamivudine for patients with chronic hepatitis B and

advanced liver disease. N Engl J Med 2004;351:1521–31.

24. Marcellin P, Gane E, Buti M, et al. Regression of cirrhosis during treatment with tenofovir disoproxil fumarate for chronic hepatitis B: a 5-year open-label follow-up study. Lancet 2013;381:468–75.

25. Maylin S, Martinot-Peignoux M, Moucari R, et al. Eradication of hepatitis C virus in patients successfully treated for chronic hepatitis C. Gastroenterology 2008;135:821–9.

26. Falize L, Guillygomarc'h A, Perrin M, et al. Reversibility of hepatic fibrosis in treated genetic hemochromatosis: a study of 36 cases. Hepatology 2006;44:472–7.

27. Dufour JF, DeLellis R, Kaplan MM. Reversibility of hepatic fibrosis in autoimmune hepatitis. Ann Intern Med 1997;127:981–5.

28. Czaja AJ, Carpenter HA. Decreased fibrosis during corticosteroid therapy of autoimmune hepatitis. J Hepatol 2004;40:646–652.

29. Vilar-Gomez E, Martinez-Perez Y, Calzadilla-Bertot L, et al. Weight Loss Through Lifestyle Modification Significantly Reduces Features of Nonalcoholic Steatohepatitis. Gastroenterology 2015;149:367-378.e5.

30. Pessione F, Ramond M-J, Peters L, et al. Five-year survival predictive factors in patients with excessive alcohol intake and cirrhosis. Effect of alcoholic hepatitis, smoking and abstinence. Liver Int 2003;23:45–53.

31. Fallowfield J a., Mizuno M, Kendall TJ, et al. Scar-Associated Macrophages Are a Major Source of Hepatic Matrix Metalloproteinase-13 and Facilitate the Resolution of Murine Hepatic Fibrosis. J Immunol 2007;178:5288–5295.

32. Ramachandran P, Iredale JP, Fallowfield JA. Resolution of liver fibrosis: Basic mechanisms

and clinical relevance. Semin Liver Dis 2015;35:119–131.

33. Issa R, Zhou X, Constandinou CM, et al. Spontaneous recovery from micronodular cirrhosis: Evidence for incomplete resolution associated with matrix cross-linking. Gastroenterology 2004;126:1795–1808.

34. Huebert RC, Rakela J. Cellular therapy for liver disease. Mayo Clin Proc 2014;89:414–24.

35. Thomas JA, Pope C, Wojtacha D, et al. Macrophage therapy for murine liver fibrosis recruits host effector cells improving fibrosis, regeneration, and function. Hepatology 2011;53:2003–15.

36. Teo GSL, Yang Z, Carman C V, et al. Intravital imaging of mesenchymal stem cell trafficking and association with platelets and neutrophils. Stem Cells 2015;33:265–77.

37. Eseonu OI, Bari C De. Homing of mesenchymal stem cells: mechanistic or stochastic? Implications for targeted delivery in arthritis. Rheumatology (Oxford) 2015;54:210–218.

38. Rustad KC, Gurtner GC. Mesenchymal Stem Cells Home to Sites of Injury and Inflammation. Adv wound care 2012;1:147–152.

39. Aldridge V, Garg A, Davies N, et al. Human mesenchymal stem cells are recruited to injured liver in a β1-integrin and CD44 dependent manner. Hepatology 2012;56:1063–73.

40. Quintanilha LF, Takami T, Hirose Y, et al. Canine mesenchymal stem cells show antioxidant properties against thioacetamide-induced liver injury in vitro and in vivo. Hepatol Res 2014;44:E206-17.

41. Cho K-A, Woo S-Y, Seoh J-Y, et al. Mesenchymal stem cells restore CCl4-induced liver injury by an antioxidative process. Cell Biol Int 2012;36:1267–74.

42. Ricciardi M, Malpeli G, Bifari F, et al. Comparison of epithelial differentiation and immune

regulatory properties of mesenchymal stromal cells derived from human lung and bone marrow. PLoS One 2012;7:e35639.

43. Houlihan DD, Newsome PN. Critical review of clinical trials of bone marrow stem cells in liver disease. Gastroenterology 2008;135:438–50.

44. Henderson NC, Iredale JP. Liver fibrosis: cellular mechanisms of progression and resolution. Clin Sci (Lond) 2007;112:265–80.

45. Haldar D, Henderson NC, Hirschfield G, et al. Mesenchymal stromal cells and liver fibrosis: a complicated relationship. FASEB J 2016;30:3905–3928.

46. Bataller R, Brenner D a. Science in medicine - liver fibrosis. J Clin Invest 2005;115:209–218.

47. Mederacke I, Hsu CC, Troeger JS, et al. Fate tracing reveals hepatic stellate cells as dominant contributors to liver fibrosis independent of its aetiology. Nat Commun 2013;4:2823.

48. Kisseleva T, Cong M, Paik Y, et al. Myofibroblasts revert to an inactive phenotype during regression of liver fibrosis. Proc Natl Acad Sci U S A 2012;109:9448–53.

49. Gressner AM, Weiskirchen R, Breitkopf K, et al. Roles of TGF-beta in hepatic fibrosis. Front Biosci 2002;7:d793-807.

50. Novo E, Marra F, Zamara E, et al. Overexpression of Bcl-2 by activated human hepatic stellate cells: Resistance to apoptosis as a mechanism of progressive hepatic fibrogenesis in humans. Gut 2006;55:1174–1182.

51. Liu X, Xu J, Brenner DA, et al. Reversibility of Liver Fibrosis and Inactivation of Fibrogenic Myofibroblasts. Curr Pathobiol Rep 2013;1:209–214.

52. Duffield JS, Forbes SJ, Constandinou CM, et al. Selective depletion of macrophages reveals distinct, opposing roles during liver injury and repair. J Clin Invest 2005;115:56–65.

53. Wijesundera KK, Izawa T, Murakami H, et al. M1- and M2-macrophage polarization in thioacetamide (TAA)-induced rat liver lesions; a possible analysis for hepato-pathology. Histol Histopathol 2014;29:497–511.

54. Karlmark KR, Weiskirchen R, Zimmermann HW, et al. Hepatic recruitment of the inflammatory Gr1+ monocyte subset upon liver injury promotes hepatic fibrosis. Hepatology 2009;50:261–74.

55. Baeck C, Wei X, Bartneck M, et al. Pharmacological inhibition of the chemokine C-C motif chemokine ligand 2 (monocyte chemoattractant protein 1) accelerates liver fibrosis regression by suppressing Ly-6C(+) macrophage infiltration in mice. Hepatology 2014;59:1060–72.

56. Pradere J-P, Kluwe J, Minicis S De, et al. Hepatic macrophages but not dendritic cells contribute to liver fibrosis by promoting the survival of activated hepatic stellate cells in mice. Hepatology 2013;58:1461–73.

57. Liaskou E, Zimmermann HW, Li K-K, et al. Monocyte subsets in human liver disease show distinct phenotypic and functional characteristics. Hepatology 2013;57:385–98.

58. Tacke F, Zimmermann HW. Macrophage heterogeneity in liver injury and fibrosis. J Hepatol 2014;60:1090–6.

59. Ramachandran P, Iredale JP. Liver fibrosis: a bidirectional model of fibrogenesis and resolution. QJM 2012;105:813–7.

60. Pellicoro A, Aucott RL, Ramachandran P, et al. Elastin accumulation is regulated at the level of degradation by macrophage metalloelastase (MMP-12) during experimental liver fibrosis. Hepatology 2012;55:1965–75.

61. Radaeva S, Sun R, Jaruga B, et al. Natural killer cells ameliorate liver fibrosis by killing activated stellate cells in NKG2D-dependent and tumor necrosis factor-related apoptosis-inducing ligand-dependent manners. Gastroenterology 2006;130:435–52.

62. Ide M, Kuwamura M, Kotani T, et al. Effects of gadolinium chloride (GdCl(3)) on the appearance of macrophage populations and fibrogenesis in thioacetamide-induced rat hepatic lesions. J Comp Pathol 2005;133:92–102.

63. Pellicoro A, Ramachandran P, Iredale JP, et al. Liver fibrosis and repair: immune regulation of wound healing in a solid organ. Nat Rev Immunol 2014;14:181–94.

64. Elsharkawy A, Oakley F, Mann D. The role and regulation of hepatic stellate cell apoptosis in reversal of liver fibrosis. Apoptosis 2005;10:927–39.

65. Zhou X, Murphy FR, Gehdu N, et al. Engagement of alphavbeta3 integrin regulates proliferation and apoptosis of hepatic stellate cells. J Biol Chem 2004;279:23996–4006.

66. Pittenger MF, Mackay AM, Beck SC, et al. Multilineage potential of adult human mesenchymal stem cells. Science 1999;284:143–7.

67. Liu SB, Ikenaga N, Peng Z-W, et al. Lysyl oxidase activity contributes to collagen stabilization during liver fibrosis progression and limits spontaneous fibrosis reversal in mice. FASEB J 2016;30:1599–1609.

68. Barry-Hamilton V, Spangler R, Marshall D, et al. Allosteric inhibition of lysyl oxidase–like-2 impedes the development of a pathologic microenvironment. Nat Med 2010;16:1009–1017.

69. Kinnman N, Housset C. Peribiliary myofibroblasts in biliary type liver fibrosis. Front Biosci 2002;7:d496-503.

70. Tuchweber B, Desmoulière A, Bochaton-Piallat ML, et al. Proliferation and phenotypic

modulation of portal fibroblasts in the early stages of cholestatic fibrosis in the rat. Lab Invest 1996;74:265–78.

71. Cassiman D, Libbrecht L, Desmet V, et al. Hepatic stellate cell/myofibroblast subpopulations in fibrotic human and rat livers. J Hepatol 2002;36:200–9.

72. Bosselut N, Housset C, Marcelo P, et al. Distinct proteomic features of two fibrogenic liver cell populations: hepatic stellate cells and portal myofibroblasts. Proteomics 2010;10:1017–28.

73. Trautwein C, Friedman SL, Schuppan D, et al. Hepatic fibrosis: Concept to treatment. J Hepatol 2015;62:S15–S24.

74. Zoubek ME, Trautwein C, Strnad P. Reversal of liver fibrosis: From fiction to reality. Best Pract Res Clin Gastroenterol 2017;31:129–141.

75. Friedenstein AJ. Osteogenetic activity of transplanted transitional epithelium. Acta Anat (Basel) 1961;45:31–59.

76. Murray IR, West CC, Hardy WR, et al. Natural history of mesenchymal stem cells, from vessel walls to culture vessels. Cell Mol Life Sci 2014;71:1353–74.

77. Seki A, Sakai Y, Komura T, et al. Adipose tissue-derived stem cells as a regenerative therapy for a mouse steatohepatitis-induced cirrhosis model. Hepatology 2013;58:1133–42.

78. Tsai P-C, Fu T-W, Chen Y-MA, et al. The therapeutic potential of human umbilical mesenchymal stem cells from Wharton's jelly in the treatment of rat liver fibrosis. Liver Transpl 2009;15:484–95.

79. Lei M, Li K, Li B, et al. Mesenchymal stem cell characteristics of dental pulp and periodontal ligament stem cells after in vivo transplantation. Biomaterials 2014;35:6332–43.

80. Ogata Y, Mabuchi Y, Yoshida M, et al. Purified Human Synovium Mesenchymal Stem Cells as a Good Resource for Cartilage Regeneration. PLoS One 2015;10:e0129096.

81. Dominici M, Blanc K Le, Mueller I, et al. Minimal criteria for defining multipotent mesenchymal stromal cells. The International Society for Cellular Therapy position statement. Cytotherapy 2006;8:315–7.

82. Horwitz EM, Blanc K Le, Dominici M, et al. Clarification of the nomenclature for MSC: The International Society for Cellular Therapy position statement. Cytotherapy 2005;7:393–5.

83. Horwitz EM, Prockop DJ, Fitzpatrick LA, et al. Transplantability and therapeutic effects of bone marrow-derived mesenchymal cells in children with osteogenesis imperfecta. Nat Med 1999;5:309–13.

84. Blanc K Le, Mougiakakos D. Multipotent mesenchymal stromal cells and the innate immune system. Nat Rev Immunol 2012;12:383–396.

85. Rasmusson I, Uhlin M, Blanc K Le, et al. Mesenchymal stem cells fail to trigger effector functions of cytotoxic T lymphocytes. J Leukoc Biol 2007;82:887–93.

86. Krampera M, Glennie S, Dyson J, et al. Bone marrow mesenchymal stem cells inhibit the response of naive and memory antigen-specific T cells to their cognate peptide. Blood 2003;101:3722–9.

87. Glennie S, Soeiro I, Dyson PJ, et al. Bone marrow mesenchymal stem cells induce division arrest anergy of activated T cells. Blood 2005;105:2821–7.

88. Anderson JD, Johansson HJ, Graham CS, et al. Comprehensive Proteomic Analysis of Mesenchymal Stem Cell Exosomes Reveals Modulation of Angiogenesis via NFkB Signaling. Stem Cells 2016.

89. Jang Y, Kim M, Cho M, et al. Effect of bone marrow-derived mesenchymal stem cells on hepatic fibrosis in a thioacetamide-induced cirrhotic rat model. BMC Gastroenterol 2014;14:198.

90. Mohamadnejad M, Alimoghaddam K, Mohyeddin-Bonab M, et al. Phase 1 trial of autologous bone marrow mesenchymal stem cell transplantation in patients with decompensated liver cirrhosis. Arch Iran Med 2007;10:459–466.

91. Kharaziha P, Hellström PM, Noorinayer B, et al. Improvement of liver function in liver cirrhosis patients after autologous mesenchymal stem cell injection: a phase I-II clinical trial. Eur J Gastroenterol Hepatol 2009;21:1199–205.

92. Amer M-EM, El-Sayed SZ, El-Kheir WA, et al. Clinical and laboratory evaluation of patients with end-stage liver cell failure injected with bone marrow-derived hepatocyte-like cells. Eur J Gastroenterol Hepatol 2011;23:936–941.

93. Peng L, Xie D, Lin B-L, et al. Autologous bone marrow mesenchymal stem cell transplantation in liver failure patients caused by hepatitis B: short-term and long-term outcomes. Hepatology 2011;54:820–8.

94. Shi M, Zhang Z, Xu R, et al. Human mesenchymal stem cell transfusion is safe and improves liver function in acute-on-chronic liver failure patients. Stem Cells Transl Med 2012;1:725–31.

95. El-Ansary M, Abdel-Aziz I, Mogawer S, et al. Phase II trial: undifferentiated versus differentiated autologous mesenchymal stem cells transplantation in Egyptian patients with HCV induced liver cirrhosis. Stem Cell Rev 2012;8:972–81.

96. Zhang Z, Lin H, Shi M, et al. Human umbilical cord mesenchymal stem cells improve liver

function and ascites in decompensated liver cirrhosis patients. J Gastroenterol Hepatol 2012;27 Suppl 2:112–20.

97. Mohamadnejad M, Alimoghaddam K, Bagheri M, et al. Randomized placebo-controlled trial of mesenchymal stem cell transplantation in decompensated cirrhosis. Liver Int 2013;33:1490–6.

98. Salama H, Zekri A-RN, Medhat E, et al. Peripheral vein infusion of autologous mesenchymal stem cells in Egyptian HCV positive patients with end stage liver disease. Stem Cell Res Ther 2014;5:70.

99. Wang L, Li J, Liu H, et al. Pilot study of umbilical cord-derived mesenchymal stem cell transfusion in patients with primary biliary cirrhosis. J Gastroenterol Hepatol 2013;28 Suppl 1:85–92.

100. Suk KT, Yoon JH, Kim MY, et al. Transplantation with autologous bone marrow-derived mesenchymal stem cells for alcoholic cirrhosis: Phase 2 trial. Hepatology 2016;64:2185–2197.

101. Lin BL, Chen JF, Qiu WH, et al. Allogeneic bone marrow–derived mesenchymal stromal cells for hepatitis B virus–related acute-on-chronic liver failure: A randomized controlled trial. Hepatology 2017;66:209–219.

102. Liang J, Zhang H, Zhao C, et al. Effects of allogeneic mesenchymal stem cell transplantation in the treatment of liver cirrhosis caused by autoimmune diseases. Int J Rheum Dis 2017;20:1219–1226.

103. Voswinkel J, Francois S, Simon JM, et al. Use of mesenchymal stem cells (MSC) in chronic inflammatory fistulizing and fibrotic diseases: A comprehensive review. Clin Rev Allergy

Immunol 2013;45:180–192.

104. Panés J, García-Olmo D, Assche G Van, et al. Expanded allogeneic adipose-derived mesenchymal stem cells (Cx601) for complex perianal fistulas in Crohn's disease: a phase 3 randomised, double-blind controlled trial. Lancet 2016;388:1281–1290.

105. Wu C, Li F, Niu G, et al. PET imaging of inflammation biomarkers. Theranostics 2013;3:448–66.

106. Ezquer M, Ezquer F, Ricca M, et al. Intravenous administration of multipotent stromal cells prevents the onset of non-alcoholic steatohepatitis in obese mice with metabolic syndrome. J Hepatol 2011;55:1112–20.

107. Shi Z, Wakil AE, Rockey DC. Strain-specific differences in mouse hepatic wound healing are mediated by divergent T helper cytokine responses. Proc Natl Acad Sci U S A 1997;94:10663–10668.

108. Chen X, Gan Y, Li W, et al. The interaction between mesenchymal stem cells and steroids during inflammation. Cell Death Dis 2014;5:e1009.

109. Jung KH, Shin HP, Lee S, et al. Effect of human umbilical cord blood-derived mesenchymal stem cells in a cirrhotic rat model. Liver Int 2009;29:898–909.

110. Chang Y-J, Liu J-W, Lin P-C, et al. Mesenchymal stem cells facilitate recovery from chemically induced liver damage and decrease liver fibrosis. Life Sci 2009;85:517–25.

111. Zhao D-C, Lei J-X, Chen R, et al. Bone marrow-derived mesenchymal stem cells protect against experimental liver fibrosis in rats. World J Gastroenterol 2005;11:3431–40.

112. Carvalho AB, Quintanilha LF, Dias J V, et al. Bone marrow multipotent mesenchymal stromal cells do not reduce fibrosis or improve function in a rat model of severe chronic liver injury.

Stem Cells 2008;26:1307–14.

113. Mannheimer EG, Quintanilha LF, Carvalho AB, et al. Bone marrow cells obtained from cirrhotic rats do not improve function or reduce fibrosis in a chronic liver disease model. Clin Transplant 2011;25:54–60.

114. Briquet A, Grégoire C, Comblain F, et al. Human bone marrow, umbilical cord or liver mesenchymal stromal cells fail to improve liver function in a model of CCl4-induced liver damage in NOD/SCID/IL-2Rγ(null) mice. Cytotherapy 2014;16:1511–1518.

115. Rabani V, Shahsavani M, Gharavi M, et al. Mesenchymal stem cell infusion therapy in a carbon tetrachloride-induced liver fibrosis model affects matrix metalloproteinase expression. Cell Biol Int 2010;34:601–5.

116. Kamada Y, Yoshida Y, Saji Y, et al. Transplantation of basic fibroblast growth factor-pretreated adipose tissue-derived stromal cells enhances regression of liver fibrosis in mice. Am J Physiol Gastrointest Liver Physiol 2009;296:G157-67.

117. Motawi TMK, Atta HM, Sadik NAH, et al. The therapeutic effects of bone marrow-derived mesenchymal stem cells and simvastatin in a rat model of liver fibrosis. Cell Biochem Biophys 2014;68:111–25.

118. Baligar P, Mukherjee S, Kochat V, et al. Molecular and Cellular Functions Distinguish Superior Therapeutic Efficiency of Bone Marrow CD45 Cells Over Mesenchymal Stem Cells in Liver Cirrhosis. Stem Cells 2016;34:135–47.

119. Abdel Aziz M, Atta H, Roshdy N, et al. Amelioration of Murine Schistosoma mansoni Induced Liver Fibrosis by Mesenchymal Stem Cells. J Stem Cells Regen Med 2012;8:28–34.

120. Newby AC. Metalloproteinase expression in monocytes and macrophages and its

relationship to atherosclerotic plaque instability. Arterioscler Thromb Vasc Biol 2008;28:2108–14.

121. Watanabe T, Niioka M, Hozawa S, et al. Gene expression of interstitial collagenase in both progressive and recovery phase of rat liver fibrosis induced by carbon tetrachloride. J Hepatol 2000;33:224–35.

122. Iredale JP, Benyon RC, Arthur MJ, et al. Tissue inhibitor of metalloproteinase-1 messenger RNA expression is enhanced relative to interstitial collagenase messenger RNA in experimental liver injury and fibrosis. Hepatology 1996;24:176–84.

123. Benyon RC, Hovell CJ, Gaça M Da, et al. Progelatinase A is produced and activated by rat hepatic stellate cells and promotes their proliferation. Hepatology 1999;30:977–86.

124. Siller-López F, Sandoval A, Salgado S, et al. Treatment with human metalloproteinase-8 gene delivery ameliorates experimental rat liver cirrhosis. Gastroenterology 2004;126:1122–33; discussion 949.

125. Jiao J, Sastre D, Fiel MI, et al. Dendritic cell regulation of carbon tetrachloride-induced murine liver fibrosis regression. Hepatology 2012;55:244–255.

126. Winwood PJ, Schuppan D, Iredale JP, et al. Kupffer cell-derived 95-kd type IV collagenase/gelatinase B: characterization and expression in cultured cells. Hepatology 1995;22:304–15.

127. Iredale JP, Thompson A, Henderson NC. Extracellular matrix degradation in liver fibrosis: Biochemistry and regulation. Biochim Biophys Acta - Mol Basis Dis 2013;1832:876–883.

128. Issa R, Williams E, Trim N, et al. Apoptosis of hepatic stellate cells: involvement in resolution of biliary fibrosis and regulation by soluble growth factors. Gut 2001;48:548–57.

129. Wright MC, Issa R, Smart DE, et al. Gliotoxin stimulates the apoptosis of human and rat hepatic stellate cells and enhances the resolution of liver fibrosis in rats. Gastroenterology 2001;121:685–98.

130. Kisseleva T, Brenner DA. The phenotypic fate and functional role for bone marrow-derived stem cells in liver fibrosis. J Hepatol 2012;56:965–72.

131. Chen S, Xu L, Lin N, et al. Activation of Notch1 signaling by marrow-derived mesenchymal stem cells through cell-cell contact inhibits proliferation of hepatic stellate cells. Life Sci 2011;89:975–81.

132. Meier RPH, Mahou R, Morel P, et al. Microencapsulated human mesenchymal stem cells decrease liver fibrosis in mice. J Hepatol 2015;62:634–641.

133. Li T, Yan Y, Wang B, et al. Exosomes derived from human umbilical cord mesenchymal stem cells alleviate liver fibrosis. Stem Cells Dev 2013;22:845–54.

134. Phinney DG, Pittenger MF, Cells SS. Concise Review : MSC-Derived Exosomes for Cell-Free Therapy. Stem Cells 2013;35:8–11.

135. Liu J, Pan G, Liang T, et al. HGF/c-Met signaling mediated mesenchymal stem cell-induced liver recovery in intestinal ischemia reperfusion model. Int J Med Sci 2014;11:626–33.

136. Ishikawa T, Factor VM, Marquardt JU, et al. Hepatocyte growth factor/c-met signaling is required for stem-cell-mediated liver regeneration in mice. Hepatology 2012;55:1215–26.

137. Parekkadan B, Poll D van, Megeed Z, et al. Immunomodulation of activated hepatic stellate cells by mesenchymal stem cells. Biochem Biophys Res Commun 2007;363:247–52.

138. Pan R-L, Wang P, Xiang L-X, et al. Delta-like 1 serves as a new target and contributor to liver fibrosis down-regulated by mesenchymal stem cell transplantation. J Biol Chem

2011;286:12340–8.

139. Nicola M Di, Carlo-Stella C, Magni M, et al. Human bone marrow stromal cells suppress T-lymphocyte proliferation induced by cellular or nonspecific mitogenic stimuli. Blood 2002;99:3838–43.

140. Tse WT, Pendleton JD, Beyer WM, et al. Suppression of allogeneic T-cell proliferation by human marrow stromal cells: implications in transplantation. Transplantation 2003;75:389–97.

141. Baba S, Fujii H, Hirose T, et al. Commitment of bone marrow cells to hepatic stellate cells in mouse. J Hepatol 2004;40:255–60.

142. Russo FP, Alison MR, Bigger BW, et al. The bone marrow functionally contributes to liver fibrosis. Gastroenterology 2006;130:1807–21.

143. Forbes SJ, Russo FP, Rey V, et al. A significant proportion of myofibroblasts are of bone marrow origin in human liver fibrosis. Gastroenterology 2004;126:955–963.

144. Li C, Kong Y, Wang H, et al. Homing of bone marrow mesenchymal stem cells mediated by sphingosine 1-phosphate contributes to liver fibrosis. J Hepatol 2009;50:1174–83.

145. Kong Y, Wang H, Wang S, et al. FTY720, a sphingosine-1 phosphate receptor modulator, improves liver fibrosis in a mouse model by impairing the motility of bone marrow-derived mesenchymal stem cells. Inflammation 2014;37:1326–36.

146. Bonzo LV di, Ferrero I, Cravanzola C, et al. Human mesenchymal stem cells as a two-edged sword in hepatic regenerative medicine: engraftment and hepatocyte differentiation versus profibrogenic potential. Gut 2008;57:223–31.

147. Miyata E, Masuya M, Yoshida S, et al. Hematopoietic origin of hepatic stellate cells in the

adult liver. Blood 2007;111:2427–2435.

148. Higashiyama R, Moro T, Nakao S, et al. Negligible contribution of bone marrow-derived cells to collagen production during hepatic fibrogenesis in mice. Gastroenterology 2009;137:1459–66.e1.

149. Magness ST, Bataller R, Yang L, et al. A dual reporter gene transgenic mouse demonstrates heterogeneity in hepatic fibrogenic cell populations. Hepatology 2004;40:1151–9.

150. Kisseleva T, Uchinami H, Feirt N, et al. Bone marrow-derived fibrocytes participate in pathogenesis of liver fibrosis. J Hepatol 2006;45:429–38.

151. Kramann R, Schneider RK, DiRocco DP, et al. Perivascular Gli1+ Progenitors Are Key Contributors to Injury-Induced Organ Fibrosis. Cell Stem Cell 2014;16:51–66.

152. Caplan A, Correa D. The MSC: an injury drugstore. Cell Stem Cell 2012;9:11–15.

153. Witte SFH de, Lambert EE, Merino A, et al. Aging of bone marrow– and umbilical cord–derived mesenchymal stromal cells during expansion. Cytotherapy 2017;19:798–807.

154. Wilhelm A, Aldridge V, Haldar D, et al. CD248/endosialin critically regulates hepatic stellate cell proliferation during chronic liver injury via a PDGF-regulated mechanism. Gut 2016;65:1175–85.

155. Bai T, Yang Y, Wu Y-L, et al. Thymoquinone alleviates thioacetamide-induced hepatic fibrosis and inflammation by activating LKB1–AMPK signaling pathway in mice. Int Immunopharmacol 2014;19:351–357.

156. Miranda AS de, Rodrigues DH, Vieira LB, et al. A thioacetamide-induced hepatic encephalopathy model in C57BL/6 mice: a behavioral and neurochemical study. Arq Neuropsiquiatr 2010;68:597–602.

157. Lacoste B, Raymond V-A, Lapierre P, et al. Protection against Acute Hepatocellular Injury Afforded by Liver Fibrosis Is Independent of T Lymphocytes Avila MA, ed. PLoS One 2016;11:e0165360.

158. Livak KJ, Schmittgen TD. Analysis of relative gene expression data using real-time quantitative PCR and the 2(-Delta Delta C(T)) Method. Methods 2001;25:402–8.

159. Russell W, Burch R, Hume C. *The principles of humane experimental technique*. 1959.

160. Jang JH, Kang KJ, Kim YH, et al. Reevaluation of experimental model of hepatic fibrosis induced by hepatotoxic drugs: an easy, applicable, and reproducible model. Transplant Proc 2008;40:2700–3.

161. Constandinou C, Henderson N, Iredale JP. Modeling Liver Fibrosis in Rodents. Fibros Res 2005;117:237–250.

162. Scholten D, Trebicka J, Liedtke C, et al. The carbon tetrachloride model in mice. Lab Anim 2015;49:4–11.

163. Weber LWD, Boll M, Stampfl A. Hepatotoxicity and mechanism of action of haloalkanes: Carbon tetrachloride as a toxicological model. Crit Rev Toxicol 2003;33:105–136.

164. Plaa GL, Witschi H. Chemicals, drugs, and lipid peroxidation. Annu Rev Pharmacol Toxicol 1976;16:125–41.

165. Popov Y, Sverdlov DY, Sharma AK, et al. Tissue transglutaminase does not affect fibrotic matrix stability or regression of liver fibrosis in mice. Gastroenterology 2011;140:1642–52.

166. Yanguas SC, Cogliati B, Willebrords J, et al. *Experimental models of liver fibrosis*. 2016.

167. Wallace MC, Hamesch K, Lunova M, et al. Standard operating procedures in experimental liver research: thioacetamide model in mice and rats. Lab Anim 2015;49:21–9.

168. Liedtke C, Luedde T, Sauerbruch T, et al. Experimental liver fibrosis research: update on animal models, legal issues and translational aspects. Fibrogenesis Tissue Repair 2013;6:19.

169. Yada A, Iimuro Y, Uyama N, et al. Splenectomy attenuates murine liver fibrosis with hypersplenism stimulating hepatic accumulation of Ly-6C(lo) macrophages. J Hepatol 2015;63:905–16.

170. Weston CJ, Shepherd EL, Claridge LC, et al. Vascular adhesion protein-1 promotes liver inflammation and drives hepatic fibrosis. J Clin Invest 2015;125:501–20.

171. Honda H, Ikejima K, Hirose M, et al. Leptin is required for fibrogenic responses induced by thioacetamide in the murine liver. Hepatology 2002;36:12–21.

172. Feng M, Ding J, Wang M, et al. Kupffer-derived matrix metalloproteinase-9 contributes to liver fibrosis resolution. Int J Biol Sci 2018;14:1033–1040.

173. Huang Y, Bastiaan De Boer W, Adams LA, et al. Image analysis of liver biopsy samples measures fibrosis and predicts clinical outcome. J Hepatol 2014;61:22–27.

174. Caplan AI, Dennis JE. Mesenchymal stem cells as trophic mediators. J Cell Biochem 2006;98:1076–1084.

175. Caplan AI. Why are MSCs therapeutic? New data: new insight. J Pathol 2009;217:318–24.

176. British Standards Institute. PAS 93: Characterization of Human Cells for Clinical Applications Guide. 2011.

177. Commottee for Advanced Therapies. Reflection paper on stem cell-based medicinal products Reflection paper on stem cell-based medicinal products. In: *European Medicines Agency*.Vol 44.; 2010:1–11.

178. Phinney DG, Sensebé L. Mesenchymal stromal cells: Misconceptions and evolving concepts.

Cytotherapy 2013;15:140–145.

179. Harichandan A, Bühring HJ. Prospective isolation of human MSC. Best Pract Res Clin Haematol 2011;24:25–36.

180. Simmons PJ, Torok-Storb B. Identification of stromal cell precursors in human bone marrow by a novel monoclonal antibody, STRO-1. Blood 1991;78:55–62.

181. Jones EA, English A, Kinsey SE, et al. Optimization of a flow cytometry-based protocol for detection and phenotypic characterization of multipotent mesenchymal stromal cells from human bone marrow. Cytometry B Clin Cytom 2006;70:391–9.

182. Bühring H-J, Treml S, Cerabona F, et al. Phenotypic characterization of distinct human bone marrow-derived MSC subsets. Ann N Y Acad Sci 2009;1176:124–34.

183. Gronthos S, Fitter S, Diamond P, et al. A novel monoclonal antibody (STRO-3) identifies an isoform of tissue nonspecific alkaline phosphatase expressed by multipotent bone marrow stromal stem cells. Stem Cells Dev 2007;16:953–63.

184. Battula VL, Treml S, Bareiss PM, et al. Isolation of functionally distinct mesenchymal stem cell subsets using antibodies against CD56, CD271, and mesenchymal stem cell antigen-1. Haematologica 2009;94:173–84.

185. Alfaifi M, Eom YW, Newsome PN, et al. Mesenchymal stromal cell therapy for liver diseases. J Hepatol 2018;68:1272–1285.

186. Scarfe L, Taylor A, Sharkey J, et al. Non-invasive imaging reveals conditions that impact distribution and persistence of cells after in vivo administration. Stem Cell Res Ther 2018;9:332.

187. Afratis NA, Nikitovic D, Multhaupt HAB, et al. Syndecans - key regulators of cell signaling

and biological functions. FEBS J 2017;284:27–41.

188. Leonova EI, Galzitskaya O V. Cell communication using intrinsically disordered proteins: what can syndecans say? J Biomol Struct Dyn 2015;33:1037–1050.

189. Chen E, Hermanson S, Ekker SC. Syndecan-2 is essential for angiogenic sprouting during zebrafish development. Blood 2004;103:1710–1719.

190. Niu F, Wen J, Fu X, et al. Stool DNA Test of Methylated Syndecan-2 for the Early Detection of Colorectal Neoplasia. Cancer Epidemiol Biomarkers Prev 2017;26:1411–1419.

191. Mytilinaiou M, Nikitovic D, Berdiaki A, et al. Emerging roles of syndecan 2 in epithelial and mesenchymal cancer progression. IUBMB Life 2017;69:824–833.

192. Obraztsova K, Evans J, Krymskaya VP. Syndecan-2: Old Player in a New Field. Am J Respir Cell Mol Biol 2019:rcmb.2019-0033ED.

193. Renga B, Francisci D, Schiaroli E, et al. The HIV matrix protein p17 promotes the activation of human hepatic stellate cells through interactions with CXCR2 and Syndecan-2. PLoS One 2014;9.

194. Chen L, Klass C, Woods A. Syndecan-2 regulates transforming growth factor-beta signaling. J Biol Chem 2004;279:15715–8.

195. Ruiz XD, Mlakar LR, Yamaguchi Y, et al. Syndecan-2 is a novel target of insulin-like growth factor binding protein-3 and is over-expressed in fibrosis. PLoS One 2012;7:2–9.

196. Tsoyi K, Chu SG, Patino-Jaramillo NG, et al. Syndecan-2 attenuates radiation-induced pulmonary fibrosis and inhibits fibroblast activation by regulating PI3K/Akt/ROCK pathway via CD148. Am J Respir Cell Mol Biol 2018;58:208–215.

197. Shi Y, Gochuico BR, Yu G, et al. Syndecan-2 exerts antifibrotic effects by promoting caveolin-

1-mediated transforming growth factor-β receptor I internalization and inhibiting transforming growth factor-β1 signaling. Am J Respir Crit Care Med 2013;188:831–41.

198. Krampera M, Galipeau J, Shi Y, et al. Immunological characterization of multipotent mesenchymal stromal cells-The international society for cellular therapy (ISCT) working proposal. Cytotherapy 2013;15:1054–1061.

199. Galipeau J, Krampera M, Barrett J, et al. International Society for Cellular Therapy perspective on immune functional assays for mesenchymal stromal cells as potency release criterion for advanced phase clinical trials. 2016;18:151–159.

200. Haack-Sørensen M, Hansen SK, Hansen L, et al. Mesenchymal Stromal Cell Phenotype is not Influenced by Confluence during Culture Expansion. Stem Cell Rev Reports 2013;9:44–58.

201. Ren J, Wang H, Tran K, et al. Human bone marrow stromal cell confluence: effects on cell characteristics and methods of assessment. Cytotherapy 2015;17:897–911.

202. Vigneswara V, Alfaifi M, Hedegaard D, et al. Cd362+ Human Mesenchymal Stromal Cells Reduce Hepatic Inflammation and Induce M2 Macrophage Polarisation in Murine Models of Primary Sclerosing Cholangitis. J Hepatol 2016;64:S179.

203. Krampera M. Mesenchymal stromal cell "licensing": a multistep process. Leuk Off J Leuk Soc Am Leuk Res Fund, UK 2011;25:1408–1414.

204. Galleu A, Riffo-Vasquez Y, Trento C, et al. Apoptosis in mesenchymal stromal cells induces in vivo recipient-mediated immunomodulation. Sci Transl Med 2017;9:1–12.

205. Dazzi F, Marelli-Berg FM. Mesenchymal stem cells for graft-versus-host disease: close encounters with T cells. Eur J Immunol 2008;38:1479–82.

206. Schuppan D, Afdhal NH. Liver Cirrhosis. Lancet 2008;371:838–851.

207. Miryounesi M, Piryaei A, Pournasr B, et al. Repeated versus single transplantation of mesenchymal stem cells in carbon tetrachloride-induced liver injury in mice. Cell Biol Int 2013;37:340–7.

208. Monsel A, Zhu Y-G, Gennai S, et al. Cell-based therapy for acute organ injury: preclinical evidence and ongoing clinical trials using mesenchymal stem cells. Anesthesiology 2014;121:1099–121.

209. Hong J, Jin H, Han J, et al. Infusion of human umbilical cord-derived mesenchymal stem cells effectively relieves liver cirrhosis in DEN-induced rats. Mol Med Rep 2014;9:1103–11.

210. Schu S, Nosov M, O'Flynn L, et al. Immunogenicity of allogeneic mesenchymal stem cells. J Cell Mol Med 2012;16:2094–103.

211. Elahi KC, Klein G, Avci-Adali M, et al. Human Mesenchymal Stromal Cells from Different Sources Diverge in Their Expression of Cell Surface Proteins and Display Distinct Differentiation Patterns. Stem Cells Int 2016;2016:5646384.

212. Munir H, Luu N-T, Clarke LSC, et al. Comparative Ability of Mesenchymal Stromal Cells from Different Tissues to Limit Neutrophil Recruitment to Inflamed Endothelium Ivanovic Z, ed. PLoS One 2016;11:e0155161.

213. Sacchetti B, Funari A, Remoli C, et al. No Identical "Mesenchymal Stem Cells" at Different Times and Sites: Human Committed Progenitors of Distinct Origin and Differentiation Potential Are Incorporated as Adventitial Cells in Microvessels. Stem Cell Reports 2016;6:897–913.

214. Grégoire C, Ritacco C, Hannon M, et al. Comparison of Mesenchymal Stromal Cells From

Different Origins for the Treatment of Graft-vs.-Host-Disease in a Humanized Mouse Model. Front Immunol 2019;10:619.

215. Phinney DG, Galipeau J, Krampera M, et al. MSCs: science and trials. Nat Med 2013;19:812–812.

216. Keating A. Mesenchymal stromal cells: new directions. Cell Stem Cell 2012;10:709–716.

217. Blanc K Le, Tammik C, Rosendahl K, et al. HLA expression and immunologic properties of differentiated and undifferentiated mesenchymal stem cells. Exp Hematol 2003;31:890–6.

218. Huang X-P, Sun Z, Miyagi Y, et al. Differentiation of allogeneic mesenchymal stem cells induces immunogenicity and limits their long-term benefits for myocardial repair. Circulation 2010;122:2419–29.

219. Ren G, Su J, Zhang L, et al. Species variation in the mechanisms of mesenchymal stem cell-mediated immunosuppression. Stem Cells 2009;27:1954–62.

220. Akiyama K, Chen C, Wang D, et al. Mesenchymal-stem-cell-induced immunoregulation involves FAS-ligand-/FAS-mediated T cell apoptosis. Cell Stem Cell 2012;10:544–55.

221. Nemeth K, Keane-Myers A, Brown JM, et al. Bone marrow stromal cells use TGF-beta to suppress allergic responses in a mouse model of ragweed-induced asthma. Proc Natl Acad Sci U S A 2010;107:5652–7.

222. Ren G, Zhang L, Zhao X, et al. Mesenchymal stem cell-mediated immunosuppression occurs via concerted action of chemokines and nitric oxide. Cell Stem Cell 2008;2:141–50.

223. Ingersoll MA, Spanbroek R, Lottaz C, et al. Comparison of gene expression profiles between human and mouse monocyte subsets. Blood 2010;115:e10-9.

224. Ramachandran P, Pellicoro A, Vernon MA, et al. Differential Ly-6C expression identifies the

recruited macrophage phenotype, which orchestrates the regression of murine liver fibrosis. Proc Natl Acad Sci U S A 2012;109:E3186-95.

225. Rak-Raszewska A, Marcello M, Kenny S, et al. Quantum Dots Do Not Affect the Behaviour of Mouse Embryonic Stem Cells and Kidney Stem Cells and Are Suitable for Short-Term Tracking Linden R, ed. PLoS One 2012;7:e32650.

226. Eggeling C, Volkmer A, Seidel CAM. Molecular Photobleaching Kinetics of Rhodamine 6G by One- and Two-Photon Induced Confocal Fluorescence Microscopy. ChemPhysChem 2005;6:791–804.

227. Luk F, Witte SFH de, Korevaar SS, et al. Inactivated Mesenchymal Stem Cells Maintain Immunomodulatory Capacity. Stem Cells Dev 2016;25:1342–1354.

228. Muller-Borer BJ, Collins MC, Gunst PR, et al. Quantum dot labeling of mesenchymal stem cells. J Nanobiotechnology 2007;5:9.

229. Bansal A, Pandey MK, Demirhan YE, et al. Novel 89Zr cell labeling approach for PET-based cell trafficking studies. EJNMMI Res 2015;5:19.

230. Roy D, Breen M, Salvado O, et al. Imaging system for creating 3D block-face cryo-images of whole mice. In: Manduca A, Amini AA, eds. *Proceedings of SPIE--the International Society for Optical Engineering*.Vol 6143.; 2006:61431E.

231. Witte SFH de, Lambert EE, Merino A, et al. Aging of bone marrow– and umbilical cord–derived mesenchymal stromal cells during expansion. Cytotherapy 2017;19:798–807.

232. Huang X, Zhang F, Wang Y, et al. Design considerations of iron-based nanoclusters for noninvasive tracking of mesenchymal stem cell homing. ACS Nano 2014;8:4403–4414.

233. Bexell D, Gunnarsson S, Tormin A, et al. Bone marrow multipotent mesenchymal stroma

cells act as pericyte-like migratory vehicles in experimental gliomas. Mol Ther 2009;17:183–90.

234. Harting MT, Jimenez F, Xue H, et al. Intravenous mesenchymal stem cell therapy for traumatic brain injury. J Neurosurg 2009;6:1189–1197.

235. Iso Y, Spees JL, Serrano C, et al. Multipotent human stromal cells improve cardiac function after myocardial infarction in mice without long-term engraftment. Biochem Biophys Res Commun 2007;354:700–706.

236. Auletta JJ, Eid SK, Wuttisarnwattana P, et al. Human mesenchymal stromal cells attenuate graft-versus-host disease and maintain graft-versus-leukemia activity following experimental allogeneic bone marrow transplantation. Stem Cells 2015;33:601–14.

237. Krueger TEG, Thorek DLJ, Denmeade SR, et al. Concise Review: Mesenchymal Stem Cell-Based Drug Delivery: The Good, the Bad, the Ugly, and the Promise. Stem Cells Transl Med 2018;7:651–663.

238. Fischer UM, Harting MT, Jimenez F, et al. Pulmonary passage is a major obstacle for intravenous stem cell delivery: the pulmonary first-pass effect. Stem Cells Dev 2009;18:683–92.

239. Liu L, Tseng L, Ye Q, et al. A New Method for Preparing Mesenchymal Stem Cells and Labeling with Ferumoxytol for Cell Tracking by MRI. Sci Rep 2016;6:26271.

240. Phillips MR, Moore SM, Shah M, et al. A method for evaluating the murine pulmonary vasculature using micro-computed tomography. J Surg Res 2017;207:115–122.

241. Lipowsky HH, Bowers DT, Banik BL, et al. Mesenchymal Stem Cell Deformability and Implications for Microvascular Sequestration. Ann Biomed Eng 2018;46:640–654.

242. Alimperti S, Lei P, Wen Y, et al. Serum-free spheroid suspension culture maintains mesenchymal stem cell proliferation and differentiation potential. Biotechnol Prog 2014;30:974–83.

243. Zanetti A, Grata M, Etling EB, et al. Suspension-Expansion of Bone Marrow Results in Small Mesenchymal Stem Cells Exhibiting Increased Transpulmonary Passage Following Intravenous Administration. Tissue Eng Part C Methods 2015;21:683–692.

244. Hu Y, Lou B, Wu X, et al. Comparative Study on In Vitro Culture of Mouse Bone Marrow Mesenchymal Stem Cells. Stem Cells Int 2018;2018:1–14.

245. Schrepfer S, Deuse T, Reichenspurner H, et al. Stem Cell Transplantation: The Lung Barrier. Transplant Proc 2007;39:573–576.

246. Witte SFH de, Merino AM, Franquesa M, et al. Cytokine treatment optimises the immunotherapeutic effects of umbilical cord-derived MSC for treatment of inflammatory liver disease. Stem Cell Res Ther 2017;8:140.

247. Leibacher J, Dauber K, Ehser S, et al. Human mesenchymal stromal cells undergo apoptosis and fragmentation after intravenous application in immune-competent mice. Cytotherapy 2017;19:61–74.

248. Kerkelä E, Hakkarainen T, Mäkelä T, et al. Transient proteolytic modification of mesenchymal stromal cells increases lung clearance rate and targeting to injured tissue. Stem Cells Transl Med 2013;2:510–20.

249. Karp JM, Leng Teo GS. Mesenchymal stem cell homing: the devil is in the details. Cell Stem Cell 2009;4:206–16.

250. Rüster B, Göttig S, Ludwig RJ, et al. Mesenchymal stem cells display coordinated rolling and

adhesion behavior on endothelial cells. Blood 2006;108:3938–44.

251. Nitzsche F, Müller C, Lukomska B, et al. Concise Review: MSC Adhesion Cascade—Insights into Homing and Transendothelial Migration. Stem Cells 2017;35:1446–1460.

252. Daldrup-Link HE, Rudelius M, Metz S, et al. Cell tracking with gadophrin-2: a bifunctional contrast agent for MR imaging, optical imaging, and fluorescence microscopy. Eur J Nucl Med Mol Imaging 2004;31:1312–21.

253. Gao J, Dennis JE, Muzic RF, et al. The dynamic in vivo distribution of bone marrow-derived mesenchymal stem cells after infusion. Cells Tissues Organs 2001;169:12–20.

254. Witte SFH de, Luk F, Sierra Parraga JM, et al. Immunomodulation By Therapeutic Mesenchymal Stromal Cells (MSC) Is Triggered Through Phagocytosis of MSC By Monocytic Cells. Stem Cells 2018;36:602–615.

255. Cheung TS, Galleu A, Bonin M von, et al. Apoptotic mesenchymal stromal cells induce prostaglandin E2 in monocytes: implications for the monitoring of mesenchymal stromal cells activity. Haematologica 2019:haematol.2018.214767.

256. Luk F, Witte SF De, Bramer WM, et al. Efficacy of immunotherapy with mesenchymal stem cells in man: A systematic review. Expert Rev Clin Immunol 2015;11:617–636.

257. Martin I, Galipeau J, Kessler C, et al. Challenges for mesenchymal stromal cell therapies. Sci Transl Med 2019;11:1–4.

258. Couteur DG Le, Fraser R, Hilmer S, et al. The Hepatic Sinusoid in Aging and Cirrhosis. Clin Pharmacokinet 2005;44:187–200.

259. Bovenkamp M Van de, Groothuis GMM, Meijer DKF, et al. Liver fibrosis in vitro: Cell culture models and precision-cut liver slices. Toxicol Vitr 2007;21:545–557.

260. Xu L, Hui AY, Albanis E, et al. Human hepatic stellate cell lines, LX-1 and LX-2: New tools for analysis of hepatic fibrosis. Gut 2005;54:142–151.

261. Weiskirchen R, Weimer J, Meurer SK, et al. Genetic Characteristics of the Human Hepatic Stellate Cell Line LX-2. PLoS One 2013;8.

262. Cao Q, Mak KM, Lieber CS. Leptin enhances alpha1(I) collagen gene expression in LX-2 human hepatic stellate cells through JAK-mediated H2O2-dependent MAPK pathways. J Cell Biochem 2006;97:188–97.

263. Mukherjee P, Mani S. Methodologies to decipher the cell secretome. Biochim Biophys Acta 2013;1834:2226–32.

264. Shibata N, Watanabe T, Okitsu T, et al. Establishment of an immortalized human hepatic stellate cell line to develop antifibrotic therapies. Cell Transplant 2003;12:499–507.

265. Kawaida K, Matsumoto K, Shimazu H, et al. Hepatocyte growth factor prevents acute renal failure and accelerates renal regeneration in mice. Proc Natl Acad Sci U S A 1994;91:4357–61.

266. Chang HK, Kim PH, Cho HM, et al. Inducible HGF-secreting human umbilical cord blood-derived MSCs produced via TALEN-mediated genome editing promoted angiogenesis. Mol Ther 2016;24:1644–1654.

267. Lou G, Chen Z, Zheng M, et al. Mesenchymal stem cell-derived exosomes as a new therapeutic strategy for liver diseases. Exp Mol Med 2017;49:e346.

268. An SY, Jang YJ, Lim HJ, et al. Milk Fat Globule-EGF Factor 8, Secreted by Mesenchymal Stem Cells, Protects Against Liver Fibrosis in Mice. Gastroenterology 2017;152:1174–1186.

269. Sobrevals L, Rodriguez C, Romero-Trevejo JL, et al. Insulin-like growth factor I gene transfer

to cirrhotic liver induces fibrolysis and reduces fibrogenesis leading to cirrhosis reversion in rats. Hepatology 2010;51:912–21.

270. Hong F, Kim W-H, Tian Z, et al. Elevated interleukin-6 during ethanol consumption acts as a potential endogenous protective cytokine against ethanol-induced apoptosis in the liver: involvement of induction of Bcl-2 and Bcl-x(L) proteins. Oncogene 2002;21:32–43.

271. Ortiz LA, Dutreil M, Fattman C, et al. Interleukin 1 receptor antagonist mediates the antiinflammatory and antifibrotic effect of mesenchymal stem cells during lung injury. Proc Natl Acad Sci U S A 2007;104:11002–7.

272. Lai RC, Tan SS, Teh BJ, et al. Proteolytic Potential of the MSC Exosome Proteome: Implications for an Exosome-Mediated Delivery of Therapeutic Proteasome. Int J Proteomics 2012;2012:1–14.

273. Chen TS, Lai RC, Lee MM, et al. Mesenchymal stem cell secretes microparticles enriched in pre-microRNAs. Nucleic Acids Res 2010;38:215–24.

274. Hyun J, Wang S, Kim J, et al. MicroRNA125b-mediated Hedgehog signaling influences liver regeneration by chorionic plate-derived mesenchymal stem cells. Sci Rep 2015;5:14135.

275. Grunsven LA van. 3D in vitro models of liver fibrosis. Adv Drug Deliv Rev 2017;121:133–146.

276. Minicis S De, Seki E, Uchinami H, et al. Gene Expression Profiles During Hepatic Stellate Cell Activation in Culture and In Vivo. Gastroenterology 2007;132:1937–1946.

277. Li Z, Dranoff JA, Chan EP, et al. Transforming growth factor-β and substrate stiffness regulate portal fibroblast activation in culture. Hepatology 2007;46:1246–1256.

278. Gilbert PM, Havenstrite KL, Magnusson KEG, et al. Substrate elasticity regulates skeletal muscle stem cell self-renewal in culture. Science 2010;329:1078–81.

279. Olsen AL, Bloomer SA, Chan EP, et al. Hepatic stellate cells require a stiff environment for myofibroblastic differentiation. Am J Physiol Liver Physiol 2011;301:G110–G118.

280. Soofi SS, Last JA, Liliensiek SJ, et al. The elastic modulus of Matrigel™ as determined by atomic force microscopy. J Struct Biol 2009;167:216–219.

281. Krause P, Saghatolislam F, Koenig S, et al. Maintaining hepatocyte differentiation in vitro through co-culture with hepatic stellate cells. In Vitro Cell Dev Biol Anim 2009;45:205–12.

282. Brown RA. In the beginning there were soft collagen-cell gels: towards better 3D connective tissue models? Exp Cell Res 2013;319:2460–2469.

283. Rocha-Azevedo B da, Grinnell F. Fibroblast morphogenesis on 3D collagen matrices: The balance between cell clustering and cell migration. Exp Cell Res 2013;319:2440–2446.

284. Abu-Absi SF, Hansen LK, Hu W-S. Three-dimensional co-culture of hepatocytes and stellate cells. Cytotechnology 2004;45:125–140.

285. Riccalton-Banks L, Liew C, Bhandari R, et al. Long-Term Culture of Functional Liver Tissue: Three-Dimensional Coculture of Primary Hepatocytes and Stellate Cells. Tissue Eng 2003;9:401–410.

286. Messner S, Fredriksson L, Lauschke VM, et al. Transcriptomic, Proteomic, and Functional Long-Term Characterization of Multicellular Three-Dimensional Human Liver Microtissues. Appl Vitr Toxicol 2018;4:1–12.

287. Bell CC, Hendriks DFG, Moro SML, et al. Characterization of primary human hepatocyte spheroids as a model system for drug-induced liver injury, liver function and disease. Sci Rep 2016;6:25187.

288. Sadasivan S, Siddaraju N, Khan K, et al. Developing an in vitro screening assay platform for

evaluation of antifibrotic drugs using precision-cut liver slices. Fibrogenesis Tissue Repair 2015;8:1.

289. Mazza G, Rombouts K, Rennie Hall A, et al. Decellularized human liver as a natural 3D-scaffold for liver bioengineering and transplantation. Sci Rep 2015;5:13079.

290. Hoogduijn MJ, Witte S de, Luk F, et al. Effects of freeze-thawing and intravenous infusion on mesenchymal stromal cell gene expression. Stem Cells Dev 2016;25:scd.2015.0329.

291. Otsuru S, Hofmann TJ, Raman P, et al. Genomic and functional comparison of mesenchymal stromal cells prepared using two isolation methods. Cytotherapy 2015;17:262–270.

292. Blanc K Le, Frassoni F, Ball L, et al. Mesenchymal stem cells for treatment of steroid-resistant, severe, acute graft-versus-host disease: a phase II study. Lancet (London, England) 2008;371:1579–86.

293. Kwong GA, Maltzahn G von, Murugappan G, et al. Mass-encoded synthetic biomarkers for multiplexed urinary monitoring of disease. Nat Biotechnol 2013;31:63–70.

294. Nielsen MJ, Veidal SS, Karsdal MA, et al. Plasma Pro-C3 (N-terminal type III collagen propeptide) predicts fibrosis progression in patients with chronic hepatitis C. Liver Int 2015;35:429–437.

295. Ozturker C, Karagoz E, Incedayi M. Non-invasive Evaluation of Liver Fibrosis: 2-D Shear Wave Elastography, Transient Elastography or Acoustic Radiation Force Impulse Imaging? Ultrasound Med Biol 2016.

296. Taouli B, Ehman RL, Reeder SB. Advanced MRI methods for assessment of chronic liver disease. AJR Am J Roentgenol 2009;193:14–27.

297. Bility MT, Cheng L, Zhang Z, et al. Hepatitis B virus infection and immunopathogenesis in a

humanized mouse model: induction of human-specific liver fibrosis and M2-like macrophages. PLoS Pathog 2014;10:e1004032.

298. Walsh NC, Kenney LL, Jangalwe S, et al. Humanized Mouse Models of Clinical Disease. Annu Rev Pathol Mech Dis 2017;12:187–215.

299. Ito R, Takahashi T, Ito M. Humanized mouse models: Application to human diseases. J Cell Physiol 2018;233:3723–3728.